

ACCEPTED MANUSCRIPT • OPEN ACCESS

A Review of the Fraction of Four-Coordinated Boron in Binary Borate Glasses

To cite this article before publication: Oliver L G Alderman *et al* 2025 *Rep. Prog. Phys.* in press <https://doi.org/10.1088/1361-6633/adc69c>

Manuscript version: Accepted Manuscript

Accepted Manuscript is “the version of the article accepted for publication including all changes made as a result of the peer review process, and which may also include the addition to the article by IOP Publishing of a header, an article ID, a cover sheet and/or an ‘Accepted Manuscript’ watermark, but excluding any other editing, typesetting or other changes made by IOP Publishing and/or its licensors”

This Accepted Manuscript is © 2025 The Author(s). Published by IOP Publishing Ltd .



As the Version of Record of this article is going to be / has been published on a gold open access basis under a CC BY 4.0 licence, this Accepted Manuscript is available for reuse under a CC BY 4.0 licence immediately.

Everyone is permitted to use all or part of the original content in this article, provided that they adhere to all the terms of the licence <https://creativecommons.org/licenses/by/4.0>

Although reasonable endeavours have been taken to obtain all necessary permissions from third parties to include their copyrighted content within this article, their full citation and copyright line may not be present in this Accepted Manuscript version. Before using any content from this article, please refer to the Version of Record on IOPscience once published for full citation and copyright details, as permissions may be required. All third party content is fully copyright protected and is not published on a gold open access basis under a CC BY licence, unless that is specifically stated in the figure caption in the Version of Record.

View the [article online](#) for updates and enhancements.

A Review of the Fraction of Four-Coordinated Boron in Binary Borate Glasses and Melts

Oliver L. G. Alderman^a, Nagia S. Tagiara^b, Ian Slagle^c, Rebecca M. Gabrielsson^d, Piper Boggs^d, Molly Wagner^e, Aaron Rossini^e, Sophia John^d, Leilani Rocha^d, Robert M. Wilson^d, Harry Hawbaker^d, Steve W. Martin^f, Alex C. Hannon^a, Efstratios I. Kamitsos^b, Steve A. Feller^d

- a. ISIS Facility, Rutherford Appleton Laboratory, Chilton, Didcot, Oxon OX11 0QX, UK
- b. Theoretical and Physical Chemistry Institute, National Hellenic Research Foundation, 48 Vassileos Constantinou Ave, 11635 Athens, Greece
- c. Department of Materials Science, Georgia Institute of Technology, Atlanta, GA USA 30332
- d. Physics Department, Coe College, Cedar Rapids, IA USA 52402
- e. Ames National Lab, Ames, IA 50011
- f. Materials Science and Engineering Department, Iowa State University, Ames, IA 50011

Abstract

In borate materials, boron is found predominantly in either trigonal planar, or tetrahedral coordination states with oxygen, which are the two most ubiquitous building blocks of borate glasses. The fraction of tetrahedral boron, N_4 , is found to vary considerably with both glass composition and applied pressure, as well as with fictive temperature – a result of its underlying dependence on temperature in the molten and supercooled liquid states. As such, the parameter N_4 is of fundamental structural importance, along with the mechanisms driving its evolution and its strong influence on thermophysical material properties. N_4 in glasses has been experimentally determined using a variety of means including nuclear magnetic resonance (NMR) spectroscopy, vibrational spectroscopy, and x-ray and neutron diffraction. In this review, we discuss how the techniques for the measurement of N_4 have evolved and improved since the pioneering x-ray diffraction measurements of the 1930s, up to the present day. A database is compiled of the available *high-quality* numerical experimental data for N_4 , with a non-exclusive focus on binary borate glasses of the form $RM_2O_z-B_2O_3$ where R is the molar ratio of modifier to boron oxide and M is a metal cation of formal charge $z+$, other than boron. In addition, we report new N_4 values for a series of strontium borate glasses, measured by ^{11}B magic angle spinning (MAS) NMR, where a disparity in the literature is found. Based on the findings of the review, we are able to point to the gaps in our knowledge where future resources could best be focused, as well as summarizing overarching trends, the present state-of-the-art, and making recommendations for best practices.

Table of Contents

Abstract	1
Table of Contents	2
1. Introduction	4
2. Nuclear Magnetic Resonance Methods	8
2.1 Introduction	8
2.2 Historical Determination of N_4 by NMR	10
2.3 Review of NMR Measurements of N_4	17
2.4 An example of a discrepancy between strontium borate results	20
2.5 Summary of NMR-Determined N_4 Measurements	21
3. Vibrational Spectroscopy Methods	23
3.1 Introduction	23
3.2. Lithium borate glasses, $xLi_2O-(1-x)B_2O_3$	26
3.3. Silver borate glasses, $xAg_2O-(1-x)B_2O_3$	31
3.4. Alkaline earth borate glasses, $xMO-(1-x)B_2O_3$	33
3.5. IR spectroscopy of borate glasses in thin film and other forms	39
3.6. Bismuth borate glasses, $xBi_2O_3-(1-x)B_2O_3$	43
3.7. Raman spectroscopy of borate glasses	46
4. Neutron and X-ray Methods	48
4.1 Introduction	48
4.2 Outline of diffraction theory	50
4.3 Methods for extracting N_4 from diffraction data	55
4.3.1 Direct integration of the pair distribution function	55
4.3.2 Peak fitting	56
4.3.3 Mapping mean B–O bond length to N_4 using the bond valence method	62
4.3.4 Holistic bulk structural modeling using diffraction data	67
4.4 Diffraction studies of binary borate glasses	67
4.4.1 Monovalent alkali and group 11 modifiers	67
4.4.2 Divalent alkaline earth and group 12 modifiers	69
4.4.3 T^{1+} borate glasses	71
4.4.4 Mn^{2+} borate glasses	72
4.4.5 Sn^{2+} and Pb^{2+} borate glasses	74
4.4.6 Sb^{3+} and Bi^{3+} borate glasses	76
4.4.7 Te^{4+} borate glasses	78
4.4.8 Water borate glasses	80
4.5 Diffraction studies of binary borate melts	80
4.6 X-ray spectroscopic and high-pressure studies of binary borate glasses and melts	83
4.7 Future prospects	83
5. Conclusions	84

1
2
3 **6. Future prospects and recommendations**

4 **Acknowledgments**

5 **References**

89

92

92

Accepted Manuscript

1
2
3
4
5
6
7
8
9
10
11
12
13
14
15
16
17
18
19
20
21
22
23
24
25
26
27
28
29
30
31
32
33
34
35
36
37
38
39
40
41
42
43
44
45
46
47
48
49
50
51
52
53
54
55
56
57
58
59
60

1. Introduction

In borate glasses, boron atoms commonly bond either to three oxygen atoms in a BO_3 trigonal planar arrangement, or to four oxygen atoms in a BO_4 tetrahedral arrangement. For pure boron oxide, B_2O_3 , the ambient pressure forms are known to contain only trigonal BO_3 units. For example, in the ambient pressure crystal phase $\text{B}_2\text{O}_3\text{-I}^1$, each boron atom is bonded to three oxygen atoms with mean bond length of 1.369 Å and mean O-B-O bond angle of 119.89°. There is considerable evidence to show that in B_2O_3 glass there are similar trigonal BO_3 sites². However, as we will discuss in this review, the addition of a modifier (*i.e.* metal oxide, such as Li_2O) to B_2O_3 , or the application of pressure, can result in a structure in which a fraction, N_4 , of the boron atoms are tetrahedral. The main emphasis of this paper is to review the various methods of measuring N_4 in a wide variety of borate glass systems.

The mechanism for the formation of 4-coordinated borons is illustrated in this section. Figure 1.1a shows a fragment of a borate glass network formed of trigonal BO_3 units, as in pure, glassy B_2O_3 . The addition of a modifier oxide, $M_2\text{O}_z$, (where M^{z+} is a modifier cation of valence z) to the material introduces surplus oxygen, which needs to be accommodated in the structure. Figure 1.1b shows how an additional oxygen atom can be incorporated into the borate network by breaking a B-O-B bridge (the oxygen forming the bridge is called a bridging oxygen \emptyset), and creating two non-bridging oxygens (NBOs). The breaking of bridges and the creation of NBOs is the normal mechanism for the incorporation of additional oxygen in systems such as silicates and phosphates. Alternatively, as shown in Figure 1.1c, an additional oxygen atom can be incorporated into the borate network by converting two boron atoms from three-coordination to four-coordination. For a binary borate of composition $\text{RM}_2\text{O}_z\text{-B}_2\text{O}_3$, the number of surplus oxygen atoms per boron atom is $Rz/2$, where z is related to the theoretical rate at which four-coordinated borons are formed. Thus, if all surplus oxygen atoms are incorporated by the mechanism shown in Figure 1.1c, the number of BO_4 units per boron atom is $N_4=Rz$. For $z=1$, the relation is $N_4=R$. For $z=2$ the glass composition is simply $\text{RMO-B}_2\text{O}_3$ and, again, $N_4=R$.

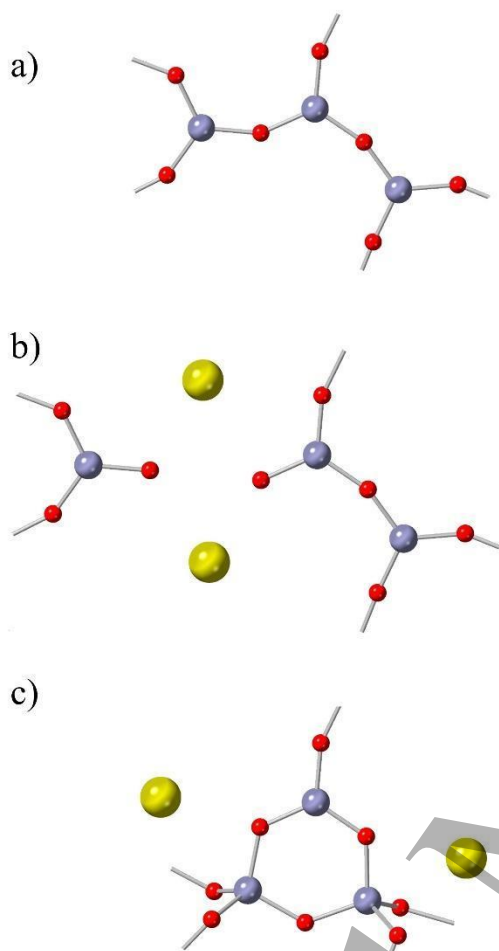


Figure 1.1

(a) A fragment of the borate network (larger blue spheres are boron atoms, and smaller red spheres are oxygen atoms).

(b) The network fragment in Figure 1.1a is shown after the incorporation of one unit of M_2O modifier by the conversion of one bridging oxygen to two non-bridging oxygens (yellow spheres without bonds are modifier cations, M^+).

(c) The network fragment in Figure 1.1a is shown after the incorporation of one unit of M_2O modifier by the conversion of two BO_3 units to BO_4 .

(Note that this arrangement of atoms has been drawn to illustrate simply the way in which four-coordinated boron arises; it should not be taken to indicate whether or not BO_4 units exist in close proximity to each other, or to imply the presence of a particular superstructural unit).

The compositions of binary borate glasses are commonly expressed in terms of either the molar ratio, R , or the molar fraction of modifier, x (in which case the composition is $xM_{2/z}O_z-(1-x)B_2O_3$). These two parameters are related according to the following equations:

$$R = \frac{x}{1-x} \quad \text{and} \quad x = \frac{R}{1+R} \quad (1.1)$$

There is interest in the behavior of N_4 due to its probable relation to the borate anomaly (also called the boron anomaly). The composition dependence of most thermophysical properties of borate glasses shows a maximum or minimum, typically at ~ 15 -30 mol% $M_{2/z}O$. The physical property measurements reported by Shelby³ are an excellent example of this behavior in alkali borate glasses. This behavior has been known for many decades (for example, see Gooding and Turner⁴), and it is in sharp contrast to the monotonic behavior for silicate glasses, which has led to it being regarded as anomalous. The first evidence for the evolution of four-coordinated boron in borate glass was reported by Biscoe and Warren⁵, who used x-ray diffraction on sodium borate

1
2
3 glasses to show an increase in the boron-oxygen coordination number as Na₂O is added to B₂O₃.
4 It was proposed that the property maxima and minima could be explained in terms of the change
5 in boron coordination number. However, the extrema of different properties occur at different
6 compositions, and a more modern view is that the change in boron coordination number is one of
7 several factors that govern the borate anomaly³.
8
9

10 As we show in this review, most experimental evidence for binary borate glass systems
11 shows that for low modifier content, the measured values of N_4 are commonly close to the ideal
12 $N_4=R$ relation. Then, as the modifier content increases, the measured values of N_4 generally reach
13 a maximum and subsequently decrease, exhibiting a behavior that is similar to the changes in
14 physical properties associated with the borate anomaly. This behavior is evidence that BO₄
15 formation (Figure 1.1c) is the dominant mechanism for incorporation of modifiers for low values
16 of R , but that NBO formation is the dominant mechanism for high values of R .
17
18

19 In principle, other structural mechanisms are possible. For example, the high pressure
20 crystal phase B₂O₃-II⁶ has only tetrahedral BO₄ units (*i.e.* it has $N_4=1$, even though $R=0$); each
21 boron atom is bonded to four oxygen atoms with mean bond length 1.476 Å and mean O-B-O
22 bond angle 109.35°. To understand how this higher coordination number arises, it is useful to note
23 that the O-B and B-O coordination numbers are necessarily related:
24
25

$$n_{O-B} = n_{B-O} \frac{c_B}{c_O} \quad (1.2)$$

26 where c_B and c_O are the atomic fractions of boron and oxygen. Thus, for pure B₂O₃, a B-O
27 coordination of four corresponds to an O-B coordination number $8/3 \approx 2.67$. In B₂O₃-II, two thirds
28 of the oxygen atoms are three-coordinated by boron, rather than acting as bridging oxygen (BOs)
29 between two boron atoms (as in Figure 1.1a). Thus, the formation of three-coordinated oxygen
30 causes an increase in the value of N_4 , and can lead to values greater than predicted by the $N_4=R$
31 relation. On the other hand, linear BO₂ units are rare, but not unknown, in crystal structures⁷.
32 Topologically, a BO₂ unit can be formed in a network of BO₃ units (as in Figure 1.1a) by breaking
33 a single B-O bond; in that case, the presence of BO₂ units leads to an increase in the number of
34 NBOs.
35
36
37
38

39 Borates are unusual in that they have superstructural units (well-defined rings formed by a small
40 number of boron triangles and tetrahedra, most commonly three). It is well established that the
41 structure of pure B₂O₃ glass includes a large number of B₃O₃O₃ boroxol groups² (highly planar
42 rings of three BO₃ units). The structure of B₂O₃ glass in terms of the fraction of B atoms in boroxol-
43 rings have been found to corresponds to the majority of boron atoms; this is ~ 0.82 - 0.85 based on
44 ¹⁰B, ¹¹B and ¹⁷O NMR^{8,9} and the nuclear quadrupole resonance (NQR) studies of Bray and
45 coworkers^{10,11}, 0.80 ± 0.05 according to neutron diffraction and inelastic neutron scattering studies
46 of Hannon *et al.*¹², 0.72 based on the NMR study by Kroeker and Stebbins¹³, as 0.73 ± 0.01 by ¹¹B
47 double rotation (DOR) NMR spectroscopy¹⁴ and by other means such as inelastic neutron
48 scattering which determined the fraction to be very close to $2/3$ ². The remainder of the boron
49 atoms are arranged in independent BO₃ units, as shown in Figure 1.2a. As the modifier content is
50 increased, and the number of BO₄ units increases and then declines, a succession of different
51 superstructural units occurs. Figure 1.2 shows some of the more important superstructural units in
52 borates. A comprehensive consideration of the superstructural units in borate structures has been
53 given by Wright¹⁵. The number of basic units (BO₃ or BO₄) in the rings of the superstructural units
54
55
56
57
58
59
60

is relatively small (usually three) compared to the rings that occur in other glass forming systems, due to the relatively large O-B-O bond angle of 120° in the BO_3 units^{2,16}. As a result of the small size of the rings, they are well defined and often planar, leading to sharp vibrational modes that are detectable by Raman spectroscopy^{16,17}.

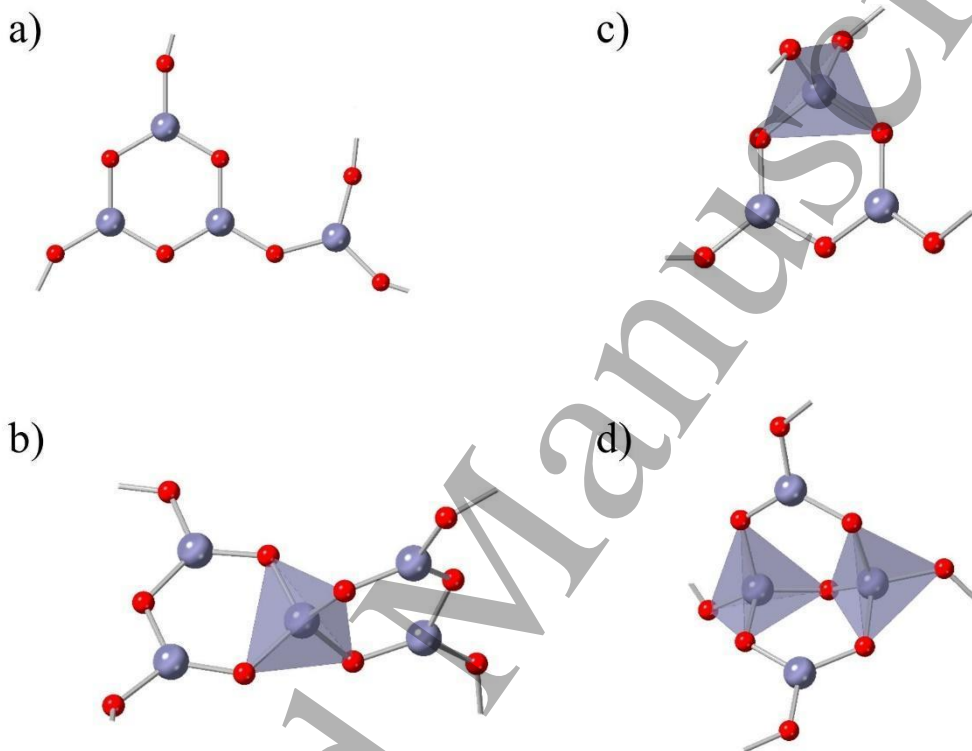


Figure 1.2. Some of the more important superstructural units in borates, shown for increasing concentration of BO_4 tetrahedra. Larger blue spheres are boron atoms, and smaller red spheres are oxygen atoms. Four-coordinated boron atoms are shown surrounded by a tetrahedron. (a) a boroxol ring, shown bonded to an independent BO_3 unit, (b) a pentaborate ring, (c) a triborate unit, (d) a diborate unit.

Recently, it has been discovered that edge-sharing can occur between two BO_4 tetrahedra in some crystalline borates (see Figure 1.3). This structural feature was first observed in the high-pressure phase of $\text{Dy}_4\text{B}_6\text{O}_{15}$ ¹⁸, where it involves a very short B...B distance of 2.098 Å. Then it was found to occur in additional high-pressure phases, before subsequently being discovered in ambient pressure phases, starting with KZnB_3O_6 ¹⁹. Typically, it has been found in metaborate crystals (*i.e.* 50 mol% B_2O_3). Figure 1.3 shows the sharing of an edge between two BO_4 tetrahedra in the ambient pressure crystal phase of $\text{Li}_4\text{Na}_2\text{CsB}_7\text{O}_{14}$ ²⁰. It should be noted that BO_2 units and edge-shared BO_4 tetrahedra have only been discovered relatively recently in crystalline compounds, and to our knowledge evidence has not currently been found for the presence of these structural features in glasses. It will be interesting to see if such evidence emerges in the future.

The occurrence of edge-shared tetrahedra does not have a direct effect on the value of N_4 , but it would be likely to have an indirect influence.

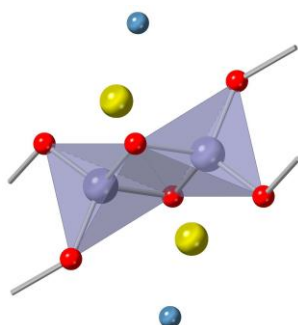


Figure 1.3.

The pair of edge-sharing BO_4 tetrahedra in the ambient pressure crystal phase $\text{Li}_4\text{Na}_2\text{CsB}_7\text{O}_{14}$ ²⁰. Boron atoms are shown by the larger gray spheres at the center of a tetrahedron of four oxygen atoms, shown as smaller red spheres. Spheres without bonds show sodium (larger yellow spheres) and lithium (smaller blue spheres) atoms.

Now, we shift our attention to the fact that borates are not the only glass-forming system in which the glass former cation can change coordination number. For example, the average Ge coordination number can become larger than four in germanate glasses²¹, whilst the Te coordination number may become less than four in tellurite glasses²². However, the exact nature of the structural changes in germanates and tellurites is still under discussion. In contrast, it has been thoroughly established that ambient B_2O_3 glass involves only three-coordinated boron, and that there are two possible boron coordination numbers in borates, either three or four. We can represent the coordination change by the relationship: $\text{B}\text{O}_3 + \frac{1}{2} \text{O}^{2-} \rightarrow [\text{B}\text{O}_4]^-$, where O is a bridging oxygen. Also, the creation of non-bridging oxygens (O^-) is a possibility by the following formula: $\text{B}\text{O}_3 + \frac{1}{2} \text{O}^{2-} \rightarrow [\text{B}\text{O}_2\text{O}]^-$. Thus there is an equilibrium relationship, $[\text{B}\text{O}_2\text{O}]^- \rightleftharpoons [\text{B}\text{O}_4]^-$. It is observed that the formation of $[\text{B}\text{O}_4]^-$ is energetically preferred at low modifications of the borate network (see further discussion below). Thus, borates are ideally suited to the study of the phenomenon of changing coordination numbers in glasses.

In this review, we mostly restrict our attention to binary borate systems. Nevertheless, the structural study of these systems is of direct relevance to glasses with more complex compositions (for example the commercial borosilicate Pyrex®²³ or to thioborates based on the glass former B_2S_3).

We will now discuss the various methods that have been used to measure N_4 : NMR, vibrational spectroscopy, and neutron and x-ray scattering techniques.

2. Nuclear Magnetic Resonance Methods

2.1 Introduction

NMR spectroscopy principally relies on the interaction of the magnetic dipole moments of atoms' nuclei with the external magnetic field (Zeeman effect). Various additional interactions give rise to a spectrum with rich structural implications. These interactions include the magnetic dipole-dipole interaction (the alteration of the magnetic field seen by a given nucleus due to its

neighboring dipole moments), the chemical shift (the shielding effect due to the electrons opposing the external magnetic field), and for nuclei with a spin greater than or equal to 1 ($I \geq 1$), the quadrupole interaction (the changes in the energy levels due to the interaction of the quadrupole moment of the nucleus with the gradient of the electric field from bonding electrons)²⁴.

¹¹B, the most common isotope for determining N_4 by NMR due to abundance, has a spin of 3/2. This results in quadrupolar perturbed transitions including a central transition ($-1/2 \rightarrow 1/2$) and two satellite transitions ($1/2 \rightarrow 3/2$ and $-3/2 \rightarrow -1/2$). In static NMR, it was usually the case that the central transition was observed. In magic angle spinning (MAS) NMR, effects due to the satellite transitions are perceived and must be accounted for.

MAS NMR allows for the elimination of the dipole-dipole interaction. To accomplish this, the sample is spun at tens of kilohertz at the magic angle of 54.74 degrees. The result is a narrowing and sharpening of the resulting NMR spectrum, allowing for more precise determination of N_4 , particularly at high magnetic fields.

For ¹¹B MAS NMR the chemical shift results in an isotropic shift that is different for three- and four-coordinated borons and is proportional to the applied magnetic field (for relatively large fields, 14.1 T or greater, substantial separation occurs between the three- and four-coordinated borons, allowing clear separation and quantification of each).

The quadrupole interaction is characterized by two parameters: the quadrupole coupling constant C_Q , which is proportional to the z-component (largest component) of the electric field gradient tensor, and the asymmetry parameter η , which is a measure of the cylindrical symmetry in the xy-plane (η may take values between 0, completely cylindrically symmetric, and 1). Trigonal borons with either three bridging oxygens or three non-bridging oxygens have η near 0. For trigonal borons with one or two non-bridging oxygens, η is typically greater than 1/2. The C_Q of the three- and four-coordinated ¹¹B in borate glasses are roughly 2.5 MHz and 0.5 MHz respectively. For ¹⁰B, these values are approximately doubled.

Boron NMR is notable in its use to determine N_4 due to its inherent quantitative results: in the integrated NMR spectrum, the areas of the peaks associated with the three- and four-coordinated borons are nearly proportional to the population of each of the species:

$$N_4 = \frac{n_4}{n_3+n_4} \approx \frac{A_4}{A_3+A_4} \quad (2.1)$$

where n is the population of the n^{th} species, and A_n is the relative area of the peak corresponding to the n^{th} species. Equation 2.1 is subject to usually small corrections such as the effects of the spinning sidebands on the areas of the three- and four-coordinated borons as accounted for by Massiot²⁵. The lower C_Q leads to a different shape to the two peaks arising from the two different coordinations of boron, aiding identification.

2.2 Historical Determination of N_4 by NMR

In 1958, Arnold Silver and Phil Bray published pioneering work on NMR in borate glass²⁶. Figure 2.1a, obtained from glassy B_2O_3 , depicts the first derivative of a classic second order quadrupole line shape characteristic of trigonal planar boron. The spectrum was observed using a permanent magnet of field strength just over 0.5 T (^{11}B radiofrequency of 7.177 MHz), and the measured C_Q was 2.76 MHz.

In the same paper, Silver and Bray also explored sodium borate glasses²⁶; Figure 2.1b shows a boron spectrum, composed of the quadrupolar broadened second order response due to trigonal boron, as well as a narrow symmetric response near the Larmor (operating) frequency. This new line was identified as originating from tetrahedral boron that resulted from sodium oxide modifying the borate network. This peak was narrower due to the reduced quadrupolar coupling constant, though later it was found to still be quadrupolar broadened²⁵, just to a lesser extent than the response from the trigonal borons²⁷.

Silver and Bray didn't integrate the spectrum computationally; rather they assumed the normalized shape of the peaks to be constant, used the height as a proxy for area, and utilized the observation that B_2O_3 is fully three-coordinated. By this methodology, Silver and Bray found N_4 as a function of sodium oxide concentration, as shown in Figure 2.1c²⁶.

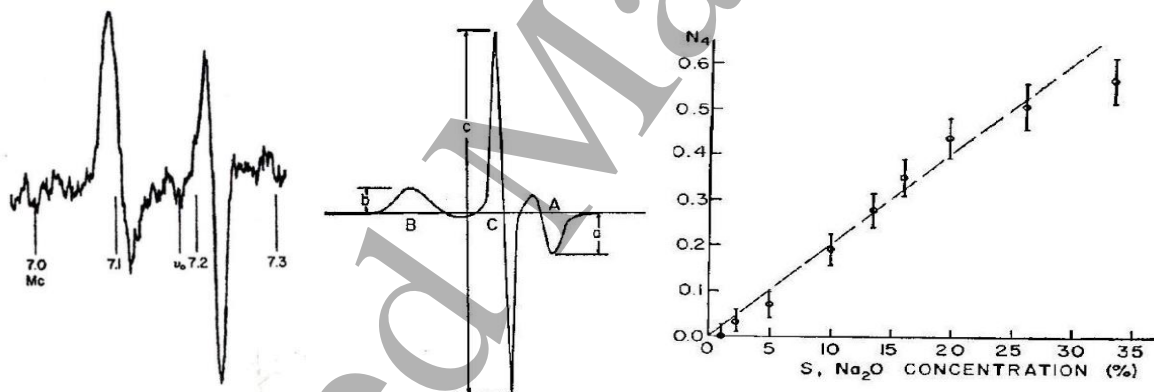


Figure 2.1. All figures above are from Silver and Bray²⁶, (a, left) ^{11}B NMR derivative spectrum from boron oxide glass, (b, middle) Typical NMR derivative response from a sodium borate glass that shows three and four coordinated boron, (c, right) The fraction of four-coordinated boron as a function of sodium oxide content in sodium borate glasses. Reproduced from Silver, A.; Bray, P. Nuclear Magnetic Resonance Absorption in Glass. I. Nuclear Quadrupole Effects in Boron Oxide, Soda-Boric Oxide, and Borosilicate Glasses. *J. Chem. Phys.* **1958**, 29 (5), 984–990, <https://doi.org/10.1063/1.1744697>, with the permission of AIP Publishing.

By 1963, Bray and O'Keefe²⁸ determined the fraction of four-coordinated boron in alkali borate glasses, see Figure 2.2. In this paper, the fraction of four-coordinate boron was found by a comparison of the NMR intensity to a standard. This standard was chosen to be crystalline sodium borohydride because N_4 in this crystal is equal to one²⁹. This resulted in a relative error in N_4 of about ± 0.04 ; this is similar to the relative error in Silver and Bray's 1958 paper²⁶. However, there is additional systematic error in the 1958 paper due to the broadening of the wide line part

of the spectrum, resulting in an overestimation of N_4 . This explains why N_4 is too high by a considerable amount. In fact, the authors themselves discussed this bias at some length^{26,28}.

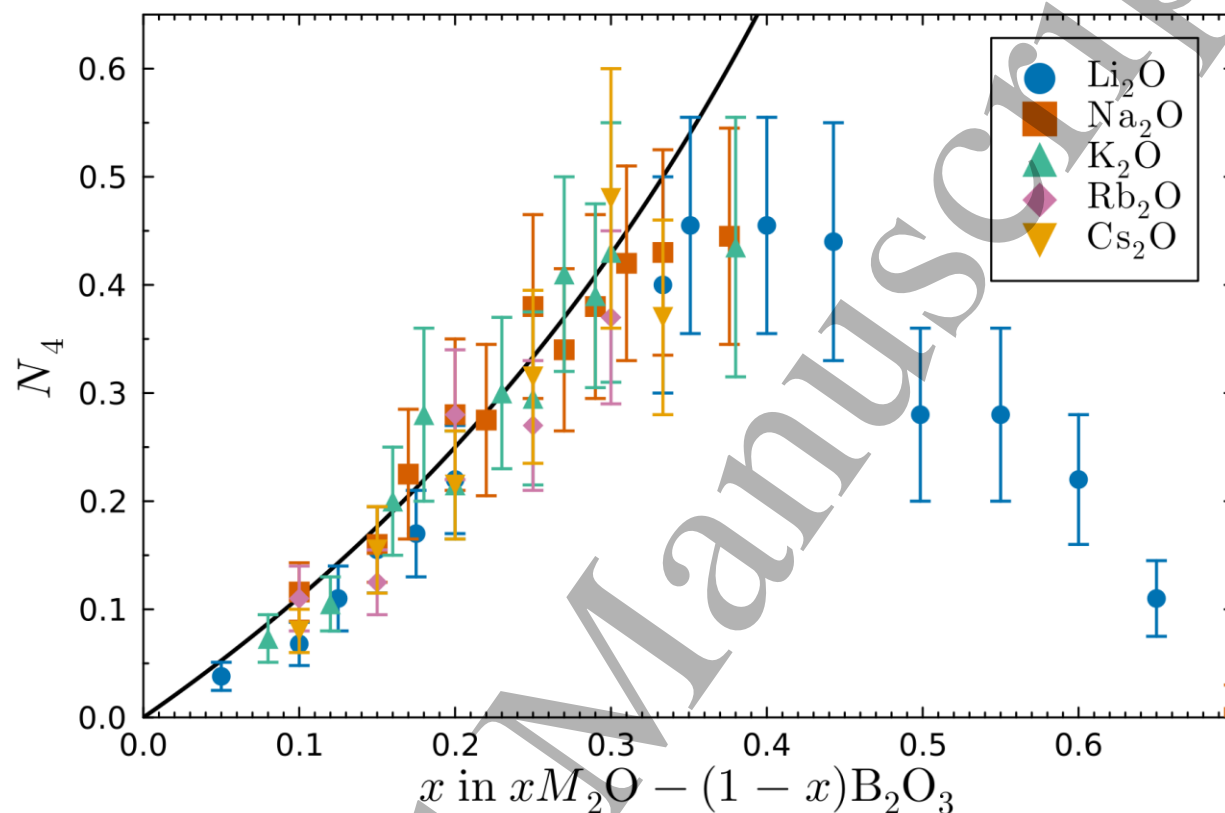


Figure 2.2. The fraction of four-coordinated boron in alkali borate glasses as found by Bray and O'Keefe²⁸. The black curved line is the relation $N_4 = x/(1-x)$ where x is the molar fraction of alkali oxide. From *Phys. Chem. Glasses* used with permission.

By 1970, computerized techniques began to be used; before this time, chart recorders were employed for the output. With digital computers, spectra could be signal averaged and programs could be written to automatically determine numerical integrals or areas under curves (see Figure 2.3a for part of the experimental spectrometer setup for doing solid state wide-line NMR during this time period). The fitting program of P.C. Taylor and P.J. Bray allowed NMR line shapes to be simulated^{30,31}; however, a significant practical drawback was that it used a mainframe computer that required batch jobs. Another approach allowed for the derivative spectrum, a result of modulation, output from the signal averager to be numerically integrated, allowing area to be measured directly (see Figure 2.3b). The first to employ this methodology for binary borate glasses was the group of Werner Müller-Warmuth, and Bray employed this in 1976^{32,33}.

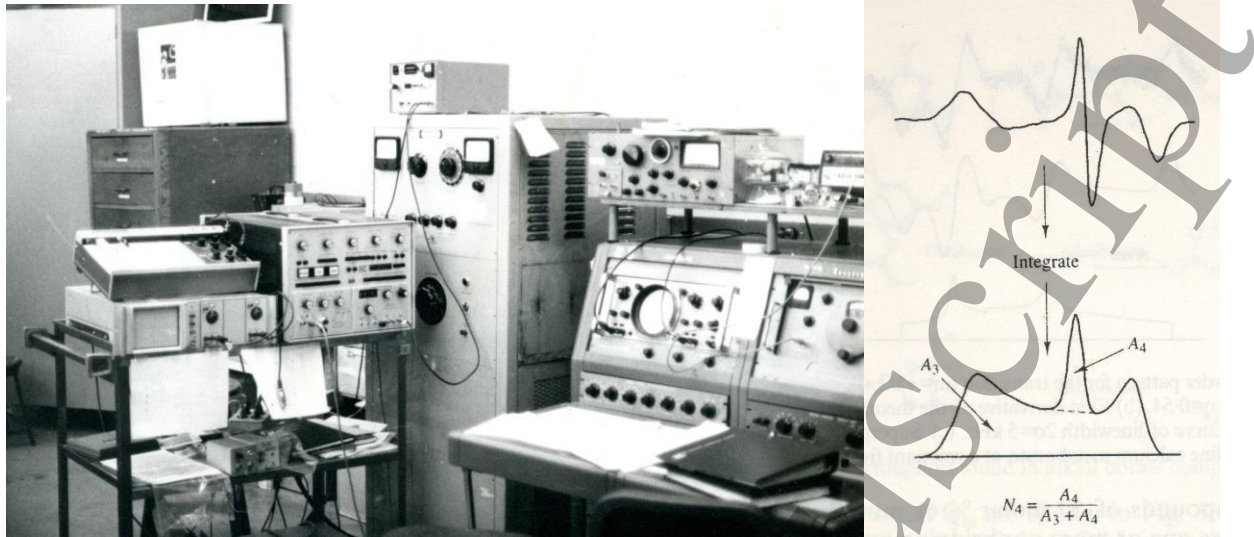


Figure 2.3. (a) Wideline NMR spectrometer for measuring N_4 circa 1975 from Prof. Phil Bray's lab at Brown University. The chart recorder sits on an oscilloscope and is the furthest instrument to the left. The computerized signal averager is to the right of the chart recorder. The magnet power supply is to the right of the signal averager. In this *Continuous Wave* (CW) setup the magnetic field was swept by varying the magnet's electric current for a fixed Larmor NMR radio frequency, (b) Signal averaged wide line NMR derivative spectrum circa 1975-1980. Shown below the experimental spectrum is the numerical integration from which areas were determined digitally.

Such techniques were employed by Jellison, Feller, and Bray³⁴ to find more precise values for N_4 in lithium borate glasses, as shown in Figure 2.4a. The error in N_4 was reduced to about ± 0.01 , considerably better than earlier results. As shown earlier in 1963²⁸, for lithium borate glasses, N_4 initially closely follows the $N_4 = x/(1-x) = R$ curve shown in Figure 2.4a. Also, the region greater than $R = 0.5$ shows a linear decline. Therefore, it is often useful to plot N_4 as a function of R , see Figure 2.4b.

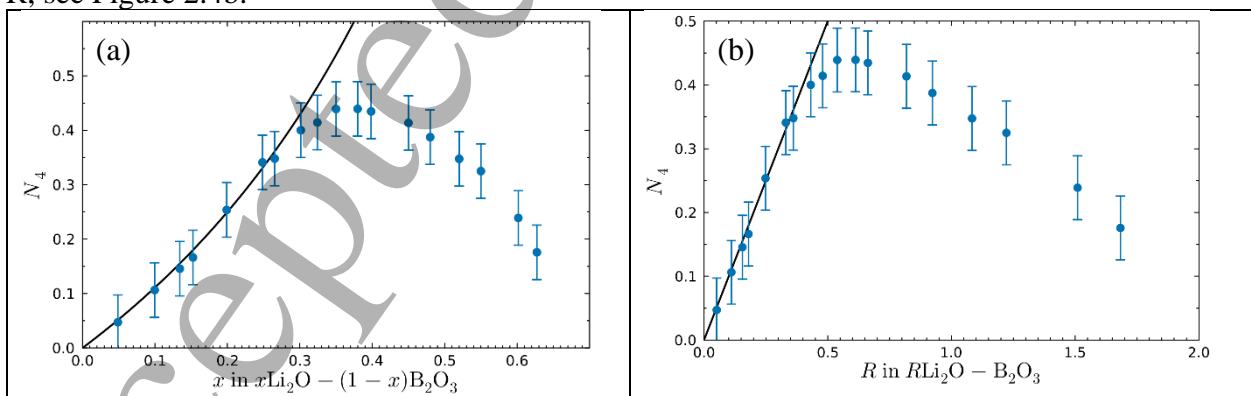


Figure 2.4. (a) Jellison, Feller, and Bray³⁴ reported N_4 versus mole fraction Li_2O , x , from lithium borate glasses. (b) N_4 as a function of R , the molar ratio of lithium oxide to boron oxide. Note the resulting linear regions that simplify modeling. From *Phys. Chem. Glasses* used with permission.

In 1989, another study of N_4 for alkali borates was conducted by Zhong and Bray³⁵ who found an alkali dependence on N_4 after $R = 0.2$ as shown in Figure 2.5a. An alternative method of

acquiring the experimental data, known as adiabatic fast passage, was employed in this work. At $R = 0.167$, the N_4 from each of the alkali borate glasses was essentially the same at $N_4 = 0.16$ ^{30,31}. Above $R = 0.4$, the N_4 values were found to be alkali dependent with N_4 decreasing as atomic number of the modifier increases.

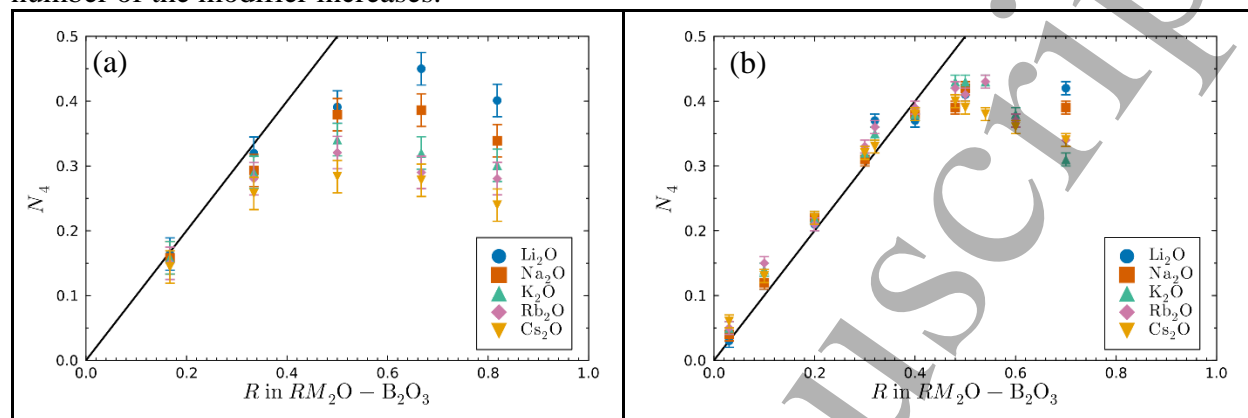


Figure 2.5. (a) Zhong and Bray's N_4 for alkali borate glasses.³⁵ We note that the figure is discrepant compared to the text in the paper in that $R = 0.2$ is shown in the figure whereas the text mentions $R = 0.167$. (b) N_4 for alkali borate glasses after Kroeker *et al.*³⁶ The plot represents results from ^{11}B MAS NMR taken at 14.1 T. From *J. Non-Cryst. Solids* used with STM guideline permission.

In 1990, magic angle spinning (MAS) was first applied to binary borate glasses^{37,38}, and most N_4 measurements since have been done using MAS NMR. Magic angle spinning eliminates effects due to dipolar and 1st order quadrupolar broadening, narrowing the spectra, allowing for more precise N_4 determination. However, the correction required to account for the satellite transitions²⁵ in MAS NMR measurements was first applied in 2000³⁹, and is unfortunately not ubiquitous in modern MAS NMR N_4 determinations. Due to the narrowing of the spectra, N_4 determination from MAS NMR benefits from increasing the magnetic field, and that has also taken off since 1990 (Figure 2.6).

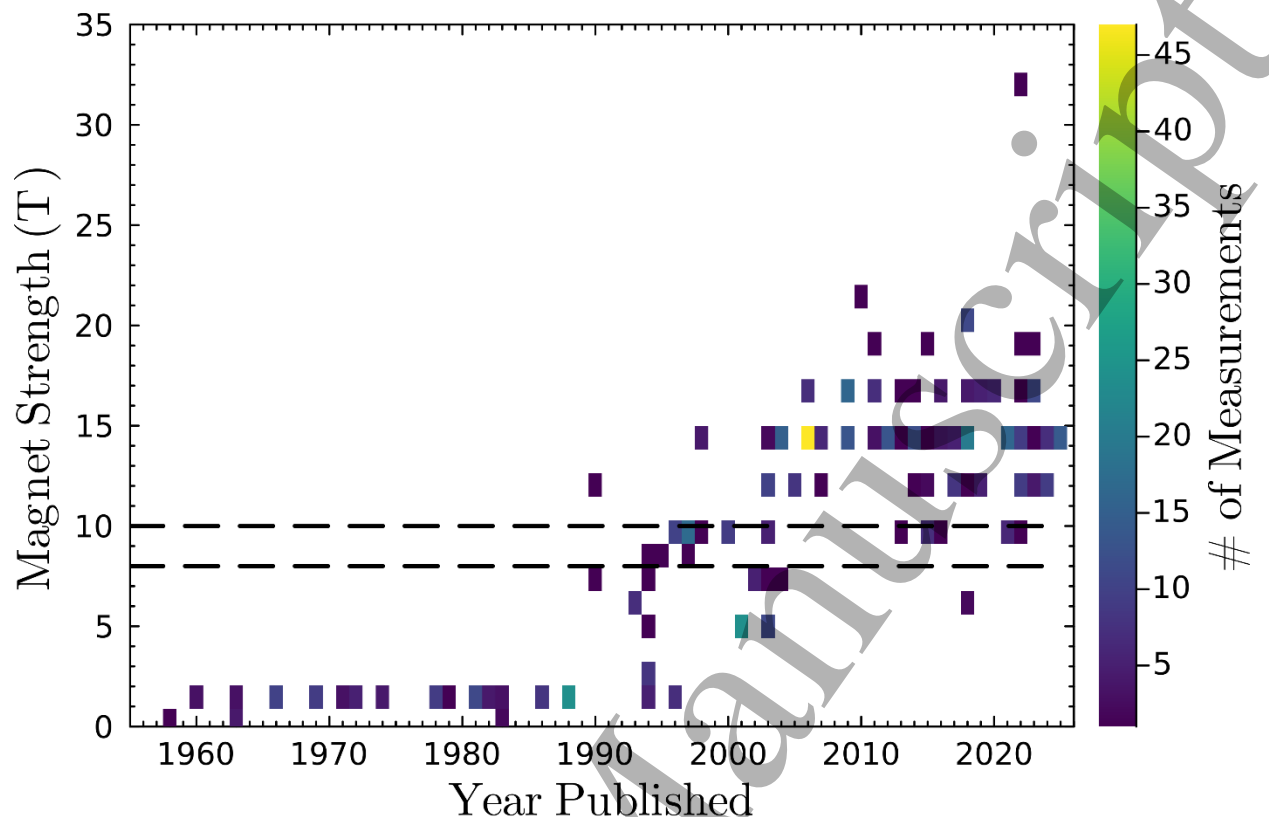


Figure 2.6. The historical distribution of the magnet strength of N_4 measurements where the magnet strength is unambiguously specified, and the measurements are otherwise high quality^{6,28,31,36-38,40-44,46,47,49-56,58,59,62,64-69,71-80,82-91,93-103,105-142,144-154,156-171,172,173,174,175,176-183}. Dashed horizontal lines indicate 8 and 10 T, the range of magnetic field strength for which N_4 determinations cannot be considered high quality.

One issue that arose in this transition to higher fields is that at 8-10 T, the four-coordinated peak overlaps with one of the quadrupolar peaks from the three-coordinated borons, which makes the deconvolution require computer simulation, and even then, there are enough degrees of freedom in the fitting that the N_4 determination can be unreliable. The first binary borate glass measurement, with the four-coordinated environment separated from that of the three-coordinated was published in 1998 and used a 14.1 T field⁴⁰, which has become a popular field strength for such measurements, though 11.7 T is also sufficient to separate the field. The increased magnetic fields (in the most extreme case exceeding 30 T⁴¹) have allowed ^{11}B NMR to yield rapid and precise measurements of the fraction of four-coordinated boron, though higher fields do limit the information that can be gained from the quadrupolar interactions.

In 2005, Kroeker *et al.*³⁶ studied alkali borates using MAS NMR performed at 14.1 T. At that magnetic field, the chemical shift difference between the three- and four-coordinated boron is enough to nearly separate the respective spectral features, making determination of N_4 easier.

The resulting N_4 fractions are shown in Figure 2.5b. Like the Zhong and Bray results³⁵, N_4 is initially independent of alkali. Above $R \approx 0.5$, N_4 is alkali dependent, in the same direction as,

but to a lesser extent than reported by Zhong and Bray³⁵. Also, whereas the data of Zhong and Bray initially fell below $N_4 = R$, Kroeker *et al.* initially very slightly exceeded $N_4 = R$ ³⁶.

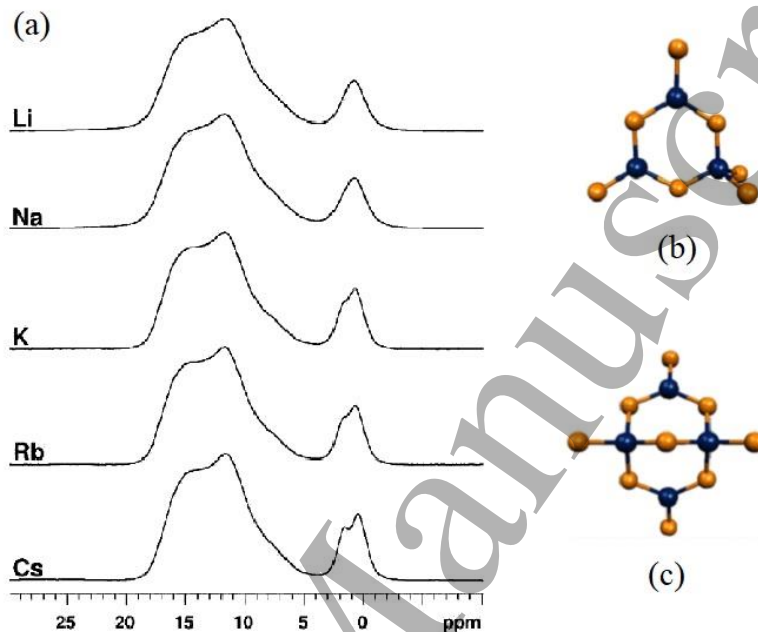


Figure 2.7. (a) ¹¹B MAS NMR from alkali borate glasses with $R = 0.1$ at a 14.1 T field³⁶ (b) trisubstituted superstructural unit, and (c) disubstituted superstructural unit. From *Phys. Chem. Glasses-Eur. J Glass Sci. Tech Proc. Fifth Int. Conf. Borate Glass Cryst. Melts* used with permission.

Additionally, due to the high magnet strength, a new feature revealed itself in the four-coordinated boron peak. Two tetrahedral environments are visible for K, Rb, Cs, and possibly Na borate glasses. Kroeker *et al.*³⁶ show that this was due to distinct chemical shifts of tetrahedral boron in different superstructural groups, see Figure 2.7a, b, and c. Kroeker *et al.* speculated that it is likely that the high frequency component is due to the disubstituted or di-trisubstituted groups and the low frequency feature is due to the trisubstituted superstructural grouping.

In 2018 ¹¹B MAS NMR was performed on the lithium borate system at 20 T (Larmor frequency of 272.8 MHz)⁴². The boron-free rotor was spun at 20 kHz. With stronger fields, the chemically shifted trigonal and tetrahedral boron features separate even more. Notice the superb signal to noise ratio and the complete separation of the three and four-coordinated boron species in Figure 2.8. A plot of N_4 vs R is provided in Figure 2.9 and shows that $N_4=R$ up to $R=0.43$.

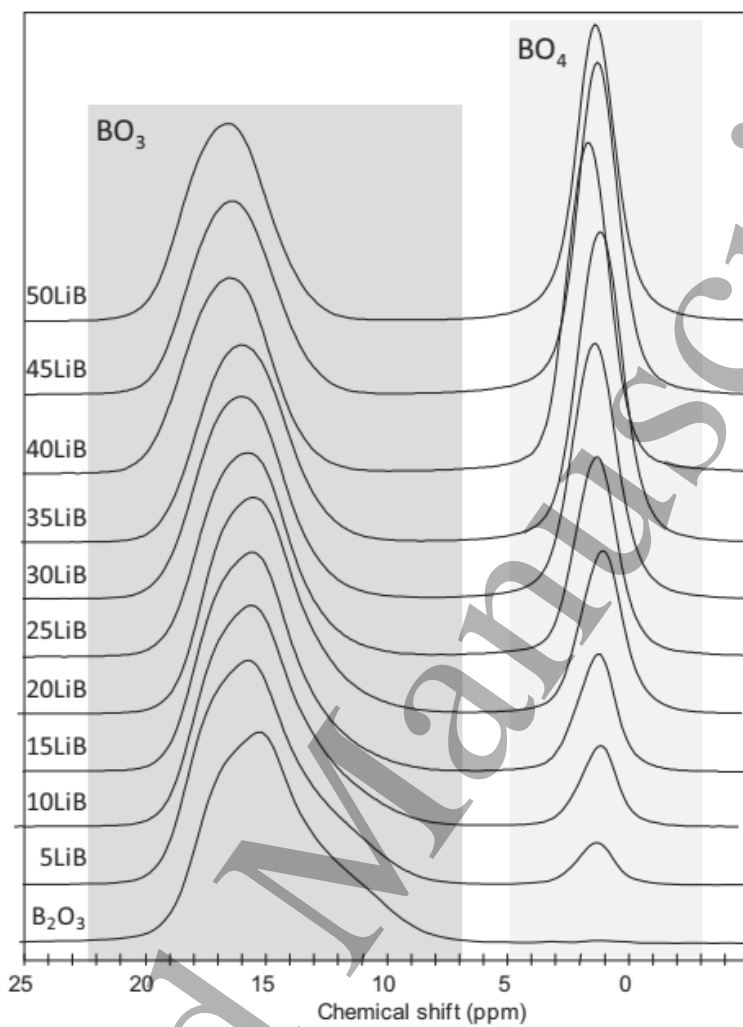


Figure 2.8. ^{11}B MAS NMR spectra of lithium borate glasses obtained at 20 T⁴². From *J. Non-Cryst. Solids* used with STM guideline permission.

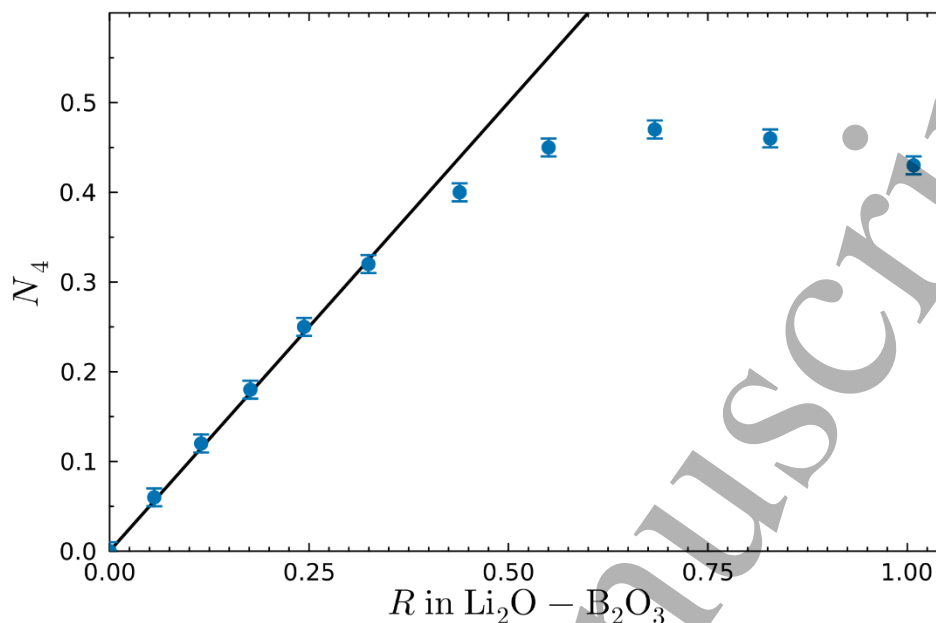


Figure 2.9. N_4 vs R for lithium borates from the study of Montouillout et al⁴².

2.3 Review of NMR Measurements of N_4

A survey of the literature was conducted for N_4 measurements of binary borate glasses^{26,28,31,33,36-38,40-59,61-152,156-158,172,173,174,176-183}. In total, 646 high-quality measurements were collected, with 25 different modifying oxides. The distribution of modifiers as found in the literature is shown in Figure 2.10a. This table is color coded to indicate the number of N_4 values reported for each element employed. Figure 2.10b is the full compilation of the N_4 values from binary borate glasses found using NMR shown in Figure 2.10a. High-quality measurements means that the method of analyzing the spectra is appropriate, no crystallization was observed, the magnet strength was not between 8-10 T (or unspecified and published 1990 or later), the glass was not pressurized, and either the glass synthesis was a solution technique, or the melting container is specified and is not silica or alumina without measuring for this material leaching into the glass. It is likely that these criteria are on the side of being too strict, as many older papers do not specify the melting container, for example. But this also does not reject measurements done with MAS NMR without accounting for spinning sideband corrections. Two studies have measurements excluded for being otherwise unexplained severe outliers^{52,153}. One study with binary alumina borates is excluded, as the melting temperature is substantially below the liquidus^{60,184}. The strontium borate glasses were checked by synthesizing the glasses and measuring them for this paper.

We recognize that other criteria that are not major issues in the data as a whole would be needed to fully satisfy the statement that the data are “high quality” This includes the fictive temperature effect, the possible composition change due to volatilization of one or more components of the glass, and possible nanoscale phase separation or unobserved crystallization in otherwise clear glasses. However, we have chosen out of necessity to proceed without further consideration of these effects. The supplemental section further discusses the quality of the data. Several of these binary borate glass systems contain immiscibility regions, where two liquids are

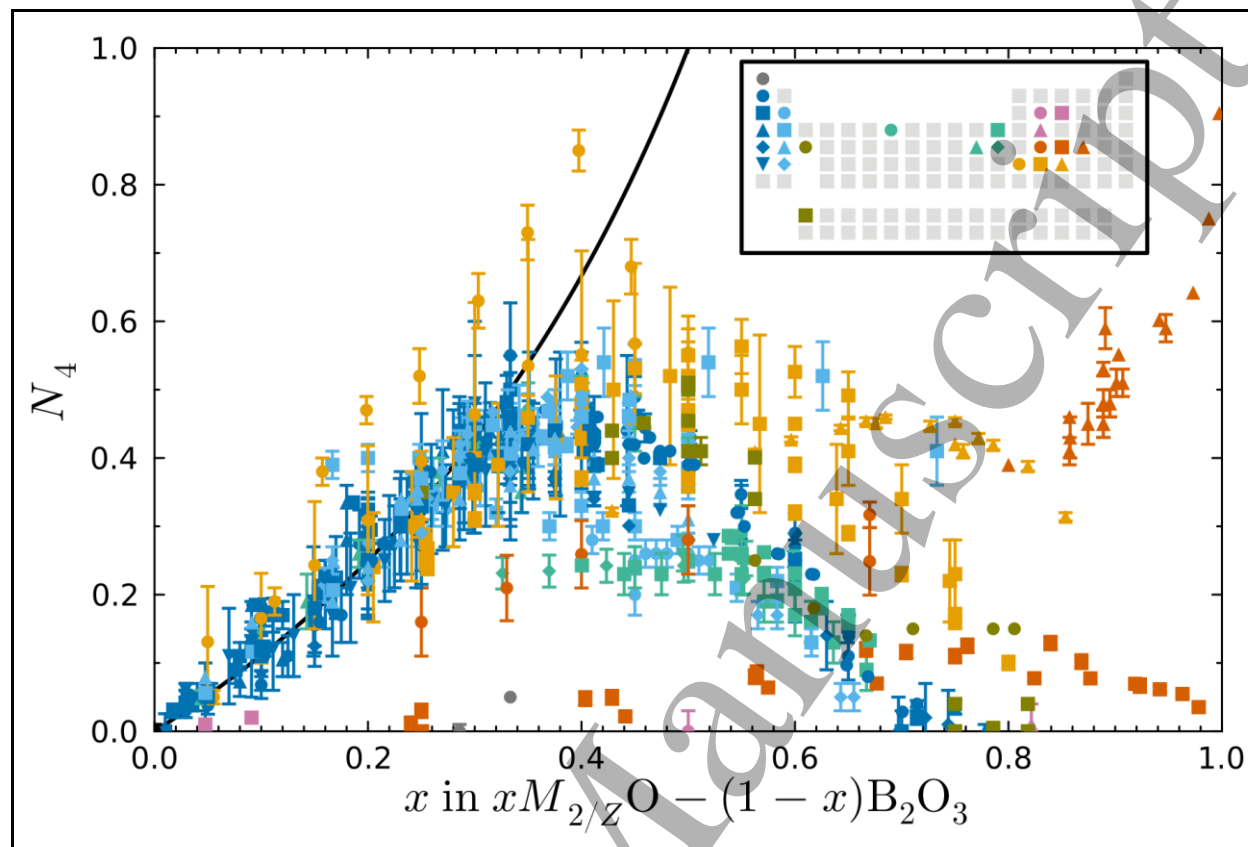


Figure 2.10. (a) Number of NMR data points for N_4 with each modifying element, as found in the literature. The data are color coordinated by the amount of reported values, according to the legend on the right. Small plots of N_4 vs. x are overlaid to give the general shape of the spectra for each modifier (b) N_4 values as determined by NMR measurements from the literature literature^{26,28,31,33,36-38,40-59,61-152,156-158,172,173,174,176-183}. Color indicates the modifier and the black curve shows $N_4 = x/(1-x)$. Values are normalized so that a single $N_4 = R$ curve may be used for all data sets.

Additionally, we can investigate the observation that N_4 is equal to R at low modification for alkali and alkaline earth borate glasses, as observed by Jellison, Feller, and Bray for lithium borate glasses³⁴. Linear regressions were performed on both alkali and alkaline earth borate systems to determine the slope, see Figure 2.11 a and 2.11 b. The intercept was fixed at zero during fitting, as this is likely the most agreed-upon point in all of borate glass NMR^{38,42,43,50,65,68,75,126}, but unmodified $x = 0$ glasses are not used in this analysis. Figures 2.11 a and b and Table 2.1 show the regression results. While the analysis of the alkali borate glasses rejects the hypothesis that $N_4 = R$ in this region, the slope being only slightly higher may instead be explained by the systematic errors caused by not correcting for spinning sideband effects, for example.

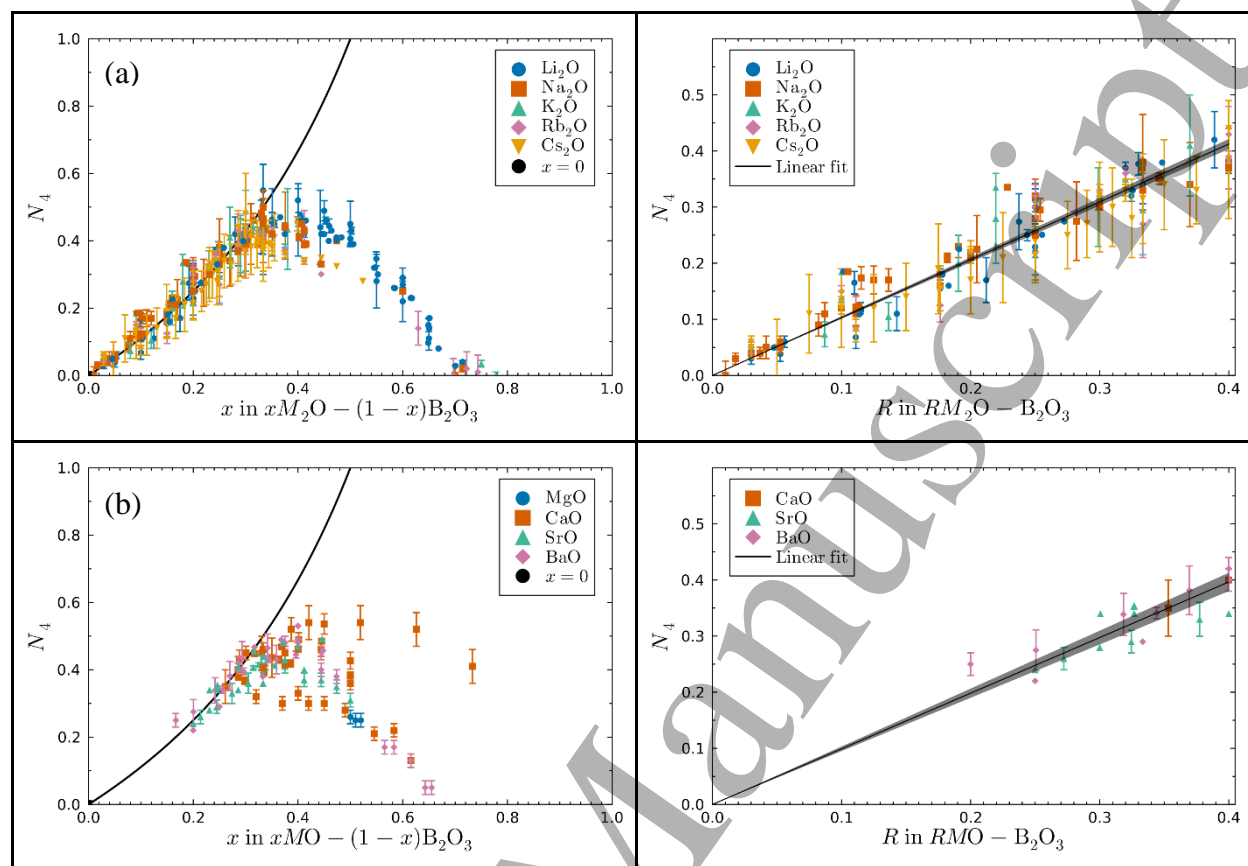


Figure 2.11. N_4 values as determined by NMR measurements of (a, upper panels) alkali borate glasses in literature^{6,28,31,36,38,40-43,45,47,50-51,58,63,65-66,68,70-72,75-79,81-82,85,89-91,94,97,99,102,104,107-109,112,114-116,118,121-122,126-128,130,133,138-140,142-149,152,156,173,174,176-180,182-183} and (b, bottom panels) alkaline earth borates^{38,42-43,46,48,50,52,55,63,65,67-68,75,87,92,96,99,101,105-106,111,117,120,125-126,132,136-137,140-141,172}.

Color indicates the modifier.

Table 2.1. Linear regression results for the $0 < R \leq 0.4$ alkali and alkaline earth borate systems with intercept 0. The p-value is for a comparison against the null hypothesis of $N_4 = R$.

System	n	Slope	Standard Error	p-value	Reject/Fail to Reject H_0 of $N_4 = R$ with 95% confidence
Alkali	147	1.031	0.011	0.0070	Reject
Alkaline Earth	21	0.991	0.020	0.6609	Fail to Reject

2.4 An example of a discrepancy between strontium borate results

As can be seen from Figure 2.11b there is a discrepancy between literature values for N_4 from the strontium borate system. In particular, the values reported by Park and Bray⁵² are significantly higher than other reported values in the literature⁶⁷. In order to resolve this, a series of strontium borate glasses were prepared by plate quenching from the melt and ^{11}B MAS NMR was performed on the samples.

The strontium borate glasses ($R = 0.5, 0.6, 0.7, 0.8, 0.9,$ and 1.0) were prepared by melting appropriate amounts of reagent grade or better SrCO_3 and H_3BO_3 at 1200°C in platinum crucibles. The samples were heated for 25 minutes, a weight loss was performed after 15 minutes, and the melts were plate quenched. Weight loss measurements on 6 gram batches were accurate to between 0.04 g to 0.10 g confirming the reactions proceeded to completion. The samples were crushed to a powder for subsequent ^{11}B MAS NMR experiments. No further treatment was done to the samples.

Solid-state NMR spectroscopy experiments were performed on a 14.1 T ($\nu_0(^1\text{H}) = 600$ MHz; $\nu_0(^{11}\text{B}) = 192.51$ MHz) Bruker wide-bore magnet equipped with a Bruker Neo console and a 2.5 mm triple resonance MAS NMR probe configured in double resonance (^1H - ^{11}B) mode. The ^1H and ^{11}B channels were isolated with bandpass filters.

The ^{11}B CT-selective $\pi/2$ and π pulse lengths were $15\ \mu\text{s}$ and $30\ \mu\text{s}$, respectively, corresponding to an 8.3 kHz RF field and 16.7 kHz CT nutation frequency. Quantitative $\pi/18$ single-pulse ^{11}B NMR spectra were recorded with a pulse duration of $1.4\ \mu\text{s}$ and recycle delay of 7.5 s. ^{11}B dipolar DQ-SQ homonuclear correlations were performed with the homonuclear dipolar recoupling sequence to generate DQ coherence. The CT-selective π pulse in the block was 1 rotor cycle in duration ($40\ \mu\text{s}$ @ 25 kHz MAS). DM-FIT was used to deconvolute the spectra. Corrections for spinning sidebands were made.²⁵

An example of a spectrum and resulting fit is shown in Figure 2.12a and the N_4 results are shown below in Figure 2.12b. Comparison to Figure 2.11b indicates that the results of Park and Bray⁵² are not verified whereas those of Yang, Torimoto, Jin and Moon were closely replicated and with increased precision^{67,117,120,132}.

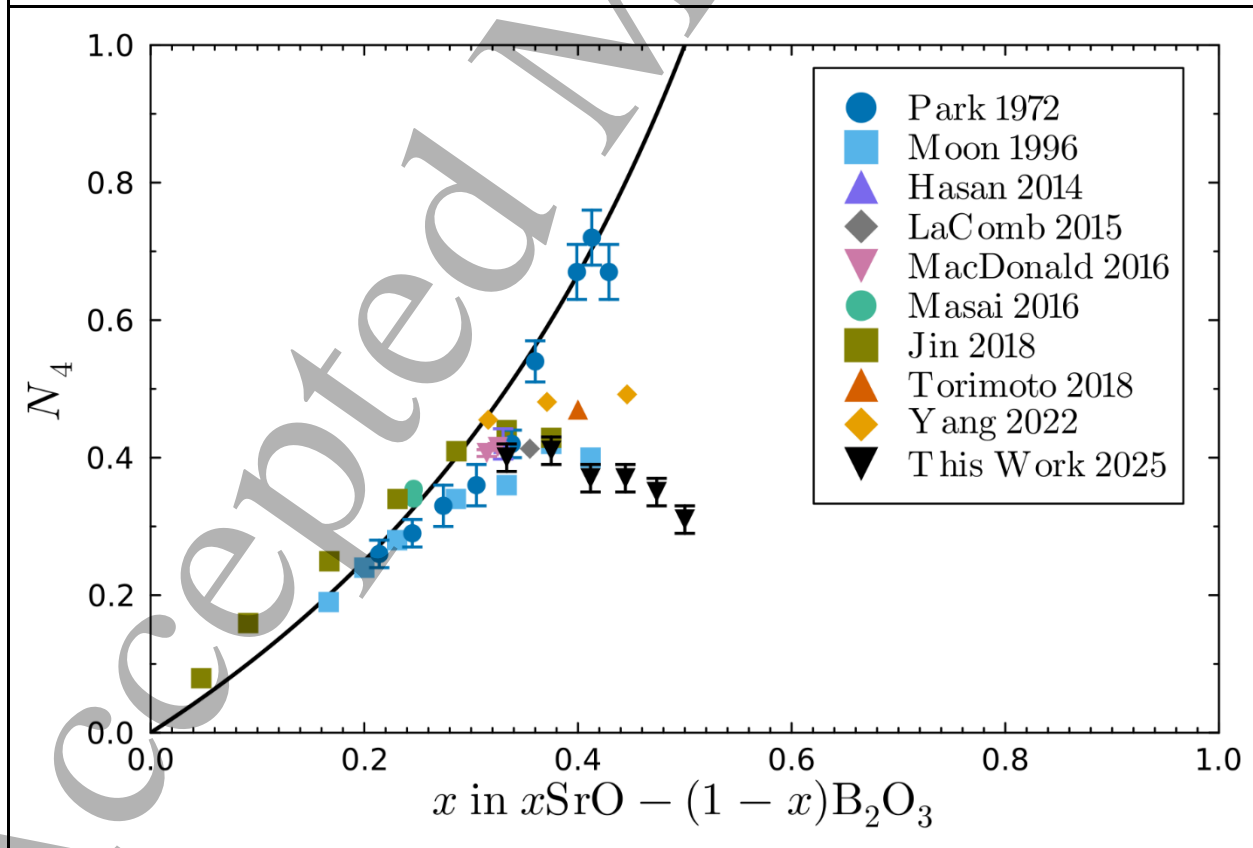
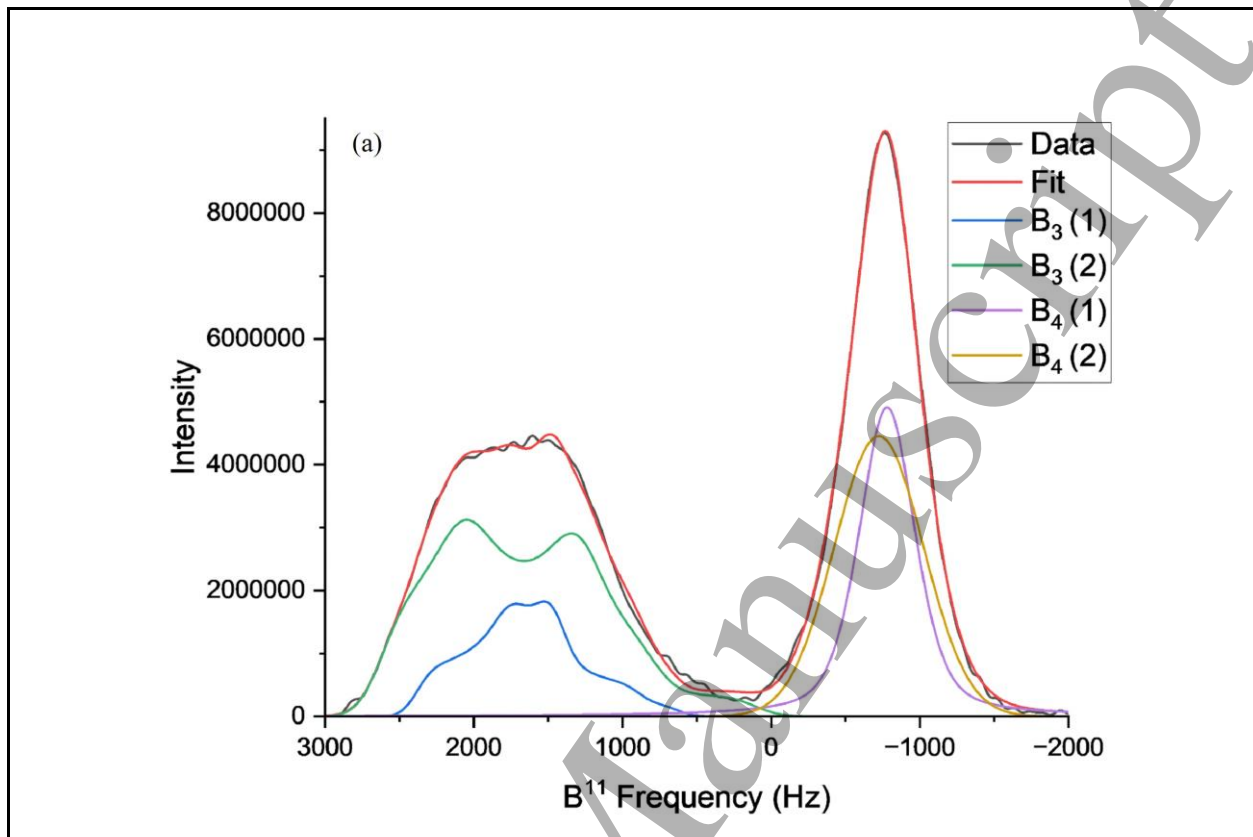


Figure 2.12. (a) NMR spectra from the $0.7\text{SrO-B}_2\text{O}_3$ ($x = 0.41$) glass sample produced for this study. It is composed of two B_3 and two B_4 peaks, as specified in the legend, and corresponds to an N_4 value of 0.37, (b) New N_4 values from strontium borates performed for this study compared to values from past studies^{52,67,96,101,105,106,117,120,132}.

2.5 Summary of NMR-Determined N_4 Measurements

We presented here numerous NMR determinations of N_4 . This was accomplished by doing a thorough literature review. An example of an application of the utility of this approach was discussed in section 2.4 where strontium borate NMR results were reviewed. Based on the literature there was a large discrepancy between reported values (Park and Bray vs Yang, Torimoto, Jin and Moon)^{52,67,117,120,132}. This discrepancy was resolved by making a series of strontium borate glasses and independently determining N_4 using ^{11}B MAS NMR. The results of Park and Bray were found to be discrepant.

N_4 may also be found by other spectroscopic techniques including infrared and Raman as well as x-ray and neutron scattering. In the next part of the paper, we examine vibrational techniques that have been used to determine N_4 . In the following section, x-ray and neutron scattering methods will be discussed.

3. Vibrational Spectroscopy Methods

3.1 Introduction

Infrared (IR) and Raman are complementary techniques of vibrational spectroscopy, and are well-known analytical tools for structural studies of glasses, since bonds constituting the glass structure can vibrate in a broad part of the spectrum covering the far-IR ($10\text{-}500\text{ cm}^{-1}$) and mid-IR ($500\text{-}5000\text{ cm}^{-1}$) frequency ranges²¹⁵⁻²¹⁷. While both techniques are important for structural studies, this section focuses on IR spectroscopy because it is more effective than Raman in quantifying the borate structure in terms of the fraction of four-coordinated boron atoms, N_4 .

Early comprehensive studies by IR spectroscopy on crystalline anhydrous borates were reported by Weir and Lippincott²¹⁸, Hart and Smallwood²¹⁹ and Weir and Schroeder²²⁰, and concern mainly borate compounds with relatively high modification levels. IR spectra were recorded on thin films produced in a diamond cell²¹⁸, on powdered materials dispersed in KBr pressed disks²¹⁹, and on films deposited on KBr and CsBr windows by evaporating suspensions in light petroleum oil, i.e., the mull sampling technique²²⁰. Measured IR bands were assigned to borate anionic species like metaborates, $[\text{BO}_2]^-$, pyroborates, $[\text{B}_2\text{O}_5]^{4-}$ and orthoborates, $[\text{BO}_3]^{3-}$. Also, absorption bands tabulated for more than 80 borate compounds allowed the identification of IR bands characteristic of boron in 3-fold and 4-fold coordination²²⁰. More recent studies include the IR spectra of crystalline metaborates with infinite chain structures, $(\text{BO}_2)_n^{n-}$, using dispersions in KBr discs²²¹, and the combination of Raman with IR reflectance spectroscopy to classify

1
2
3 metaborate crystals according to their tendency to form chain-, $(\text{BO}_2)_n^{n-}$, or ring-type, $[\text{B}_3\text{O}_6]^{3-}$,
4 metaborate structures²²².
5

6
7 Applications of IR spectroscopy to borate glasses go back to the fifties and earlier, and
8 refer to glasses such as boron oxide and soda borates²²³, alkali borates²²⁴, boron oxide and lithium
9 borates²²⁵, and vitreous $\text{B}_2\text{O}_3 \cdot x\text{H}_2\text{O}$ ²²⁶. These early IR investigations were conducted on powdered
10 glasses using the KBr disk technique²²³, on polished glass samples employing the reflectance
11 technique²²⁴, on thin film specimens drawn from the melt by dipping a platinum ring or by blowing
12 bulbs with very thin walls²²⁵, and by the Nujol mull technique²²⁶. The study of Anderson *et al.*²²³
13 showed that hydrogen bonds play an important role in the atomic arrangement of the B_2O_3 and the
14 low soda content glasses. For the B_2O_3 glass in particular, it was suggested that it consists of
15 $[\text{B}_9\text{O}_{14}]^-$ complexes held together by hydrogen bonds between oxygen atoms²²³. One of the nine
16 borons in the complex is tetrahedrally coordinated and the other borons are triangularly
17 coordinated to oxygen. When Na_2O is added to the glass, the number of $[\text{B}\text{O}_4]^-$ tetrahedra and B-
18 O-B bridges increase. Other IR studies suggested a structure for B_2O_3 glass made up of boron-
19 oxygen triangles, BO_3 , where each oxygen atom is shared by two boron atoms in adjacent
20 triangles²²⁴⁻²²⁶, noting that weak absorption measured at about $1000\text{-}1110\text{ cm}^{-1}$ was taken to
21 indicate the presence of a small proportion of $[\text{B}\text{O}_4]^-$ tetrahedral units²²⁵. Also, water was detected
22 in boron oxide glass as manifested by strong IR absorption at 3300 cm^{-1} due to the O-H stretching
23 vibration²²⁵, and was suggested to lead to hydrogen bonding between oxygen atoms^{225,226}. The IR
24 absorption spectra of alkali borate glasses showed a lower proportion of water than that retained
25 in boron oxide glass. Addition of alkali oxides to B_2O_3 was found to decrease the intensity of bands
26 attributed to BO_3 -containing units ($400, 719, 885, 1250, 1430\text{ cm}^{-1}$) in favor of new bands ($950,$
27 $1055, 1330\text{ cm}^{-1}$) associated with $[\text{B}\text{O}_4]^-$ -containing units²²⁵.
28
29
30
31

32 In his pioneering studies^{227,228}, Krogh-Moe showed that the IR spectra of alkali borate
33 glasses are consistent with the group model where the borate triangular and tetrahedral units are
34 arranged into superstructural groups similar to those found in crystalline borates like pentaborate
35 ($\text{K}_2\text{O} \cdot 5\text{B}_2\text{O}_3$), triborate ($\text{Cs}_2\text{O} \cdot 3\text{B}_2\text{O}_3$), and diborate ($\text{Li}_2\text{O} \cdot 2\text{B}_2\text{O}_3$), see Figure 1.2 of the NMR
36 section. For boron oxide glass, Krogh-Moe reviewed previous IR studies and concluded that the
37 BO_3 triangles are arranged in planar boroxol rings (see ring in Figure 1.2a) which form the glass
38 network^{227,228}. Raman spectroscopy provided strong support to the group structural model of
39 Krogh-Moe. For B_2O_3 glass, the Raman spectrum is dominated by a strong and highly polarized
40 band at 806 cm^{-1} ; this band was shown to arise from the symmetric breathing mode of the boroxol
41 ring and involves only the motion of the three oxygen atoms in the ring²²⁹⁻²³². We note in particular
42 the Windisch and Risen Raman study of $\nu\text{-B}_2\text{O}_3$ with different isotopic substitutions for both B
43 and O, which beautifully identified the breathing mode of oxygens in the boroxol ring as
44 responsible for the sharp Raman peak at 808 cm^{-1} .²³²
45
46
47

48 The presence of superstructural groups in modified borate glasses is supported also by more
49 recent Raman and IR studies, with some of these superstructural entities containing directly linked
50 $[\text{B}\text{O}_4]^-$ units²³³⁻²³⁸. A review of the earlier literature on the structural peculiarities of borate glasses
51 has been reported by Griscom²³⁹, while an extensive review on the different models and
52 superstructural groups proposed for borate glasses was given by Wright¹⁵.
53
54
55
56
57
58
59
60

1
2
3
4 The earlier IR studies provided valuable qualitative information for the evolution of the
5 borate structure as metal oxides are added to B_2O_3 , but gave no quantitative measure of the borate
6 structure such as the fraction of four-coordinated boron atoms. This difficulty is related to the fact
7 that most of the earlier IR measurements were made by transmission on pellets of powdered glasses
8 dispersed in non-absorbing matrix materials such as alkali metal halides. However, this technique
9 often leads to sample hydrolysis²³⁶ and ion-exchange²⁴⁰ during glass grinding and pellet processing
10 at high pressures. As a result, frequency shifts of absorption bands are observed as well as the
11 appearance of bands which are not representative of the pristine glass. The use of alkali halide salts
12 as matrices also causes spectral distortions and non-reproducible intensities of absorption bands
13 because they represent a combination of transmission and reflection phenomena, the extent of
14 which depends on the size and aggregation of glass particles and on the dielectric constant of the
15 salt matrix^{241,242}. An alternative method is to measure infrared transmission on thin films, if the
16 viscosity of the molten borate permits the preparation of such films²⁴³. It is noted though that the
17 quantitative assessment of the infrared spectra of glass films is more complicated compared to
18 bulk glasses. This is because thin films may exhibit the Berreman effect under oblique incidence
19 of the IR radiation, and this causes the mixing of transverse optical (TO) and longitudinal optical
20 (LO) modes²⁴⁴, or could suffer from band distortions caused by a strong interference wave which
21 develops under nearly perpendicular incidence of the IR radiation²⁴⁵.

22
23
24
25 Among the various IR sampling techniques, infrared reflectance spectroscopy on bulk
26 glasses is advantageous for quantitative studies. First, the same glass sample, i.e., a polished slab,
27 is used for data acquisition over a broad frequency range covering the entire infrared spectrum.
28 Second, the capabilities of modern Fourier-transform spectrometers, combined with the
29 availability of software for analysis of reflectivity data, allow for the quantitative determination of
30 the frequency-dependent optical and dielectric properties of the glass. This is because the true
31 shapes and relative intensities of IR bands related to vibrational modes can be obtained and, thus,
32 can permit the quantitative analysis of glass structure. These features make IR reflectance a
33 powerful tool in glass science, as manifested by the steadily increasing interest in the field²⁰⁷. It is
34 noted that in early studies by IR reflectance²¹⁵, no quantification of the borate structure was
35 discussed. This is because the measured reflectance, $R(\nu)$, depends both on the real, $n(\nu)$, and the
36 imaginary, $k(\nu)$, parts of the complex refractive index, in comparison to the absorption coefficient
37 $\alpha(\nu)$ which depends only on the extinction coefficient $k(\nu)$ ^{216,236}. Here ν is the infrared frequency
38 in wavenumbers, cm^{-1} . It is noted that glasses absorb strongly the infrared radiation, especially in
39 the mid-IR region where the stretching vibrations of the glass network are active. For example, the
40 absorption coefficient for the strong IR band at 1370 cm^{-1} for glass $0.33Li_2O-0.67B_2O_3$ (see Fig
41 3.2 below) is $\alpha=13.0 \times 10^3\text{ cm}^{-1}$, suggesting that the penetration depth of the infrared radiation into
42 the glass is limited to $d_p=1/\alpha=0.77\text{ }\mu\text{m}$. This indicates that IR reflectance spectroscopy is a surface-
43 sensitive techniques and, thus, very capable for studying surface corrosion effects.²⁴⁶ For this
44 reason, the evaluation of structure of bulk glasses by IR reflectance spectroscopy requires
45 measurements on flat and fresh glass surfaces to avoid hydrolysis phenomena. Therefore, IR
46 reflectance spectra are useful for the quantitative assessment of the bulk glass structure, provided
47 that proper analysis is made to separate the $n(\nu)$ and $k(\nu)$ contributions to $R(\nu)$. For a review on
48 infrared reflectance spectroscopy of glasses and techniques for analyzing the $R(\nu)$ spectra see
49 "Infrared Spectroscopy of Glasses" by Kamitsos²¹⁶.

1
2
3 In the following sections, we will review applications of IR reflectance spectroscopy to
4 evaluate N_4 in different families of modified borate glasses. A case of IR transmission
5 measurements on borate thin films will be presented to highlight precautions to be taken when
6 applying this technique for quantitative studies. Semi quantitative descriptions of the borate
7 structure from Raman spectroscopy will be also given.
8
9

10 11 12 3.2. Lithium borate glasses, $x\text{Li}_2\text{O}-(1-x)\text{B}_2\text{O}_3$ 13

14
15 The transmittance of bulk glasses is practically zero in the region of their fundamental
16 vibrational modes, because glasses are strong absorbers of IR radiation. This facilitates the
17 measurement of good quality reflectance spectra on bulk glasses and allows for their quantitative
18 treatment. Lithium borate glasses, $x\text{Li}_2\text{O}-(1-x)\text{B}_2\text{O}_3$ with $0 \leq x \leq 0.73$, were studied by specular
19 reflectance in the continuous spectral region $30-4,000 \text{ cm}^{-1}$. Figure 3.1a shows reflectance spectra,
20 $R(\nu)^{236}$ for some lithium borate glass compositions. The reflectance spectra were analyzed by the
21 Kramers-Krönig (KK) transformation to calculate the corresponding $n(\nu)$ and $k(\nu)$ spectra^{216,236},
22 as well as the absorption coefficient spectra using the expression $\alpha(\nu)=4\pi\nu k(\nu)$ where ν is the
23 frequency in wavenumbers (cm^{-1}). The calculated $\alpha(\nu)$ spectra are shown in Figure 3.1b and
24 demonstrate a progressive evolution with Li_2O addition. To understand the origin of the induced
25 spectral changes, we will briefly review the assignments for the main absorption profiles and
26 employ the experimental IR data to obtain N_4 .
27
28
29
30
31
32
33
34
35
36
37
38
39
40
41
42
43
44
45
46
47
48
49
50
51
52
53
54
55
56
57
58
59
60

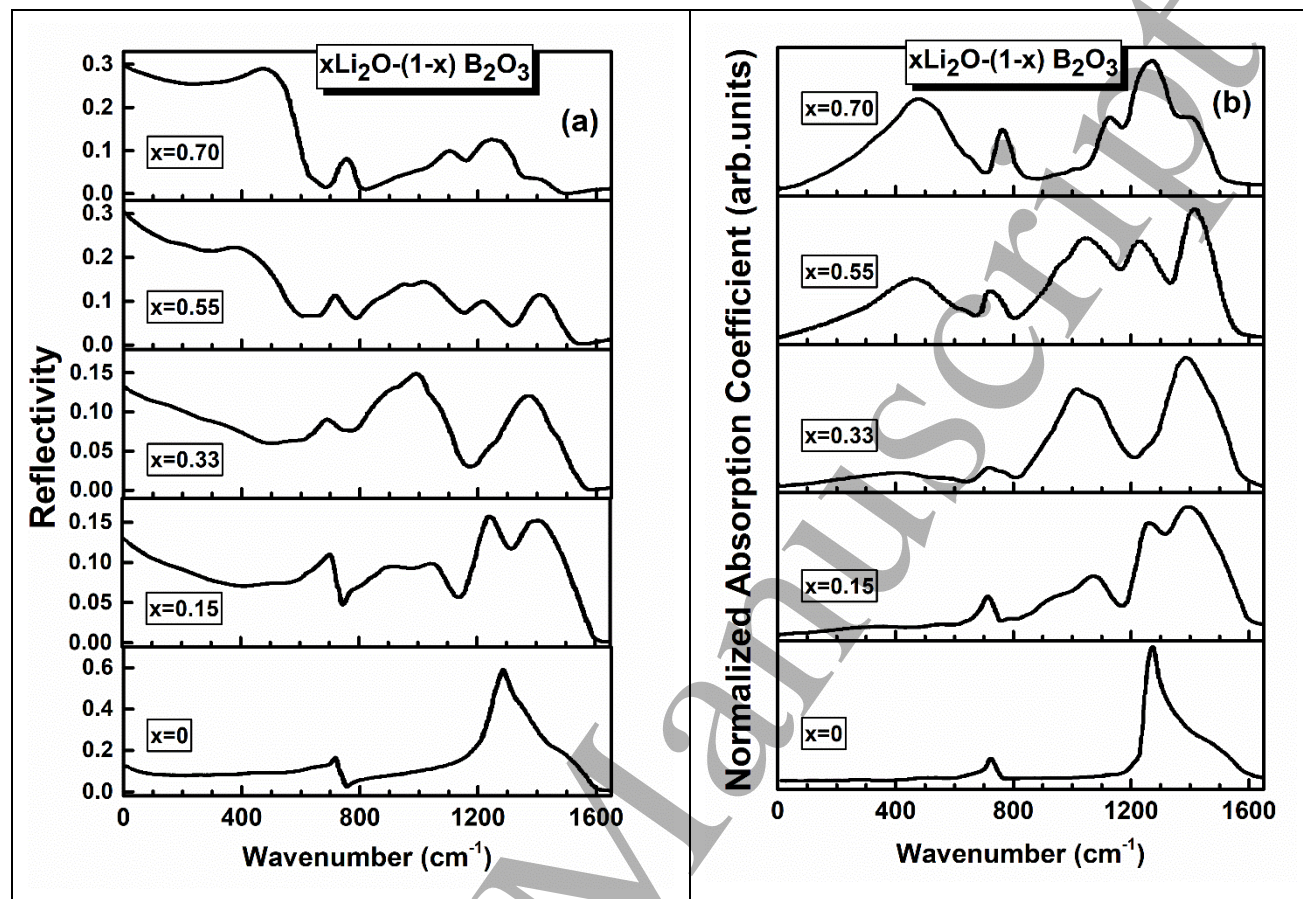


Figure 3.1. (a) Infrared reflectance spectra (left), and (b) calculated absorption coefficient spectra (right) of lithium-borate glasses $x\text{Li}_2\text{O}-(1-x)\text{B}_2\text{O}_3$ with $0 \leq x \leq 0.70$ (reproduced from Ref. 236).

As discussed in the original study²³⁶, absorption in the range 800-1200 cm^{-1} can be attributed to the B-O stretching vibrations in structural groups containing $[\text{B}\text{O}_4]^-$ tetrahedra, with anhydrous B_2O_3 glass naturally showing no absorption in this spectral range ($x=0$, Figure 3.1b). The high frequency absorption profile (ca. 1200-1650 cm^{-1}) originates from the stretching vibration of B-O and B-O⁻ bonds in borate triangular units, which are of the BO_3 and $[\text{B}\text{O}_2\text{O}]^-$ type for glasses below the metaborate stoichiometry, $x < 0.5$. At higher Li_2O contents, $x > 0.5$, asymmetric stretching vibrations of the pyro-borate $[\text{B}_2\text{O}_5]^{4-}$ and ortho-borate $[\text{BO}_3]^{3-}$ units also contribute to the high frequency envelope. Thus, the evolution of the ca. 800-1200 cm^{-1} envelope with x in the range $0 < x \leq 0.40$ shows the progressive change of boron coordination number from three to four. For higher Li_2O contents ($x \geq 0.45$), the decrease of the relative intensity of the $[\text{B}\text{O}_4]^-$ absorption envelop denotes the destruction of $[\text{B}\text{O}_4]^-$ units in favor of borate triangles with increasing number of non-bridging oxygen atoms, and this leads to the change of boron coordination number from four to three. Deformation modes of the borate units give rise to weaker absorption bands in the ca. 550-800 cm^{-1} range, while absorption in the far-IR range (below 550 cm^{-1}) is due to Li ion-site vibrations and exhibits increasing intensity and frequency with Li_2O content (Figure 3.1b).

To quantify the effect of Li_2O on the borate structure, the $\alpha(\nu)$ spectra were deconvoluted and the component bands were assigned to borate species (BO_3 , $[\text{B}\text{O}_4]^-$, $[\text{B}\text{O}_2\text{O}]^-$, $[\text{B}_2\text{O}_5]^{4-}$ and $[\text{BO}_3]^{3-}$) and to Li ion-site vibrations²³⁶. This allowed the mapping of the network structure in the entire glass-forming range in terms of the relative integrated intensities of borate species; however, no attempt was made to calculate N_4 from the IR data. In a subsequent study on alkali diborate glasses, $\text{M}_2\text{O}-2\text{B}_2\text{O}_3$ with $\text{M}=\text{Li}, \text{Na}, \text{K}, \text{Rb}, \text{Cs}$, the total integrated intensity A_4 of $[\text{B}\text{O}_4]^-$ units was found to vary linearly with the fraction N_4 determined from NMR measurements²⁴⁷. In the following, we revisit the IR data of lithium-borate glasses to calculate N_4 .

The integrated IR intensities of borate tetrahedral (A_4) and triangular (A_3) units can be obtained by spectral deconvolution or integration. Examples are shown in Figure 3.2 and Figure 3.3 for the $x=0.33$ glass, noting that the spectral deconvolution involved 13 Gaussian component bands as it was done earlier for the $x=0.55$ composition.²³⁶

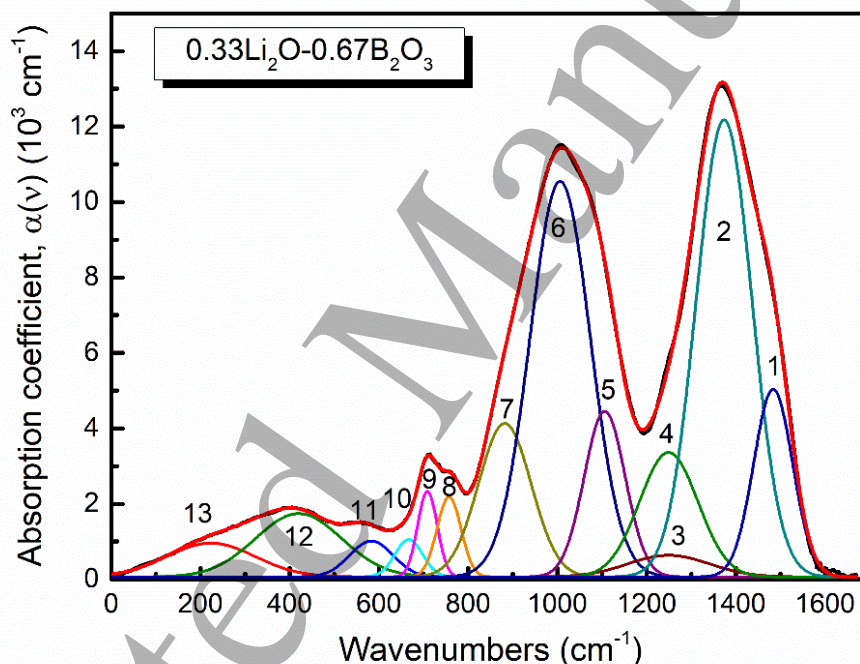


Figure 3.2. Deconvolution into Gaussian component bands of the absorption coefficient spectrum of glass $0.33\text{Li}_2\text{O}-0.67\text{B}_2\text{O}_3$. Black solid line represents the experimental spectrum, the red line is the simulated spectrum and the Gaussian component bands are labeled 1-13.

From spectral deconvolution, A_4 is obtained as the sum of the integrated intensities of bands 5-7 and A_3 is the sum of the integrated intensities of bands 1-4 (Figure 3.2). From spectral integration, A_4 is calculated as the total integrated intensity of the absorption envelope at ca. $800-1200\text{ cm}^{-1}$ and A_3 corresponds to the total integrated intensity of the ca. $1200-1650\text{ cm}^{-1}$ absorption envelope (Figure 3.3).

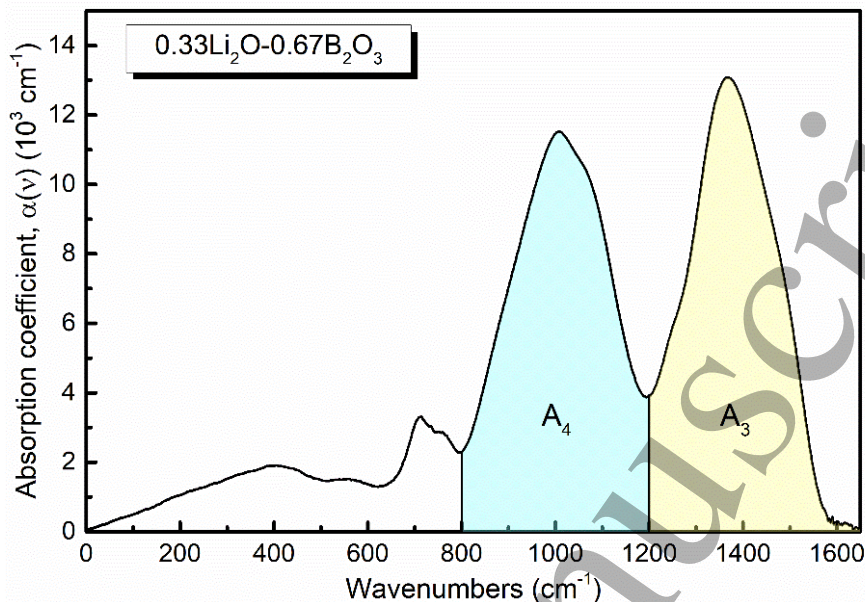


Figure 3.3. Example of spectral integration for the infrared absorption bands of borate tetrahedral units (800-1200 cm^{-1} , A_4) and triangular units (1200-1600 cm^{-1} , A_3) for glass $0.33\text{Li}_2\text{O}-(1-x)\text{B}_2\text{O}_3$.

Denoting by $[\text{B}_4]$ and $[\text{B}_3]$ the concentrations of borate tetrahedral and trigonal units, then $N_4 = [\text{B}_4]/([\text{B}_4] + [\text{B}_3])$ with $[\text{B}_4] = A_4/\alpha_4$ and $[\text{B}_3] = A_3/\alpha_3$, where α_4 and α_3 are the absorption coefficients of boron tetrahedral and triangular units. Combination of these relations gives the following simple expression for the fraction of boron atoms in four-fold coordination:

$$N_4 = \frac{A_r}{\alpha_r + A_r} \quad (3.1)$$

where $A_r = A_4/A_3$ and $\alpha_r = \alpha_4/\alpha_3$ is the relative absorption coefficient of boron tetrahedra versus triangles²⁴⁸. The composition dependence of A_r as obtained by fitting and integration is presented in Figure 3.4 and demonstrates the change of boron coordination number from three to four up to about $x=0.40$ and then back to three at higher Li_2O contents.

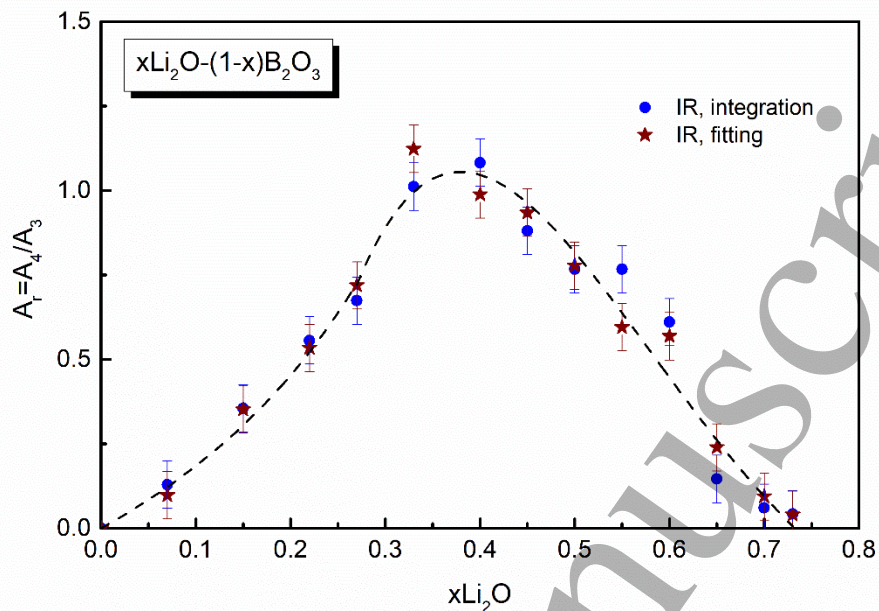


Figure 3.4. Relative integrated absorption $A_r = A_4/A_3$ as a function of Li_2O content obtained by fitting or integration of the absorption profiles corresponding to borate tetrahedral (A_4) and triangular (A_3) units for lithium-borate glasses. The line through the data points is drawn to guide the eye.

The use of the A_r data to calculate N_4 through Equation 3.1 requires the knowledge of the relative absorption coefficient, α_r . As presented in Figure 2.4(a) of the NMR section, the structural modification of glasses with Li_2O contents below ca. 27 mol% involves only the transformation of BO_3 into $[\text{B}\text{O}_4]^-$ units and, thus, the relation $N_4 = x/(1-x)$ is obeyed. Then, Equation 3.1 can be rewritten in the following form for $x < 0.27$:

$$\alpha_r = \frac{A_r (1 - N_4)}{N_4} = \frac{A_r (1 - 2x)}{x} \quad (3.2)$$

The A_r data for glasses $x = 0.07$, 0.15 and 0.22 and Equation 3.2 lead to the average value of the relative absorption coefficient $\langle \alpha_r \rangle = 1.48 \pm 0.07$. The obtained value is in good agreement with that reported for lithium-metaborate glass ($\alpha_r = 1.50$, $x = 0.5$)²⁴⁸, and the value $\langle \alpha_r \rangle = 1.6 \pm 0.1$ found for ternary glasses in the system $y\text{Li}_2\text{O} - (1-y)[x(2\text{TeO}_2) - (1-x)\text{B}_2\text{O}_3]$ with $y = 0.33$ and 0.40 and $0 \leq x \leq 1$ ²⁴⁹.

Therefore, we use the obtained value $\langle \alpha_r \rangle = 1.48 \pm 0.07$ for lithium borate glasses in the entire glass-forming range and apply Equation 3.1 to convert the A_r data into N_4 values. The N_4 results from the IR analysis are shown in Figure 3.5 in comparison with N_4 data from earlier ^{11}B ³⁴ and ^{10}B NMR^{34,250,251} and more recent ^{11}B NMR⁴² studies. It is observed that the agreement between infrared and NMR results is good in the entire glass-forming range, indicating the usefulness of IR reflectance spectroscopy to quantify the borate glass structure.

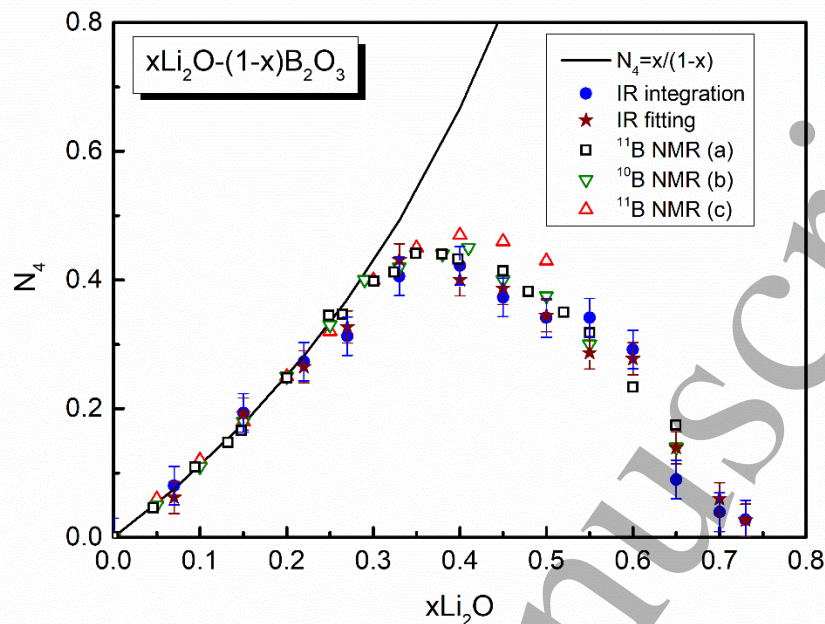


Figure 3.5. Fraction of four-coordinated boron atoms, N_4 , for glasses $x\text{Li}_2\text{O}-(1-x)\text{B}_2\text{O}_3$. N_4 was calculated from the IR data using Equation 3.1 where A_T was derived by integration or fitting of the absorption profiles for borate tetrahedral and triangular units (Figures 3.2 and 3.3). Comparison is made with N_4 from NMR, (a)Ref. 34, (b)Ref. 250 and (c)Ref. 42, and the $x/(1-x)$ values when each oxygen atom from the added Li_2O converts two triangular BO_3 units into two tetrahedral $[\text{B}\text{O}_4]^-$ units (O =bridging oxygen atom).

3.3. Silver borate glasses, $x\text{Ag}_2\text{O}-(1-x)\text{B}_2\text{O}_3$

Silver borate glasses, $x\text{Ag}_2\text{O}-(1-x)\text{B}_2\text{O}_3$, have attracted interest because they form the basis of fast-ion-conducting glasses like those in the ternary system $\text{AgI-Ag}_2\text{O-B}_2\text{O}_3$ ^{252,253}. The structure of the borate network of the binary glasses $x\text{Ag}_2\text{O}-(1-x)\text{B}_2\text{O}_3$ ($0 \leq x \leq 0.33$) was studied by IR reflectance and Raman spectroscopy²⁵⁴. The absorption coefficient spectra were calculated by KK transformation of the specular reflectance spectra and are shown in Figure 3.6. Comparison with Figure 3.1b shows that the lithium and silver borate glasses exhibit similar spectral evolutions suggesting the presence of similar short-range order borate units. Therefore, the same approach is applied here for the derivation of N_4 from the infrared data.

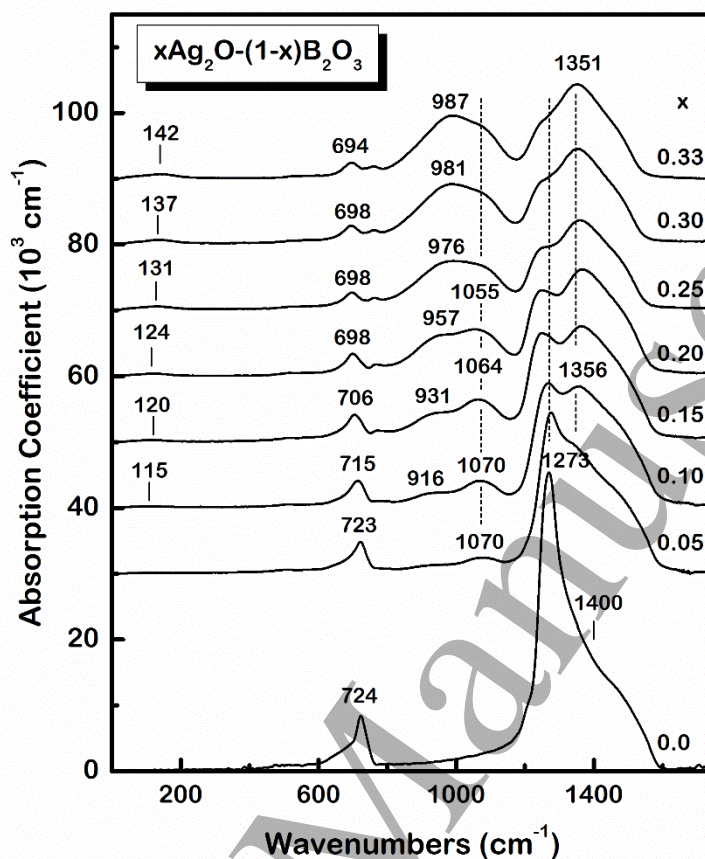


Figure 3.6. Infrared absorption coefficient spectra of glasses $x\text{Ag}_2\text{O}-(1-x)\text{B}_2\text{O}_3$ (reproduced from Ref. 245). The spectra for $x=0.05$ to $x=0.33$ have been offset to allow comparison.

The integrated intensities A_4 ($800-1200\text{ cm}^{-1}$) and A_3 ($1299-1550\text{ cm}^{-1}$) were calculated and their ratio $A_r=A_4/A_3$ is presented in Figure 3.7a, demonstrating the progressive change in boron coordination number. Application of Equation 3.2 for glasses $x=0.05$ and 0.07 gives the average value for the relative absorption coefficient $\langle\alpha_r\rangle=1.25$, which is then used to calculate N_4 from the A_r data. The results in Figure 3.7b show good agreement between the IR-based N_4 data and those derived from the NMR study of Kim and Bray⁵³ and from neutron diffraction of Wright et al²⁵⁵. Clearly, N_4 follows the theoretical curve $x/(1-x)$ up to about $x=0.25$ and deviates from this curve at higher Ag_2O contents, indicating the formation of non-bridging oxygen atoms on triangular metaborate units, $[\text{BO}_2\text{O}]^-$.

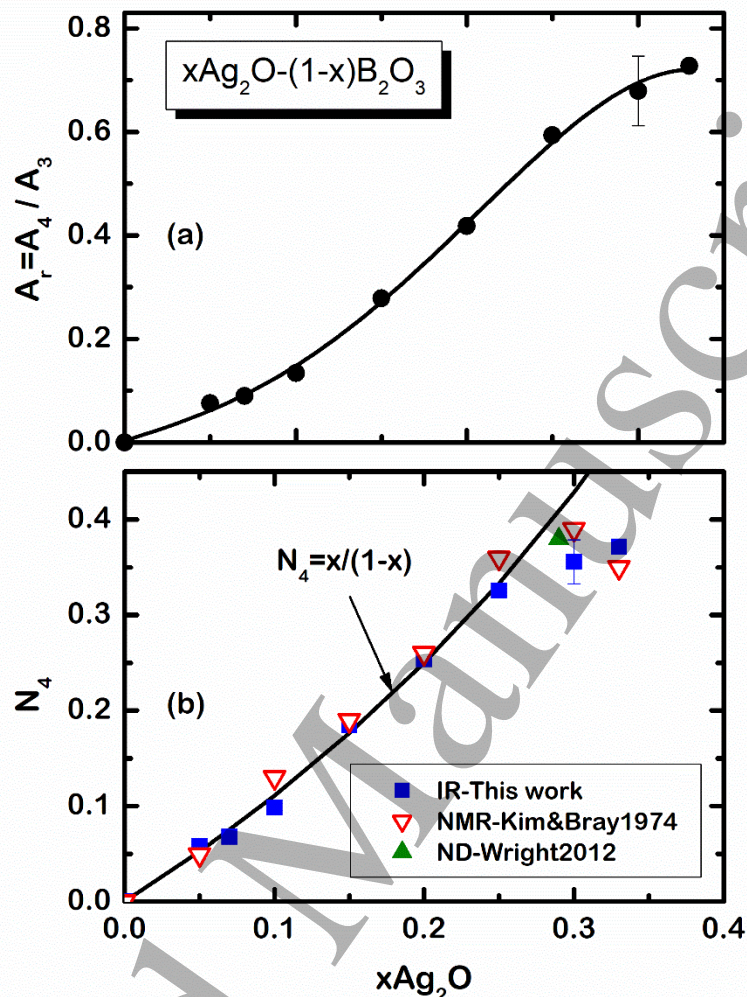


Figure 3.7. Effect of Ag_2O content on the relative integrated intensity $A_r = A_4/A_3$ (a), and the fraction N_4 calculated from Equation 3.1 using $\alpha_r = 1.25$ (b) for glasses $x\text{Ag}_2\text{O}-(1-x)\text{B}_2\text{O}_3$. The line in (a) is a guide to the eye and in (b) is the theoretical value $N_4 = x/(1-x)$. Comparison is made with experimental N_4 data from NMR spectroscopy⁵³ and neutron diffraction²⁵⁵.

3.4. Alkaline earth borate glasses, $x\text{MO}-(1-x)\text{B}_2\text{O}_3$

Compared to alkali borate glasses, less structural information is available for alkaline-earth borates ($x\text{MO}-(1-x)\text{B}_2\text{O}_3$, $\text{M}=\text{Mg}, \text{Ca}, \text{Sr}, \text{Ba}$) including, for example, the M -dependence of N_4 (see Figure 2.11(b)). In this context, results obtained by infrared spectroscopy will be reviewed in this section and compared to those obtained by other techniques.

Absorption coefficient spectra, obtained by KK analysis of the measured reflectance spectra^{256,257}, are shown in Figure 3.8 for MO contents $x=0.33$ and 0.45 . To facilitate spectral comparison, the spectra of glasses with the same MO content were scaled at the high frequency

absorption band. It is clear that the absorption profiles depend not only on the MO content but also on the type of alkaline-earth metal.

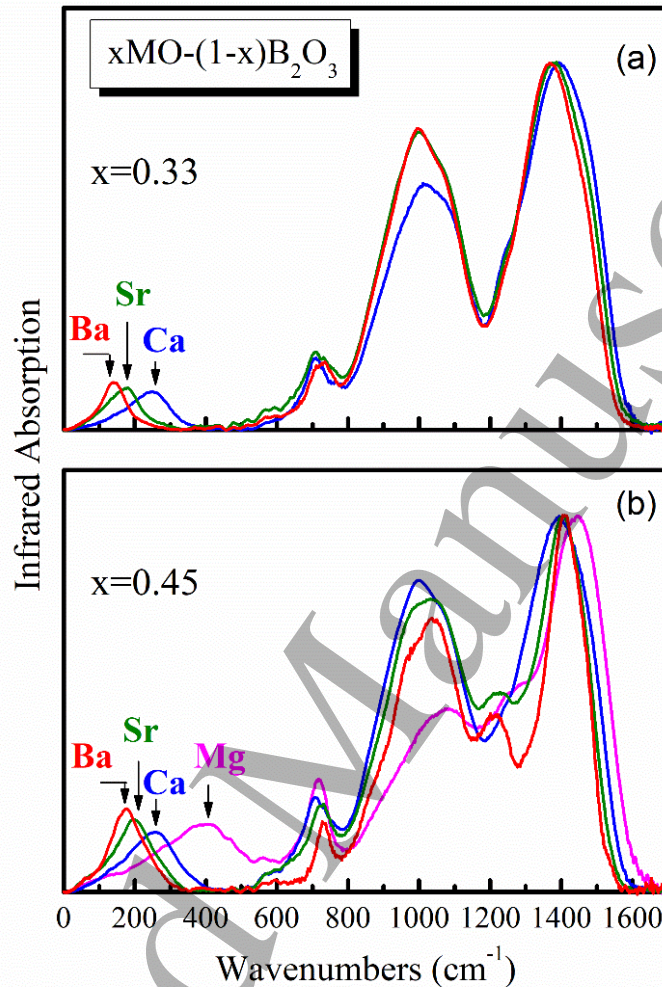


Figure 3.8. Infrared absorption spectra of alkaline earth borate glasses, $\text{MO}-(1-x)\text{B}_2\text{O}_3$, with composition $x=0.33$ (a) and $x=0.45$ (b), reproduced^{256,257}. For each composition, the spectra have been normalized on the strongest high-frequency band at $1370\text{-}1450\text{ cm}^{-1}$ to facilitate comparison.

To quantify the effects on the short-range order structure by IR spectroscopy, we have calculated the integrated intensity of the absorption envelopes $800\text{-}1150\text{ cm}^{-1}$ (A_4 , borate tetrahedral units) and $1150\text{-}1550\text{ cm}^{-1}$ (A_3 , borate triangular units), noting that the frequency ranges for absorption of the triangular and tetrahedral borate units depend slightly on the modifier cation i.e., the cation mass and the strength of interactions between the cation and the borate unit. The relative integrated intensity, $A_r=A_4/A_3$, is shown in Figure 3.9 as a function of MO content and type. The change in boron coordination from three to four as the MO content increases towards the metaborate composition ($x=0.50$) is illustrated in this figure, noting that the x value at which A_r exhibits its maximum is a function of the type of alkaline-earth oxide. Also, for glasses of the same MO content the value of A_r decreases in the order $\text{Ba}>\text{Sr}>\text{Ca}>>\text{Mg}$ for x up to ca. $x=0.45$, and changes to $\text{Ca}>\text{Sr}>\text{Ba}>>\text{Mg}$ for $x>0.45$.

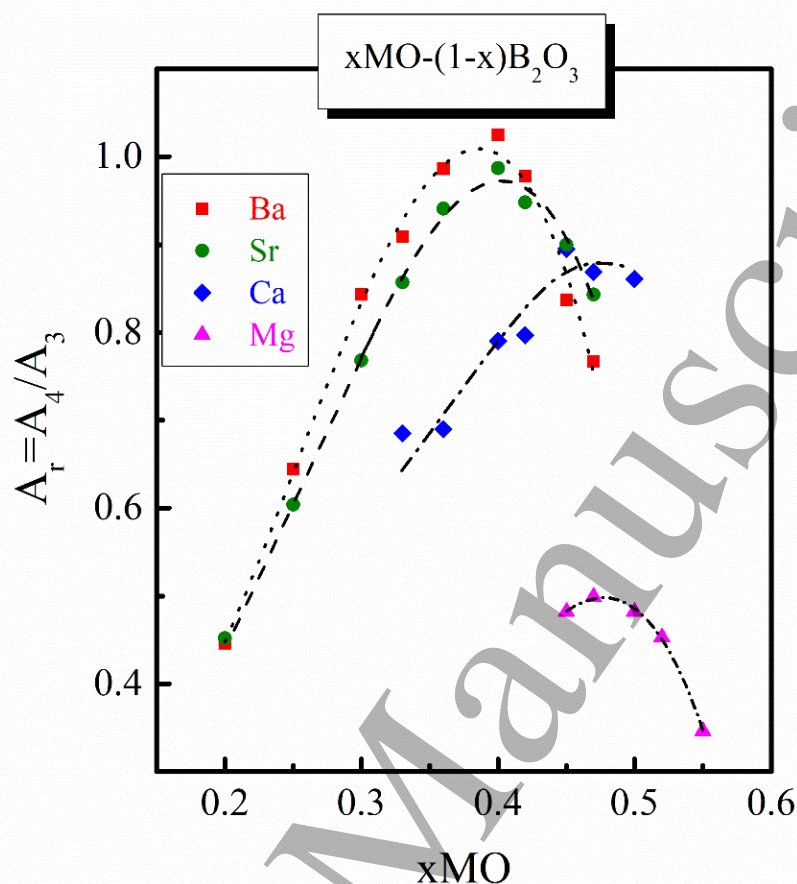


Figure 3.9. Relative integrated IR absorption $A_r = A_4/A_3$ as a function of the MO content and type in alkaline earth borate glasses $MO-(1-x)B_2O_3$ ($M = Mg, Ca, Sr, Ba$)^{256,257}.

The relative integrated intensities A_r can be used to calculate N_4 from Equation 3.1, once the relative absorption coefficients, α_r , are known for all four glass systems. We note that the glass-forming ranges of alkaline earth borates made by splat quenching are considerably narrower than those of the alkali borates, i.e., Mg: $0.45 \leq x \leq 0.55$, Ca: $0.33 \leq x \leq 0.50$, Sr: $0.20 \leq x \leq 0.47$ and Ba: $0.15 \leq x \leq 0.47$. Therefore, only the low modification Ba- and Sr-borate glasses offer the possibility to apply Equation 3.2 for the evaluation of α_r . Application of this approach to Ba-borate glasses with $x=0.20$ and $x=0.25$ gives the average value $\alpha_r(Ba) = 1.32 \pm 0.05$, while the $x=0.20$ Sr-borate glass composition gives $\alpha_r(Sr) = 1.36 \pm 0.05$. For Ca-borates the IR data (A_r) have been scaled with the NMR data of Wu and Stebbins⁹⁹ at $x=0.5$ ($N_4 = 0.383$) to obtain $\alpha_r(Ca) = 1.40 \pm 0.05$. For Mg-borate glasses Dell and Bray¹⁴¹ reported $N_4 = 0.20$ for the $0.45MgO-0.55B_2O_3$ glass and this gives $\alpha_r(Mg) = 1.90 \pm 0.075$. These findings show that α_r increases with increasing cation field strength, noting that in earlier studies the average value $\alpha_r = 1.30$ was employed for $M = Ba, Sr$ and Ca ^{256,257}.

The results for the IR-based N_4 values are shown in Figure 3.10 versus MO content and are compared with the theoretical curve $x/(1-x)$, as well as with N_4 values obtained by other techniques including neutron diffraction²⁵⁵, NMR^{63,67,99,117,132,137,141,172}, neutron diffraction and molecular dynamics²⁵⁸ and x-ray diffraction²⁵⁹.

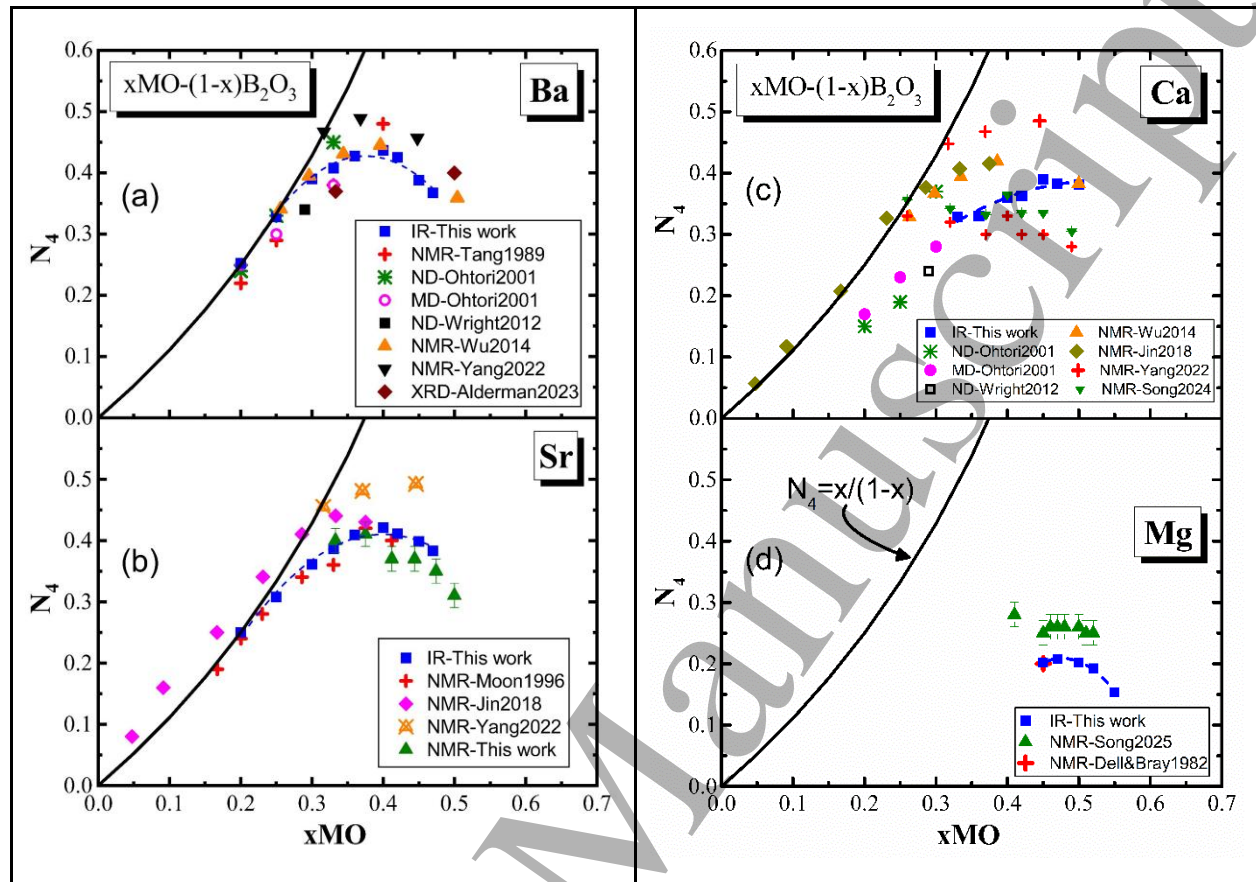


Figure 3.10. Composition dependence of N_4 in alkaline earth borate glasses $M_2O-(1-x)B_2O_3$ (M=Ba (a), Sr (b), Ca (c) and Mg (d)) obtained by IR, NMR, neutron diffraction (ND), molecular dynamics (MD), and x-ray diffraction (XRD) studies^{63,67,99,117,132,137,141,255,258,259,260}. Dashed lines through IR data points are guides to the eyes. The figures were compiled from those in Refs. 256 and 257 by using the new $\alpha_r(M)$ values and adding recent N_4 data from other techniques.

The following observations can be made from Figure 3.10: (i) In general, there is good agreement between the infrared results and those of other techniques, noting the presence of scattering in the N_4 values among various techniques. IR reflectance spectroscopy is shown again to be a useful tool for the quantification of the borate glass structure; (ii) For Ba- and Sr-glasses of low MO contents (up to ca. $x=0.25$) the N_4 value follows the theoretical $x/(1-x)$ curve, but it deviates for M=Ca and Mg; (iii) The MO content at which N_4 attains its maximum value shifts to higher x values as the field strength of the M^{2+} ion increases, in line with the earlier observations of Holland *et al.* for various borate systems⁷⁵; (iv) Borate glasses of the same alkaline-earth content exhibit a decreasing trend in N_4 with increasing field strength of the M^{2+} ion, i.e. from Ba to Mg. Note that this N_4 trend with M^{2+} cation field strength is opposite to that found for alkali borate glasses for compositions $x>0.3$ ³⁶.

As presented above, the relative absorption coefficient of boron tetrahedra versus triangles, $\alpha_r = \alpha_4/\alpha_3$, depends on the type of alkaline-earth cation. To quantify this effect, we consider the role of the cation field strength, F , defined according to Dietzel²⁶⁰ as follows:

$$F = \frac{z}{(r_c + r_o)^2} \quad (3.3)$$

Here z is the cation valence ($z=2$ for M^{2+} cations), r_c is the cation radius for an assumed coordination number (CN) and r_o is the oxygen radius. We take here $r_o = 1.35 \text{ \AA}^{261}$ for two-fold coordination of oxygen in all alkaline-earth borate compositions studied in this work. While this is an approximation, a constant r_o value has been employed in other studies as well²⁶². In any case, the oxygen coordination is expected to have a small effect on the cation-oxygen distance, and so on the values of F . Taking CN=4 for Mg^{2+} , CN=6 for Ca^{2+} and Sr^{2+} and CN=8 for Ba^{2+} , the corresponding ionic radii are $r(Mg^{2+}) = 0.57 \text{ \AA}$, $r(Ca^{2+}) = 1.00 \text{ \AA}$, $r(Sr^{2+}) = 1.18 \text{ \AA}$, and $r(Ba^{2+}) = 1.42 \text{ \AA}^{261}$. The relative IR absorption coefficient (α_r) and cation field strength (F) values for $M = Ba, Sr, Ca$ and Mg cations are presented in **Table 3.1** and plotted Figure 3.11, where the correlation between α_r and F can be described by the quadratic equation:

$$\alpha_r = 1.75 (\pm 0.14) - 3.41 (\pm 0.74) F + 6.79 (\pm 0.90) F^2 \quad (3.4)$$

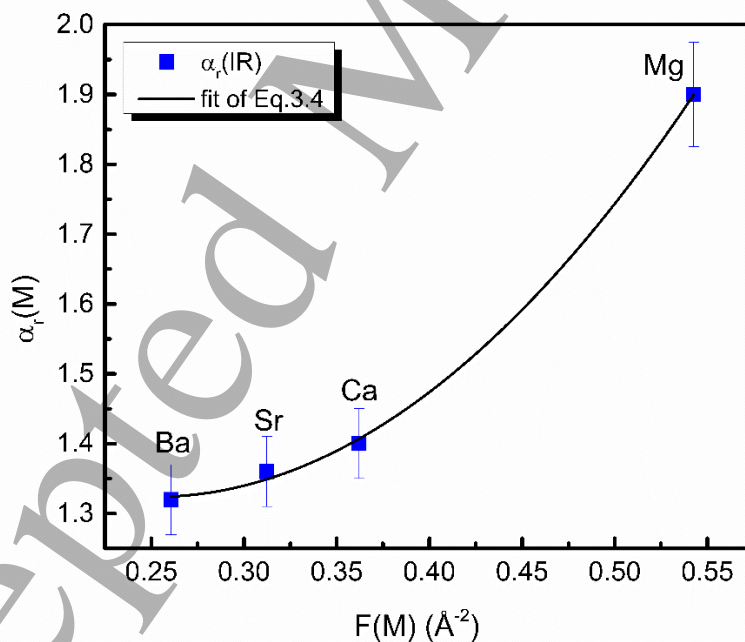


Figure 3.11. Relative IR absorption coefficient, $\alpha_r(M)$, as a function of cation field strength, $F(M)$, for $M = Ba, Sr, Ca$ and Mg -borate glasses. The line is the fit of Equation 3.4 to the data.

Table 3.1. Coordination number (CN), ionic radius (r_c), cation field strength (F) calculated by Equation 3.3 with $r_o=1.35 \text{ \AA}^{261}$, and relative IR absorption coefficient ($\alpha_r=\alpha_4/\alpha_3$) for the M^{2+} cations considered in this work.

Cation	CN	r_c (\AA)	F (\AA^{-2})	α_r
Mg ²⁺	4	0.57	0.54	1.90±0.07 ^(a)
Ca ²⁺	6	1.00	0.36	1.40±0.05 ^(a)
Sr ²⁺	6	1.18	0.31	1.36±0.05 ^(a)
Ba ²⁺	8	1.42	0.26	1.32±0.05 ^(a)
Pb ²⁺	6	1.19	0.31	1.35 ^(b)
Mn ²⁺	4	0.66	0.50	1.74 ^(b)
Mn ²⁺	6	0.67	0.49	1.71 ^(b)
Fe ²⁺	4	0.63	0.51	1.78 ^(b)
Fe ²⁺	6	0.77	0.44	1.56 ^(b)
Cu ²⁺	4	0.57	0.54	1.89 ^(b)
Cu ²⁺	6	0.73	0.46	1.62 ^(b)
Zn ²⁺	4	0.60	0.53	1.85 ^(b)

^(a) Obtained in this work and ^(b) Calculated by Equation 3.4.

To test the predictive value of Equation 3.4, we consider here the case of lead-borate glasses, $x\text{PbO}-(1-x)\text{B}_2\text{O}_3$, for which A_r data are available from IR reflectance measurements²⁶³, and N_4 data have been obtained by NMR spectroscopy^{28,80,86,88,129,154} and neutron diffraction^{264,265}. For lead ions with a network-modifier role, i.e. with primarily ionic Pb-O bonds, we assume CN=6^{80,86,88,129,154,155,264,265} and take $r(\text{Pb}^{2+})=1.19 \text{ \AA}^{261}$, which result in the cation field strength value $F(\text{Pb}^{2+})=0.31 \text{ \AA}^{-2}$ and then in $\alpha_r(\text{Pb}^{2+})=1.35$ by application of Equation 3.4. Thus, the A_r infrared data²⁶³ can be converted to N_4 data by Equation 3.1 and compared in Figure 3.12 with N_4 obtained from other experimental techniques^{28,80,86,88,129,154,264,265}.

The agreement between the N_4 -IR, and the N_4 data from other techniques^{28,80,86,88,129,154,172,264,265}, found in Figure 3.12 for Pb-borates demonstrates the usefulness of Equation 3.4 and Equation 3.1 for predicting N_4 from infrared spectra of borate glasses containing divalent cations such as Zn^{2+} . With $\alpha_r(\text{Zn}^{2+})=1.85$ (Table 3.1) one expects a similar evolution of the IR spectra and structure of Zn- and Mg-borate glasses; for example, $N_4(\text{Zn})=0.26$ for $x=0.54$ ¹³⁵ in comparison to $N_4(\text{Mg})=0.20$ for $x=0.50$ ¹⁴¹ and $N_4(\text{Mg})=0.25$ for $x=0.50$ ¹⁷² in Figure 3.10. Also, Equation 3.4 should be helpful for glasses with paramagnetic ions for which no NMR data are available²⁶⁶; predicted values for α_r are given in Table 1 for Mn^{2+} , Fe^{2+} and Cu^{2+} ions and can be employed in future structural studies to determine N_4 . It is noted though that Equation 3.4 should be applied with caution to divalent transition metal ions since the presence of d-electrons would contribute to partially covalent M-O bonding. This is in comparison to metal ions with noble gas electron configurations, like the alkaline-earths, where the M-O bonding is primarily ionic.

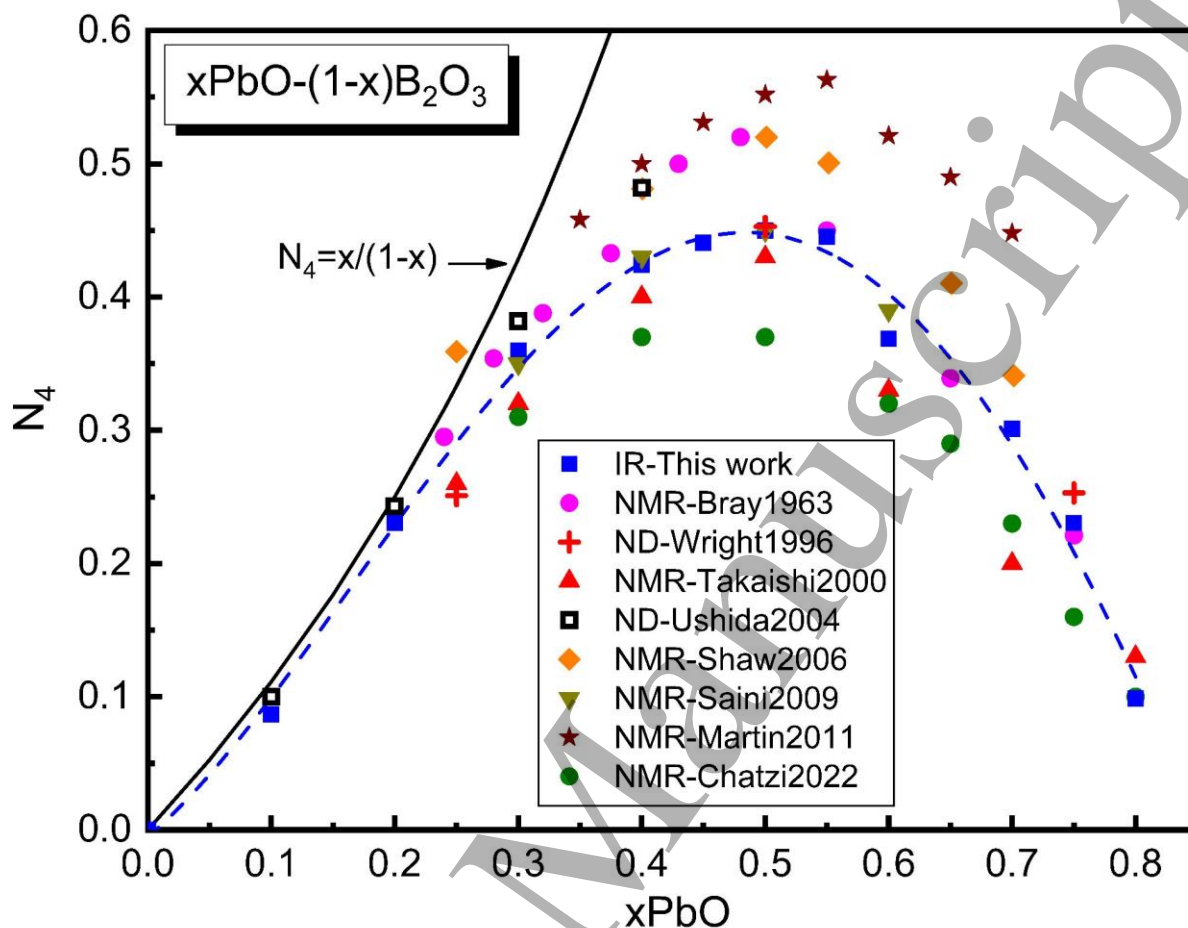


Figure 3.12. N_4 data obtained by IR results (A_r from Ref. 263) using Equation 3.1 and $\alpha_r(\text{Pb}^{2+})=1.35$, NMR spectroscopy^{28,80,86,88,129,154}, and neutron diffraction^{264,265}. Dashed line between the IR data points is a guide to the eye.

3.5. IR spectroscopy of borate glasses in thin film and other forms

IR spectra of thin film glasses are often used to assess their structure in relation to the corresponding bulk glasses. We show here that such comparisons and relevant conclusions should be made with caution. We use as an example the silver diborate glass doped with 20 mol% AgI, i.e., $0.2\text{AgI}-0.8[\text{Ag}_2\text{O}-2\text{B}_2\text{O}_3]$. The specular reflectance spectrum of the bulk glass was measured and then KK-transformed to calculate the optical properties $n(\nu)$ and $k(\nu)$ shown in Figure 3.13^{245(a)}.

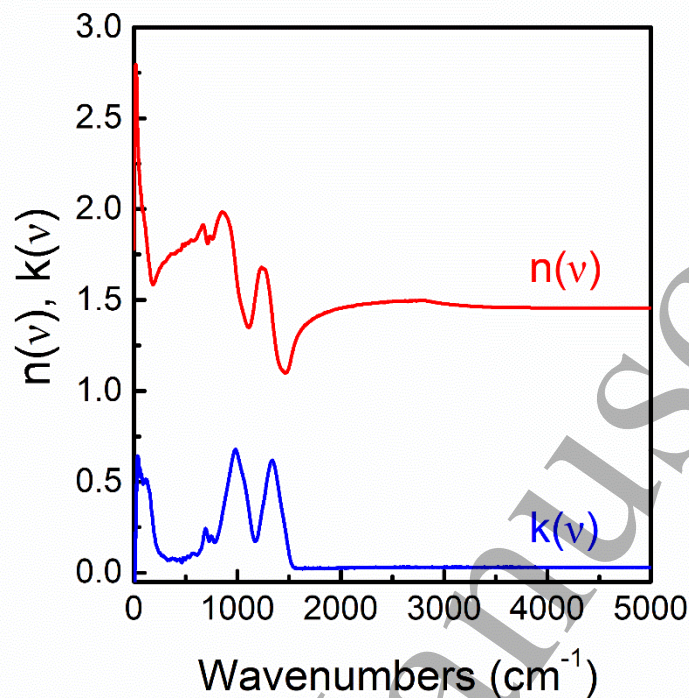


Figure 3.13. Refractive index, $n(\nu)$, and extinction coefficient, $k(\nu)$, spectra of the bulk glass 0.2AgI-0.8[Ag₂O-2B₂O₃] obtained by Kramers-Krönig transformation of the measured reflectance spectrum (reproduced from Ref. 245(a)).

The $n(\nu)$ and $k(\nu)$ spectra are then used as inputs to calculate the transmittance spectra, $T(\nu)$, of thin films using a formalism^{245(a)} to account for multiple reflections in the films. The thin films considered here have different thickness, t , but the same chemical composition and structure as they all have exactly the same $n(\nu)$ and $k(\nu)$ properties of the bulk glass. The simulated transmittance spectra $T(\nu)$ for films of different thickness are shown in the left panel of Figure 3.14. The absorbance spectra were calculated using $A(\nu)=-\log_{10}T(\nu)$ and are depicted in the right panel of Figure 3.14.

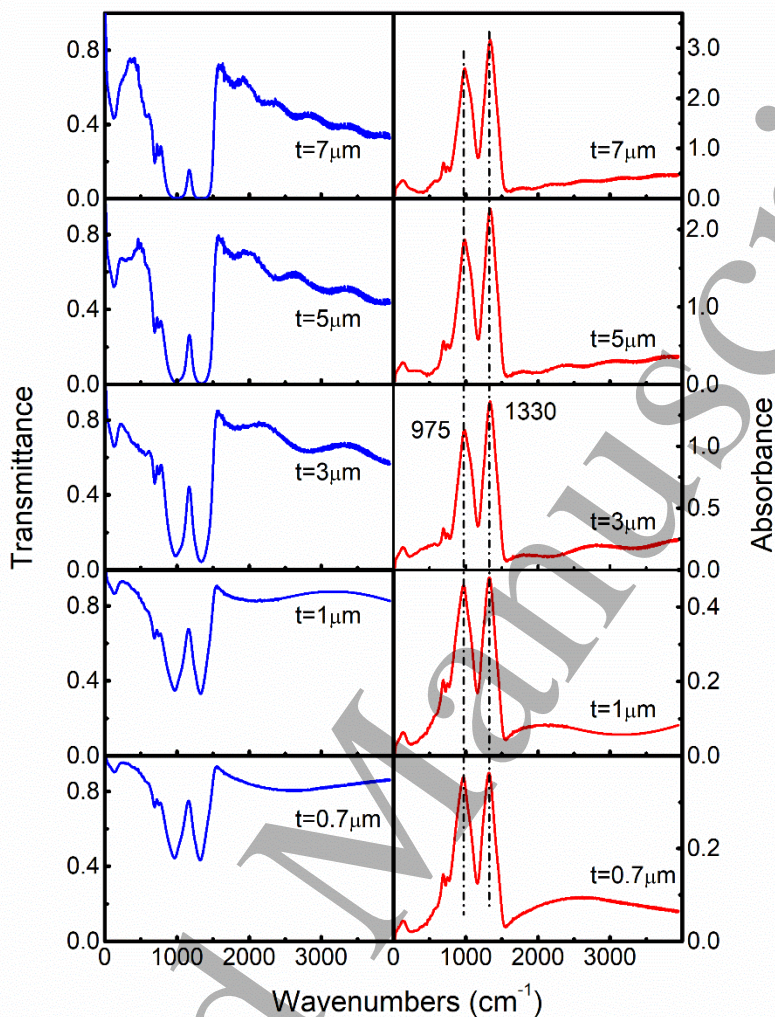


Figure 3.14. Effect of film thickness on the calculated transmittance (left) and absorbance (right) spectra of free-standing films, using as input the $n(\nu)$ and $k(\nu)$ spectra of Figure 3.13 for glass films with composition $0.2\text{AgI}-0.8[\text{Ag}_2\text{O}-2\text{B}_2\text{O}_3]$, and variable thickness ($0.7 \mu\text{m} \leq t \leq 7 \mu\text{m}$). Reproduced from Ref. 245(a).

It is observed that all spectra exhibit similar profiles below 1500 cm^{-1} . The strongest absorption envelopes are at ca. 970 cm^{-1} (due to borate tetrahedra, $[\text{B}\text{O}_4]^-$) and 1330 cm^{-1} (due to triangular borate units, BO_3 and $[\text{B}\text{O}_2\text{O}]^-$). The position of these envelopes varies from 965 to 985 cm^{-1} and from 1320 to 1340 cm^{-1} , respectively, as the film thickness increases from 0.7 to $7.0 \mu\text{m}$. Considering the origin of the ca. 970 and 1330 cm^{-1} envelopes, it would be tempting to associate the obvious dependence of their peak frequency on film thickness with variations in the nature of the borate tetrahedral and triangular units. In addition, the relative intensity $A_r = A_4/A_3$ of these envelopes changes with film thickness as seen in Figure 3.15, and this could be interpreted as a change in N_4 . Obviously, none of these interpretations are correct since all film spectra were

derived from the same $n(\nu)$ and $k(\nu)$ spectra and, thus, they should have the same bonding and structure.

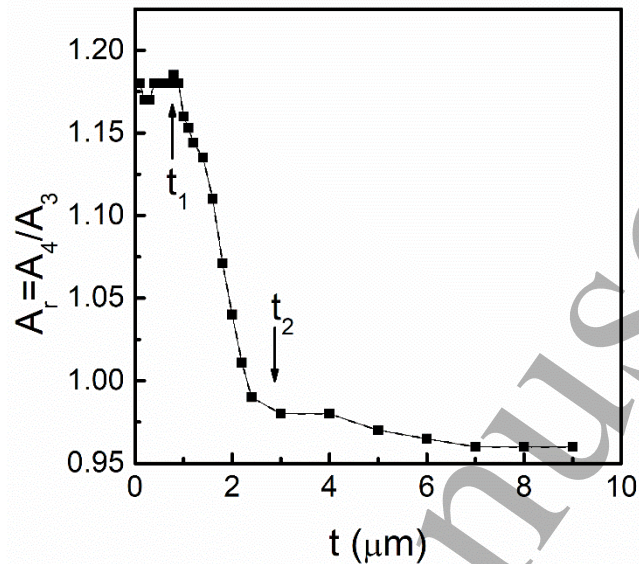


Figure 3.15. Dependence of the relative integrated absorption $A_r=A_4/A_3$ on film thickness (t) for glassy films with composition $0.2\text{AgI}-0.8[\text{Ag}_2\text{O}-2\text{B}_2\text{O}_3]$. For $t_1 < t < t_2$ the ratio $A_r=A_4/A_3$ shows a strong dependence on the film thickness. Reproduced from Ref. 245(a).

The phenomena described above result directly from the influence of film thickness on the IR absorption profiles. As seen in Figure 3.14, all films exhibit interference patterns which are well visible in the region above 1500 cm^{-1} where the glass absorption is very small. The interference patterns extend over the entire IR region, and this results in absorption spectra which are superpositions of the true vibrational profile of the bulk glass and a pure optical effect, i.e., interference due to multiple reflections in the film. The period and amplitude of interference change with film thickness and, thus, these parameters influence the frequency and relative intensity of vibrational bands in a manner which depends on film thickness.

It is noted that the studied borate thin films exhibit larger values of the $A_r=A_4/A_3$ ratio than bulk glasses of the same composition, while the decrease of A_4/A_3 upon increasing film thickness was observed also for experimental thin films blown from the melt^{245(a)}. However, the A_4/A_3 values of thin films and bulk glasses can never be the same even for thick films. A key reason for this statement is that the $A(\nu)$ spectra of thin films, derived from the $T(\nu)$ spectra, are functions of both $n(\nu)$ and $k(\nu)$ as compared to the $\alpha(\nu)$ spectra of bulk glasses which depend only on $k(\nu)$ ^{245(a)}. Besides this difference in $A(\nu)$ and $\alpha(\nu)$ spectra and the optical effects in thin films, there are usually differences in thermal histories of thin films and bulk glasses and this may introduce structural differences because of the different fictive temperatures²⁴⁵.

The example presented above shows that a safe interpretation of measured infrared spectra on thin films requires the comparison of measured and simulated spectra, taking into account purely optical effects as well as differences in thermal history between thin films and bulk glasses.

1
2
3
4 The use of the relative integrated intensity A_r to obtain N_4 in borate glasses has been applied
5 also to IR transmission spectra measured on powdered glasses dispersed in KBr pellets^{267–274}. In
6 such studies, the relation $N_4=A_4/(A_3+A_4)=A_r/(1+A_r)$ has been employed which implies that $\alpha_r=1$
7 according to Equation 3.1. However, this is not the case at least for the glasses considered here. In
8 any case, the experimental parameter A_4/A_3 derived from IR spectroscopy by the KBr pellet
9 technique is a useful tool to probe structural trends caused by, e.g., variations in borate glass
10 composition; its conversion though to N_4 requires the knowledge of α_r for the particular borate
11 system. Recently, proper application of Equation 3.1 was made by Osipova et al.²⁷⁵ for iron-
12 containing zinc borate glasses using $\alpha_r=1.36$ ²⁷⁵, relative to the $\alpha_r(\text{Zn})=1.85$ value found in the
13 present study.
14
15
16
17
18

19 3.6. Bismuth borate glasses, $x\text{Bi}_2\text{O}_3-(1-x)\text{B}_2\text{O}_3$

20
21 The previous paragraphs presented IR-derived N_4 data for borate glasses modified by metal
22 oxides of univalent (e.g., Li^+) and divalent (e.g., Ba^{2+}) metal ions. Here we consider the trivalent
23 metal ion Bi^{3+} in the binary glasses $x\text{Bi}_2\text{O}_3-(1-x)\text{B}_2\text{O}_3$. Glasses in the bismuth-borate system can
24 be prepared in an extended glass forming range up to ca. 88.2 mol% Bi_2O_3 by employing the twin
25 roller quenching technique²⁷⁶, and attract interest for a range of applications, e.g., in photonics²⁷⁷
26 and radiation shielding²⁷⁸.
27

28
29 Glasses for IR reflectance measurements were prepared by splat-quenching the melt
30 between two polished stainless-steel blocks²⁷⁶. With this method, bulk glasses were obtained in
31 the range $0.2 \leq x \leq 0.8$. The glass specimens have smooth and flat surfaces, suitable for specular
32 reflectance measurements without any further treatment.
33

34
35 Figure 3.16 presents the absorption coefficient spectra, $\alpha(\nu)$, calculated from the measured
36 specular reflectance spectra of glasses $x\text{Bi}_2\text{O}_3-(1-x)\text{B}_2\text{O}_3$ ²⁷⁹. It is observed that the $750\text{--}1150\text{ cm}^{-1}$
37 envelope originating from asymmetric boron–oxygen stretching vibration modes of tetrahedral
38 borate units exhibits considerable activity even at very high modification levels, $x > 0.70$ (Figure
39 3.16, right); in this composition range lithium borate glasses show practically no absorption of
40 metaborate tetrahedral species, $[\text{B}\text{O}_4]^-$ (Figure 3.1b). This peculiarity of bismuth-borate glasses
41 with very high modification was explained by the formation of orthoborate-type tetrahedral units,
42 $[\text{B}\text{O}_2\text{O}_2]^{3-}$, which coexist with their isomeric triangular orthoborate species $[\text{BO}_3]^{3-}$ ($[\text{B}\text{O}_2\text{O}_2]^{3-}$
43 $\rightleftharpoons [\text{BO}_3]^{3-}$).
44
45
46
47
48
49
50
51
52
53
54
55
56
57
58
59
60

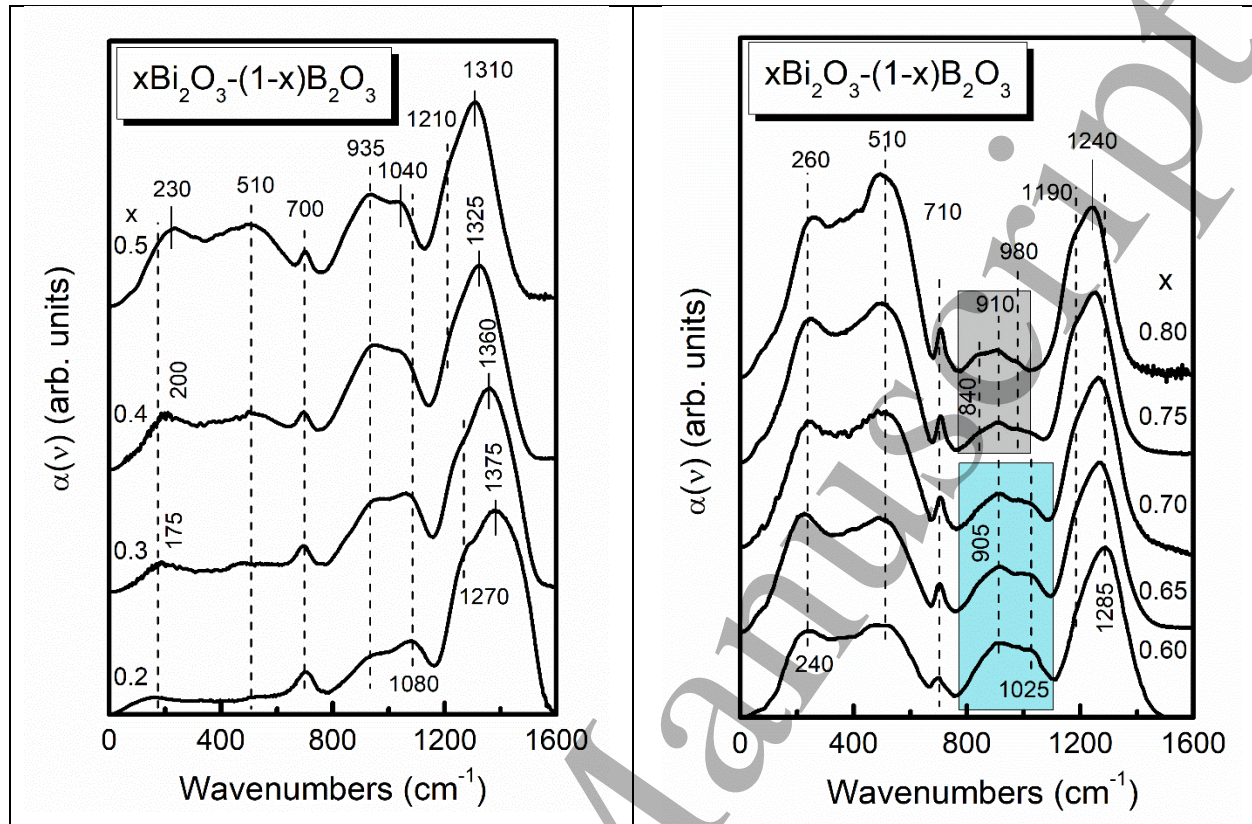


Figure 3.16. Calculated absorption coefficient spectra, $\alpha(\nu)$, for glasses $x\text{Bi}_2\text{O}_3-(1-x)\text{B}_2\text{O}_3$ with $0.2 \leq x \leq 0.5$ (left) and $0.6 \leq x \leq 0.8$ (right), reproduced from Ref. 279.

To quantify the effect of Bi_2O_3 on the borate structure, the $\alpha(\nu)$ spectra were deconvoluted and the integrated intensities of component bands above 800 cm^{-1} were used in combination with mass and charge balance equations to evaluate the molar fractions of the short-range borate units: X_{4m} , X_{4o} , X_3 , X_2 , X_1 and X_0 which correspond to borate units $[\text{B}\text{O}_4]^-$, $[\text{B}\text{O}_2\text{O}_2]^{3-}$, BO_3 , $[\text{B}\text{O}_2\text{O}]^-$, $[\text{B}\text{O}\text{O}_2]^{2-}$ and $[\text{B}\text{O}_3]^{3-}$ (O and O^- denote bridging and non-bridging oxygen atoms). Thus, this extensive infrared analysis provides the molar fractions of all borate units as compared to the approach presented in previous sections, which gives only the fraction N_4 on the basis of $A_T = A_4/A_3$. The composition dependence of the total fraction of boron atoms in four-fold coordination, $N_4 = X_{4m} + X_{4o}$, is presented in Figure 3.17a as derived from IR²⁷⁹ and NMR spectroscopy⁸³, while the evolution of the fractions of units BO_3 , $[\text{B}\text{O}_2\text{O}]^-$, $[\text{B}\text{O}\text{O}_2]^{2-}$ and $[\text{B}\text{O}_3]^{3-}$ is also given²⁷⁹.

It is evident from Figure 3.17a that in the composition range $0.2 \leq x \leq 0.65$, the N_4 data from IR and NMR are, generally, in good agreement. The experimental N_4 data are compared in the same figure with the theoretical value obtained if all oxygen atoms introduced by Bi_2O_3 are forming $[\text{B}\text{O}_4]^-$ units, $N_{4th} = 3x/(1-x)$. Clearly, the experimental rate for $[\text{B}\text{O}_4]^-$ formation is considerably lower than $3x/(1-x)$. For $x=0.2$ the experimental rate is $1.3x/(1-x)$, indicating that only 43% of the introduced oxygen forms $[\text{B}\text{O}_4]^-$ units. For $x=0.3$ the experimental N_4 rate reduces to $x/(1-x)$, showing that 33% of the oxygen forms $[\text{B}\text{O}_4]^-$ units. Therefore, the rest of the added oxygen participates in other kinds of structural groups including the non-bridging oxygen containing $[\text{B}\text{O}_2\text{O}]^-$ and $[\text{B}\text{O}\text{O}_2]^{2-}$ units²⁷⁹.

It was also possible to separate the contributions of the $[\text{B}\emptyset_4]^-$ and $[\text{B}\emptyset_2\text{O}_2]^{3-}$ tetrahedral species to the total N_4 value as resulted from the analysis of the IR spectra. The results are shown in Figure 3.17b in terms of the fractional contributions of the metaborate tetrahedral units $[\text{B}\emptyset_4]^-$, X_{4m}/N_4 , and of the orthoborate tetrahedral units $[\text{B}\emptyset_2\text{O}_2]^{3-}$, X_{4o}/N_4 , to the total N_4 fraction of borate tetrahedral species in the $x\text{Bi}_2\text{O}_3-(1-x)\text{B}_2\text{O}_3$ glasses. Clearly, $[\text{B}\emptyset_4]^-$ constitute the dominating tetrahedral units for $0.20 \leq x \leq 0.70$ and the $[\text{B}\emptyset_2\text{O}_2]^{3-}$ units prevail at higher Bi_2O_3 levels ($x > 0.7$), where they coexist with their isomeric triangular borate species $[\text{BO}_3]^{3-}$.

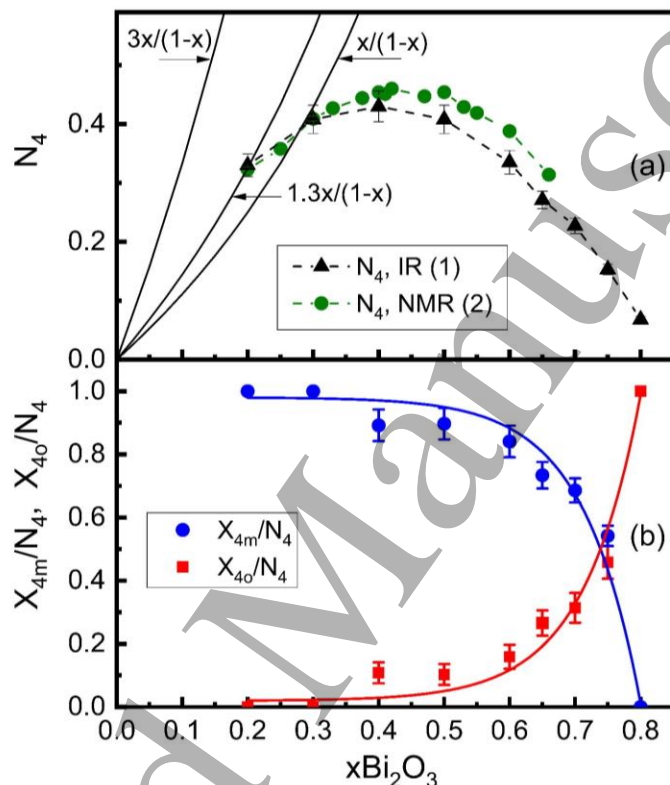


Figure 3.17. (a) Comparison of the molar fractions of borate tetrahedral units N_4 in glasses $x\text{Bi}_2\text{O}_3-(1-x)\text{B}_2\text{O}_3$ obtained by IR, (1)Ref. 279, and NMR, (2)Ref. 83, spectroscopy. The solid black lines present the theoretical value for the mole fraction of $[\text{B}\emptyset_4]^-$ units formed at rates $3x/(1-x)$, $1.3x/(1-x)$ and $x/(1-x)$. (b) Fractional contributions of the metaborate tetrahedral units $[\text{B}\emptyset_4]^-$, X_{4m}/N_4 , and of the orthoborate tetrahedral units $[\text{B}\emptyset_2\text{O}_2]^{3-}$, X_{4o}/N_4 , to the total fraction N_4 of borate tetrahedra in these bismuth borate glasses²⁷⁹. Dashed lines in (a) and solid lines in (b) are drawn as guides to the eye.

The formation of $[\text{B}\emptyset_2\text{O}_2]^{3-}$ tetrahedral species could be at the origin of the very broad glass-forming region of glasses $x\text{Bi}_2\text{O}_3-(1-x)\text{B}_2\text{O}_3$. While the nominal orthoborate composition ($\text{O}/\text{B}=3/1$) corresponds to $x=0.5$ in this system, the glass-forming region extends well-above this limit and reaches $x=0.80$ by splat-quenching and even $x=0.88$ by twin roller quenching²⁷⁶. This is in contrast to lithium-borate glasses $x\text{Li}_2\text{O}-(1-x)\text{B}_2\text{O}_3$ for which glass formation by splat-quenching was possible up to $x=0.73$, i.e. the pure orthoborate glass ($x=0.75$) could not be prepared due to crystallization²³⁶. This can be rationalized in terms of the main structural difference between the two glass systems: while $[\text{BO}_3]^{3-}$ triangles are the only borate species present in Li-orthoborate, they coexist, with their isomeric tetrahedral orthoborate units $[\text{B}\emptyset_2\text{O}_2]^{3-}$ in highly-modified Bi-borate glasses, in addition to the parallel glass-forming role of Bi_2O_3 at high x values i.e., formation

of BiO_n polyhedral species²⁷⁹; both these factors prevent crystallization and extend the glass-forming region of the Bi-borate system. Recently, the preparation of the $x=0.75$ Li-borate glass was achieved by intentionally leaving some carbonate species $[\text{CO}_3]^{2-}$ in the melt, from the starting Li_2CO_3 material, to avoid crystallization upon quenching²⁸⁰.

The glass-forming role of Bi_2O_3 in bismuthate glasses above the orthoborate composition ($x>0.5$) is probably related to the involvement of the d-electrons of Bi in primarily covalent Bi-O bonds in BiO_n polyhedral species.²⁷⁹ The fact that part of the added oxygen is involved in covalent bonding with Bi allows the borate component to maintain its orthoborate composition by the coexisting $[\text{BO}_3]^{3-}$ and $[\text{B}\emptyset_2\text{O}_2]^{3-}$ isomeric units, with the latter forming at increasing rates for $x>0.5$ (see Fig. 3.17b). This trend is consistent with the composition dependence of the glass transition temperature which decreases from $T_g=407$ °C at $x=0.50$ to $T_g=312$ °C at $x=0.80$.⁸³ Assuming that the fictive temperature shows a behavior similar to T_g , then the structure of the supercooled liquid for $x=0.80$ would be arrested into the glassy state at lower temperature than that for $x=0.50$ and, naturally, this would drive the structure to the more condensed orthoborate units. As reported by Lower et al.²⁸¹, the $[\text{B}\emptyset_4]^-$ tetrahedral unit has smaller effective volume than its isomeric $[\text{B}\emptyset_2\text{O}]^-$ triangular species. Assuming that the same trend is exhibited by the orthoborate isomers, then the $[\text{B}\emptyset_2\text{O}_2]^{3-}$ tetrahedra would have smaller effective volume than their $[\text{BO}_3]^{3-}$ isomers and, thus, the decreasing fictive temperature would favor the formation of the tetrahedral orthoborate isomers.

3.7. Raman spectroscopy of borate glasses

Compared to IR, the number of Raman studies devoted to the quantification of the borate structure are limited. This is due to the lack of knowledge about the Raman scattering cross section of vibrations related to borate species. Instead, Raman spectroscopy can provide a semi quantitative description of the structure in terms of relative band intensities of borate species. Such an approach was employed in the Raman study of glasses $x\text{Na}_2\text{O}-(1-x)\text{B}_2\text{O}_3$ with $0\leq x\leq 0.75$ ²⁸², noting that glass-formation for $x=0.45, 0.50$ and 0.55 was achieved by replacing $0.05, 0.07$ and 0.05 moles B_2O_3 by equal number of moles Al_2O_3 , respectively. Assignment of the complex Raman profiles supported the use of the following characteristic bands: 805 cm^{-1} for boroxol rings; $545, 765, 780,$ and 1120 cm^{-1} for $[\text{B}\emptyset_4]^-$ tetrahedral units; 1490 cm^{-1} for triangular metaborate units $[\text{B}\emptyset_2\text{O}]^-$; 820 cm^{-1} for pyroborate units $[\text{B}_2\text{O}_5]^{4-}$ and 890 cm^{-1} for orthoborate triangular units $[\text{BO}_3]^{3-}$. Assuming that the bandwidths of the Raman bands do not change with composition, the band intensity of a specific borate unit was approximated by the peak height of its Raman band, or by the sum of peak heights of the four bands related to $[\text{B}\emptyset_4]^-$ units.

The composition dependence of the relative Raman intensity of the previously mentioned borate units has been estimated and the results are given in Figure 3.18. As depicted in this figure, the analysis of the Raman spectra gives a semi quantitative mapping of the borate structure in the entire glass forming range; it starts with boroxol rings of neutral $\text{B}\emptyset_3$ triangles at $x=0$ and progresses, through $[\text{B}\emptyset_4]^-$, $[\text{B}\emptyset_2\text{O}]^-$, and $[\text{B}_2\text{O}_5]^{4-}$ formation and destruction, to a completely depolymerized borate structure of highly charged orthoborate units $[\text{BO}_3]^{3-}$. Figure 3.18 also shows corresponding N_4 data from NMR spectroscopy^{35,36,173,283}. Considering the approximations

made to analyze the Raman spectra, the agreement in the composition dependence of $[\text{B}\text{O}_4]^-$ species from Raman and N_4 from NMR is satisfactory especially for glasses with $x < 0.33$.

Despite the semi quantitative nature of the trends exhibited by the Raman data in Fig. 13.18, it is observed that non-bridging oxygens appear to form on $[\text{B}\text{O}_2\text{O}]^-$ units well below the ca. $x=0.25$ composition, which signals the formation of NBOs according to NMR spectroscopy on the same glasses (Fig. 2.11(a)). The effectiveness of Raman spectroscopy in probing NBOs may be related to the strong Raman cross-section of $\text{B}-\text{O}^-$ stretching in comparison to $\text{B}-\text{O}$ stretching. It is noted that NBO formation starts at about $x=0.30$ in Li-borate glasses (see Fig. 2.4(a), Fig. 3.5 and Ref. 277), while increasing alkali cation size was found to favor the early formation of NBOs for compositions $x < 0.50$.²⁸⁴ This was associated with the decreasing polarizing power, i.e. increasing softness of the alkali cations (Lewis acids).

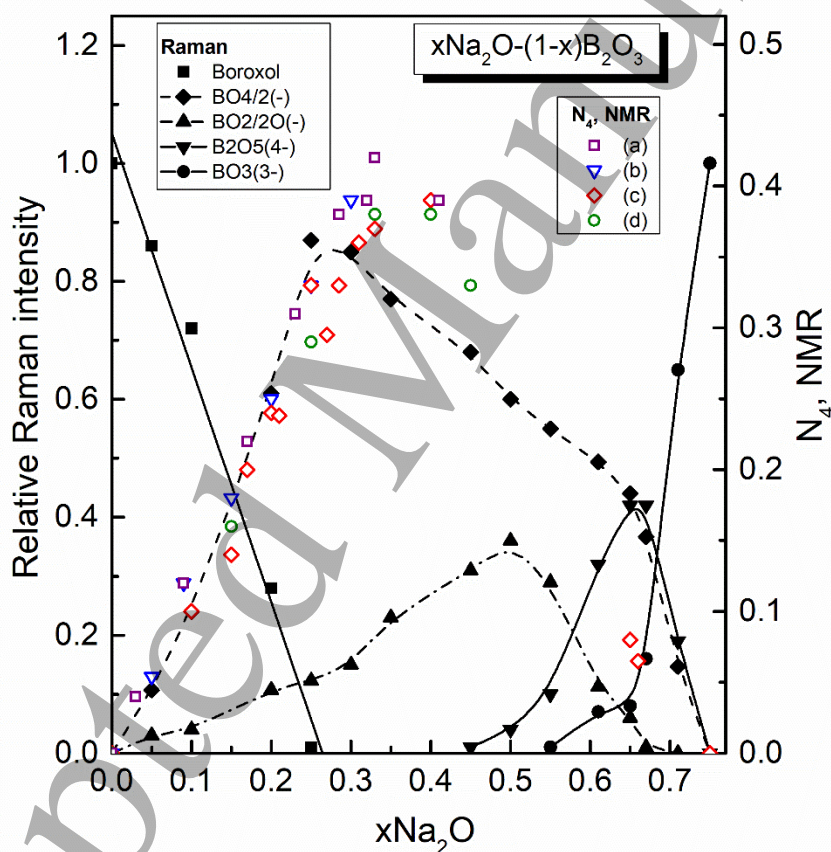


Figure 3.18. Composition dependence of the relative Raman intensity of borate units in sodium borate glasses $x\text{Na}_2\text{O}-(1-x)\text{B}_2\text{O}_3$ spanning the composition range $0 \leq x \leq 0.75$ (reproduced from Ref. 281). The Raman results for BO_4^- tetrahedral units are compared with N_4 data from NMR spectroscopy, (a)Ref. 36, (b)Ref. 282, (c)Ref. 283 and (d)Ref. 35. Lines connecting the Raman data points are guides to the eye.

In a later study of glasses $x\text{Na}_2\text{O}-(1-x)\text{B}_2\text{O}_3$ with $0 \leq x \leq 0.33$ ²⁸⁵, the Raman spectra were fitted in the entire frequency range with Gaussian-type bands which were attributed to different

borate species. The scaling of Raman data with corresponding NMR data allowed the evaluation from Raman spectroscopy of N_{3a}/N_{3s} and N_4 , where N_{3a} and N_{3s} stand for the relative population of $[B\emptyset_2O]^-$ and $B\emptyset_3$ species. The composition and temperature dependence of N_4 as derived from Raman spectroscopy is shown in Figure 3.19²⁸⁵. It is clear that at each Na_2O content there is a decreasing trend of N_4 with temperature, indicating the conversion of $[B\emptyset_4]^-$ to $[B\emptyset_2O]^-$ species at high temperatures. This is an example of the effectiveness of Raman spectroscopy to characterize melt structures, using instrumentation and experimental set-ups more accessible than those of other techniques.

The temperature-induced conversion $[B\emptyset_4]^- \rightarrow [B\emptyset_2O]^-$ in alkali borate glasses has been supported by a range of studies including statistical mechanical calculations²⁸⁶, high-temperature NMR^{40,287}, high temperature Raman^{285,288,289}, molecular dynamics simulations^{290,291}, neutron diffraction^{292,293}, and high-energy x-ray diffraction^{294,295}.

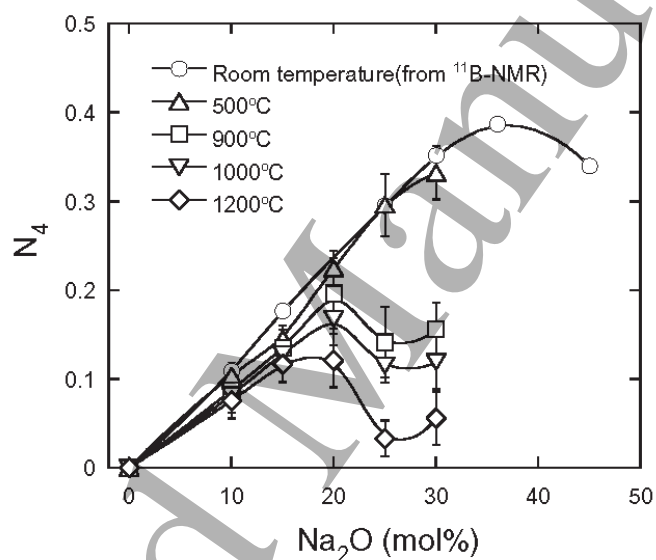


Figure 3.19. Plot of N_4 at various temperatures as a function of Na_2O content for glasses $xNa_2O-(1-x)B_2O_3$ (reproduced from Ref. 285). ^{11}B -NMR data are employed to scale the room temperature Raman data³⁵. Lines between the data points are guides to the eye. From *J. Non-Cryst. Solids* used with STM guideline permission.

4. Neutron and X-ray Methods

4.1 Introduction

The application of x-ray diffraction methods to study the structure of glasses was developed by Warren and coworkers in the 1930s^{296,297}, applied to sodium borate glasses to determine N_4 for the very first time in 1938⁵, and subsequently to calcium²⁹⁸ and potassium²⁹⁹ borate glasses in the early 1940s. In the late 1940s, neutron diffraction methods at reactor sources became available, and subsequently, in the early 1970s, the pulsed neutron scattering technique was developed for

particle accelerator based sources of neutrons. Importantly, this latter method enabled the exploitation of more energetic, epithermal, neutrons and to collect diffraction patterns to high momentum transfers. This is important for studying glass structure since the maximum momentum transfer is reciprocally related to the real-space resolution in the resulting pair distribution functions, which are the weighted histograms of all of the interatomic separations occurring in the scattering material. At a similar time, Mozzi and Warren^{300,301} demonstrated the collection of higher quality x-ray diffraction data from glasses, in part by use of higher energy x-rays derived from a heavier metal source (Rh $K\alpha$ as opposed to Mo $K\alpha$). A step change came in the mid-1990s with the use of much higher-energy x-rays, produced at intense synchrotron sources, being applied to study glass structure by diffraction^{302,303}. As for pulsed neutron sources, these ‘hard’ x-rays allowed for measurements of high real-space resolution pair distribution functions. In addition, the use of pulsed neutrons or high-energy synchrotron x-rays have several other advantages that allow the collection of high quality diffraction patterns from glasses, including reduced neutron capture and photoelectric absorption cross-sections respectively. As such, the study of glass structure by diffraction methods has come to be dominated by pulsed neutrons and hard synchrotron x-rays, although reactor neutrons also play a strong part. What these sources have in common is that they are too large and costly for a typical laboratory to house, and tend to be run as national or international facilities. This has meant that, whilst such large-scale facilities provide diffraction data of much higher quality than can be obtained with small-scale laboratory sources of x-rays (or even neutrons or electrons), there is, at least a perception of, lower accessibility. The result is that, as can be seen from this review, the number of studies of N_4 in borate glasses by diffraction methods is much lower than by NMR or vibrational spectroscopy, techniques which are more widely available. The opportunity to reduce this gap is already ripe for the picking, given the increases in brightness and throughput of both synchrotron and neutron sources over recent decades, along with the development of improved analysis techniques, as discussed below.

Historically, the first reports of the measurement of binary borate glass structure by neutron diffraction appeared in the late 1980s, with pulsed neutron diffraction studies of heavy metal borate glasses by Yasui *et al.*^{304,305}. However, it wasn’t until the early 1990s that neutron diffraction measurements were used to derive N_4 values, by Wright & Vedishcheva *et al.* in lead borate glasses^{264,306,307}, and by Kita *et al.* in sodium borate melts³⁰⁸. The first use of high-energy synchrotron x-ray diffraction to study binary borate glasses (and melts) came in the late 1990s with a study including 15Li₂O-85B₂O₃ by Herms *et al.*³⁰⁹, with the first reports of N_4 coming from Herms & Sakowski in 2000, on more highly modified alkali borate glasses and melts³¹⁰. As such, the vast majority of diffraction studies reviewed below are those originating in the 1990s and the decades since, representing 30 years of research, because these studies are the ones in which reasonably accurate quantitative determinations of N_4 in binary borate glasses and melts have been made. In total we review about 315 diffraction measurements where N_4 has been reported, with half of those being from the borate melt studies of Alderman *et al.*^{259,294,295,311,312}. This covers about 32 studies and 17 different modifiers.

4.2 Outline of diffraction theory

As is evident from the introduction above, diffraction based determinations of N_4 in binary borate glasses and melts have historically been made using either x-rays or neutrons. The theoretical background and equations used to interpret such measurements are introduced below, using a superscript R to denote a dependence on radiation type, and $R = N$ or X to denote neutrons or x-rays respectively. Other types of radiation used for diffraction measurements, such as electrons, have thus far played a minor role and are therefore considered beyond the scope of the present article, although many of the concepts are identical. In a total scattering diffraction experiment, the measured quantity is the differential scattering cross section:

$$\frac{d\sigma^N}{d\Omega}(Q) = I^N(Q) = S^N(Q) + \sum_{\alpha=1}^n c_{\alpha} \bar{b}_{\alpha}^2, \quad (4.1)$$

$$\frac{d\sigma^X}{d\Omega}(Q) = I^X(Q) = S^{X'}(Q) + \sum_{\alpha=1}^n c_{\alpha} f_{\alpha}^2(Q) + \sum_{\alpha=1}^n c_{\alpha} C_{\alpha}(Q) \quad (4.2)$$

Here $Q = (4\pi/\lambda)\sin\theta$ is the scattering vector magnitude for elastic scattering, between radiation quanta with incident and scattered wavelength λ and 2θ is the scattering angle between their wavevectors \mathbf{k}_i and \mathbf{k}_f , with $|\mathbf{k}_f| = |\mathbf{k}_i| = k = 2\pi/\lambda$. For isotropic media, including most glasses, the cross section depends only on the magnitude of $\mathbf{Q} = \mathbf{k}_i - \mathbf{k}_f$, that is $|\mathbf{Q}| = Q$. σ^R is the scattering cross section and Ω the solid angle. $S^R(Q)$ is the distinct scattering which contains all of the structural information relating to distances between pairs of atoms within the scattering volume. The meaning of the prime in the x-ray distinct scattering is explained below. The remaining terms on the right hand side of equations (4.1) and (4.2) are self-scattering terms which do not contain structural information and contribute only an incoherent background signal which must be subtracted from the measured differential cross sections to obtain the distinct scattering. The summations represent compositional averaging over the n unique elements present, with c_{α} the fractions of atoms of identity α within the scattering volume. The \bar{b}_{α} are the neutron scattering lengths averaged over all isotopes and spin states of the nucleus-neutron system for a given element α . The $f_{\alpha}(Q)$ and $C_{\alpha}(Q)$ are respectively the x-ray form factors and Compton scattering for element α . The distinct scattering term can be represented as a summation over pair terms:

$$S^N(Q) = \sum_{\alpha \geq \beta}^n \sum_{\beta=1}^n (2 - \delta_{\alpha\beta}) c_{\alpha} c_{\beta} \bar{b}_{\alpha} \bar{b}_{\beta} (S_{\alpha\beta}(Q) - 1) \quad (4.3)$$

$$S^X(Q) = \frac{S^{X'}(Q)}{(\sum_{\alpha=1}^n c_{\alpha} f_{\alpha}(Q))^2} = \sum_{\alpha \geq \beta}^n \sum_{\beta=1}^n \frac{(2 - \delta_{\alpha\beta}) c_{\alpha} c_{\beta} f_{\alpha}(Q) f_{\beta}(Q) (S_{\alpha\beta}(Q) - 1)}{(\sum_{\alpha=1}^n c_{\alpha} f_{\alpha}(Q))^2} \quad (4.4)$$

where $\delta_{\alpha\beta}$ is the Kronecker delta with α and β the chemical elements within the scattering volume. The $S_{\alpha\beta}(Q)$ are known as the partial structure factors, encoding the information on distances between atoms of type α and β , there being $(n^2 + n)/2$ unique pair terms. The x-ray distinct scattering $S^{X'}(Q)$ is divided by a sharpening function $(\sum_{\alpha=1}^n c_{\alpha} f_{\alpha}(Q))^2$ in order to approximately remove its form-factor related Q -dependence, this approximation becomes exact only for monatomic scatterers.

Note that the $S_{\alpha\beta}(Q)$ partial structure factors depend only on the structure of the material, and not on the radiation type. The influence of the radiation type is encapsulated in the pair weighting factors which we define as:

$$W_{\alpha\beta}^N = (2 - \delta_{\alpha\beta}) c_{\alpha} c_{\beta} \overline{b_{\alpha}} \overline{b_{\beta}}, \quad (4.5)$$

$$W_{\alpha\beta}^X(Q) = \frac{(2 - \delta_{\alpha\beta}) c_{\alpha} c_{\beta} f_{\alpha}(Q) f_{\beta}(Q)}{(\sum_{\alpha=1}^n c_{\alpha} f_{\alpha}(Q))^2}. \quad (4.6)$$

Such that

$$S^R(Q) = \sum_{\alpha \geq \beta}^n \sum_{\beta=1}^n W_{\alpha\beta}^R(Q) (S_{\alpha\beta}(Q) - 1). \quad (4.7)$$

An example of both $QS^N(Q)$ and $QS^X(Q)$ are shown in Figure 4.1 for the case of a barium diborate glass²⁵⁹. In this example there is considerable contrast due to the relatively high weighting of the Ba- β pair terms in the x-ray scattering. Nonetheless, many similar features can be observed in the two interference functions, including the positions of the first two peaks at $Q_1 \approx 1.25 \text{ \AA}^{-1}$ and $Q_2 \approx 1.91 \text{ \AA}^{-1}$, as well as the oscillations at high- Q which are dominated by the B-O pair term. These similarities stem from the fact that both functions are based on the same set of $S_{\alpha\beta}(Q)$, only with different pair weightings.

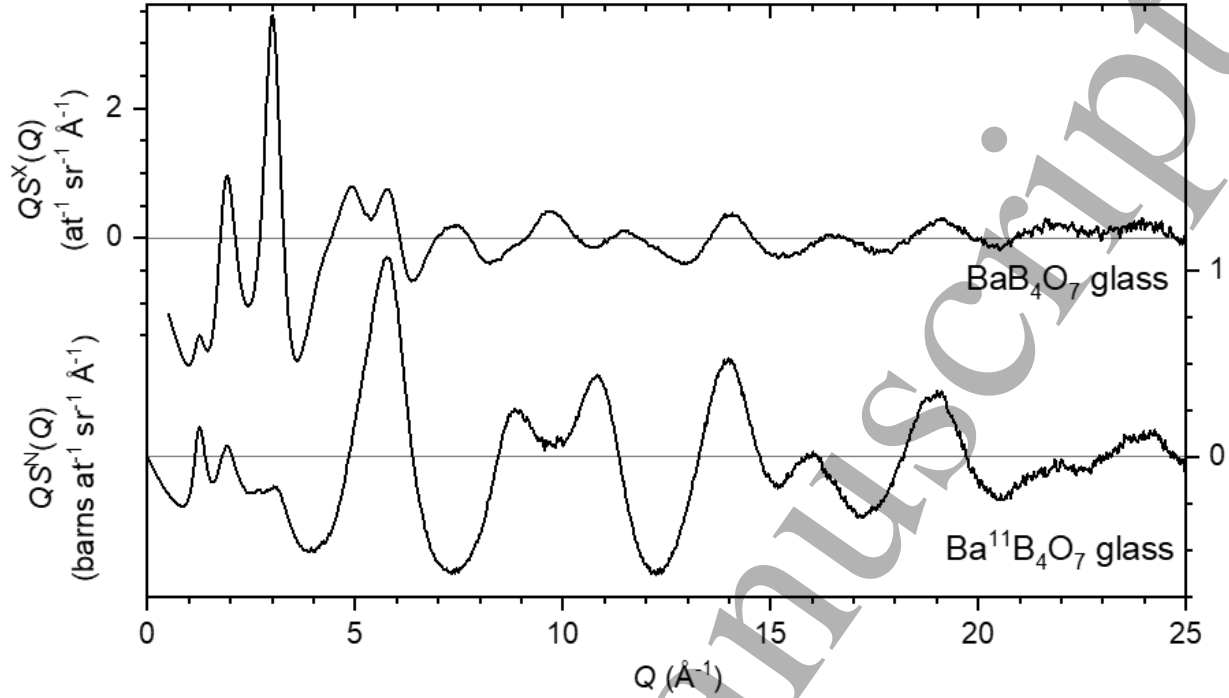


Figure 4.1: Interference functions for $\text{Ba}^{11}\text{B}_4\text{O}_7$ glass as measured with neutrons on the GEM instrument at the ISIS Neutron and Muon Source (lower)²⁵⁹, and for BaB_4O_7 glass as measured with x-rays at sector 6-ID-D of the Advanced Photon Source (upper)²⁵⁹.

Defining the partial radial distribution function $\rho_{\alpha\beta}(r)$ as the average number of β atoms within a spherical shell at separations between r and $r + dr$ of an α atom, the site-site partial pair distribution function is defined by:

$$g_{\alpha\beta}(r) \equiv \frac{\rho_{\alpha\beta}(r)}{4\pi r^2 \rho_0} \quad (4.8)$$

where ρ_0 is the number of atoms per unit volume. Likewise, the partial differential distribution function is defined by:

$$d_{\alpha\beta}(r) = 4\pi r \rho_0 [g_{\alpha\beta}(r) - 1] \quad (4.9)$$

and relates by sine Fourier transform to the partial structure factor:

$$d_{\alpha\beta}(r) = \frac{2}{\pi} \int_0^\infty Q [S_{\alpha\beta}(Q) - 1] \sin Qr dQ \quad (4.10)$$

Average coordination numbers can be determined by integration as:

$$n_{\alpha\beta}(r_1, r_2) = c_\beta \int_{r_1}^{r_2} \rho_{\alpha\beta}(r) dr = c_\beta \int_{r_1}^{r_2} r t_{\alpha\beta}(r) dr = 4\pi \rho_0 c_\beta \int_{r_1}^{r_2} r^2 g_{\alpha\beta}(r) dr \quad (4.11)$$

where

$$t_{\alpha\beta}(r) = d_{\alpha\beta}(r) + 4\pi r \rho_0 \quad (4.12)$$

This is key to the subject of our review, because within the assumption that boron in borate glasses coordinates either to 3 or 4 oxygen atoms:

$$N_4 = n_{BO} - 3 \quad (4.13)$$

where it is implicit that the integration limits encompass only the first coordination shell.

Since in practice it is rare that all of the partial $S_{\alpha\beta}(Q)$ and $d_{\alpha\beta}(r)$ can be determined experimentally, it is usual to define x-ray or neutron differential distribution functions:

$$D^R(r) = \frac{2}{\pi} \int_0^{Q_{max}} Q S^R(Q) M(Q) \sin Qr dQ \quad (4.14)$$

wherein it is explicitly acknowledged that measurements can only attain a certain finite maximum $Q = Q_{max}$, and a modification function, $M(Q)$, is used to describe the truncation at Q_{max} . This truncation can be performed sharply with a step function:

$$M_{step}(Q) = 1 \text{ for } Q \leq Q_{max} \text{ or } 0 \text{ for } Q > Q_{max} \quad (4.15)$$

or more smoothly with, for example, a Lorch function:

$$M_{Lorch}(Q) = \frac{Q_{max}}{\pi Q} \sin\left(\frac{\pi Q}{Q_{max}}\right) \text{ for } Q \leq Q_{max} \text{ or } 0 \text{ for } Q > Q_{max} \quad (4.16)$$

The total correlation functions are given by:

$$T^R(r) = D^R(r) + 4\pi r \rho_0 \sum_{\alpha \geq \beta}^n \sum_{\beta=1}^n W_{\alpha\beta}^R(Q=0) \quad (4.17)$$

where it should be noted that within our formalism the summation over pair weighting factors is unity for x-rays and equal to the compositionally averaged neutron scattering length squared, $\langle \bar{b} \rangle^2$, for neutrons:

$$T^N(r) = D^N(r) + 4\pi r \rho_0 \langle \bar{b} \rangle^2 \quad (4.18)$$

$$T^X(r) = D^X(r) + 4\pi r \rho_0 \quad (4.19)$$

An example of $T^N(r)$ is shown in Figure 4.2 for the case of a barium diborate glass²⁵⁹.

In terms of partial pair correlations:

$$T^R(r) = \sum_{\alpha \geq \beta}^n \sum_{\beta=1}^n P_{\alpha\beta}^R(r) \otimes t_{\alpha\beta}(r) \quad (4.20)$$

where \otimes denotes a convolution and the peak shape functions are given by

$$P_{\alpha\beta}^R(r) = \frac{1}{\pi} \int_0^\infty W_{\alpha\beta}^R(Q) M(Q) \cos Qr dQ \quad (4.21)$$

From the above, it is clear that care must be taken when determining coordination numbers from $T^R(r)$. This is because even when, e.g. the B–O bond length distribution *circa* 1.4 Å, is apparently fully resolved from other partial pair contributions, its peak shape function will mean that its total area is spread out. Thus, strictly speaking a broad integration range is needed which may not be possible due to correlations at higher r . Furthermore, there may still be subtle influences from other partial pair contributions, especially in the case of x-rays where the weighting factors are Q -dependent, as well as in the case of relatively low Q_{\max} . For this reason, peak fitting methods are often applied, as described in the following sections.

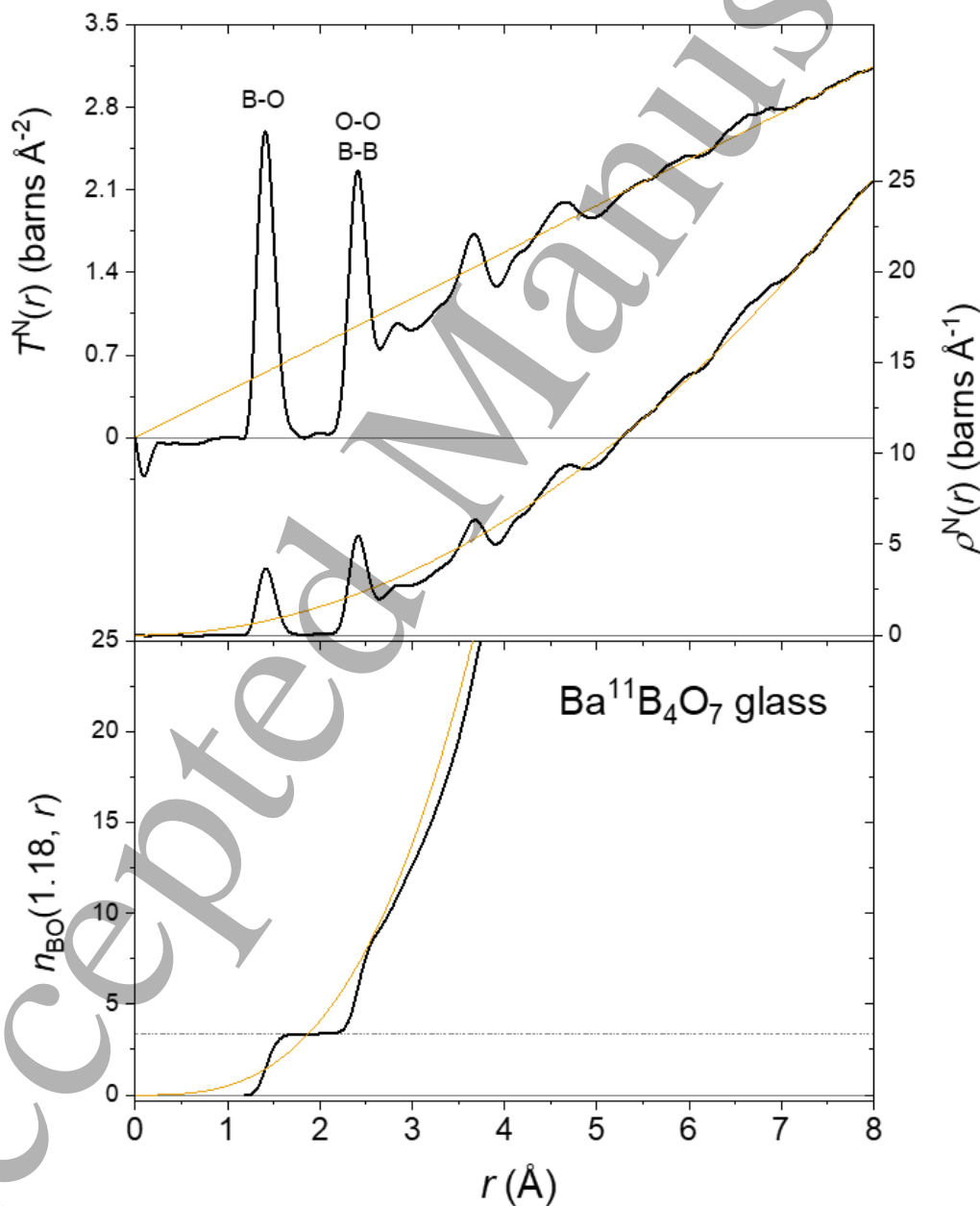


Figure 4.2: Neutron (a) total correlation function; (b) radial distribution function; (c) running B–O coordination number for Ba¹¹B₄O₇ glass as measured on the GEM instrument at the ISIS Neutron and Muon Source. The yellow curves represent the average density contributions which are a) $4\pi r \rho_0 \langle \bar{b} \rangle^2$; b) $4\pi r^2 \rho_0 \langle \bar{b} \rangle^2$; c) $\frac{4}{3}\pi r^3 \rho_0 \langle \bar{b} \rangle^2 \frac{c_0}{W_{BO}^N}$. Since $n_{BO}(1.18, r)$ is calculated from the total $\rho^N(r)$, it corresponds only to $n_{BO}(r)$ below about 2 Å. The plateau prior to this indicates $n_{BO} = 3.35(10)$, as indicated by the chained horizontal line, and $N_4 = 0.35(10)^{259}$. The data were obtained by Fourier transform of the interference function in Figure 4.1, using a Lorch modification function and $Q_{\max} = 40 \text{ \AA}^{-1}$.

4.3 Methods for extracting N_4 from diffraction data

Note that all methods for calculation of N_4 from diffraction data are based on measurement of the mean coordination number, n_{BO} , and predicated on the assumption that only 3- and 4-coordinated boron atoms are present, such that $N_4 = n_{BO} - 3$.

4.3.1 Direct integration of the pair distribution function

In order to determine the B–O coordination number by direct integration, one needs access to the partial radial distribution function $\rho_{BO}(r)$. For determination of N_4 , it is only the local coordination number that is of interest, and so only $\rho_{BO}(1.0 \lesssim r \lesssim 1.8 \text{ \AA})$ is actually required. Thus, even though it is $T^N(r)$ or $T^X(r)$ that are determined from a single neutron or x-ray diffraction measurement, rather than $\rho_{BO}(r) = r t_{BO}(r)$, in the cases where there is no real-space overlap with other pair terms, then n_{BO} and N_4 can be determined by suitable integration of the total correlation function. For the case of neutrons, the pair weighting factors are independent of Q , and therefore the W_{BO}^N can be divided out in real-space. Thus, the integral of equation 4.11 becomes:

$$n_{BO}(r_1, r_2) = c_0 \int_{r_1}^{r_2} r t_{BO}(r) dr = \frac{c_0}{W_{BO}^N} \int_{r_1}^{r_2} r T^N(r) dr \quad (4.22)$$

where the second equality holds only for integration limits chosen to encompass the B–O bond length distribution, without overlap with any other non-zero partial pair distribution. An example of this is shown in Figure 4.2 for the case of a barium diborate glass²⁵⁹.

For the x-ray case, the Q -dependence of the weighting factors necessitates the division by $W_{BO}^X(Q)$ in reciprocal space:

$$S_{BO}^X(Q) = \frac{s^X(Q)}{W_{BO}^X(Q)} \quad (4.23)$$

Fourier transform of this modified structure factor using equation 4.14 leads to a real-space function $D_{BO}^X(r)$ and

$$T_{BO}^X(r) = D_{BO}^X(r) + 4\pi r \rho_0 \sum_{\alpha \geq \beta}^n \sum_{\beta=1}^n \frac{W_{\alpha\beta}^R(Q=0)}{W_{BO}^X(Q=0)} \quad (4.24)$$

Then finally,

$$n_{BO}(r_1, r_2) = c_O \int_{r_1}^{r_2} r T_{BO}^X(r) dr \quad (4.25)$$

As for equation 4.22, equation 4.25 holds only for integration limits chosen to encompass the B–O bond length distribution, without overlap with any other non-zero partial pair distributions. In practice a small amount of overlap with other partial pair terms can be difficult to avoid, especially due to the complex peak function, in the pair terms other than B–O, in the x-ray case.

If there is overlap of the B–O nearest-neighbor peak with peaks arising from other pair terms, then integration of the total $T^N(r)$ or $T_{BO}^X(r)$ will not yield the desired result. It may be possible to remove the overlap by defining a suitable difference function taken between differently weighted measurements. This could be either a difference between a neutron and x-ray measurement, or between neutron measurements made on suitable isotopically distinct samples. Since this method is not commonly practiced for boron or oxygen isotopes in borates, we do not discuss it any further herein. Alternatively, more commonly practiced methods for removal of overlap are to use some kind of model for the overlapping peaks, or to rely on peak fitting methods.

4.3.2 Peak fitting

Peak fitting is often performed to real-space diffraction data at short interatomic separations typical of the bonded (B–O, M–O) and nearest neighbor non-bonded (O–O, M–M, B–B, M–B) pair distances. Whilst any underlying distribution of interatomic distances can in principle be used, normal Gaussian distributions are the most commonly applied, being the expected peak shapes for bonded interactions within the harmonic approximation. Such peaks have the following form:

$$\tilde{t}_{\alpha\beta}(r) = \frac{n_{\alpha\beta}}{c_\beta r_{\alpha\beta} \sqrt{2\pi\langle u_{\alpha\beta}^2 \rangle}} \exp\left(-\frac{(r-r_{\alpha\beta})^2}{2\langle u_{\alpha\beta}^2 \rangle}\right) \otimes P_{\alpha\beta}^R(r) \quad (4.26)$$

where again \otimes denotes a convolution by the peak shape function. The mean bond length between the α – β pair is denoted $r_{\alpha\beta}$, with $\langle u_{\alpha\beta}^2 \rangle$ its mean-square deviation due to static and thermal disordering and $n_{\alpha\beta}$ the coordination number. In reciprocal space this takes the form:

$$S_{\alpha\beta}(Q) = \frac{n_{\alpha\beta} W_{\alpha\beta}^R(Q)}{c_\beta} \frac{\sin Q r_{\alpha\beta}}{Q r_{\alpha\beta}} \exp\left(-\frac{\langle u_{\alpha\beta}^2 \rangle Q^2}{2}\right) \quad (4.27)$$

where it is implicit that to transform this to real-space, the same Q_{\max} and modification function must be used in the Fourier transform as for the experimental data, such that the peak function is identical.

Clearly, in the case of borates, there can be both trigonal and tetrahedral species present which will have different r_{BO} , $\langle u_{BO}^2 \rangle$ and abundances. It is important to note that the trigonal and tetrahedral B–O bond lengths are about $r_{BO3} = 1.37 \text{ \AA}$ and $r_{BO4} = 1.48 \text{ \AA}$, respectively, and, to date, these have never been resolved from one another in a measured pair distribution function. Using

pulsed neutrons to obtain high $Q_{\max} = 50 \text{ \AA}^{-1}$ Hoppe *et al*³¹³ resolved the bridging P–O and terminal P=O bonds in P_2O_5 glass. These occur respectively at $r_{\text{P-O}_b} = 1.58 \text{ \AA}$ and $r_{\text{P-O}_t} = 1.43 \text{ \AA}$, which is a larger separation than for r_{BO_3} and r_{BO_4} . Furthermore, the terminal double bond leads to a rather small $\langle u_{\text{P-O}_t}^2 \rangle^{1/2} = 0.028 \text{ \AA}$, both factors make resolving the two P–O more accessible than the two B–O bond length distributions. Indeed, even for arbitrarily high Q_{\max} , it may never be possible to resolve the two B–O bond length distributions, which would require that their widths were both, on average, $\langle u_{\text{BO}}^2 \rangle^{1/2} < 0.05 \text{ \AA}$, which may not be the case. Nonetheless, the existence of the two boron coordination species needs to be considered when peak fitting. When Q_{\max} is relatively low, and real-space resolution $\Delta r \sim 1/Q_{\max}$ relatively poor, it can be sufficient to fit a single B–O bond length distribution. This is typical in the case of both x-ray diffraction^{259,294,295,311,312} and reactor source neutron diffraction, where often $Q_{\max} \lesssim 25 \text{ \AA}^{-1}$ and B–O peaks appear relatively symmetric. Clearly a single peak is also likely sufficient in the limiting cases of $N_4 = 0$ or 1. Using pulsed neutrons, larger Q_{\max} are routinely obtained, typically in the range $30 \lesssim Q_{\max} \lesssim 50 \text{ \AA}^{-1}$, and asymmetry in the B–O peak becomes apparent when $0 < N_4 < 1$ ²⁵⁹.

When fitting a single Gaussian B–O bond length distribution to the real-space diffraction data, the N_4 follows directly from the n_{BO} in equation 4.26 using $N_4 = n_{\text{BO}} - 3$. If two peaks have been fitted, then their individual coordination numbers can be summed and $N_4 = n_{\text{BO}} - 3 = n_{\text{BO}(1)} + n_{\text{BO}(2)} - 3$. In this manner, the two peak fit can be considered as an arbitrary characterisation of an asymmetric peak using two symmetric ones, where only their averaged or summed properties are considered. On the other hand, if one considers the fitting capable of distinguishing the bonds within trigonal and tetrahedral species, then the two peak fit can be considered to yield:

$$n_{\text{BO}} = n_{\text{BO}_4} + n_{\text{BO}_3} = 4N_4 + 3(1 - N_4) = N_4 + 3 \quad (4.28)$$

such that N_4 follows not only from the total coordination number, but also from the coordination numbers obtained from either of the two individual peaks. I.e.:

$$N_4 = n_{\text{BO}_4}/4 \quad (4.29)$$

$$N_4 = 1 - n_{\text{BO}_3}/3 \quad (4.30)$$

Furthermore, N_4 may also be obtained by ratio, a method which is independent of the absolute normalization (scaling) of the dataset:

$$N_4 = n_{\text{BO}_4}/(n_{\text{BO}_4} + n_{\text{BO}_3}) \quad (4.31)$$

In the author's (OLGA) experience, sensible two-peak fitting results are only reliably obtained with the use of some kind of fitting constraint. For example, the positions of the two peaks can be fixed at the expected positions for ideal trigonal and tetrahedral species from empirical bond-valence theory (1.371 \AA and 1.477 \AA). An example using this constraint is shown in Figure 4.3, for the neutron diffraction measurement of $\text{Ba}^{11}\text{B}_4\text{O}_7$ glass²⁵⁹. Final fitting parameters are given in Table 4.1. Interestingly, the $\langle u_{\text{BO}}^2 \rangle^{1/2}$ obtained indicate that the peaks are unlikely to be resolvable, even with arbitrarily high real-space resolution, since their sum is very similar to the peak separation. The total area of the two peaks together yields a similar $N_4 = 0.32(10)$ to direct integration ($N_4 = 0.35(10)$, see Table 4.2). This is to be expected, whilst the

slightly smaller value appears to arise from the inability of the fit to account for the small shoulder *circa* 1.7 Å, Figure 4.3. This might indicate either distortion (static disorder) or anharmonicity in the thermal vibrations of the BO₄ units, indicating that the harmonic approximation made in the use of Gaussian bond length distributions is beginning to break down. Notably, using the areas of the individual peaks yields higher N_4 values, of 0.45(5) and 0.42(4) for the BO₃ and BO₄ peaks respectively (Table 4.1 and 4.2). At first it might seem counterintuitive that the individual peaks could yield higher N_4 than that derived from their total summed area. However, it can be seen from equation 4.28 that the two instances of N_4 partially cancel out (since one is preceded by a minus sign), and will only give agreement with the N_4 from their area if they are equal. Such a condition could be used as an additional fitting constraint. Note that inclusion of the ‘missing area’ *circa* 1.7 Å into the BO₄ peak area improves agreement slightly, to $N_4 = 0.43(4)$. Another method for extracting N_4 from the two-peak fit is to use their coordination number ratio, as in equation 4.31. For our example, this method yields a slightly larger $N_4 = 0.50(10)$. Notably this method is often applied in the literature, but to the ratio of the peak *areas*. If the peak areas are determined from the $\rho_{\text{BO}}(r)$, then this is equivalent to the coordination number ratio. However, if the peak areas are determined from $t_{\text{BO}}(r) = \rho_{\text{BO}}(r)/r$, then N_4 will be underestimated, with $N_4 = 0.48(10)$ in our example. The underestimation will be more extreme if peak areas are determined for $g_{\text{BO}}(r) = \rho_{\text{BO}}(r)/4\pi\rho_0r^2$.

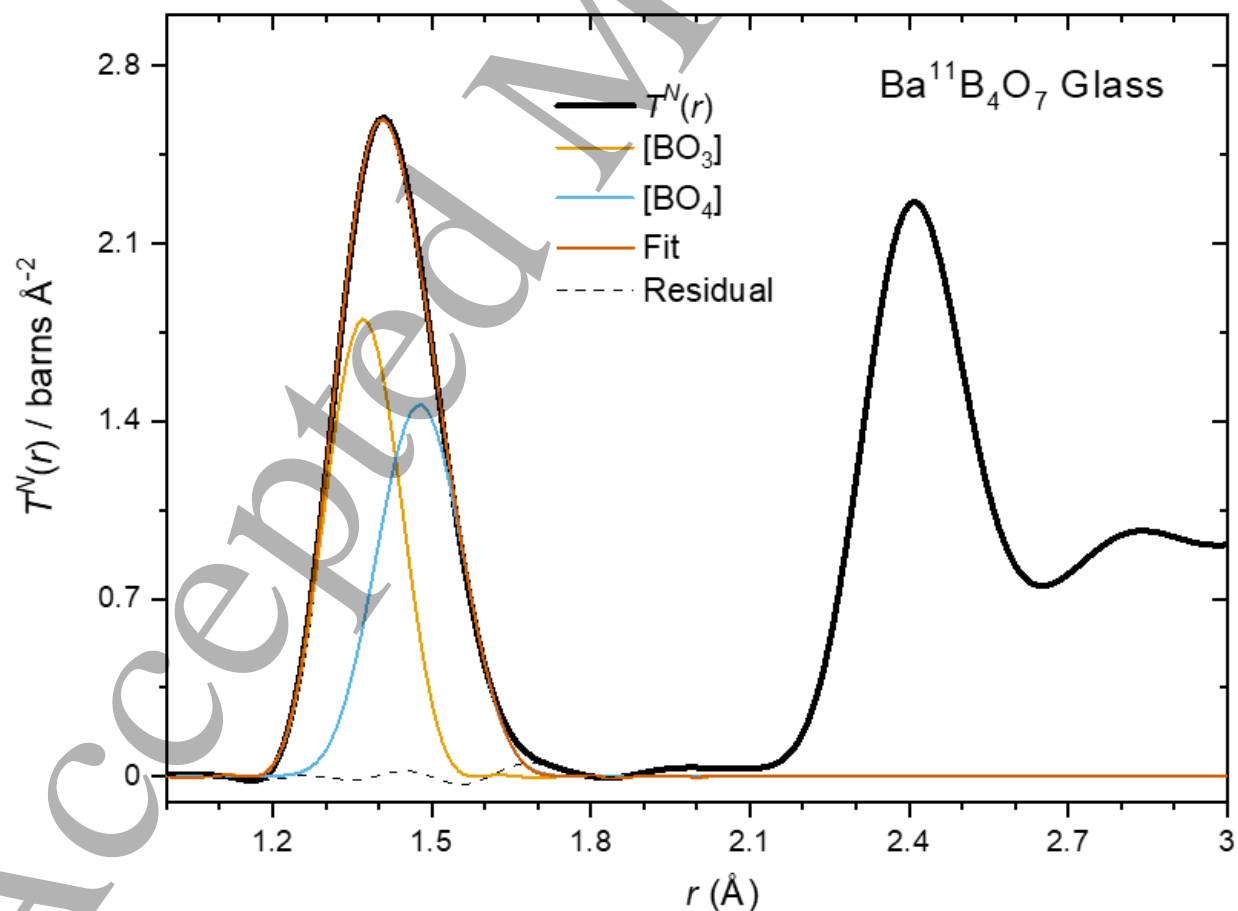


Figure 4.3: Two peak fit to the neutron total correlation function for Ba¹¹B₄O₇ glass, as measured on the GEM instrument at the ISIS Neutron and Muon Source (Figure 4.2)²⁵⁹. The two individual peaks are shown, along with their sum, and the residual between this and the data fitted to.

Table 4.1: Parameters derived from the peak fit shown in Figure 4.3 for Ba¹¹B₄O₇ glass. *The individual BO₃ and BO₄ bond lengths were kept fixed at their ideal bond-valence expectation values. N_4 can be calculated from the individual peak areas (equations 4.29 and 4.30) as well as the total area (equation 4.28, see Table 4.2 for additional methods). $n_{\text{OB}} = c_{\text{B}}n_{\text{BO}}/c_{\text{O}}$ are also shown, along with the fraction of non-bridging oxygen, $f_{\text{nbr}} = 2 - n_{\text{OB}}$, which is non-zero at this composition if $N_4 < 0.5$ (assuming oxygen are either bridging or non-bridging and coordinate to either 2 or 1 boron atoms respectively).

Peak	r_{BO} (Å)	$\langle u_{\text{BO}}^2 \rangle^{1/2}$ (Å)	n_{BO}	N_4	n_{OB}	f_{nbr}
BO ₃	1.371*	0.047(2)	1.65(15)	0.45(5)	0.94(5)	0.03(3)
BO ₄	1.4774*	0.062(3)	1.67(15)	0.42(4)	0.95(5)	0.05(2)
Total	1.4225	n.a.	3.32(10)	0.32(10)	1.90(7)	0.10(7)

Table 4.2: N_4 derived for a single neutron diffraction dataset for Ba¹¹B₄O₇ glass, in 7 different ways. These can be grouped into 4 methods i) from total area of the B–O bond length distribution; ii) from the areas of the BO₃ or BO₄ bond length distributions; iii) from the ratio of the coordination numbers of the two bond length distributions; iv) from the mean bond length using bond-valence methods.

Method	N_4	Equation
Integration	0.35(10) ²⁶	4.22
Fitted BO ₃ peak	0.45(5)	4.29
Fitted BO ₄ peak	0.42(4)	4.30
Fitted total area	0.32(10)	4.28
Fitted peaks ratio	0.50(10)	4.31
Bond valence, mean $r_{\text{BO}} = 1.4225$ Å from fit	0.45(1)	4.36
Bond valence, mean $r_{\text{BO}} = 1.4251$ Å from integration	0.47(1) ²⁶	4.36

Another example of peak fitting, this time taken from the literature³¹², is shown in Figure 4.4. In this case, x-rays were used to measure the structure factor for supercooled liquid lithium pyroborate. In contrast to the previous example of barium diborate glass measured with neutrons, here the Q_{max} is lower, at 22.8 Å⁻¹, and hence only a single B–O bond length distribution has been fitted. The example highlights the effects of overlap with the B–O peak, which occur here due to the presence of short modifier-oxygen bonds, lower real-space resolution and the complex peak shape functions arising from the electron density distributions from which the x-rays scatter. As such, it is often instructive to fit and/or model peaks to higher r , in order to extract the most accurate B–O peak parameters and hence N_4 .

1
2
3 In summary there are three main ways that peak fitting is used to obtain N_4 from the:
4

- 5 i) total area of the B–O bond length distribution, akin to the direct integration method
6 ii) individual (unresolved) BO_3 and BO_4 peak areas
7 iii) ratio of the (unresolved) BO_3 and BO_4 peak areas
8

9 Note that method i) is largely insensitive to the details of the fitting model, as long as it
10 gives a good fit. Methods ii) and iii) are highly sensitive to the partitioning of the B–O bond length
11 distribution into those from BO_3 and BO_4 units, and this cannot in general be done uniquely due
12 to the unresolved nature of the two features. This sensitivity notwithstanding, methods ii) and iii)
13 have the advantage that they are independent of the absolute scaling or normalization of the dataset
14 being fitted.
15
16

17 Another means to determine N_4 from fitting parameters also exists, which is to exploit the
18 high sensitivity of diffraction methods to length-scales and to use the bond-valence method for
19 mapping mean B–O bond lengths to mean coordination numbers, and this is discussed in the
20 following section.
21
22
23
24
25
26
27
28
29
30
31
32
33
34
35
36
37
38
39
40
41
42
43
44
45
46
47
48
49
50
51
52
53
54
55
56
57
58
59
60

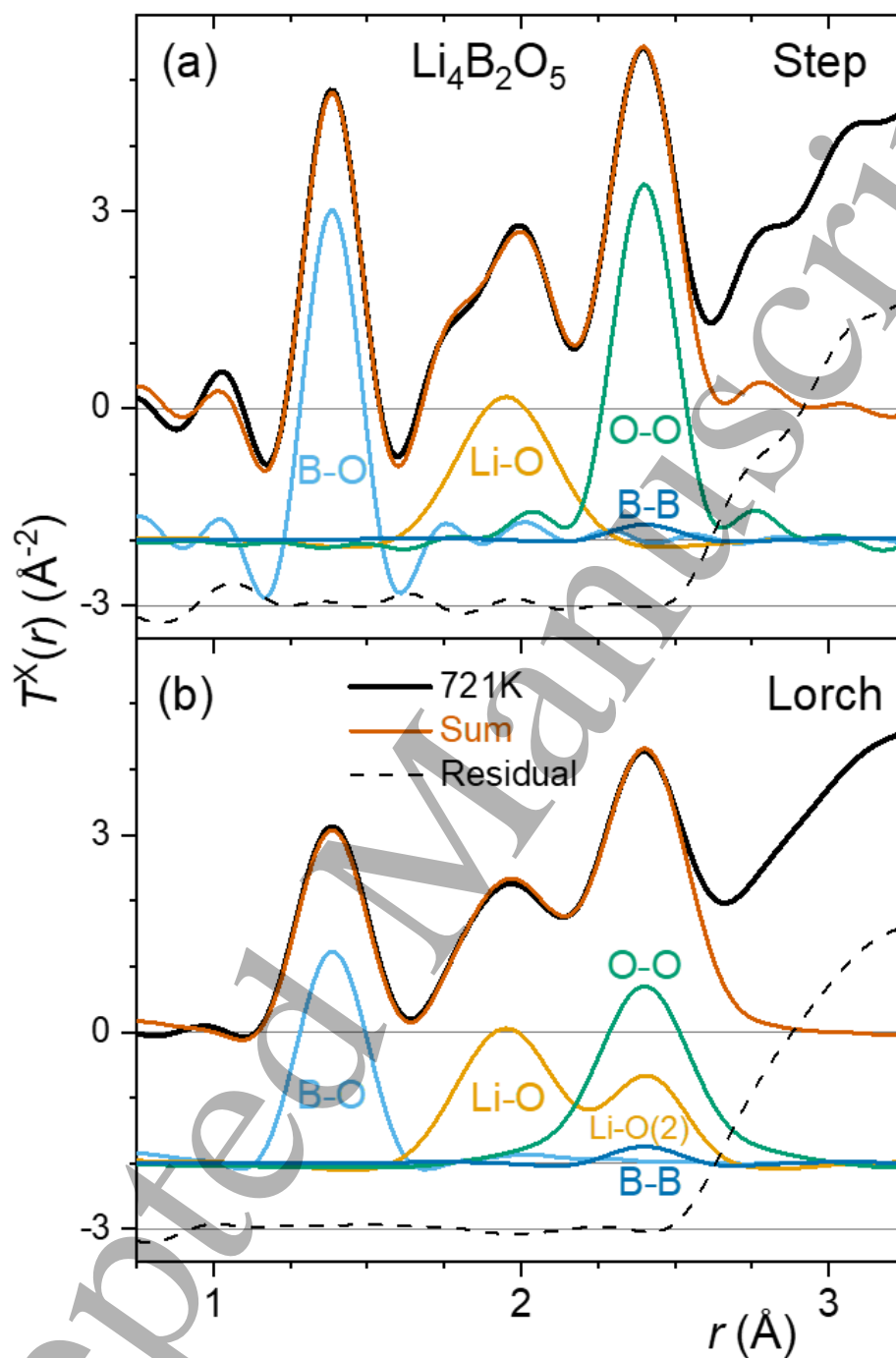


Figure 4.4: Peak fits to the X-ray total correlation function for supercooled liquid $\text{Li}_4\text{B}_2\text{O}_5$ at $T = 721 \text{ K}$ ³¹², obtained using $Q_{\text{max}} = 22.8 \text{ \AA}^{-1}$ and (a) step modification; (b) Lorch modification function. (a) shows results from a 4-peak simultaneous fit, with the small B-B peak estimate held fixed. This method leads to overestimation of the O-O coordination number, at the expense of longer Li-O bonds. (b) shows results from a 5-peak sequential fit, including a second distribution of longer Li-O bonds, with the O-O peak modeled at the expected coordination number. Individual peaks are offset vertically by -2 \AA^{-2} and the residual by -3 \AA^{-2} for clarity.

4.3.3 Mapping mean B–O bond length to N_4 using the bond valence method

The structural information contained within a diffraction measurement arises from the path length differences between radiation quanta scattered from different scattering centers. As such, diffraction is an interference technique which is highly sensitive to length scales and distances within the scattering material. This means that mean bond lengths, $r_{\alpha\beta}$, are typically determined with much higher precision than are coordination numbers, $n_{\alpha\beta}$, because the latter depend on the absolute normalization of the scattering data, as well as on a host of corrections that are necessary in real experiments due to effects including attenuation, multiple and inelastic scattering in the sample under study, as well as in any container and sample environment apparatus. Meanwhile, the length (or Q) scaling is calibrated by measurement of a crystalline powder standard of precisely known cell parameter. Therefore, if a means exists to quantitatively relate $r_{\alpha\beta}$ to $n_{\alpha\beta}$, this could serve, at the very least, as a consistency check on the $n_{\alpha\beta}$ determined by direct integration or peak fitting, or, in cases where these lack the desired precision, to determine $n_{\alpha\beta}$ more precisely. The bond-valence (BV) methodology provides such a means and is introduced and discussed below.

The bond-valence method splits the formal valence of a central ion, V_α , between its bonds, depending upon the length of those bonds:

$$V_\alpha = \sum_{\beta} v_{\alpha\beta} \quad (4.32)$$

where the summation is over the bonds, and with the bond valences (strengths), $v_{\alpha\beta}$, related exponentially to the bond lengths $r_{\alpha\beta}$:

$$v_{\alpha\beta} = \exp\left(\frac{R_{\alpha\beta} - r_{\alpha\beta}}{b}\right) \quad (4.33)$$

In equation 4.33 the $R_{\alpha\beta}$ are the bond-valence parameters for the α – β pair and b is often treated as a universal constant. Using a large database of crystal structures, Brown and Altermatt³¹⁴ derived an empirical value of $b = 0.37 \text{ \AA}$ and $R_{\text{BO}} = 1.371(1) \text{ \AA}$. A useful simplification can be made by assuming that all bond lengths within a coordination polyhedron are equivalent, such that

$$V_\alpha = n_{\alpha\beta} \exp\left(\frac{R_{\alpha\beta} - r_{\alpha\beta}}{b}\right) \quad (4.34)$$

and the $r_{\alpha\beta}$ can be directly related to the $n_{\alpha\beta}$ by

$$n_{\alpha\beta} = V_\alpha \exp\left(\frac{r_{\alpha\beta} - R_{\alpha\beta}}{b}\right) \quad (4.35)$$

This simplification has been shown to be a useful approximation,^{259,294,295,311,312} despite the fact that certain (if not all) borate polyhedra are expected *not* to have equivalent bonds, such as the asymmetrical metaborate $\text{B}\text{O}_2\text{O}^-$ and pyroborate BO_2O^{2-} triangles. In these cases the distortion theorem states that the mean bond will be elongated due to the non-equivalence of the three

individual bonds, an effect arising from the exponential nature of the bond-valence relationship. As such, use of equation 4.36 below could lead to overestimation of N_4 in highly modified borates. This effect is nonetheless small when compared to the changes in mean bond length induced by boron coordination change from 3 to 4, and neglecting it therefore has only a small impact on the precision of N_4 determination via the mean bond length. Note that when $n_{\alpha\beta} = V_\alpha$, then it follows that $r_{\alpha\beta} = R_{\alpha\beta}$. For boron, $V_\alpha = V_B = 3$ and

$$N_4 = 3 \left\{ \exp \left(\frac{r_{BO} - R_{BO}}{b} \right) - 1 \right\} \quad (4.36)$$

So in pure B_2O_3 , where $n_{BO} = 3$, indeed the mean bond length r_{BO} is very close to $R_{BO} = 1.371(1) \text{ \AA}$, as can be seen in Table 4.3 which lists total scattering diffraction measurements of r_{BO} in pure B_2O_3 glass. Equation 4.36, plotted in Figure 4.5, can therefore be used to map measured mean r_{BO} to N_4 , providing a means of interpolation between the integer values of $N_4 = 0$ and 1 ($n_{BO} = 3$ and 4). To fully exploit the sensitivity of this method, a BV parameter can be derived from a measurement of r_{BO} in pure B_2O_3 glass using the same experimental setup and calibration as applied to the binary borate glasses under investigation, and for which precise N_4 are sought. This has been exploited for a range of binary borate glasses and melts^{259,294,295,311,312}, including a correction for the observed temperature dependence (thermal expansion) of the B–O bond³¹⁵ in B_2O_3 , used to derive $R_{BO}(T) = 1.375 + (5.14 \times 10^{-6})T$ in K and \AA units, using 100 keV synchrotron x-rays. Some examples are shown in Figure 4.6. The N_4 derived using the BV method have typical uncertainties as low as 0.01, approaching the sensitivity of high-field solid-state ^{11}B NMR, but with the advantage that diffraction methods are equally applicable in the high-temperature molten state. Notably, if a BV parameter is not calibrated under the same conditions as the diffraction experiment, then an uncertainty in N_4 of 0.05 can be inferred from the range of r_{BO} measured for pure B_2O_3 glass in Table 4.3, and represented by the blue shaded area in Figure 4.5. The N_4 values for $Ba^{11}B_4O_7$ glass derived using equation 4.36 and the standard $R_{BO} = 1.371(1) \text{ \AA}$ are given at the bottom of Table 4.2. Systematic uncertainties which could arise using this method include the violation of the bond length equivalence within individual polyhedra discussed above, as well as variability of the thermal expansion coefficient for different borate polyhedra. Despite these challenges, the method appears, to date, to be the most precise and accurate means for extracting N_4 from diffraction data.

Table 4.3: Summary of total scattering diffraction measurements of the mean B–O bond length in B_2O_3 glass ($^{11}B_2O_3$ for neutrons). Unweighted mean values are also given for x-rays (excluding the earliest measurement at $1.39(2) \text{ \AA}$, and the high temperature measurement at $1.38(1) \text{ \AA}$, denoted by *), neutrons, and both together, along with the standard deviations in parentheses. The r_{BO} obtained as part of high-pressure studies are systematically lower, with larger uncertainties, and have also been excluded (denoted by †). The r_{BO} from Suzuya *et al.*³¹⁶ was determined by our own Fourier transform and peak fitting to their data (denoted by ‡). In the final row is the mean B–O bond length in crystalline B_2O_3 -I, calculated from the crystallographic unit cell by averaging over the six unique bonds present. Notably the value thus obtained is slightly different from the 1.372 \AA quoted by Gurr *et al.*³¹⁷ Furthermore it should be noted that crystallographic bond lengths

are determined from the long-range average structure, as opposed to the local structure probed by total scattering diffraction, and can in cases with local disorder differ appreciably.

r_{BO} (Å)	R	Q_{max} (Å ⁻¹)	Mod. function	Year	Authors	Ref
1.39(2)*	X Cu & Mo $K\alpha$	11.3	Step	1936	Warren, Krutter & Morningstar	318
1.37	X Cu & Rh $K\alpha$	20	Gaussian	1970	Mozzi & Warren	301
1.38(1)*	X Mo $K\alpha$ @ 973K	15	Step	1995	Sugiyama, Nomura & Kimura	319
1.3656(5)‡	X 40.9 keV sync.	24.47	Lorch	2000	Suzuya <i>et al.</i>	316
1.3600	X 61.5 keV sync.	25	?	2003	Kajinami <i>et al.</i>	320
1.351(10)†	X E dispersive	10	?	2008	Brazhkin <i>et al.</i>	321
1.3765(5)	X 100 keV sync.	24.47	Lorch	2015	Alderman <i>et al.</i>	315
1.3680(70)	Mean X					
1.366	N pulsed	40	Lorch	1982	Johnson, Wright & Sinclair	322
1.375	N pulsed	36	?	1990	Misawa	323
1.365(1)	N pulsed	44.56	Lorch	1994	Hannon <i>et al.</i>	12
1.3655(2)	N pulsed	40	Lorch	2009	Hannon, Barney & Holland	324
1.347(10)†	N pulsed	19.5	step	2014	Zeidler <i>et al.</i>	325
1.353(10)†	N reactor	21.7	step	2014	Zeidler <i>et al.</i>	325
1.3741(2)	N pulsed, V cell	38.8	Lorch	2025	Alderman	326
1.3732(5)	N pulsed, Pt cell	38.8	Lorch	2025	Alderman	326
1.3698(48)	Mean N					
1.3691(54)	Mean					
1.371(20)	X crystallography	n.a.	n.a.	1970	Gurr <i>et al.</i>	317

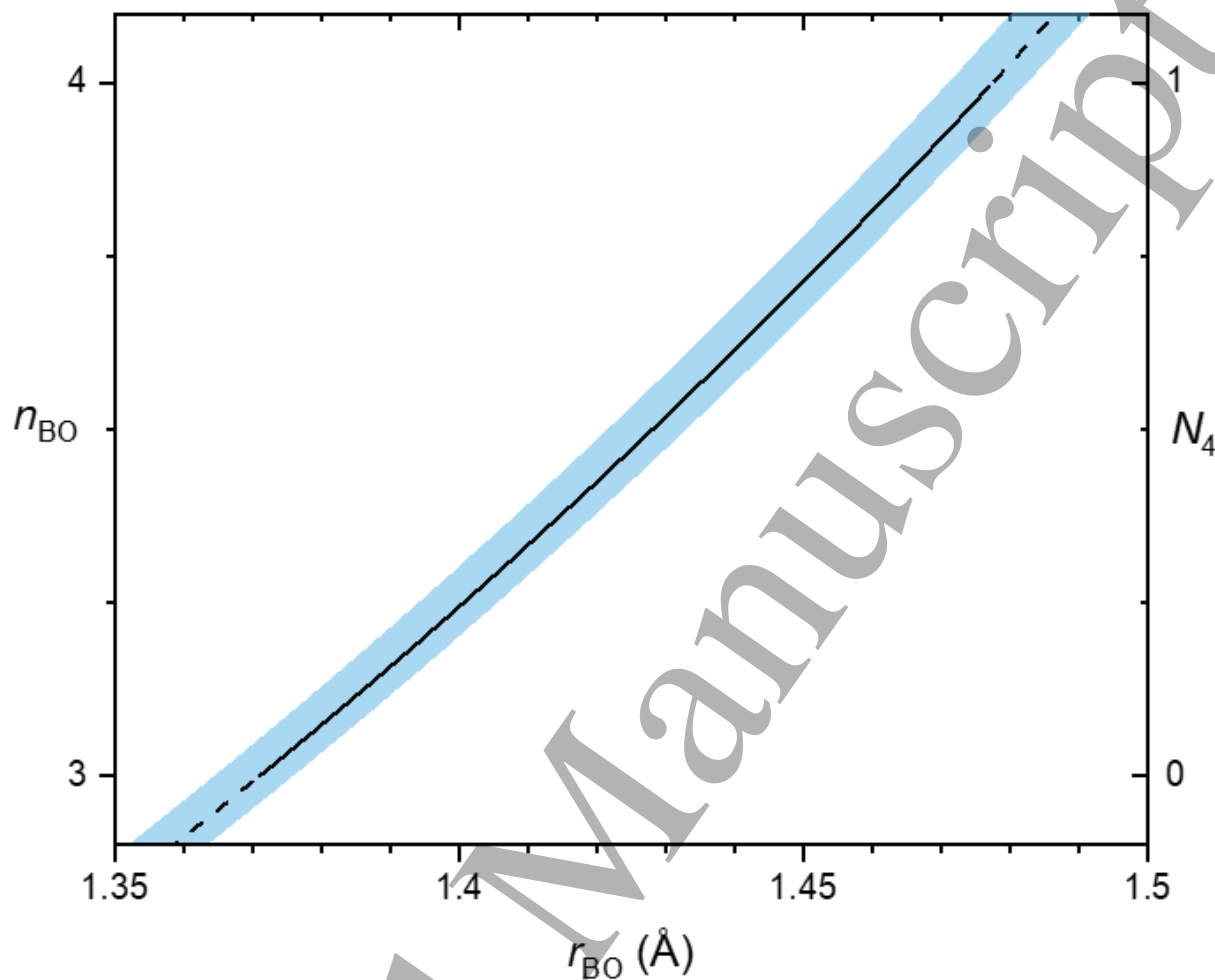


Figure 4.5: Exponential relationship between $n_{BO} = N_4 + 3$ and mean bond length r_{BO} , using the bond-valence methodology for equivalent bonds, equation 4.36. The black curve uses the standard BV parameters from Brown and Altermatt³¹⁴ ($b = 0.37$ Å and $R_{BO} = 1.371(1)$ Å). The blue shaded area represents the uncertainty bounds inferred from the range of measured r_{BO} in pure B_2O_3 glass, Table 4.3. Specifically, based on $R_{BO} = 1.365(1)$ Å¹² and $R_{BO} = 1.3765(5)$ Å³¹⁵.

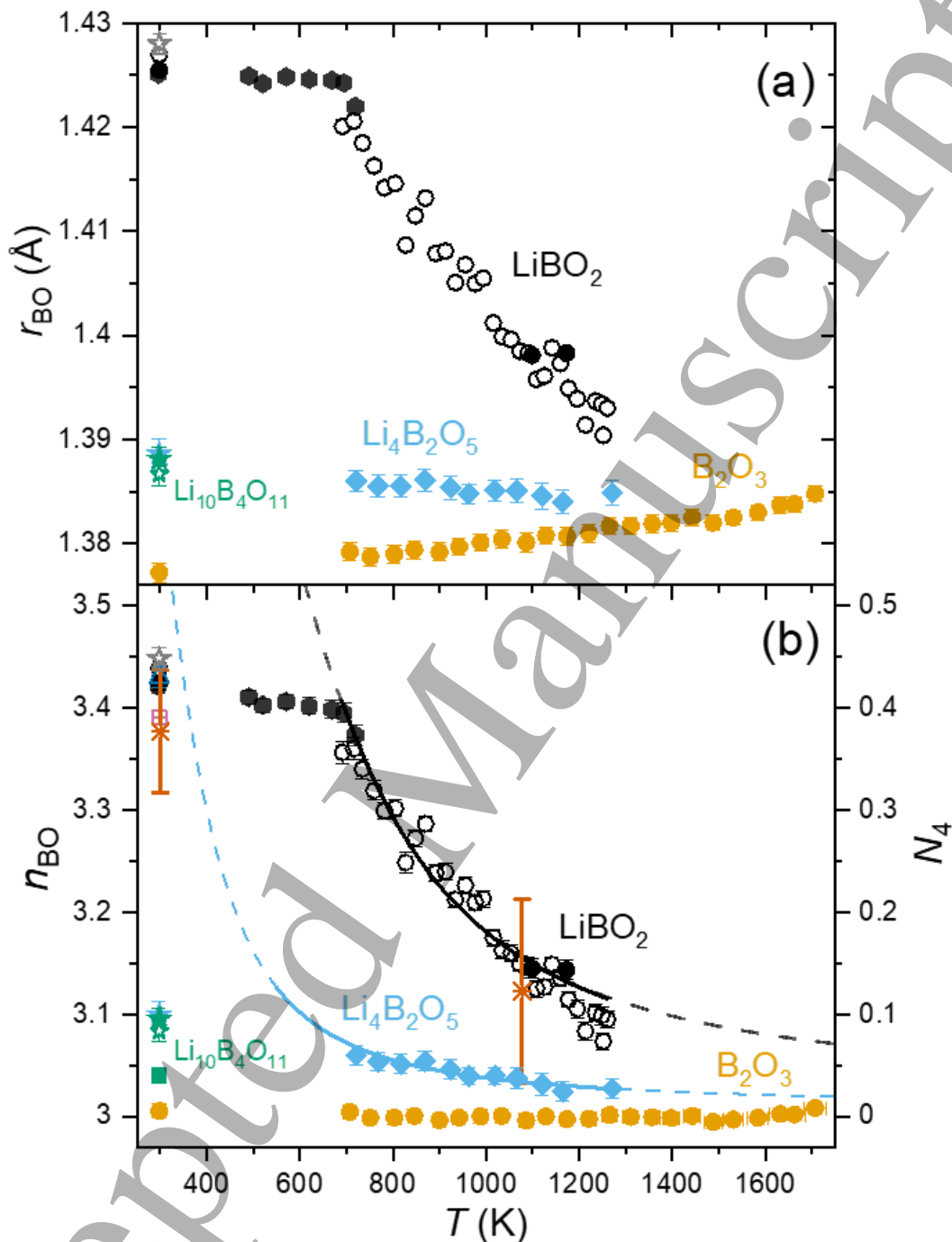


Figure 4.6: High-energy x-ray diffraction results for the (a) Mean B–O bond lengths, $r_{BO}(T)$ and (b) Mean B–O coordination numbers, $n_{BO}(T)$, as derived from $r_{BO}(T)$ using the temperature dependent bond-valence method^{294,311}, for $\text{Li}_4\text{B}_2\text{O}_5$ ³¹², LiBO_2 ²⁹⁵ and B_2O_3 ³¹⁵ melts and glasses, as well as $\text{Li}_{10}\text{B}_4\text{O}_{11}$ glasses³¹². The curves are the results of van't Hoff analysis based on the $[\text{BØ}_4]^- \rightleftharpoons [\text{BØ}_2\text{O}]^-$ (and related) coordination changing isomerization reaction(s), with dashed extrapolations. Exemplary N_4 values from ^{11}B NMR are shown for comparison in (b) for LiBO_2

(blue triangle⁴², pink crossed square¹⁷⁴) and $\text{Li}_{10}\text{B}_4\text{O}_{11}$ (green square⁸¹), and from non-resonant inelastic x-ray scattering for LiBO_2 (orange double crosses³²⁷).

4.3.4 Holistic bulk structural modeling using diffraction data

Popular methods for diffraction data analysis include those which refine space-filling three dimensional models of atomic configurations to the measured structure factors. These include Reverse Monte Carlo (RMC), Empirical Potential Structure Refinement (EPSR) and its successor Dissolve. As far as determining N_4 values is concerned, this might be considered analogous to the peak fitting methods discussed above, but with a more holistic consideration of the longer r contributions, and with the constraint(s) that the model be consistent with a chemically and physically plausible arrangement of atoms at the measured bulk density.

4.4 Diffraction studies of binary borate glasses

4.4.1 Monovalent alkali and group 11 modifiers

N_4 data compiled from diffraction experiments on alkali and silver borate glasses are plotted in Figure 4.7. The diffraction data are shown as filled coloured symbols such that they stand out against the representative N_4 data from NMR shown as open grey symbols. Taking an overview in this way, it becomes immediately apparent that the majority of the diffraction data are limited to modifier contents $R < 0.5$ where, largely, both diffraction and NMR measurements indicate that $N_4 = R$. The only examples of diffraction measurements of N_4 in highly modified (alkali or silver) binary borate glasses are those of Wright *et al*³²⁸ for an $R = 2.13$ rubidium borate, and those of Alderman *et al*^{295,312} for $R = 1, 2$ and 2.5 lithium borates. Interestingly, at such high modification levels ($R \geq 2$), the observed $N_4 > 0$ imply the presence of either non-bridging oxygen associated with tetrahedral boron units (e.g. $[\text{BO}\emptyset_3]^{2-}$) or a disproportionation into large borate polyanions centered around e.g. $[\text{B}\emptyset_4]^-$ metaborate units (e.g. $[\text{B}\emptyset_4 \cdot 4(\text{BO}_2\emptyset)]^{9-}$), along with orthoborate $[\text{BO}_3]^{3-}$. Given that NMR studies indicate a decrease in N_4 with increasing alkali mass^{35,36,81}, at least in the $0.5 < R < 1$ composition range, it would be instructive to confirm this result using neutron diffraction on a glass series in this range, as a function of alkali, to complement the study of Wright *et al*²⁵⁵ at $R = 0.4$.

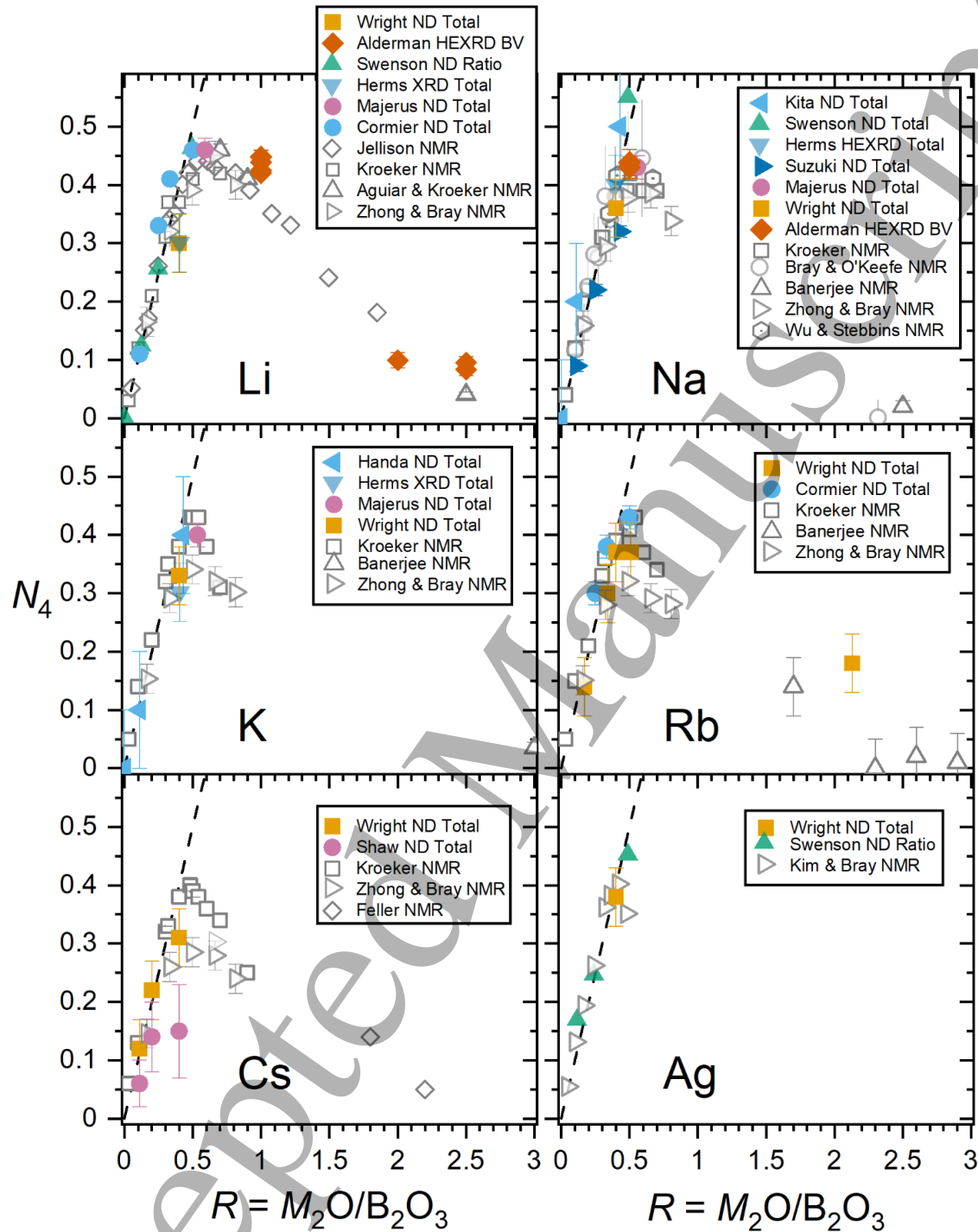


Figure 4.7: $N_4 = n_{BO} - 3$ values for M_2O - B_2O_3 borate glasses with monovalent modifier cations. For Li, using pulsed ND³²⁹, reactor ND^{255,292,330}, HEXRD^{295,310,312} and NMR^{34,35,36,81}. For Na using pulsed ND^{329,331} (including 1073 K melts by Kita *et al.*³⁰⁸), reactor ND^{255,292}, HEXRD^{310,311} and NMR^{28,35,36,78,99}. For K using pulsed ND³³², reactor ND^{255,292}, HEXRD²² and NMR^{35,36,78}. For Rb using reactor ND^{255,328,333} and NMR^{35,36,78}. For Cs using pulsed ND³³⁴, reactor ND^{255,328} and NMR^{35,36,79,81}. For Ag using pulsed ND³²⁹, reactor ND²⁵⁵ and NMR⁵³.

4.4.2 Divalent alkaline earth and group 12 modifiers

For the divalent alkaline earth and group 12 transition metals, Figure 4.8, there are far fewer diffraction data available, with no measurements at all for Mg or Cd. The largest number of diffraction studies in this category focus on Ba borate glasses, showing good agreement with NMR and IR studies. Kajinami *et al*³³⁵ used a laboratory source of Mo $K\alpha$ x-rays to study zinc borate glasses, and reported fitting parameters for a BO_3 and BO_4 2-peak fit. In addition to the total n_{BO} (N_4) reported, these allow us to calculate N_4 using the ratio and BV methods, both of which give improved agreement with the trend of decreasing N_4 with increasing R observed by NMR. The data are less accurate than those obtained with NMR due to the Zn ions dominating the x-ray scattering, and the relatively small $Q_{\text{max}} = 12 \text{ \AA}^{-1}$. Nonetheless, this points towards the importance of reporting all fitting parameters, as well as calculating N_4 by multiple methods. As for the alkali borate glasses, it would be instructive to perform neutron diffraction on a glass series in the $0.5 < R < 1$ composition range, as a function of divalent modifier, given that IR spectroscopic data indicate the opposite trend to the alkali case, that is, an increase in N_4 with increasing alkaline earth mass²⁵⁷. There is quite a large spread in datasets for Ca borate glasses, and this is discussed further in section 5.

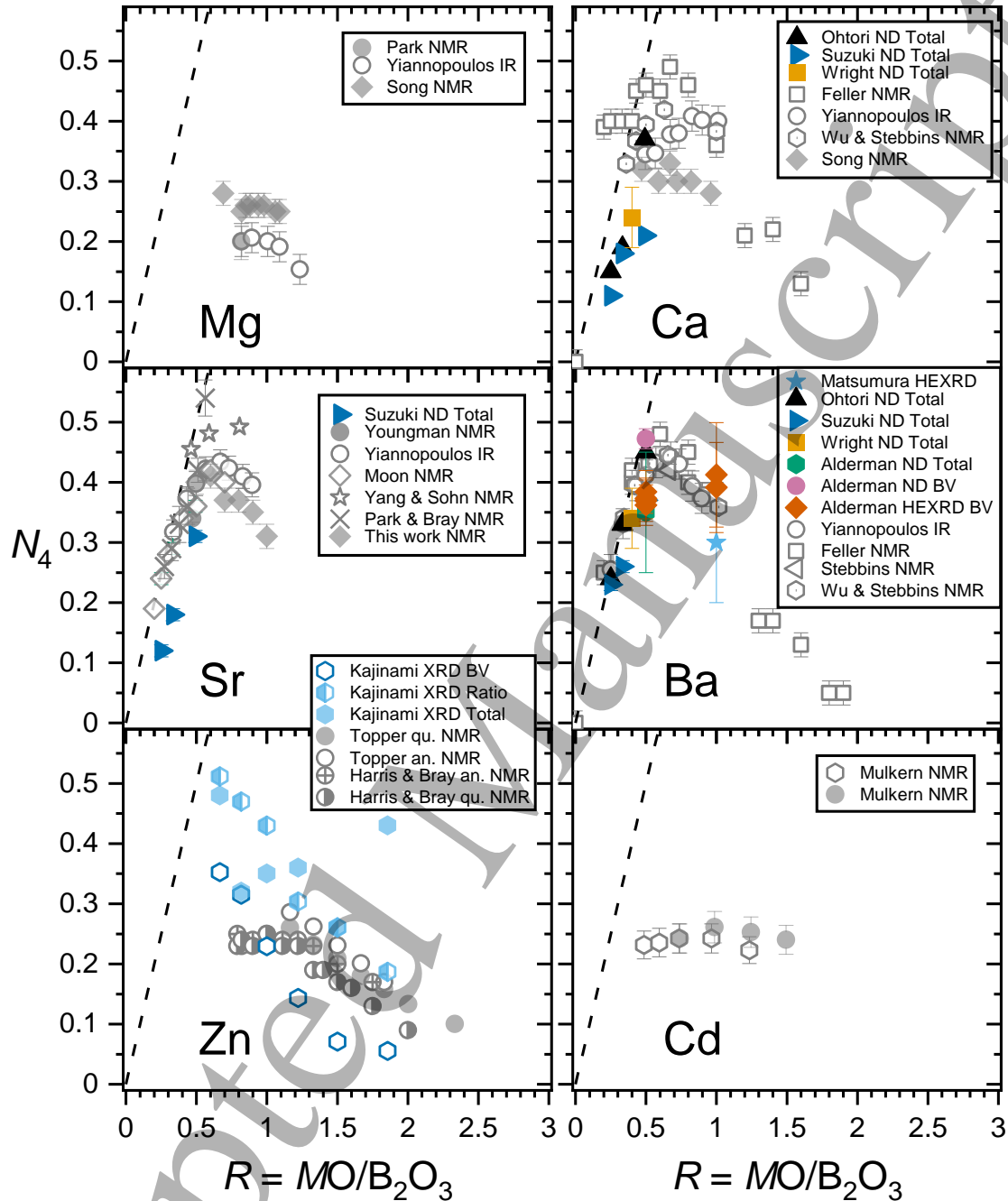


Figure 4.8: $N_4 = n_{BO} - 3$ values for $MO-B_2O_3$ borate glasses with divalent modifier cations. For Mg using NMR⁵⁵ and IR²⁵⁷. For Ca using pulsed ND^{258,331}, reactor ND²⁵⁵, NMR^{92,99} (data from Song *et al.*¹³⁷ have been corrected as discussed above) and IR²⁵⁷. For Sr using pulsed ND³³¹, NMR^{52,67,132,336} including the NMR data from the present work (Fig. 2.12), and IR²⁵⁷. For Ba using pulsed ND^{258,259,331}, reactor ND²⁵⁵, HEXRD^{259,337}, NMR^{39,92,99} and IR²⁵⁷. For Zn using Mo $K\alpha$ XRD³³⁵ and NMR^{61,135} (for both quenched and annealed glasses). For Cd using NMR⁶².

4.4.3 Tl⁺ borate glasses

The thallium borate glasses are an unusual case where $N_4 > R$ were originally observed by Baugher and Bray using NMR methods⁴⁹, Figure 4.9. Since that time, both ¹¹B NMR and pulsed neutron diffraction were applied to the Tl₂O-B₂O₃ glasses as part of the PhD thesis research of Nattapol Laorodphan⁹³. Lower N_4 than those reported by Baugher and Bray⁴⁹ were found using both techniques, but nonetheless, the glasses from 5 to 30 mol% Tl₂O were all found to have excess tetrahedral boron, with $N_4 > R$, Figure 4.9. The neutron diffraction results were obtained by constrained fitting of two peaks to the B–O bond length distribution, fixed at the positions expected from BV. However, it is not clear if the ratio method, or the absolute areas of the peaks were used to derive the N_4 values. Unfortunately, the mean B–O bond lengths were not reported, which would provide a highly instructive check on the N_4 using the BV method. This is especially so given both the considerably atypical $N_4 > R$, as well as the large values of $N_4 > 0.5$, for $R > 0.5$, which is something rarely seen for any binary borate glasses, as is evident from this review. Laorodphan discusses possible reasons for the $N_4 > R$ observations, including the possibility of water attack, for which there was some evidence for in Raman spectra (at low Tl₂O content), and which could be exacerbated in the ¹¹B NMR measurements due to the pulverization of the samples prior to measurement. It was also noted that for two crystalline compounds known to have $N_4 = R$ from their crystal structures, $N_4 > R$ was observed by NMR, which at least raises the possibility that the same systematic effect could be at play for the glasses. The neutron diffraction data would be relatively sensitive to water content, but do not appear to show evidence for this, consistent with the fact that larger glass fragments were used in those measurements. Nonetheless, confidence in the neutron diffraction derived N_4 would be enhanced considerably if error bars could be calculated, and if agreement was found using the mean bond lengths and BV based methodology. Such confirmation should be sought before concluding that unusual structural units, such as oxygen triclusters (oxygen bonded to three boron atoms), are present to charge balance excess tetrahedral boron, such as in the high-pressure B₂O₃-II phase, or other $N_4 = 1$ structures, including SrB₄O₇ and PbB₄O₇.

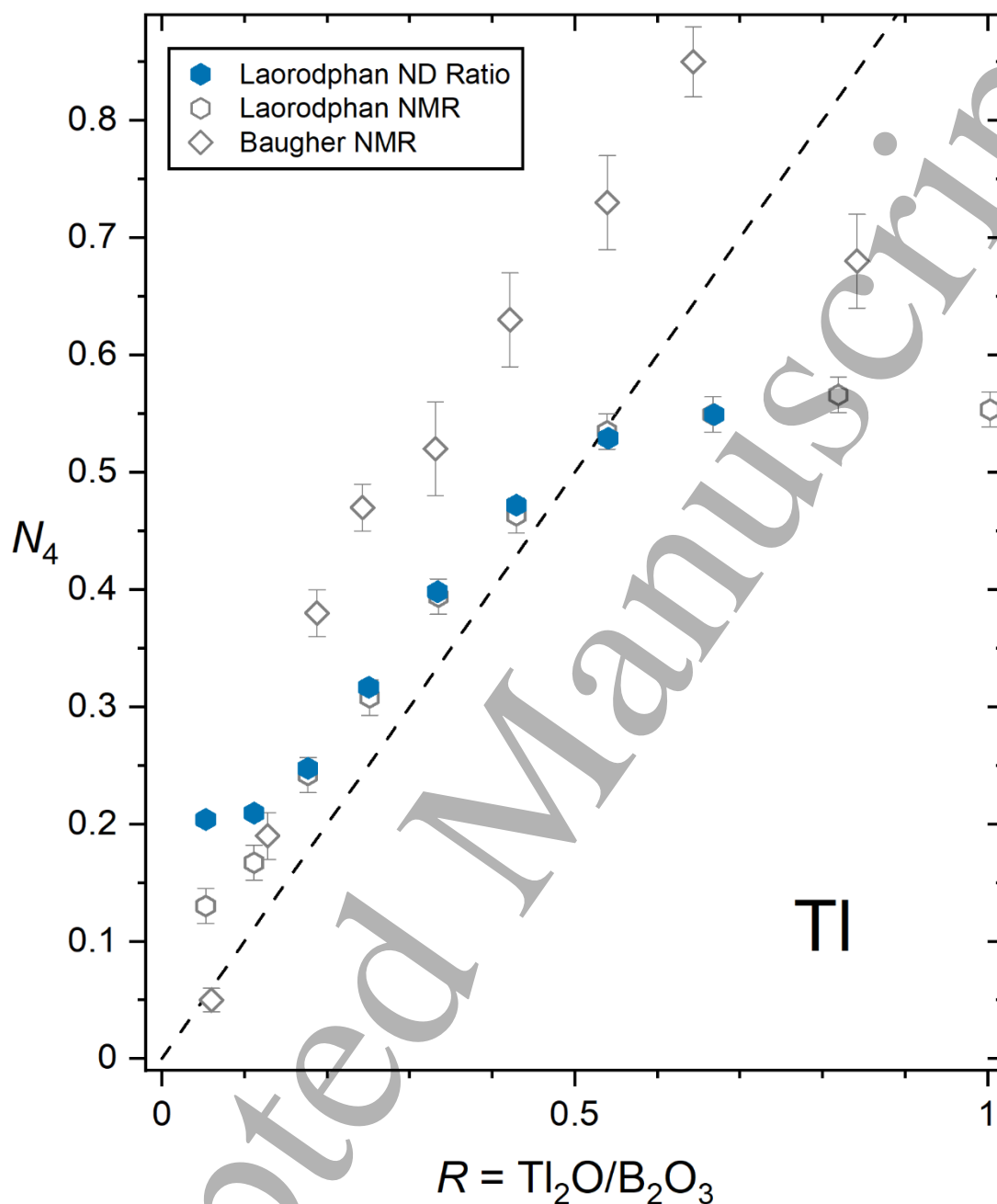


Figure 4.9: $N_4 = n_{\text{BO}} - 3$ values for $\text{Ti}_2\text{O}-\text{B}_2\text{O}_3$ glasses from the pulsed neutron diffraction study of Laorodphan *et al.*⁹³ along with the ^{11}B NMR data from the same study and from Baugher and Bray⁴⁹.

4.4.4 Mn^{2+} borate glasses

Kajinami *et al.*³²⁰ studied $\text{MnO}-\text{B}_2\text{O}_3$ glasses using 61.5 keV synchrotron x-rays. The authors used alumina crucibles, which can lead to contamination of the melts³²⁴. They state that compositions were checked by inductively coupled plasma atomic emission spectroscopy, but do not present the results. They do not discuss taking any precautions to prevent the formation of

1
2
3 Mn³⁺, the melting temperature being 1423 K. Nonetheless, the reported coordination numbers
4 yield N_4 in reasonable agreement with the wide-line NMR study of Park and Bray⁵⁷, Figure 4.10,
5 other than the outlier at $R = 0.79$ with unusually high $N_4 = 0.72$. We have used the mean B–O bond
6 lengths reported in the same study to calculate N_4 by the BV method, using their self-consistent
7 r_{BO} reported for B₂O₃ glass as the bond-valence parameter R_{BO} , see Figure 4.10. Not only is good
8 agreement observed with the reported $N_4 = n_{BO} - 3$ in the $0.27 \leq R \leq 0.54$ range, but remarkably,
9 at $R = 0.79$ we find $N_4 = 0.34$, in much closer alignment with the NMR of Park and Bray⁵⁷, and
10 the IR study of Möncke *et al.*²⁶⁶ at $R = 1$. Overall, the behavior of Mn²⁺ borate glasses, in terms of
11 N_4 , appears to be rather similar to barium borate glasses, as opposed to the higher field strength
12 Zn²⁺ and Mg²⁺ borate glasses which tend to have lower N_4 for a given composition. This is despite
13 the fact that Mn²⁺ has a field strength intermediate between Mg²⁺ (and Zn²⁺) and Ca²⁺, which could
14 imply an important effect of the 3d electrons on the bonding and resultant N_4 . We should caveat
15 this with cautionary statements regarding all of the studies represented in Fig. 4.10, including the
16 aforementioned possibility of contamination and multivalent Mn in the x-ray diffraction work, the
17 inherent challenges in collecting and quantifying NMR spectra from strongly paramagnetic
18 glasses, and the uncertainty in relative infrared absorption coefficient, α_r . Indeed, using the $\alpha_r \approx$
19 1.73 estimated herein for Mn²⁺, Table 3.1, yields a revised value of $N_4 = 0.32(2)$ at $R = 1$, based
20 on the IR data of Möncke *et al.*²⁶⁶, and as shown in Fig. 4.10.
21
22
23
24
25
26
27
28
29
30
31
32
33
34
35
36
37
38
39
40
41
42
43
44
45
46
47
48
49
50
51
52
53
54
55
56
57
58
59
60

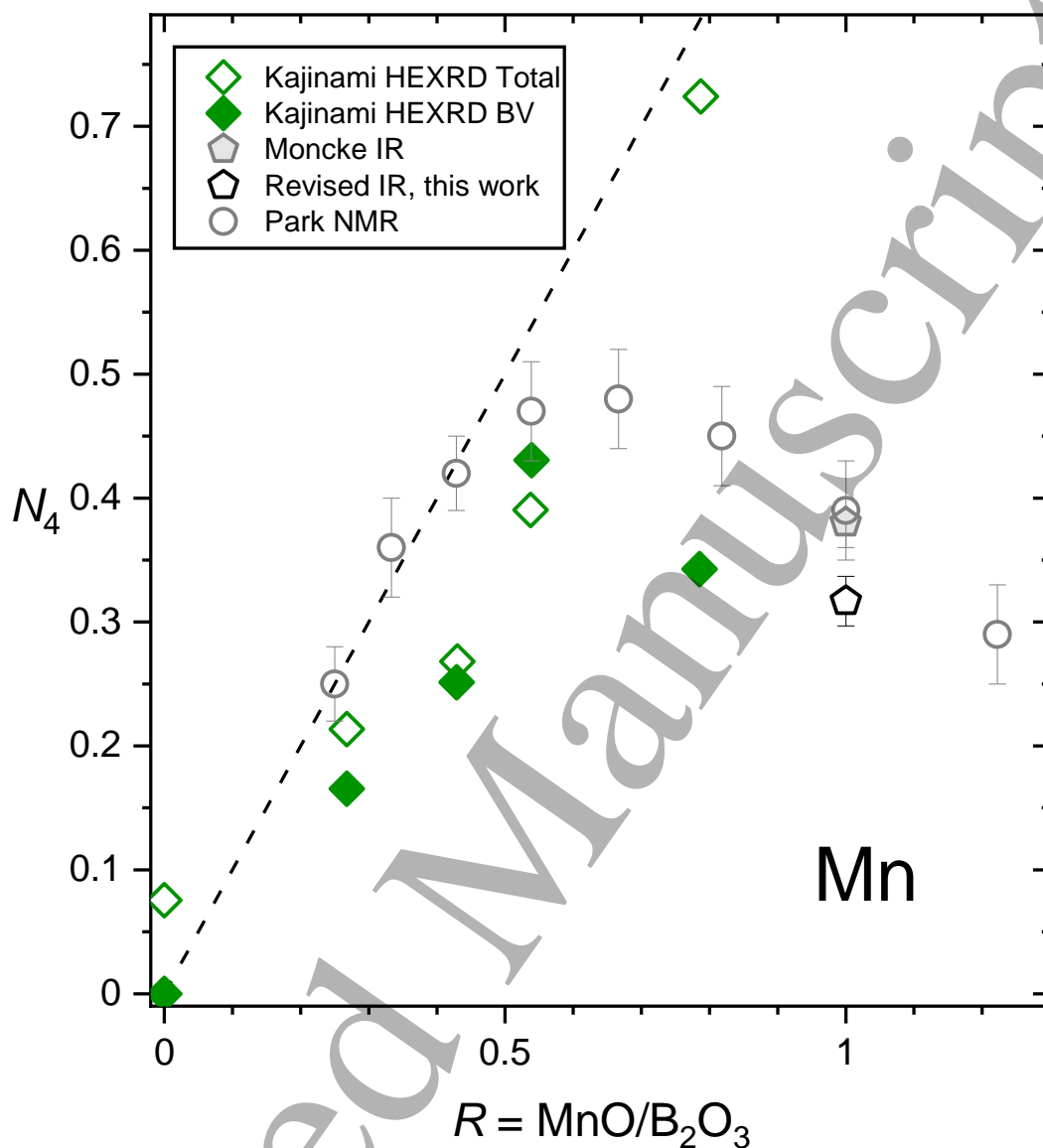


Figure 4.10: $N_4 = n_{\text{BO}} - 3$ values for MnO-B₂O₃ glasses from the high-energy x-ray diffraction study of Kajinami *et al.*³²⁰, digitized from their Figure 3. The mean B–O bond lengths digitized from the same figure were also used to calculate N_4 using the bond valence method, and using $R_{\text{BO}} = 1.360 \text{ \AA}$ from their r_{BO} measured for pure B₂O₃. Also shown is the IR reflectance spectroscopic determination of N_4 for manganese metaborate from Möncke *et al.*²⁶⁶, a revised value based on the $\alpha_r \approx 1.73$ estimated herein for Mn²⁺, Table 3.1, and the wide-line NMR derived data of Park and Bray⁵⁷.

4.4.5 Sn²⁺ and Pb²⁺ borate glasses

There are relatively few diffraction studies of binary tin borate glasses, Figure 4.11. We are aware only of the reactor neutron diffraction measurement by Gejke *et al.*³³⁸ on tin metaborate, up to the rather limited $Q_{\text{max}} = 10 \text{ \AA}^{-1}$, where they report a range of N_4 between 0.0 and 0.5 that is

consistent with their observed structure factor, with a most probable value of $N_4 = 0.3$. Hannon, Barney and Holland report on a detailed neutron diffraction study of tin borate based glasses³²⁴, melted in alumina crucibles. This led to contamination by between 3 and 9 mol% Al_2O_3 , as was well characterized and discussed by the authors, such that the glasses were in fact ternary tin aluminoborates, beyond the scope of the present review. Nonetheless, it is worth mentioning that with the corrected compositions, the authors found N_4 values in reasonable accord, if somewhat lower, than NMR on glasses made in both alumina^{324,339} and carbon³⁴⁰ crucibles. Again, we have used the mean B–O bond lengths reported in the same study to calculate N_4 by the BV method, using their self-consistent r_{BO} reported for B_2O_3 glass as the bond-valence parameter R_{BO} , see Figure 4.11. Remarkably, agreement with the NMR results is improved for all compositions, with a possible exception at the lowest tin content glass, where the same authors report a rather low N_4 from ^{11}B NMR, which is not in accord with earlier NMR studies, unlike their results for all other compositions.

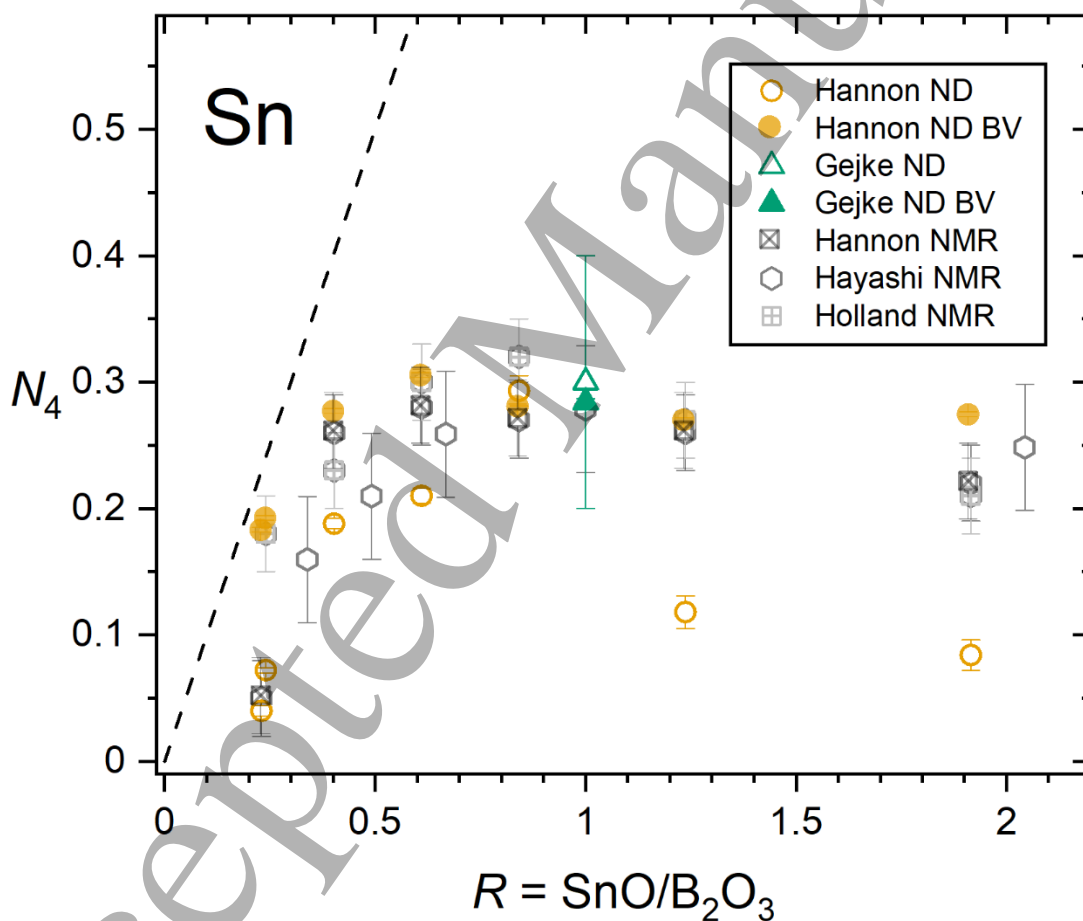


Figure 4.11: $N_4 = n_{\text{BO}} - 3$ values for $\text{SnO-B}_2\text{O}_3$ glasses from the pulsed neutron diffraction study of Hannon, Barney and Holland³²⁴ (containing 3 to 9 mol% Al_2O_3), and the reactor based neutron diffraction study of Gejke *et al.*³³⁸ Data from three ^{11}B NMR studies are shown for comparison^{324,339,340}.

Compared to tin borate glasses, lead borate glasses tend to have higher values of N_4 , see Figure 4.12. This implies that the higher-field strength lone-pair cation Sn^{2+} tends to bond somewhat more covalently, and demonstrates more network former character than does Pb^{2+} . The two pulsed neutron diffraction studies of $\text{PbO-B}_2\text{O}_3$ glasses^{263,264,306,341} show good agreement with both NMR and IR determinations of N_4 (Figure 4.12), including demonstrating the presence of tetrahedral boron at very high modifier contents.

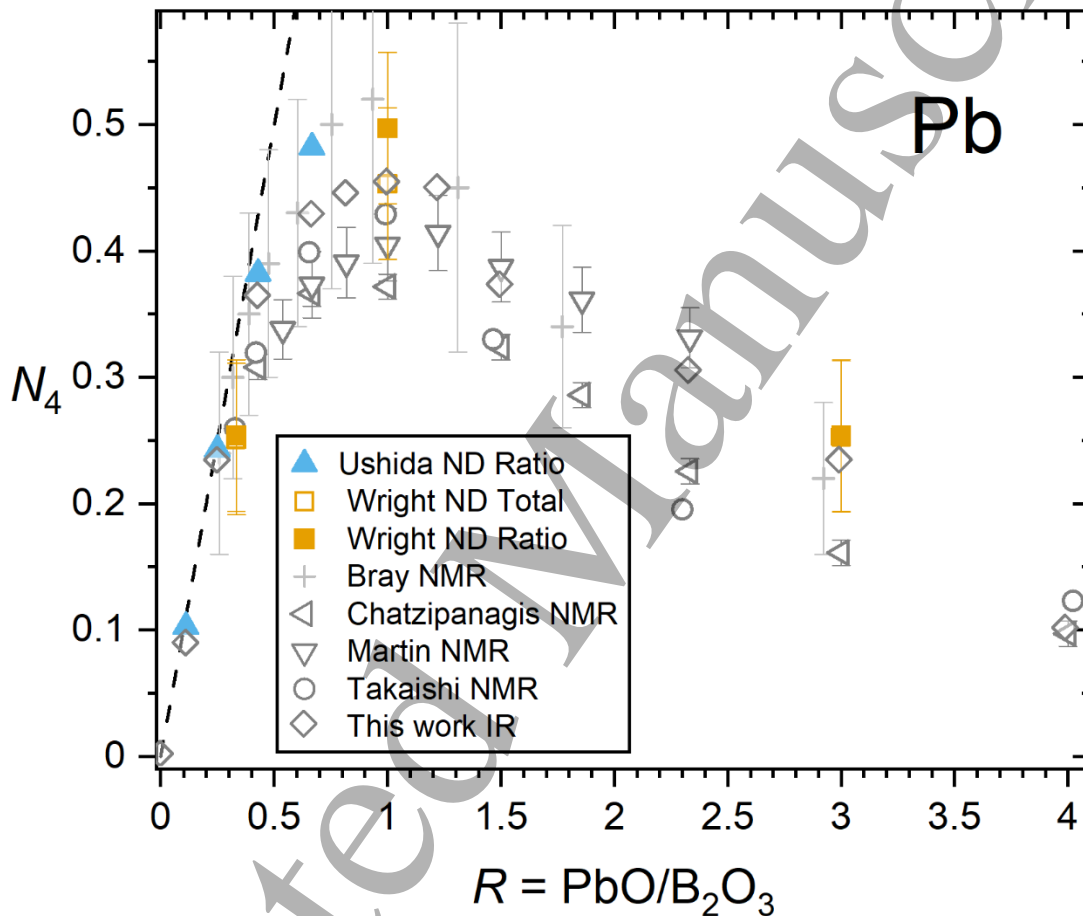


Figure 4.12: $N_4 = n_{\text{BO}} - 3$ values for $\text{PbO-B}_2\text{O}_3$ glasses from the pulsed neutron diffraction studies of Wright *et al.*^{255,307,341} and Ushida *et al.*²⁶⁵. Data from several ^{11}B NMR studies^{44,88,129,215} are also shown for comparison, along with the IR values determined in the present work.

4.4.6 Sb^{3+} and Bi^{3+} borate glasses

A single neutron diffraction study of antimony borate glasses has been reported in the PhD thesis of Robin Orman³⁴². The N_4 derived from the reported n_{BO} are plotted in Figure 4.13. Whilst Sb^{3+} is the primary modifying cation present, the Sb^{5+} content was reported to increase gradually with the total antimony content, up to about 14% of the total Sb at the highest nominal, 70 mol%, Sb_2O_3 composition⁷⁵. As can be seen, the N_4 in these glasses are remarkably low, in stark contrast

to Bi borate glasses (Figure 4.14), an observation which is analogous to the differences between the Sn and Pb borate glasses, but of greater magnitude. In other words, the Sb is apparently bonding largely covalently, with a strongly network forming character. Notably, using the $N_4 = n_{\text{BO}} - 3$ from the total B–O peak areas³⁴² leads to several unphysical negative results (Figure 4.13). This indicates systematic errors in the normalization of the diffraction data, rather than e.g. two-coordinated boron species, as can be concluded using the BV method to map the reported mean B–O bond lengths onto N_4 values. As can be seen in Figure 4.13, this leads to $N_4 \geq 0$, as expected, and much better agreement with the available ^{11}B NMR data^{74,75,175}, in all cases.

For bismuth borate glasses, again, only a single neutron diffraction study has been made^{341,343} and the N_4 derived from the reported n_{BO} are plotted in Figure 4.14. There is largely good agreement with available ^{11}B NMR⁸¹ and IR spectroscopic²⁷⁹ data, with the exception of the $R = 2$ diffraction measurement, and the $R = 1$ measurement derived using the peak ratio method, which is expected to be less reliable owing to the non-uniqueness of such fits.

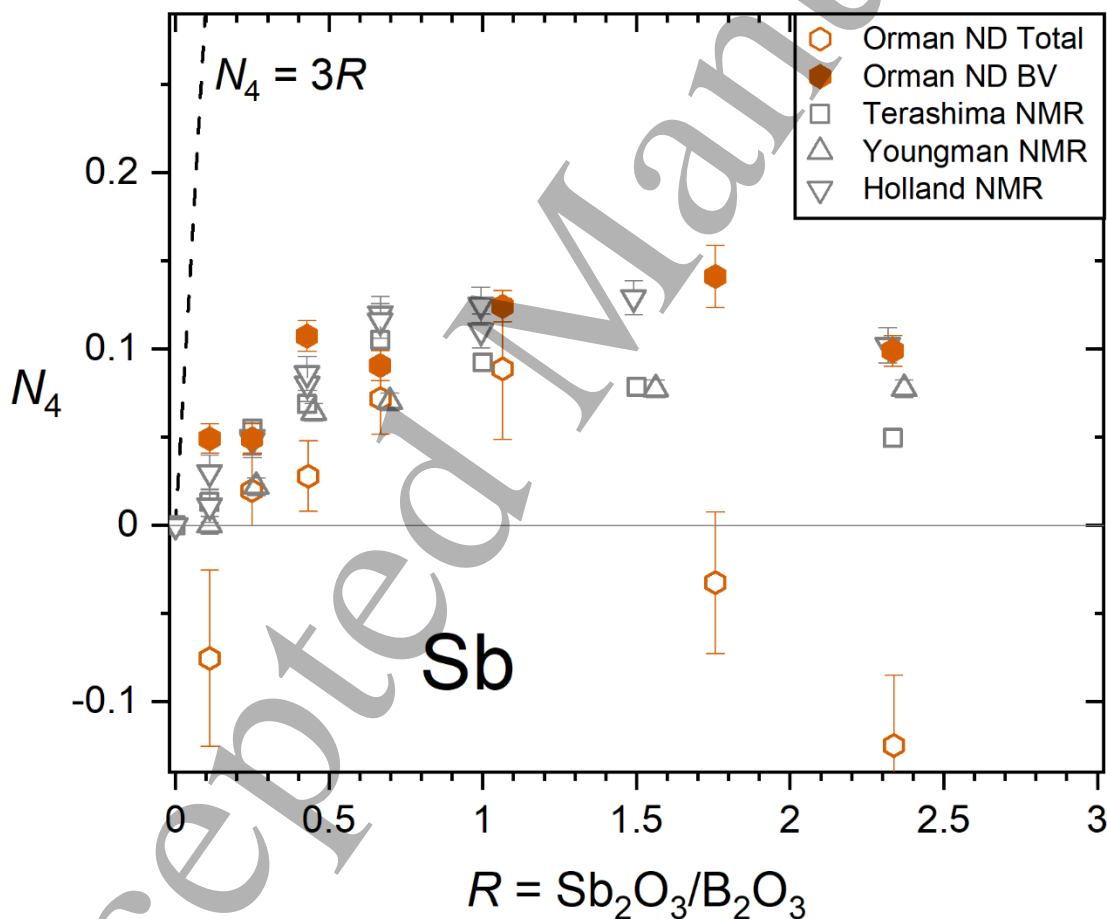


Figure 4.13: $N_4 = n_{\text{BO}} - 3$ values for $\text{Sb}_2\text{O}_3\text{-B}_2\text{O}_3$ glasses from the pulsed neutron diffraction study of Orman³⁴² N_4 derived from the total area of the B–O bond length distribution are plotted (open hexagons), as reported in the doctoral thesis of Orman. In addition, the mean bond lengths reported in the thesis, obtained from single peak fits to the B–O bond length distribution, have been used herein to derive N_4 via the bond valence method (filled hexagons), using $R_{\text{BO}} = 1.365(1)$ Å from

the pulsed neutron diffraction determination of n_{BO} by Hannon *et al.*¹² in pure B_2O_3 . Note that the antimony borate glasses were reported to contain between 1 and 14% (increasing with R) of the antimony in the Sb^{5+} oxidation state⁷⁵. Data from several ^{11}B NMR studies^{74,75,175} are shown for comparison.

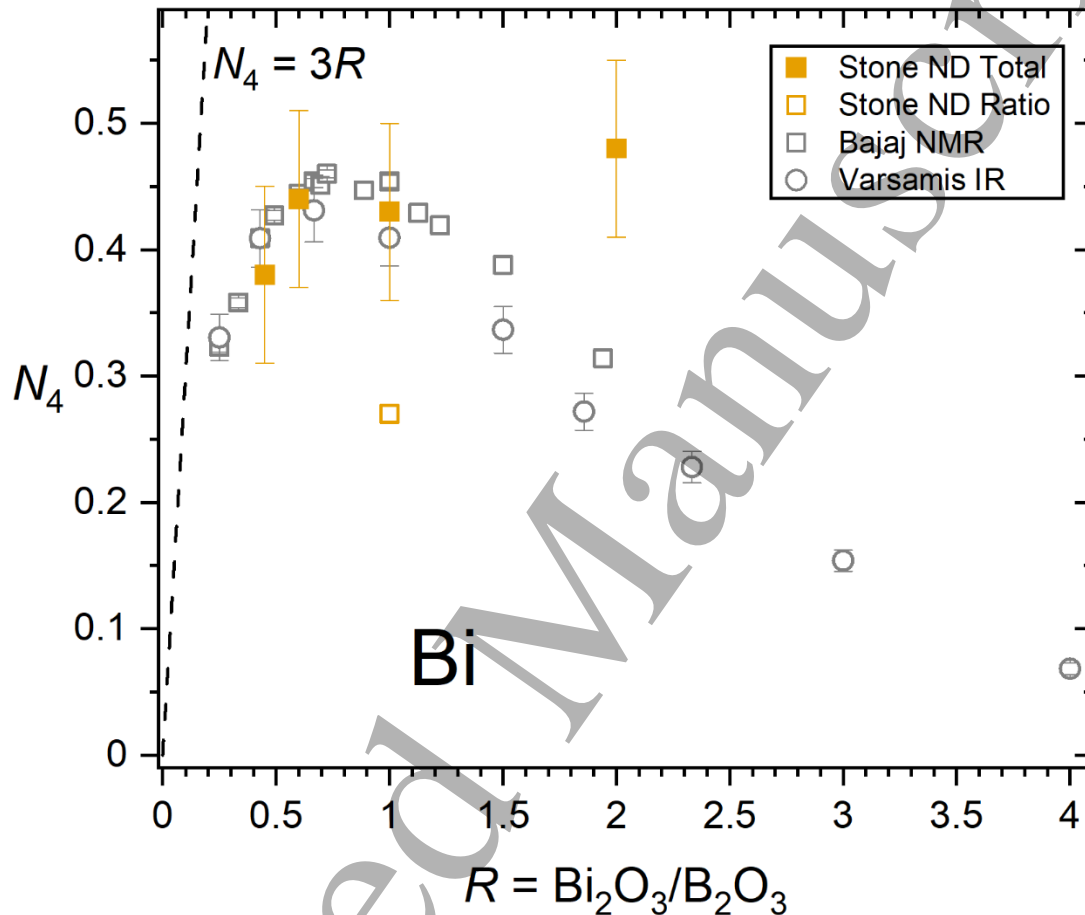


Figure 4.14: $N_4 = n_{\text{BO}} - 3$ values for Bi_2O_3 - B_2O_3 glasses from the pulsed neutron diffraction study of Stone *et al.*^{341,343}. Data from the ^{11}B NMR study of Bajaj *et al.*⁸³ and the infrared reflectance spectroscopy study of Varsamis *et al.*²⁷⁹ are shown for comparison.

4.4.7 Te^{4+} borate glasses

Tellurium borate glasses have been obtained at rather low boron contents, between R of 2 and 198⁶⁴. As such, one can consider tellurium as the primary network former (pure TeO_2 glass can also be obtained³⁴⁴, with difficulty). Remarkably, these binary borotellurite glasses have the highest N_4 values of any of the binary borate glasses reviewed herein, as measured by both neutron diffraction⁸⁴ and NMR⁶⁴, and ranging from 0.39 to 0.91, Figure 4.15. In this case, the N_4 derived from the n_{BO} reported by neutron diffraction are in excellent agreement with those derived from the mean B-O bond lengths and the BV method.

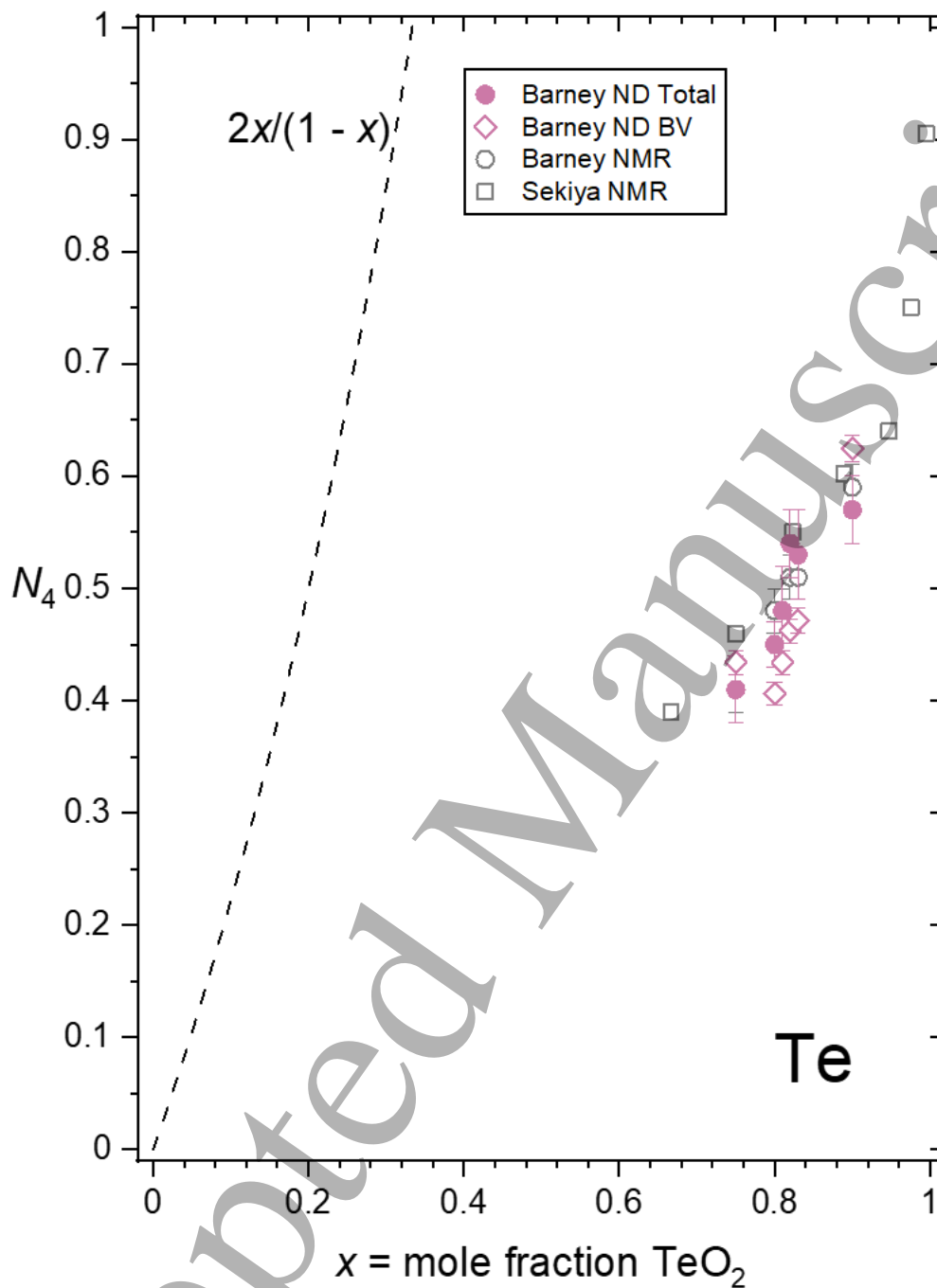


Figure 4.15: $N_4 = n_{\text{BO}} - 3$ values for $\text{TeO}_2\text{-B}_2\text{O}_3$ glasses from the pulsed neutron diffraction study of Barney *et al.*⁸⁴ along with the ^{11}B NMR data from the same study and from Sekiya *et al.*⁶⁴ Note that the abscissa is the mole fraction of TeO_2 , rather than a molar ratio as in the previous figures, because the $R = \text{TeO}_2/\text{B}_2\text{O}_3$ values are very large (3 to 9 for the ND study, 2 to 198 for the NMR study).

4.4.8 Water borate glasses

Early x-ray diffraction studies of water borate glasses ($\text{H}_2\text{O}-\text{B}_2\text{O}_3$) by Milberg & Meller in 1959³⁴⁵ ($R = 0$ and 0.33) and 1960³⁴⁶ ($R = 0, 0.42, 0.50$ and 0.63) indicated that the majority of boron were contained within trigonal planar units, but the “possibility that a small fraction of the boron atoms [were] coordinated by four oxygen atoms [was] not completely excluded”. Unfortunately, the uncertainties on the coordination numbers reported do not permit any quantitative assessment of N_4 values. Nonetheless, the authors’ conclusions were consistent with contemporary NMR measurements by Silver in 1960⁴³ who estimated an $N_4 = 0.05$ for an $R = 0.5$ water borate glass, with the spectrum for an $R = 0.6$ glass indicating a slightly lower, but non-zero, N_4 fraction. Meanwhile, for an $R = 0.4$ glass, obtained at higher temperatures, no resonance arising from tetrahedral boron was detected. Notably the three crystalline polymorphs of metaboric acid (HBO_2) provide precedent for tetrahedral boron in water borate structures, having N_4 values of 0, 0.33 and 1.0 for the orthorhombic, monoclinic and cubic forms respectively. Brüning & Patterson³⁴⁷ studied a large number of water borate glasses, from $R = 0$ to 1, and Brüning *et al*³⁴⁸. a large number of more water-rich liquids, by x-ray diffraction. They only measured to $Q_{\text{max}} = 7 \text{ \AA}^{-1}$, and do not calculate Fourier transforms or report coordination numbers or N_4 values. Wright³⁴⁹ gives an excellent discussion of water borate glasses and crystals in the context of the chemistry of B_2O_3 .

Overall, it is clear that knowledge regarding $\text{H}_2\text{O}-\text{B}_2\text{O}_3$ glasses and liquids could be improved upon using modern quantitative methods of structure and N_4 determination.

4.5 Diffraction studies of binary borate melts

One advantage of diffraction methods is that they view both glasses and melts in the same way, which is distinct to NMR methods where the timescales for nuclear spin relaxation play a key role. In particular, in high-temperature melts the exchange of boron between 3- and 4-coordinated environments becomes more rapid than the NMR timescale set by the relaxation time, and so only a single, site-averaged, resonance is observed^{287,350}. This means that N_4 cannot be quantified in melts by ^{11}B NMR in the same manner as proves so effective in the solid state. As such, diffraction methods have played a greater role in the elucidation of N_4 in borate melts, whilst ^{11}B NMR has been applied effectively for studies of glasses as a function of their *fictive* temperature. Alderman³⁵¹ reviewed structural studies of borate melts up to about 2017. All studies reviewed, including those by diffraction, show that N_4 tends to decline with increasing temperature, but the extent to which this happens is highly composition dependent. For example, the temperature dependence of N_4 is small at low Na_2O contents²⁹⁴, but is clearly significant at 33 mol% Na_2O , Figure 4.16³¹¹. Since the time of the review, a few further high-energy x-ray diffraction studies have shown a dramatic decline in N_4 with temperature for lithium metaborate²⁴⁷, Figure 4.6, a gradual decline for lithium pyroborate³¹², which has only a small N_4 fraction (Figure 4.6), and for barium metaborate and diborate²⁵⁹ similar $N_4(T)$ to sodium diborate were found, Figure 4.17. The complex temperature and composition dependence of $N_4(R,T)$ has been described within a simple boron coordination change isomerization model^{258,295,312}, and related to the configurational heat capacity and entropy contributions, as well as qualitatively to the fragility

indices. It is likely that, in general, the enthalpies and entropies of isomerization will depend not only on composition parameter R , as has been demonstrated, but also on the modifier identity. This could be verified by measurements on borate melts with other modifiers, as well as by calculating model $N_4(R, T)$ at the fictive temperature, T_f , (or glass transition temperature, T_g , as a proxy), for comparison to the N_4 measured for glasses, as reviewed herein.

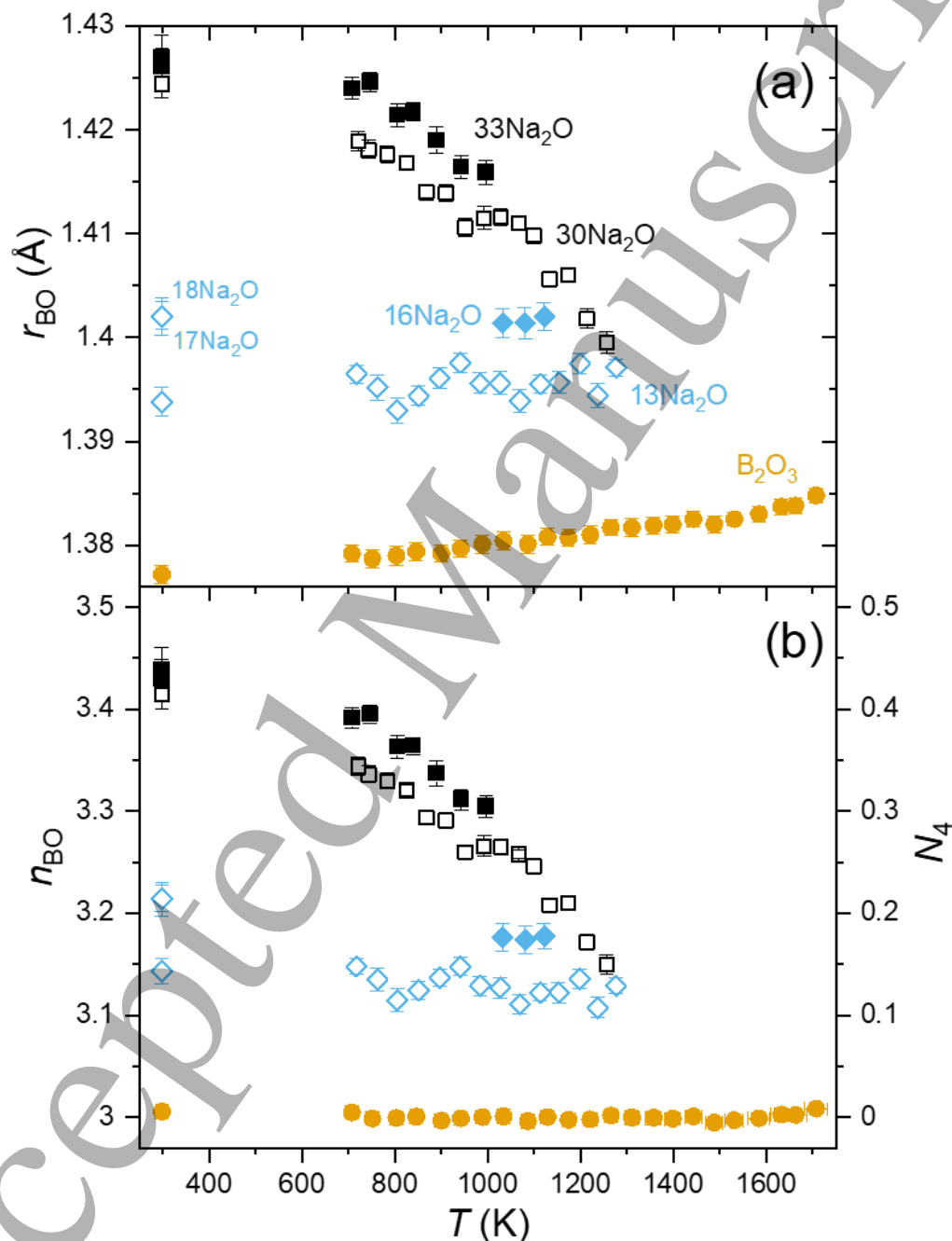


Figure 4.16: High-energy x-ray diffraction results for the (a) Mean B–O bond lengths, $r_{BO}(T)$ and (b) Mean B–O coordination numbers, $n_{BO}(T)$, as derived from $r_{BO}(T)$ using the temperature

dependent bond-valence method^{294,311}, for B_2O_3 ³¹⁵ and sodium borate melts and glasses^{294,311}. Molar percentages soda are indicated in part (a).

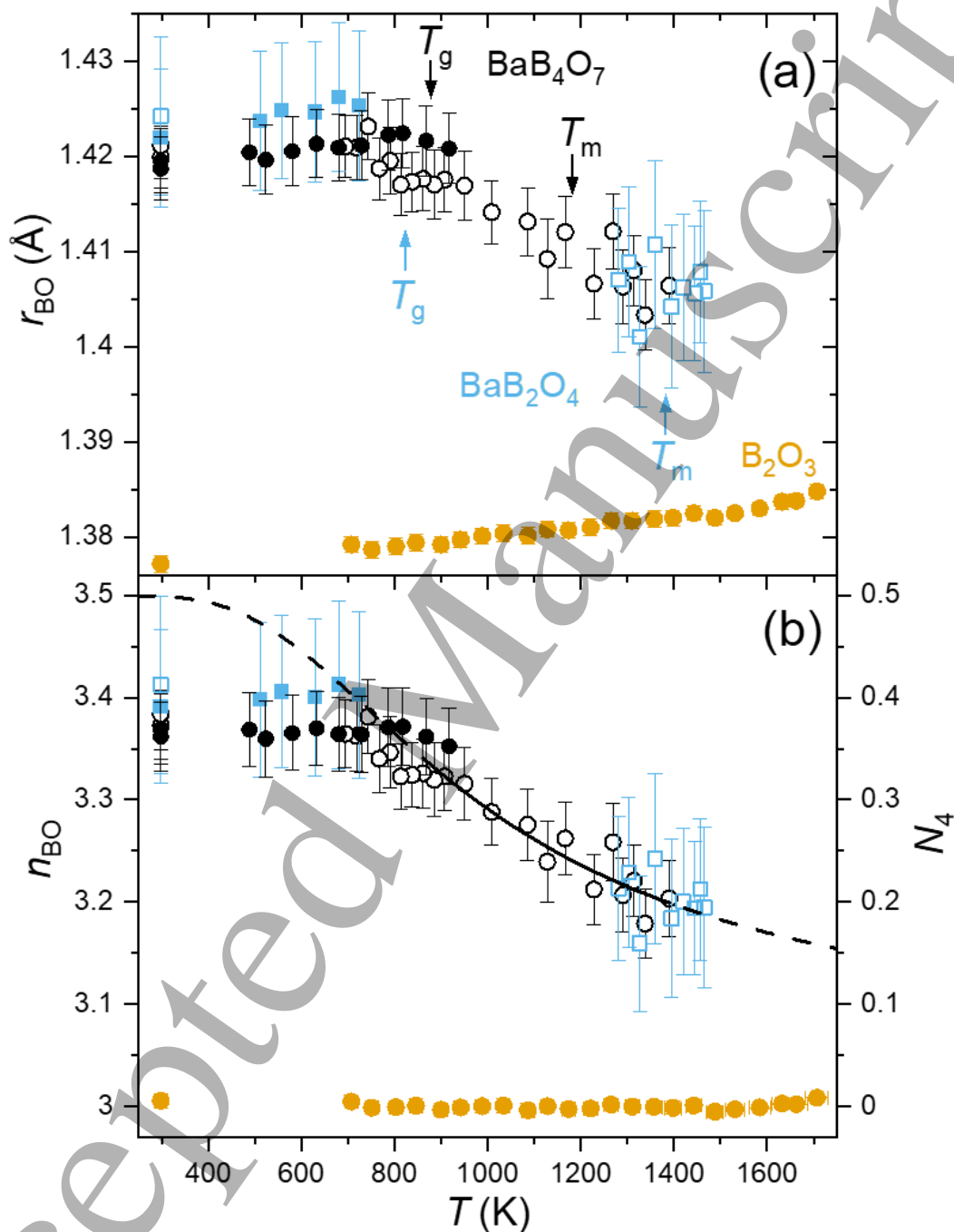


Figure 4.17: High-energy x-ray diffraction results for the (a) Mean B–O bond lengths, $r_{BO}(T)$ and (b) Mean B–O coordination numbers, $n_{BO}(T)$, as derived from $r_{BO}(T)$ using the temperature dependent bond-valence method^{294,311}, for B_2O_3 ³¹⁵ and barium borate melts and glasses²⁵⁹. The curve in (b) is the result of van't Hoff analysis for BaB_4O_7 , based on the $[B\emptyset_4]^- \rightleftharpoons [B\emptyset_2O]^-$ coordination changing isomerization reaction, with dashed extrapolations. Note the larger error

bars compared to the measurements on Li (Figure 4.6) or Na (Figure 4.16) borates, reflecting the dominance of the modifier (Ba) in the x-ray scattering signal.

4.6 X-ray spectroscopic and high-pressure studies of binary borate glasses and melts

Although this section of the review is focused on x-ray and neutron diffraction, x-ray spectroscopy has also been used to derive N_4 values in binary borate glasses and melts. In 1995 Li *et al.*³⁵² used soft x-rays and the total electron yield (TEY) method to observe B K-edge x-ray absorption near-edge structure (XANES) spectra in several potassium borophosphosilicate glasses, demonstrating that N_4 could be estimated by this method. Later, in 1999, Fleet and Muthupari³⁵³ applied the same method to borosilicate glasses, as well as a sodium diborate glass. In this work fluorescence yield (FY) spectra were collected simultaneously, which the authors point out is a more bulk-sensitive method (about 110 nm penetration depth) compared to TEY, the latter probing only about 6 nm into the surface. In 2001 a study from Yamamoto *et al.*³⁵⁴ built on the earlier work to study a series of binary sodium borate glasses with TEY B K-edge XANES spectroscopy. These authors showed that N_4 could be estimated from the spectra, mostly in good agreement with ¹¹B NMR.

Of particular note is the development of the non-resonant inelastic x-ray scattering method, also referred to as x-ray Raman scattering. This method is capable of providing spectra analogous to x-ray absorption spectroscopy, but uses high-energy x-rays, achieving greater bulk sensitivity, and obviating the need for the soft x-rays and ultra-high vacuum otherwise required for observing the boron K-edge. This method has been applied to the study of levitated liquid and glassy lithium borates³²⁷ (Figure 4.6b) as well as to cold-compressed borate glasses at up to 30 GPa^{355,356}. The high-pressure work indicates a dramatic increase in N_4 for pure B₂O₃ and Li₂B₄O₇ glasses above 4 GPa, approaching $N_4 = 1$ for the highest pressures studied³⁵⁶. Meanwhile the increase in N_4 for Na₂B₄O₇ glass was shown to be more gradual with pressure³⁵⁵.

Pure B₂O₃ has been studied at high pressures by both x-ray^{320,357} and neutron³²⁴ diffraction methods. High-pressure neutron diffraction of a 30(¹¹B₂O₃).70GeO₂ glass has been reported in the PhD thesis of Buscemi³⁵⁸.

4.7 Future prospects

It is clear from this review that despite decades of research into binary borate glasses using diffraction methods, there are still many gaps in knowledge to be filled. This is the case even if considering only the fundamental structural parameter N_4 . These gaps include:

1. There are still very few diffraction measurements of highly modified binary alkali or alkaline earth borate glasses, above the diborate composition ($R > 0.5$). This is despite this being a structurally rich region in which non-bridging oxygens begin to dominate over tetrahedral boron as charge-balancing species.

- 1
2
3
4
5
6
7
8
9
10
11
12
13
14
2. There are no diffraction measurements at all for Mg borate glasses, or for most of the transition metal and rare-earth borate glasses. X-ray diffraction measurements of some rare-earth borates have been made³⁵⁹ but since the heavy rare-earth ions dominate the x-ray scattering, N_4 were not determined. Neutron diffraction would be highly applicable here, at least for the rare-earth elements that do not have strong neutron absorption resonances. Diffraction methods have an advantage over standard ^{11}B NMR methods when it comes to paramagnetic glasses, due to paramagnetic relaxation enhancement induced broadening of the NMR spectra. Thus, diffraction methods should be taken advantage of for studying the structure of the paramagnetic rare-earth and transition metal borate glasses.

15
16
17
18
19
20

In terms of high-temperature and high-pressure measurements, the field is almost completely wide open, since only a handful of alkali and alkaline earth borate melt compositions have been studied at high temperature, and there are no *published* high-pressure diffraction studies of binary borate glasses known to the authors.

21
22
23
24
25
26
27
28
29
30

The success of the bond-valence based approach to precise and accurate determination of B–O coordination numbers, using the mean B–O bond length as proxy, is evident from this review, especially in figures 4.10, 4.11 and 4.13, as well as in the temperature dependent studies of Alderman *et al.* (e.g. Figure 4.6). Therefore, we call on all future authors reporting on diffraction measurements of borate glasses to report the mean B–O bond length if at all possible. Furthermore, to use this as a check on the directly determined coordination number, and if necessary, to provide a more precise and accurate estimate of n_{BO} and N_4 via the bond-valence method.

31 32 33 34

5. Conclusions

35
36
37
38
39
40
41
42
43

It is clear from this review that in the almost nine decades since the first measurements of N_4 in binary borate glasses by x-ray diffraction, the ability to study this aspect of borate glass structure has been transformed by the advent of new technologies and methodologies. In particular the application of nuclear magnetic resonance spectroscopies to the boron isotopes, especially ^{11}B , has become the most commonly applied technique, and gold standard for N_4 quantification, nowadays most commonly by high-field magic angle spinning, with requisite correction for the intensity in the spinning sidebands.

44
45
46
47
48
49
50
51
52
53
54
55
56
57
58
59
60

Infrared *reflectance* spectroscopy has also been shown capable of N_4 quantification, so long as suitable care is taken to address the relative absorption of borate triangles and tetrahedra. This is typically achieved by scaling IR reflectance data for a compositional series to an accurate ^{11}B NMR measurement at one or more composition, or else to $N_4 = x/(1 - x)$ if this relationship has been established at the given composition by NMR or diffraction. Importantly, it has been shown that the relative absorption is modifier cation dependent, but that it scales e.g. quadratically with the divalent modifier field strength (Figure 3.1), allowing for interpolations to be made where necessary (Table 3.1). While scaling with NMR measurement(s) is the direct way to convert IR reflectance data into N_4 , a more detailed infrared analysis combining spectral deconvolution with mass and charge balance equations is capable of providing the molar fractions of all short-range

borate units and not just of BO_4 (i.e., N_4). This has been demonstrated for bismuth borate glasses and opens the way for application to other borate glasses (see section 3.6 and Varsamis *et al.*²⁷⁹).

Total scattering diffraction methods have also come along a great deal, with the advent of both reactor and particle accelerator based neutron sources, and intense synchrotron sources of high-energy x-rays. Although inherently quantitative, the uncertainties in the direct determination of B–O coordination number, and thereby N_4 , have traditionally been larger than those associated with ^{11}B NMR. However, it has recently been demonstrated^{259,294,295,311,312} that N_4 values rivaling the accuracy and precision of ^{11}B NMR can be determined from diffraction data. This is achieved by exploiting the inherent sensitivity of total scattering diffraction, as an interference based method, to length scales, and mapping accurate and precise determinations of the mean B–O bond length onto N_4 values using bond-valence methodology.

Certain general observations about binary borate glasses can be made considering the entire corpus of studies reporting N_4 :

Firstly, ambient pressure binary borate glass structures typically tend to have $N_4 < 0.5$, such that trigonal borate species predominate. There are notable exceptions to this rule, such as the unusual $\text{TeO}_2\text{--B}_2\text{O}_3$ glasses, where B_2O_3 contents are exceptionally low, and it is quite well established by NMR and neutron diffraction that $N_4 > 0.5$ when TeO_2 content exceeds about 82 mol%⁸⁴. On the other hand, the high $N_4 > 0.5$ reported by Park and Bray⁵² for $\text{SrO--B}_2\text{O}_3$ glasses have been identified as outliers and should be discarded, as discussed above. The single $N_4 > 0.5$ reported by Kajinami *et al.*³²⁰ for $\text{MnO--B}_2\text{O}_3$ glasses by x-ray diffraction has also been ruled out by us as an outlier. This is because it is not consistent with the reported B–O bond length, and our bond-valence based determination of $N_4 < 0.5$, nor with the remarkable NMR study of Park and Bray⁵⁷ on this paramagnetic glass system. Other cases are less clear cut. A few NMR studies have reported $N_4 > 0.5$ for lead borate glasses with PbO content close to, or exceeding, 50 mol% (Figure 3.12). However, these data are not supported by existing neutron diffraction or IR reflectance data, or indeed by several other NMR studies (Figure 3.12, Figure 4.12). Very large $N_4 > 0.5$ were reported early on for $\text{Tl}_2\text{O--B}_2\text{O}_3$ glasses by Baugher and Bray⁴⁹ using NMR, including many values of $N_4 > x/(1-x)$. The thesis work of Laorodphan⁹³ using both NMR and neutron diffraction has since revised these values downwards, but not to the extent that the two anomalies, $N_4 > x/(1-x)$ for $x < 50$ mol% Tl_2O and $N_4 > 0.5$ for $x > 50$ mol% Tl_2O , disappear altogether. Overall, the general predominance of binary borate glasses having $N_4 < 0.5$ is in stark contrast to the well-established fact that many modified borosilicate glasses, especially at high SiO_2 contents, tend to have $N_4 > 0.5$. Historically this has led to development of models for borate glass structure which invoke Lowenstein type avoidance rules for the negatively charged borate tetrahedra.¹⁵ However, the foundations of such models have been strongly questioned by Möncke *et al.*²³⁸ who present evidence for corner-sharing pairs of $[\text{B}\text{O}_4]^-$, as well as $[\text{B}\text{O}_2\text{O}_2]^{3-}$, tetrahedra in glasses. Such moieties are of course also well known in borate and borosilicate crystal structures. An alternative explanation for the $N_4 < 0.5$ in binary borate glasses *could* involve the temperature dependence of $N_4(T)$ observed in the molten and supercooled liquid states. $N_4(T)$ is typically observed to progressively increase as the liquid is (super)cooled towards the glass transition at T_g . Since this boron coordination change mechanism contributes to the super-Arrhenian temperature dependence

of the liquid viscosity (liquid fragility), it has a self-limiting effect, in that the rapid rise in viscosity results in glass transition at T_g , arresting the increase in $N_4(T)$ as it falls out of equilibrium, and before it can exceed 0.5, in most cases. This idea that the equilibrium N_4 fractions in highly modified glasses could in fact be much higher than the non-equilibrium values observed to date remains to be explored.

Secondly, as discussed by Holland *et al.*⁷⁵ there is an interesting linear correlation between the composition, n^{\max} , at which N_4 reaches its maximum value, expressed as molar fraction modifier oxide $M_{2/Z}O$, and the modifier cation potential $\varphi = Z/r_M$. This makes sense if one considers that as φ increases, modifier charge becomes progressively localized, and the space available around it to pack charge balancing borate tetrahedra diminishes. In Figure 5.1 we have updated this correlation plot between n^{\max} and φ using our large database of N_4 values, and included points for additional modifier cations Tl^+ , Ag^+ , Ba^{2+} , Cd^{2+} , Mn^{2+} , Mg^{2+} , La^{3+} , and Te^{4+} , see also Table 5.1.

Table 5.1: Modal cation-oxygen bond lengths, r_{MO} , as derived from diffraction studies, together with the corresponding cation potentials φ , and observed compositions of maximum N_4 , n^{\max} (in mole fraction $M_{2/Z}O$). Cation radii are simply obtained using $r_M = r_{MO} - r_O$, with $r_O = 1.35 \text{ \AA}$, the Shannon-Prewitt radius for 2-fold oxygen (other values could be chosen, yielding qualitatively identical results). The penultimate column gives the reference used for obtaining r_{MO} , and the final column indicates the glass system used for r_{MO} , or else the cation-oxygen coordination number used to obtain the Shannon-Prewitt radius, in lieu of suitable diffraction data.

Cation	Z (e)	Modifier oxide	r_{MO} (Å)	r_M (Å)	$\varphi = Z/r_{MO}$ ($e\text{Å}^{-1}$)	n^{\max} (mol. frac. $M_{2/Z}O$)	Ref.	Glass system or n_{MO}
Cs	1	Cs ₂ O	3.13(1)	1.78	0.562(3)	0.3320	360–362	9
Rb	1	Rb ₂ O	2.85(5)	1.5	0.67(2)	0.3326	255	borate
K	1	K ₂ O	2.75(5)	1.4	0.71(3)	0.3325	255	borate
Tl	1	Tl ₂ O	2.527(1)	1.177	0.8496(7)	0.4003	363	germanate
Ag	1	Ag ₂ O	2.40(5)	1.05	0.95(5)	0.3433	329	borate
Na	1	Na ₂ O	2.295(2)	0.945	1.058(2)	0.3529	364	silicate
Ba	2	BaO	2.775(5)	1.425	1.403(5)	0.3917	259	borate
Li	1	Li ₂ O	1.96(1)	0.61	1.64(3)	0.3906	312	borate
Sr	2	SrO	2.56(1)	1.21	1.65(1)	0.3777	360–362	7
Pb	2	PbO	2.40(5)	1.05	1.90(9)	0.4861	154	borate
Ca	2	CaO	2.39(1)	1.04	1.92(2)	0.4018	21	germanate
Cd	2	CdO	2.22(1)	0.87	2.30(3)	0.4865	360–362	5
Sn	2	SnO	2.125(1)	0.775	2.581(3)	0.5950	324	borate
La	3	La _{2/3} O	2.490(1)	1.14	2.632(2)	0.4674	359	borate
Mn	2	MnO	2.10(1)	0.75	2.67(4)	0.3862	360–362	5 (high spin)
Zn	2	ZnO	2.00(1)	0.65	3.08(5)	0.5038	335	borate
Mg	2	MgO	1.97(2)	0.62	3.23(10)	0.4716	365	phosphate
Bi	3	Bi _{2/3} O	2.20(5)	0.85	3.53(21)	0.6815	343	borate
Sb	3	Sb _{2/3} O	1.978(1)	0.628	4.777(8)	0.7583	342	borate
Te	4	Te _{1/2} O	1.91(5)	0.56	7.14(64)	0.9974	84	borate

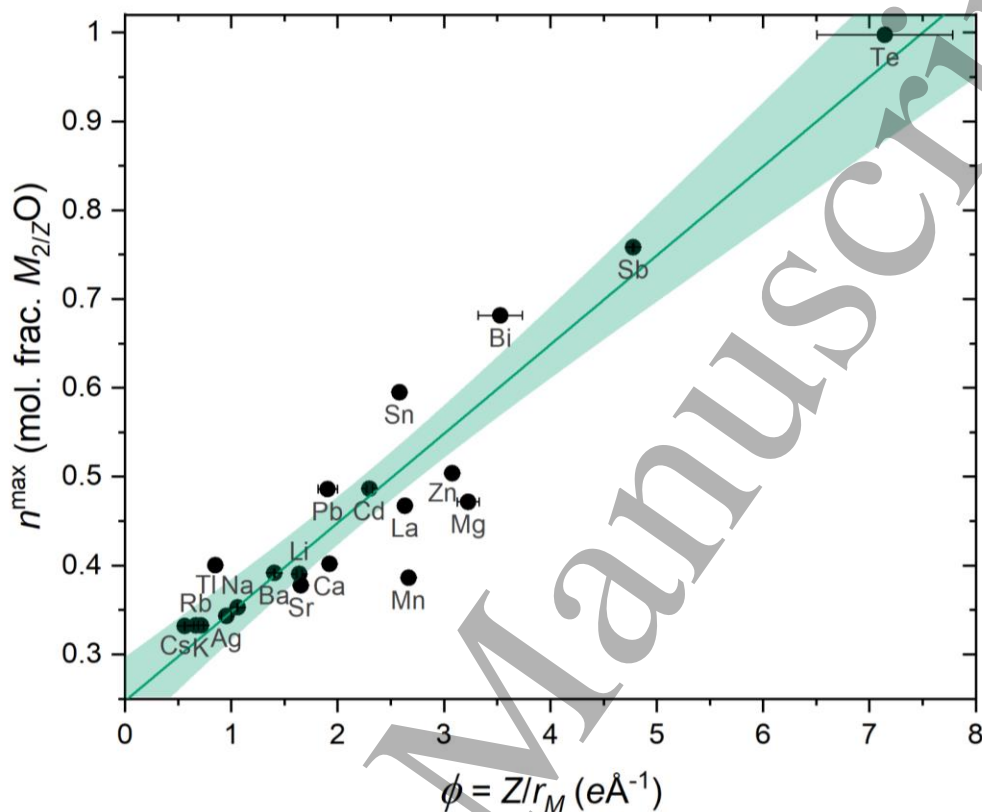


Figure 5.1: Correlation plot between composition, n^{\max} , at which N_4 reaches its maximum value, expressed as molar fraction modifier oxide $M_{2/Z}O$, and the modifier cation potential $\phi = Z/r_M$. Here Z is the formal cation charge and r_M the modifier cation radius. The unweighted linear fit is given by $n^{\max} = 0.25(2) + 0.100(8) \phi$, in the units shown on the axes, with 95% confidence bounds shaded.

To generate the data shown in Table 5.1 and Figure 5.1, n^{\max} were determined from spline fits to the NMR derived N_4 in our database, except in the case of Mg^{2+} where the IR data were used. In the cases of Cd^{2+} and Sn^{2+} , the N_4 maxima are rather broad and poorly determined. In the cases of Ag^+ and Tl^+ , there are very few points at modifier contents beyond the maxima. For Ca^{2+} , the spread in the various datasets is very large, again leading to significant uncertainty in n^{\max} . In order to derive $\phi = Z/r_M$ values, total scattering diffraction measurements of the modal $M-O$ bond lengths were used in most cases, and the oxygen radius of $r_O = 1.35 \text{ \AA}$ subtracted to yield r_M . Note that modal bond lengths are often shorter than mean bond lengths, but easier to determine, and likely more pertinent. In most cases, diffraction data on borate glasses themselves were used^{84,154,255,259,312,324,329,335,342,343,359}. In other cases data from other glass systems were used, including silicates (Na^+)³⁶⁴, germanates (Ca^{2+} and Tl^+)^{21,360} and phosphates (Mg^{2+})³⁶⁵. In the remaining cases Shannon-Prewitt ionic radii³⁶⁰⁻³⁶² were used for 5-fold Mn^{2+} (high spin) and Cd^{2+} , 7-fold Sr^{2+} and 9-fold Cs^+ .

1
2
3
4
5
6
7
8
9
10
11
12
13
14
15
16
17
18
19
20
21
22
23
24
25
26
27
28
29
Ultimately the linear relationship displayed in Figure 5.1 terminates at $\varphi \approx 7.5 \text{ e}\text{\AA}^{-1}$, where n^{max} reaches its limiting value of 1. Notably this is before the tetravalent (Si^{4+} , Ge^{4+}) and pentavalent (P^{5+}) glass formers which all have larger $\varphi \gtrsim 10$. In the case of Si^{4+} and Ge^{4+} , $N_4 = 0$ for the compositions measured^{37,366}. P_2O_5 - B_2O_3 glasses are rather curious in that they only form at rather low P_2O_5 contents, where $N_4 \gtrsim 0$ has been found⁵⁴. This limited glass forming region has been attributed to the need for perfect topological ordering between $[\text{B}\text{O}_4]^-$ and $[\text{P}\text{O}_4]^+$ units, which tends to lead to crystallization of BPO_4 . Indeed, extrapolations from ternary borophosphate glasses indicate high N_4 fractions in the hypothetical P_2O_5 -rich binary borate glasses⁵⁴. Te^{4+} appears to be right on the limit of the linear relationship, with high $\varphi \approx 7.1 \text{ e}\text{\AA}^{-1}$ and n^{max} approaching 1. Indeed, it should be noted that the $n^{\text{max}} \approx 1$ is not a true maximum in the sense that it is not clear from the available data if the derivative $\partial N_4/\partial n$ goes to zero. Interestingly, trivalent Al^{3+} has a similar $\varphi \approx 7.5 \text{ e}\text{\AA}^{-1}$ but is not known to generate tetrahedral boron in pure aluminoborate glasses⁶⁰. This is likely due to the propensity for tetrahedral aluminium $[\text{Al}\text{O}_4]^-$ units which are not suitable for charge balancing $[\text{B}\text{O}_4]^-$, whereas in the telluroborate glasses, the Te^{4+} lone pair causes a small number of short bonds to form to oxygen, and $[\text{Te}\text{O}_3]^+$ units are well suited to charge balancing $[\text{B}\text{O}_4]^-$. Overall, it is clear that the linear relationship breaks down at high φ , where the specific mechanisms of charge balance become quite different, and very much cation dependent. It is also worth mentioning that the linear relationship fitted to the data in Fig. 5.1 has no theoretical justification, it is merely the simplest functional form available. Furthermore, there are several outliers which are not described by the linear relationship, particularly Mn^{2+} , but for which the true uncertainties in n^{max} are unclear.

30
31
32
33
34
35
36
37
38
39
40
41
42
43
44
45
46
47
48
49
50
51
52
53
54
55
56
57
58
59
60
Finally, it is apparent that in some cases, particularly that of CaO - B_2O_3 glasses, that the consensus on $N_4(x)$ is quite poor, Figure 5.2. Does this point toward a particularly large sensitivity of $N_4(x)$ to thermal history in this case? Or is it simply down to the various systematic uncertainties of the individual studies, which by chance plague this system more than others? These questions can be readily answered with suitably designed studies. In the first instance, through studies of the temperature, and fictive temperature, dependencies of N_4 . In the second instance, through multi-technique approaches, whereby, for example, ^{11}B MAS NMR, IR reflectance spectroscopy and diffraction methods are all applied to a single set of glasses, with the expectation that a consensus would be obtained, at least for that set of glasses with their given thermal histories. Notably, the study by Lepry and Nazhat¹²⁵ involved sol-gel derived amorphous calcium borate solids, with a calcination temperature of 673 K, which is well below the glass transition temperatures of 870 – 930 K³⁶⁷. The low-temperature synthesis route explains the very high CaO contents achieved. It is also tempting to speculate that the relatively high N_4 values obtained by both NMR and IR methods¹²⁰, Figure 5.2, at high $R > 1$, are a result of the general expectation for higher $N_4(T_f)$ at lower fictive temperature T_f . This would however require a special mechanism enabling the metastable equilibrium for N_4 to be approached, one possibly provided by the very high surface areas of the amorphous powders, which imbues higher mobility and additional relaxation routes. However, another explanation might be the presence of organic and hydroxyl impurities which might be expected, especially considering that the glass powders were all discolored off-white, or even black in the case of the lowest CaO content.

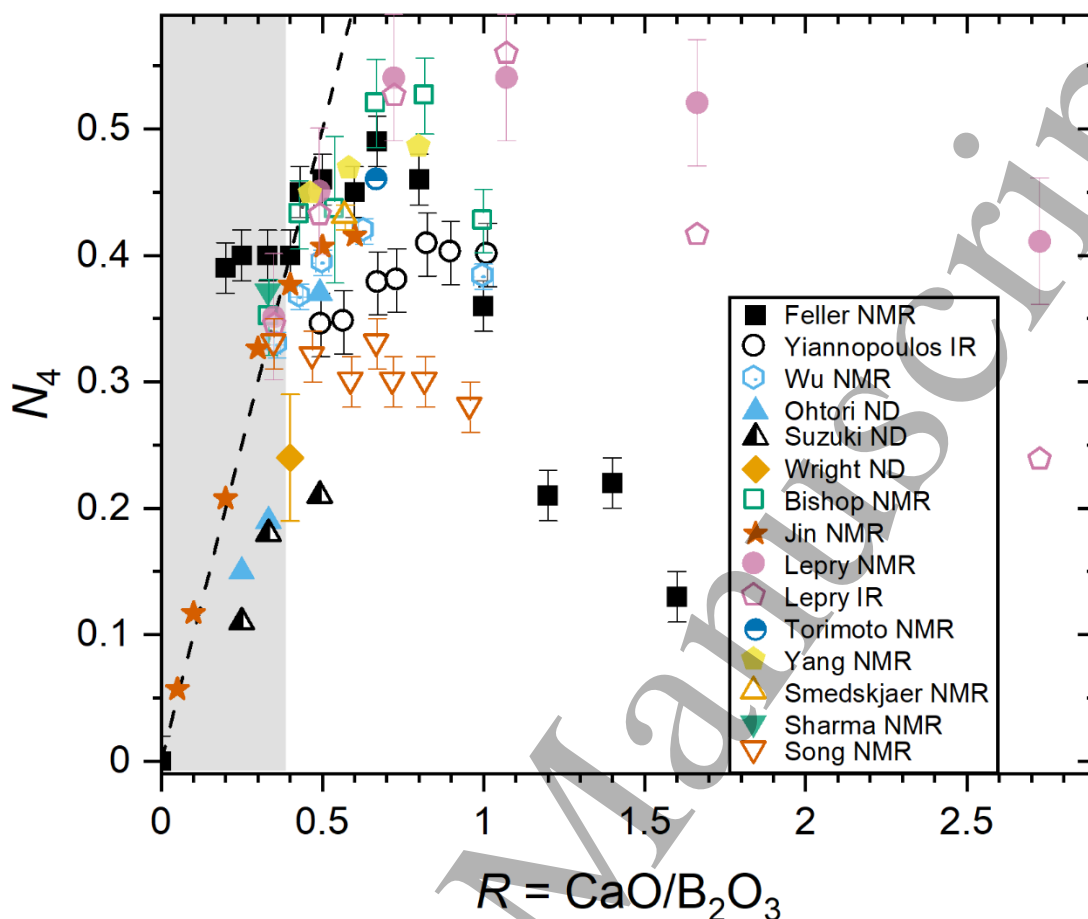


Figure 5.2: Compilation of N_4 measurements on $\text{CaO-B}_2\text{O}_3$ glasses and amorphous solids. The shaded region indicates that of stable liquid-liquid immiscibility in the equilibrium phase diagram, and therefore data in this region may refer to inhomogeneous phase separated glasses. The dashed line is $N_4 = R$. References for ND^{255,257,331}, NMR^{46,87,92,99,117,120,125,132,136,137} (data from Song *et al.*¹³⁷ have been corrected as discussed above) and IR^{125,257}. The study by Lepry and Nazhat¹²⁵ involved sol-gel derived amorphous calcium borate solids.

It is worth noting that the neutron diffraction studies by Ohtori *et al.*²⁵⁸ and Suzuki *et al.*³³¹ were seemingly based on the same experimental data, but report different N_4 values, especially for calcium diborate glass. In this latter case, the result from Ohtori *et al.*²⁵⁸ appears to be in better agreement with a wider range of other studies.

6. Future prospects and recommendations

The use of ^{11}B MAS NMR will likely remain the go-to method for N_4 measurement in borate glasses. It should be reiterated here that this method typically requires corrections to be made to account for spinning sideband intensities in order to avoid systematic inaccuracies. Nonetheless, despite the tremendous numbers of N_4 measurements made to date using ^{11}B NMR,

1
2
3 looking at Figure 2.10 it is quite clear that there are gaps in our knowledge. Most glaring are the
4 lack of N_4 measurements in paramagnetic borate glasses. This is for good reason, and largely due
5 to the severe broadening effects arising due to interactions with unpaired electrons and
6 paramagnetic relaxation enhancement of the nuclear spins, which has led to a general tendency of
7 practitioners to avoid measuring spectra from glasses containing paramagnetic ions as major
8 components (above dopant levels). The pioneering early work by Park and Bray⁵⁷ on MnO-B₂O₃
9 glasses, as well as Bucholtz and Bray⁵⁸ on Fe₂O₃-PbO-B₂O₃ glasses used low frequency field-
10 sweep methods to enable collection of the incredibly broad ¹¹B NMR spectral signals. It would be
11 a tremendous development to see a revival of such capability, particularly in light of the plethora
12 of wide-line NMR methodologies now available³⁶⁸, including those developed specifically for
13 tackling paramagnetic systems,^{369,370} and taking advantage of modern capabilities including rapid
14 MAS and pulsed Fourier transform methodologies. Indeed, progress has already been made in this
15 direction in the case of ²⁹Si NMR spectroscopy of paramagnetic minerals and glasses³⁷¹.
16
17
18
19

20 In terms of vibrational spectroscopies, infrared *reflectance* has been shown to be
21 preeminent in terms of quantifying N_4 , and this is the method which should be applied when
22 seeking accurate N_4 values and trends. Of course, it still relies to some extent on other methods in
23 order to pin down the relative absorption of borate triangles and tetrahedra. However, the
24 dependence of the relative absorption on cation field strength developed herein is now ripe for
25 exploitation and extension to other modifier cations, and to mixed-modifier glasses.
26
27

28 As demonstrated by this review, it is clear that a reasonable number of diffraction studies
29 of binary borate glasses have been made, and used to quantify N_4 . Nonetheless, diffraction methods
30 appear underutilized when compared to both NMR and IR spectroscopies. This is understandable
31 given the reliance on large-scale facilities: x-ray synchrotrons, nuclear reactors and proton
32 accelerator driven spallation neutron sources. However, this needn't be the case. The issue here is
33 perhaps largely one of a perception of difficulty in accessing these facilities, and this barrier
34 requires breaking down. For one thing, advancements in radiation sources, detectors and
35 instrumentation have led to a steady increase in throughput, and it is perfectly feasible nowadays
36 to measure the neutron or x-ray structure factors for large numbers (several 10s) of glasses in a
37 single experiment, with each measurement *typically* on the order of a few hours with neutrons, and
38 minutes with synchrotron x-rays. Furthermore, light modifier containing borate glasses can be
39 measured routinely with specialized laboratory-based x-ray sources (typically based on Ag-source
40 x-rays) on hour to day timescales. An additional barrier to the application of neutron diffraction to
41 borate glasses is the need to isotopically enrich in ¹¹B, in order to avoid significant levels of the
42 strongly neutron absorbing ¹⁰B isotope (20% natural abundance). However, ¹¹B is relatively cheap
43 as isotopes go, partly due its status as a by-product of ¹⁰B enrichment utilized by the nuclear
44 industry.
45
46
47
48
49

50 Diffraction methods present an excellent opportunity for addressing the paucity of
51 information available on the structure of paramagnetic borate glasses, and with far fewer
52 challenges than those posed by the application of NMR to such materials. Diffraction methods are
53 also relatively well suited to quantitative *in-situ* measurements under extreme conditions of high-
54 temperature and/or high-pressure, with clear opportunities in this direction.
55
56
57
58
59
60

We call on future authors of diffraction studies to report on the mean B–O bond length in borate glasses wherever possible, and at the very least to use this as a check on the directly determined B–O coordination numbers, if not to also provide a more precise and accurate estimate of N_4 using bond-valence based methodology.

Water borate glasses deserve the attention of both modern NMR methods and high- Q diffraction studies, in order to build on the early work done by Silver³⁹, Meller and Milberg^{345,346}, and later studies by Brüning *et al*^{347,348}. This could include neutron diffraction, where isotopic substitution of hydrogen by deuterium can be exploited to provide contrast and more detailed structural information than is available from a single measurement or isotopologue. An example includes recent work on aqueous potassium borate solutions³⁷².

The two apparent anomalies of the thallium borate glasses also deserve further attention, with the caveat that thallium is incredibly toxic and requires great care when working with it. Specifically, the observations that $N_4 > R$ for $R < 1$ and $N_4 > 0.5$ for $R > 1$ (Figure 4.9) require confirmation and explanation. Given sufficient safety precautions, other binary borate systems containing toxic modifiers would also be of interest, but they can pose additional challenges, including phase separation with a very wide immiscibility gap for beryllium, and likely mixed oxidation states for low melting arsenic ($\text{As}^{3+}/\text{As}^{5+}$) borates. As is apparent from Figure 2.10, there are many other binary borate systems for which no N_4 measurements have been reported, and many of which likely do form glasses. One example are vanadium borate glasses, which have been prepared containing largely only pentavalent V^{5+} .³⁷³ These would be excellent candidates for combined x-ray and neutron diffraction studies, and should be amenable to standard ^{11}B NMR methods given the absence of lower valence, paramagnetic, vanadium species.

Overall, whilst the field has been progressed a long way, we cannot claim to have a quantitative means for predicting N_4 in any arbitrary binary borate glass composition, much beyond the limited applicability of the $N_4 = x/(1 - x)$ relationship which holds for low levels ($x \lesssim 30$ mol% $M_2\text{O}$ or MO) of monovalent (excluding hydrogen) and some divalent modifiers. In this spirit, the application of machine learning to the N_4 database presented herein could be incredibly fruitful, and should be tested for predicting $N_4(x, T)$, including for the cases of modifiers for which no measurements exist. This could be achieved by characterizing modifiers by their field strengths, cation potentials, electronegativities and polarizabilities, for example. Such endeavors will not be without their challenges, but should be well worth the effort.

It is worth noting here that we have not reviewed models which do exist for predicting N_4 over extended ranges of composition and/or temperature. These include the simple axiomatic models for $N_4(x)$ proposed by Abe, Beekenkamp, Gupta, Krogh-Moe and Griscom, which have been previously reviewed and compared by Wright.¹⁵ These models have the advantage of simplicity, ease of calculation and lack of empirical adjustable parameters. On the other hand, since they do not include temperature dependence, and tend to maximize N_4 under the constraints of their assumptions, they can be considered only as low temperature limiting cases.¹⁵ Furthermore, since these models contain no explicit dependence on modifier identity, no single model can capture the plethora of different $N_4(x)$ curves observed for binary borate glasses across the periodic table of ‘modifier’ oxides (Fig. 2.10). At the other end of the scale is the model of

1
2
3 ideal associated solutions (IAS), which considers the molten state as comprised of chemical
4 groupings found in the crystalline phases, with abundances based on their relative free energies of
5 formation. This model has the advantage of including temperature (and in principle pressure)
6 dependence, as well as composition dependence, but requires knowledge of not only the stable
7 crystal structures found within a given system, but so too their temperature dependent free energies
8 of formation. The IAS model has been applied reasonably successfully to Li and Na borates.³⁷⁴
9 Intermediate between the two aforementioned approaches is the boron coordination change
10 isomerization (BCCI) model,^{259,295,312} which has been fitted to experimental $N_4(x,T)$ data. The
11 BCCI model is a relatively simple phenomenological model which allows for interpolation, and
12 perhaps limited extrapolation of, $N_4(x,T)$, but which requires empirically estimated enthalpies and
13 entropies of the boron coordination change reaction. These parameters have been shown to depend
14 somewhat on x ,^{259,312} and are also expected to depend on modifier identity, requiring further
15 measurements to constrain the model over a wider compositional space. Finally, there are now
16 numerous classical interaction potential parameterizations, as well as first principles approaches
17 for modelling borate melts and glasses using molecular dynamics. It is unlikely any of these can
18 capture the temperature and composition dependence of $N_4(x,T)$, owing to the unrealistically high
19 quenching rates necessitated by available computational resources. Or in other words, molecular
20 dynamics might allow for reasonable prediction of $N_4(x,T)$ in the equilibrium and mildly
21 supercooled liquid state, but will then tend to underestimate it in the glassy state owing to the
22 overly rapid quenching timescale. Or, if the potentials are tuned to yield agreement with
23 experimental $N_4(x)$ for glasses, they will then likely fail to capture $N_4(x,T)$ in the liquid state.
24
25
26
27
28
29

30 In limiting the scope of this review to just a single important structural parameter (N_4), and
31 to *binary* borate glasses, containing only a single cation in addition to boron, and with only a single
32 anion (O^{2-}), we have been able to be reasonably comprehensive with our review. To obtain an
33 analogous review and database for more complex, multicomponent, borate-bearing glasses will
34 likely require a large degree of automated data mining, in addition to the necessary human input,
35 given the daunting vastness of the glass-forming composition space and the correspondingly larger
36 number of studies involving such materials to date.
37
38
39

40 Acknowledgments

41
42 EIK and NST acknowledge support by the project “National Infrastructure in Nanotechnology,
43 Advanced Materials and Micro-/Nanoelectronics” (MIS 5002772), co-financed by Greece and the
44 European Union (European Regional Development Fund). This material is based upon work
45 supported by the National Science Foundation Graduate Research Fellowship under Grant No.
46 DGE-2039655 (IS). Any opinions, findings, and conclusions or recommendations expressed in
47 this material are those of the authors and do not necessarily reflect the views of the National
48 Science Foundation. Steve A. Feller, Rebecca M. Gabrielsson, Harry Hawbaker, Piper Boggs,
49 Sophia John, Leilani Rocha, and Robert M. Wilson acknowledge NSF grant DMR-2203142.
50
51

52 Professor Scott Kroeker is gratefully acknowledged for providing his perspective on the NMR
53 spectroscopy of paramagnetic materials. We wish to thank an anonymous reviewer for their careful
54 reading and extensive constructive comments that led to the improvement of our original
55 manuscript.
56
57

A supplemental section with numerical values of the data is included as well.

References

- (1) Burianek, M.; Birkenstock, J.; Mair, P.; Kahlenberg, V.; Medenbach, O.; Shannon, R. D.; Fischer, R. X. High-Pressure Synthesis, Long-Term Stability of Single Crystals of Diboron Trioxide, B₂O₃, and an Empirical Electronic Polarizability of ¹³B³⁺. *Phys. Chem. Miner.* **2016**, *43*, 527–534. <https://doi.org/10.1007/s00269-016-0813-x>.
- (2) Sinclair, R.; Stone, C.; Wright, A.; Polyakova, I.; Vedishcheva, N.; Shakhmatkin, B.; Feller, S.; Johanson, B.; Venhuizen, P.; Williams, R. Inelastic Neutron Scattering Studies of Superstructural Units in Borate Glasses and Crystalline Phases. *Phys. Chem. Glasses* **2000**, *41* (5), 286–289.
- (3) Shelby, J. E. *Introduction to Glass Science and Technology*; Royal Society of Chemistry, 2005.
- (4) Gooding, E. J.; Turner, W. E. S. A Study of the Series of Glasses Containing Sodium Oxide, Boric Oxide and Silica. *J. Soc. Glass Technol.* **1934**, *18* (69), T032–T066.
- (5) Biscoe, J.; Warren, B. E. X-Ray Diffraction Study of Soda-Boric Oxide Glass. *Journal of the American Ceramic Society* **1938**, *21* (8), 287–293. <https://doi.org/10.1111/j.1151-2916.1938.tb15777.x>.
- (6) Prewitt, C. T.; Shannon, R. D. Crystal Structure of a High-Pressure Form of B₂O₃. *Acta Cryst.* **1968**, *24* (6), 869–874. <https://doi.org/10.1107/S0567740868003304>.
- (7) Huang, C.; Mutailipu, M.; Zhang, F.; Griffith, K. J.; Hu, C.; Yang, Z.; Griffin, J. M.; Poepelmeier, K. R.; Pan, S. Expanding the Chemistry of Borates with Functional [BO₂]⁻ Anions. *Nature communications* **2021**, *12* (1), 2597. <https://doi.org/10.1038/s41467-021-22835-4>.
- (8) Jellison Jr, G.; Panek, L.; Bray, P.; Rouse Jr, G. Determinations of Structure and Bonding in Vitreous B₂O₃ by Means of B¹⁰, B¹¹, and O¹⁷ NMR. *J. Chem. Phys.* **1977**, *66* (2), 802–812. <https://doi.org/10.1063/1.433959>.
- (9) Jellison Jr, G.; Bray, P. Structural Determinations for Sodium Borate Glasses Using B¹⁰ and B¹¹ NMR. In *Borate Glasses: Structure, Properties, Applications*; Springer, 1978; pp 353–367.
- (10) Gravina, S. J.; Bray, P. J.; Petersen, G. L. Pure Nuclear Quadrupole Resonance Spectroscopy Studies of the Structure of Glasses. *J. Non-Cryst. Solids* **1990**, *123* (1–3), 165–169. [https://doi.org/10.1016/0022-3093\(90\)90781-G](https://doi.org/10.1016/0022-3093(90)90781-G).
- (11) Bray, P.; Emerson, J.; Lee, D.; Feller, S.; Bain, D.; Feil, D. NMR and NQR Studies of Glass Structure. *J. Non-Cryst. Solids* **1991**, *129* (1–3), 240–248. [https://doi.org/10.1016/0022-3093\(91\)90100-K](https://doi.org/10.1016/0022-3093(91)90100-K).
- (12) Hannon, A.; Grimley, D.; Hulme, R.; Sinclair, R. Boroxol Groups in Vitreous Boron Oxide: New Evidence from Neutron Diffraction and Inelastic Neutron Scattering Studies. *J. Non-Cryst. Solids* **1994**, *177*, 299–316. [https://doi.org/10.1016/0022-3093\(94\)90544-4](https://doi.org/10.1016/0022-3093(94)90544-4).
- (13) Kroeker, S.; Stebbins, J. F. Three-Coordinated Boron-11 Chemical Shifts in Borates. *Inorg. Chem.* **2001**, *40* (24), 6239–6246. <https://doi.org/10.1021/ic010305u>.
- (14) Hung, I.; Howes, A.; Parkinson, B.; Anupöld, T.; Samoson, A.; Brown, S. P.; Harrison, P.; Holland, D.; Dupree, R. Determination of the Bond-Angle Distribution in Vitreous B₂O₃ by

- ¹¹B Double Rotation (DOR) NMR Spectroscopy. *J. Solid State Chem.* **2009**, *182* (9), 2402–2408. <https://doi.org/10.1016/j.jssc.2009.06.025>.
- (15) Wright, A. C. Borate Structures: Crystalline and Vitreous. *Phys. Chem. Glasses-Eur. J. Glass Sci. Technol. Part B* **2010**, *51* (1), 1–39.
- (16) Galeener, F. L. Planar Rings in Glasses. *Solid State Commun.* **1982**, *44* (7), 1037–1040. [https://doi.org/10.1016/0038-1098\(82\)90329-5](https://doi.org/10.1016/0038-1098(82)90329-5).
- (17) Meera, B. N.; Ramakrishna, J. Raman Spectral Studies of Borate Glasses. *J. Non-Cryst. Solids* **1993**, *159* (1–2), 1–21. [https://doi.org/10.1016/0022-3093\(93\)91277-A](https://doi.org/10.1016/0022-3093(93)91277-A).
- (18) Huppertz, H.; von der Eltz, B. Multianvil High-Pressure Synthesis of Dy₄B₆O₁₅: The First Oxoborate with Edge-Sharing BO₄ Tetrahedra. *J. Am. Chem. Soc.* **2002**, *124* (32), 9376–9377. <https://doi.org/10.1021/ja017691z>.
- (19) Jin, S.; Cai, G.; Wang, W.; He, M.; Wang, S.; Chen, X. Stable Oxoborate with Edge-Sharing BO₄ Tetrahedra Synthesized under Ambient Pressure. *Angew. Chem. Int. Ed.* **2010**, *49* (29), 4967–4970. <https://doi.org/10.1002/anie.200907075>.
- (20) Mutailipu, M.; Zhang, M.; Li, H.; Fan, X.; Yang, Z.; Jin, S.; Wang, G.; Pan, S. Li₄Na₂CsB₇O₁₄: A New Edge-Sharing [BO₄]⁵⁻ Tetrahedra Containing Borate with High Anisotropic Thermal Expansion. *Chem. Commun.* **2019**, *55* (9), 1295–1298. <https://doi.org/10.1039/C8CC09422E>.
- (21) Alderman, O. L. G.; Hannon, A. C.; Feller, S.; Beanland, R.; Holland, D. The Germanate Anomaly in Alkaline Earth Germanate Glasses. *J. Phys. Chem. C* **2017**, *121* (17), 9462–9479. <https://doi.org/10.1021/acs.jpcc.6b12372>.
- (22) Barney, E. R.; Hannon, A. C.; Holland, D.; Umesaki, N.; Tatsumisago, M.; Orman, R. G.; Feller, S. Terminal Oxygens in Amorphous TeO₂. *J. Phys. Chem. Lett.* **2013**, *4* (14), 2312–2316. <https://doi.org/10.1021/jz4010637>.
- (23) Howes, A. P.; Vedishcheva, N. M.; Samoson, A.; Hanna, J. V.; Smith, M. E.; Holland, D.; Dupree, R. Boron Environments in Pyrex® Glass—a High Resolution, Double-Rotation NMR and Thermodynamic Modelling Study. *Phys. Chem. Chem. Phys.* **2011**, *13* (25), 11919–11928. <https://doi.org/10.1039/c1cp20771g>.
- (24) Kroeker, S. Nuclear Magnetic Resonance Spectroscopy of Glasses. In *Modern Glass Characterization*; Affatigato, M., Ed.; The American Ceramic Society and John Wiley & Sons, Inc: Hoboken, New Jersey, 2015; pp 1–30.
- (25) Massiot, D.; Bessada, C.; Coutures, J.; Taulelle, F. A Quantitative Study of ²⁷Al MAS NMR in Crystalline YAG. *Journal of Magnetic Resonance (1969)* **1990**, *90* (2), 231–242.
- (26) Silver, A.; Bray, P. Nuclear Magnetic Resonance Absorption in Glass. I. Nuclear Quadrupole Effects in Boron Oxide, Soda-Boric Oxide, and Borosilicate Glasses. *J. Chem. Phys.* **1958**, *29* (5), 984–990. <https://doi.org/10.1063/1.1744697>.
- (27) Alderman, O. L.; Iuga, D.; Howes, A. P.; Pike, K. J.; Holland, D.; Dupree, R. Spectral Assignments and NMR Parameter–Structure Relationships in Borates Using High-Resolution ¹¹B NMR and Density Functional Theory. *Phys. Chem. Chem. Phys.* **2013**, *15* (21), 8208–8221.
- (28) Bray, P. J.; O’Keefe, J. G. Nuclear Magnetic Resonance Investigations of the Structure of Alkali Borate Glasses. *Phys. Chem. Glasses* **1963**, *4* (2), 37–46.
- (29) Soldate, A. M. *J. Am. Chem. Soc.* **1938**, *21*, 287.
- (30) Taylor, P. C.; Bray, P. J. Lineshape Program Manual, 1969.
- (31) Taylor, P.; Bray, P. Computer Simulations of Magnetic Resonance Spectra Observed in Polycrystalline and Glassy Samples. *J. Magn. Reson.* **1970**, *2* (3), 305–331.

- [https://doi.org/10.1016/0022-2364\(70\)90102-2](https://doi.org/10.1016/0022-2364(70)90102-2).
- (32) Müller-Warmuth, W.; Poch, W.; Siefert, O. Bestimmung Der Mittleren Koordinationgrade Der Bor in KF–B₂O₃ Gläsern Aus Dem B-Kernresonance Spectrum. *Glastech. Ber.* **1970**, *43* (1), 5–7.
- (33) Kim, K.; Bray, P.; Merrin, S. Nuclear Magnetic Resonance Studies of the Glasses in the System PbO–B₂O₃–SiO₂. *J. Chem. Phys.* **1976**, *64* (11), 4459–4465. <https://doi.org/10.1063/1.432125>.
- (34) Jellison Jr., G. E.; Feller, S. A.; Bray, P. J. A Re-Examination of the Fraction of 4-Coordinated Boron Atoms in the Lithium Borate Glass System. *Phys. Chem. Glasses* **1978**, *19*, 52–53.
- (35) Zhong, J.; Bray, P. J. Change in Boron Coordination in Alkali Borate Glasses, and Mixed Alkali Effects, as Elucidated by NMR. *J. Non-Cryst. Solids* **1989**, *111* (1), 67–76. [https://doi.org/10.1016/0022-3093\(89\)90425-0](https://doi.org/10.1016/0022-3093(89)90425-0).
- (36) Kroeker, S.; Aguiar, P.; Cerquiera, A.; Okoro, J.; Clarida, W.; Doerr, J.; Olesiak, M.; Ongie, G.; Affatigato, M.; Feller, S. A. Alkali Dependence of Tetrahedral Boron in Alkali Borate Glasses. *Phys. Chem. Glasses-Eur. J. Glass Sci. Tech Proc. Fifth Int. Conf. Borate Glass Cryst. Melts* **2006**, *47* (4), 393–396.
- (37) Bunker, B. Multinuclear Nuclear Magnetic Resonance and Raman Investigation of Sodium Borosilicate Glass Structure. *Phys. Chem. Glasses* **1990**, *31*, 30.
- (38) Prabakar, S.; Rao, K.; Rao, C. N. R. ¹¹B NMR Spectra and Structure of Boric Oxide and Alkali Borate Glasses. *Proc. R. Soc. Lond. Math. Phys. Sci.* **1990**, *429* (1876), 1–15. <https://doi.org/10.1098/rspa.1990.0048>.
- (39) Stebbins, J. F.; Zhao, P.; Kroeker, S. Non-Bridging Oxygens in Borate Glasses: Characterization by ¹¹B and ¹⁷O MAS and 3QMAS NMR. *Solid State Nucl. Magn. Reson.* **2000**, *16* (1–2), 9–19. [https://doi.org/10.1016/S0926-2040\(00\)00050-3](https://doi.org/10.1016/S0926-2040(00)00050-3).
- (40) Sen, S.; Xu, Z.; Stebbins, J. Temperature Dependent Structural Changes in Borate, Borosilicate and Boroaluminate Liquids: High-Resolution ¹¹B, ²⁹Si and ²⁷Al NMR Studies. *J. Non-Cryst. Solids* **1998**, *226* (1–2), 29–40. [https://doi.org/10.1016/S0022-3093\(97\)00491-2](https://doi.org/10.1016/S0022-3093(97)00491-2).
- (41) Dorn, R. W.; Paterson, A. L.; Hung, I.; Gor'kov, P. L.; Thompson, A. J.; Sadow, A. D.; Gan, Z.; Rossini, A. J. Dipolar Heteronuclear Correlation Solid-State NMR Experiments between Half-Integer Quadrupolar Nuclei: The Case of ¹¹B–¹⁷O. *J. Phys. Chem. C* **2022**, *126* (28), 11652–11666. <https://doi.org/10.26434/chemrxiv-2022-srqt9>.
- (42) Montouillout, V.; Fan, H.; del Campo, L.; Ory, S.; Rakhmatullin, A.; Fayon, F.; Malki, M. Ionic Conductivity of Lithium Borate Glasses and Local Structure Probed by High Resolution Solid-State NMR. *J. Non-Cryst. Solids* **2018**, *484*, 57–64. <https://doi.org/10.1016/j.jnoncrysol.2018.01.020>.
- (43) Silver, A. Nuclear Magnetic Resonance in B₂O₃–H₂O Glasses and Boric Acids. *J. Chem. Phys.* **1960**, *32* (4), 959–962. <https://doi.org/10.1063/1.1730904>.
- (44) Bray, P.; Leventhal, M.; Hooper, H. Nuclear Magnetic Resonance Investigations of the Structure of Lead Borate Glasses. *Phys. Chem. Glasses* **1963**, *4* (2), 47–66.
- (45) Ring, P. J. *A Nuclear Magnetic Resonance Study of Some Vitreous and Crystalline Lithium-Borates*; Brown University, 1964.
- (46) Bishop, S.; Bray, P. Nuclear Magnetic Resonance Studies of Calcium Boroaluminate Glasses. *Phys. Chem. Glasses* **1966**, *7* (3), 73.
- (47) Kline, D.; Bray, P. Nuclear Magnetic Resonance Investigations of Structure of Glasses in

- System NaF-Na₂O-B₂O₃. *Phys. Chem. Glasses* **1966**, 7 (2), 41.
- (48) Greenblatt, S.; Bray, P. Nuclear Magnetic Resonance Investigations of System BaO-B₂O₃. *Physics and Chemistry of Glasses* **1967**, 8 (5), 190–193.
- (49) Baugher, J.; Bray, P. Magnetic Resonance Studies of Thallium Borate Glasses. *Phys. Chem. Glasses* **1969**, 10 (3), 77–88.
- (50) Kriz, H.; Bray, P. A Study of the Distribution of Boron Sites in Glassy B₂O₃ Using ¹¹B NMR. *J. Non-Cryst. Solids* **1971**, 6 (1), 27–36.
[https://doi.org/10.1016/0022-3093\(71\)90013-5](https://doi.org/10.1016/0022-3093(71)90013-5).
- (51) Rhee, C.; Bray, P. J. Nuclear Magnetic Resonance Studies of the Structure of Caesium Borate Glasses and Crystalline Compounds. *Phys. Chem. Glasses* **1971**, 12 (6), 165–174.
- (52) Park, M.; Bray, P. ¹¹B NMR Studies of Strontium Borate Glasses and Compounds. *Phys. Chem. Glasses* **1972**, 13 (2), 50–62.
- (53) Kim, K.; Bray, P. B¹¹ Nuclear Magnetic Resonance Studies of the System Ag₂O-B₂O₃. *J. Non-Metals* **1974**, 2 (2), 95–101.
- (54) Yun, Y.; Bray, P. Nuclear Magnetic Resonance Studies of the Glasses in the System K₂O-B₂O₃-P₂O₅. *J. Non-Cryst. Solids* **1978**, 30 (1), 45–60. [https://doi.org/10.1016/0022-3093\(78\)90055-8](https://doi.org/10.1016/0022-3093(78)90055-8).
- (55) Park, M. J.; PJ, B. The Determination of the Structures of Compounds and Glasses in the System MgO-B₂O₃ Using B¹¹ NMR. *Phys. Chem. Glasses* **1979**, 20, 31.
- (56) Göring, R.; Schnabel, B.; Buerger, H.; Nass, H. ¹¹B NMR Study on Glasses of the System TeO₂-B₂O₃. *Phys. Status Solidi Appl. Res.* **1981**, 68 (1), K29–K32.
- (57) Park, M.; Bray, P. Determination of the Structure of Glasses in the MnO-B₂O₃ System Using B¹¹ NMR. *J. Korean Phys. Soc.* **1981**, 14 (1), 67–74.
- (58) Geissberger, A.; Bucholtz, F.; Bray, P. J. ⁷Li, ¹¹B and ¹⁹F NMR in Amorphous Alkali Halogen Borate Solid Ionic Conductors. *J. Non-Cryst. Solids* **1982**, 49 (1–3), 117–127.
- (59) Bucholtz, F.; Bray, P. ¹¹B and ²⁰⁷Pb NMR Studies of Glasses in the System xFe₂O₃· yPbO· zB₂O₃ (0 ≤ x ≤ 15.3 Mol%, z/Y ≅ 3). *J. Non-Cryst. Solids* **1983**, 54 (1–2), 43–80.
- (60) Harris Jr, I.; Bray, P. B¹¹ Nuclear Magnetic Resonance Studies of Borate Glasses Containing Tellurium Dioxide. *Phys. Chem. Glasses* **1984**, 25 (2), 44–51.
- (61) Harris Jr, I.; Bray, P. B¹¹ NMR Studies of Zinc Borate Compounds and Glasses. *Phys. Chem. Glasses* **1984**, 25 (3), 69–75.
- (62) Mulkern, R.; Chung, S.; Bray, P.; Chryssikos, G.; Turcotte, D.; Risen, W. An NMR Study of the Photoconducting Glass Systems CdO-B₂O₃-GeO₂ and CdO-B₂O₃-SiO₂. *J. Non-Cryst. Solids* **1986**, 85 (1–2), 69–78. [https://doi.org/10.1016/0022-3093\(86\)90079-7](https://doi.org/10.1016/0022-3093(86)90079-7).
- (63) Yongxing, T.; Zhonghong, J.; Xiuyu, S. NMR, IR and Raman Spectra Study of the Structure of Borate and Borosilicate Glasses. *J. Non-Cryst. Solids* **1989**, 112 (1–3), 131–135.
- (64) Sekiya, T.; Mochida, N.; Ohtsuka, A.; Soejima, A.; Yasumori, A.; Yamane, M. ¹¹B MAS NMR Spectra of BO_{3/2}-TeO₂ Glasses. *Glastech. Berichte* **1993**, 66 (1), 15–20.
[https://doi.org/10.1016/0926-2040\(93\)90009-C](https://doi.org/10.1016/0926-2040(93)90009-C).
- (65) Youngman, R.; Zwanziger, J. Multiple Boron Sites in Borate Glass Detected with Dynamic Angle Spinning Nuclear Magnetic Resonance. *J. Non-Cryst. Solids* **1994**, 168 (3), 293–297.
[https://doi.org/10.1016/0022-3093\(94\)90342-5](https://doi.org/10.1016/0022-3093(94)90342-5).
- (66) Zhang, X.-Q. NMR Computer Simulation of Glassy and Powdered Samples: Application to Studies of Sodium Borovanadate Glasses, New Jersey Institute of Technology, 1994.
<https://digitalcommons.njit.edu/theses/1708>.
- (67) Moon, S.-J.; Kim, M.-S.; Chung, S.-J.; Kim, H.-T. Studies on the Structure in Strontium

- Borate Glasses. *J. Korean Phys. Soc.* **1996**, 29 (2), 213.
- (68) Berryman, J. R.; Feller, S. A.; Affatigato, M.; Kodama, M.; Meyer, B. M.; Martin, S. W.; Borsa, F.; Kroeker, S. Thermal, Acoustic, and Nuclear Magnetic Resonance Studies of Cesium Borate Glasses. *J. Non-Cryst. Solids* **2001**, 293, 483–489. [https://doi.org/10.1016/S0022-3093\(01\)00754-2](https://doi.org/10.1016/S0022-3093(01)00754-2).
- (69) Hayashi, A.; Nakai, M.; Tatsumisago, M.; Minami, T.; Himei, Y.; Miura, Y.; Katada, M. Structural Investigation of SnO–B₂O₃ Glasses by Solid-State NMR and X-Ray Photoelectron Spectroscopy. *J. Non-Cryst. Solids* **2002**, 306 (3), 227–237. [https://doi.org/10.1016/S0022-3093\(02\)01169-9](https://doi.org/10.1016/S0022-3093(02)01169-9).
- (70) Ratai, E.; Chan, J. C.; Eckert, H. Local Coordination and Spatial Distribution of Cations in Mixed-Alkali Borate Glasses. *Phys. Chem. Chem. Phys.* **2002**, 4 (14), 3198–3208. <https://doi.org/10.1039/B202492F>.
- (71) Clarida, W.; Berryman, J.; Affatigato, M.; Feller, S.; Kroeker, S.; Zwanziger, J.; Meyer, B.; Borsa, F.; Martin, S. Dependence of N₄ upon Alkali Modifier in Binary Borate Glasses. *Phys. Chem. Glasses* **2003**, 44 (3), 215–217.
- (72) Kroeker, S.; Feller, S.; Affatigato, M.; O'Brien, C.; Clarida, W.; Kodama, M. Multiple Four Coordinated Boron Sites in Caesium Borate Glasses and Their Relation to Medium Range Order. *Phys. Chem. Glasses* **2003**, 44 (2), 54–58.
- (73) Metwalli, E. Copper Redox Behavior, Structure and Properties of Copper Lead Borate Glasses. *J. Non-Cryst. Solids* **2003**, 317 (3), 221–230. [https://doi.org/10.1016/S0022-3093\(02\)01853-7](https://doi.org/10.1016/S0022-3093(02)01853-7).
- (74) Youngman, R.; Sen, S.; Cornelius, L.; Ellison, A. Novel Structural Aspects of Sb₂O₃-B₂O₃ Glasses. *Phys. Chem. Glasses* **2003**, 44 (2), 69–74.
- (75) Holland, D.; Hannon, A.; Smith, M.; Johnson, C.; Thomas, M.; Beesley, A. The Role of Sb⁵⁺ in the Structure of Sb₂O₃-B₂O₃ Binary Glasses—an NMR and Mössbauer Spectroscopy Study. *Solid State Nucl. Magn. Reson.* **2004**, 26 (3–4), 172–179. <https://doi.org/10.1016/j.ssnmr.2004.02.004>.
- (76) Epping, J. D.; Eckert, H.; Imre, Á. W.; Mehrer, H. Structural Manifestations of the Mixed-Alkali Effect: NMR Studies of Sodium Rubidium Borate Glasses. *J. Non-Cryst. Solids* **2005**, 351 (43–45), 3521–3529. <https://doi.org/10.1016/j.jnoncrysol.2005.08.034>.
- (77) Epping, J. D.; Strojek, W.; Eckert, H. Cation Environments and Spatial Distribution in Na₂O–B₂O₃ Glasses: New Results from Solid State NMR. *Phys. Chem. Chem. Phys.* **2005**, 7 (11), 2384–2389. <https://doi.org/10.1039/B502265G>.
- (78) Banerjee, J.; Ongie, G.; Harder, J.; Edwards, T.; Larson, C.; Sutton, S.; Moeller, A.; Basu, A.; Affatigato, M.; Feller, S. Structural Studies of Solution-Made High Alkali Content Borate Glasses. *J. Non-Cryst. Solids* **2006**, 352 (6–7), 674–678. <https://doi.org/10.1016/j.jnoncrysol.2005.11.051>.
- (79) Feller, S.; Nijhawan, S.; Royle, M.; MacKenzie, J.; Taylor, J.; Sharma, M.; Kamitsos, E. I.; Chryssikos, G. D.; Patsis, A.; Bray, P. Physical Properties and Spectroscopy of Rubidium and Caesium Borate Glasses with Exceptionally High Alkali Content. *Chim. Chron. New Ser.* **1994**, 23, 309–314.
- (80) Shaw, J.; Werner-Zwanziger, U.; Zwanziger, J. Correlation of Lead Borate Glass Structure with Photoelastic Response. *Phys. Chem. Glasses-Eur. J. Glass Sci. Technol. Part B* **2006**, 47 (4), 513–517.
- (81) Aguiar, P. M.; Kroeker, S. Boron Speciation and Non-Bridging Oxygens in High-Alkali Borate Glasses. *J. Non-Cryst. Solids* **2007**, 353 (18–21), 1834–1839.

- 1
2
3
4
5
6
7
8
9
10
11
12
13
14
15
16
17
18
19
20
21
22
23
24
25
26
27
28
29
30
31
32
33
34
35
36
37
38
39
40
41
42
43
44
45
46
47
48
49
50
51
52
53
54
55
56
57
58
59
60
- <https://doi.org/10.1016/j.jnoncrysol.2007.02.013>.
- (82) Michaelis, V. K.; Aguiar, P. M.; Kroeker, S. Probing Alkali Coordination Environments in Alkali Borate Glasses by Multinuclear Magnetic Resonance. *J. Non-Cryst. Solids* **2007**, *353* (26), 2582–2590. <https://doi.org/10.1016/j.jnoncrysol.2007.04.029>.
- (83) Bajaj, A.; Khanna, A.; Chen, B.; Longstaffe, J. G.; Zwanziger, U.-W.; Zwanziger, J.; Gómez, Y.; González, F. Structural Investigation of Bismuth Borate Glasses and Crystalline Phases. *J. Non-Cryst. Solids* **2009**, *355* (1), 45–53. <https://doi.org/10.1016/j.jnoncrysol.2008.09.033>.
- (84) Barney, E. R.; Hannon, A. C.; Holland, D. A Multi-Technique Structural Study of the Tellurium Borate Glass System. *Phys. Chem. Glasses-Eur. J. Glass Sci. Technol. Part B* **2009**, *50* (3), 156–164.
- (85) Chen, B.; Werner-Zwanziger, U.; Nascimento, M. L.; Ghussn, L.; Zanutto, E. D.; Zwanziger, J. W. Structural Similarity on Multiple Length Scales and Its Relation to Devitrification Mechanism: A Solid-State NMR Study of Alkali Diborate Glasses and Crystals. *J. Phys. Chem. C* **2009**, *113* (48), 20725–20732. <https://doi.org/10.1021/jp907259e>.
- (86) Saini, A.; Khanna, A.; Michaelis, V. K.; Kroeker, S.; González, F.; Hernández, D. Structure–Property Correlations in Lead Borate and Borosilicate Glasses Doped with Aluminum Oxide. *J. Non-Cryst. Solids* **2009**, *355* (45–47), 2323–2332. <https://doi.org/10.1016/j.jnoncrysol.2009.08.006>.
- (87) Smedskjaer, M. M.; Mauro, J. C.; Sen, S.; Yue, Y. Quantitative Design of Glassy Materials Using Temperature-Dependent Constraint Theory. *Chem. Mater.* **2010**, *22* (18), 5358–5365. <https://doi.org/10.1021/cm1016799>.
- (88) Martin, V.; Wood, B.; Werner-Zwanziger, U.; Zwanziger, J. Structural Aspects of the Photoelastic Response in Lead Borate Glasses. *J. Non-Cryst. Solids* **2011**, *357* (10), 2120–2125. <https://doi.org/10.1016/j.jnoncrysol.2011.01.042>.
- (89) Raguene, B.; Tricot, G.; Silly, G.; Ribes, M.; Pradel, A. Revisiting the ‘Mixed Glass Former Effect’ in Ultra-Fast Quenched Borophosphate Glasses by Advanced 1D/2D Solid State NMR. *J. Mater. Chem.* **2011**, *21* (44), 17693–17704. <https://doi.org/10.1039/C1JM12350E>.
- (90) Wu, J.; Potuzak, M.; Stebbins, J. F. High-Temperature in Situ ¹¹B NMR Study of Network Dynamics in Boron-Containing Glass-Forming Liquids. *J. Non-Cryst. Solids* **2011**, *357* (24), 3944–3951. <https://doi.org/10.1016/j.jnoncrysol.2011.08.013>.
- (91) Christensen, R.; Olson, G.; Martin, S. W. Structural Studies of Mixed Glass Former 0.35 Na₂O+0.65[xB₂O₃+(1-x) P₂O₅] Glasses by Raman and ¹¹B and ³¹P Magic Angle Spinning Nuclear Magnetic Resonance Spectroscopies. *J. Phys. Chem. B* **2013**, *117* (7), 2169–2179. <https://doi.org/10.1021/jp308494a>.
- (92) Feller, S.; Mullenbach, T.; Franke, M.; Bista, S.; O’Donovan-Zavada, A.; Hopkins, K.; Starkenberg, D.; McCoy, J.; Leipply, D.; Stansberry, J. Structure and Properties of Barium and Calcium Borosilicate Glasses. *Phys. Chem. Glasses-Eur. J. Glass Sci. Technol. Part B* **2012**, *53* (5), 210–218.
- (93) Laorodphan, N. Structural Studies of Thallium Containing Germanate and Borate Glasses and Crystalline Phases, University of Warwick, 2012. <http://webcat.warwick.ac.uk/record=b2685731~S1>.
- (94) Larink, D.; Eckert, H.; Reichert, M.; Martin, S. W. Mixed Network Former Effect in Ion-Conducting Alkali Borophosphate Glasses: Structure/Property Correlations in the System [M₂O]_{1/3} [(B₂O₃)_x(P₂O₅)_{1-x}]_{2/3} (M= Li, K, Cs). *J. Phys. Chem. C* **2012**, *116* (50), 26162–

26176. <https://doi.org/10.1021/jp307085t>.
- (95) Khanna, A.; Saini, A.; Chen, B.; González, F.; Pesquera, C. Structural Study of Bismuth Borosilicate, Aluminoborate and Aluminoborosilicate Glasses by ^{11}B and ^{27}Al MAS NMR Spectroscopy and Thermal Analysis. *J. Non-Cryst. Solids* **2013**, *373*, 34–41. <https://doi.org/10.1016/j.jnoncrysol.2013.04.020>.
- (96) Hasan, M. S.; Werner-Zwanziger, U.; Boyd, D. Composition-structure-properties Relationship of Strontium Borate Glasses for Medical Applications. *J. Biomed. Mater. Res. A* **2015**, *103* (7), 2344–2354. <https://doi.org/10.1002/jbm.a.35361>.
- (97) Maldonis, J.; North, J.; Ramm, A.; Starkenburg, D.; Hopkins, K.; Wiese-Moore, E.; Rasmussen, P.; Delgado, D.; Affatigato, M.; Feller, S. Structure Studies of Caesium and Lithium Borovanadate Glass Systems. *Phys. Chem. Glasses-Eur. J. Glass Sci. Technol. Part B* **2014**, *55* (2), 85–96.
- (98) Trégouët, H.; Caurant, D.; Majérus, O.; Charpentier, T.; Cormier, L.; Pytalev, D. Spectroscopic Investigation and Crystallization Study of Rare Earth Metaborate Glasses. *Procedia Mater. Sci.* **2014**, *7*, 131–137. <https://doi.org/10.1016/j.mspro.2014.10.018>.
- (99) Wu, J.; Stebbins, J. F. Cation Field Strength Effects on Boron Coordination in Binary Borate Glasses. *J. Am. Ceram. Soc.* **2014**, *97* (9), 2794–2801. <https://doi.org/10.1111/jace.13100>.
- (100) Kaur, N.; Khanna, A.; González-Barriuso, M.; González, F.; Chen, B. Effects of Al^{3+} , W^{6+} , Nb^{5+} and Pb^{2+} on the Structure and Properties of Borotellurite Glasses. *J. Non-Cryst. Solids* **2015**, *429*, 153–163. <https://doi.org/10.1016/j.jnoncrysol.2015.09.005>.
- (101) LaComb, M.; Stebbins, J. F. Tricuster Oxygen Atoms in Crystalline and Glassy SrB_4O_7 : High Resolution ^{11}B and ^{17}O Nuclear Magnetic Resonance Analysis. *J. Non-Cryst. Solids* **2015**, *428*, 105–111. <https://doi.org/10.1016/j.jnoncrysol.2015.08.014>.
- (102) Larink, D.; Eckert, H. Mixed Network Former Effects in Tellurite Glass Systems: Structure/Property Correlations in the System $(\text{Na}_2\text{O})_{1/3}[(2\text{TeO}_2)_x(\text{B}_2\text{O}_3)_{1-x}]_{2/3}$. *J. Non-Cryst. Solids* **2015**, *426*, 150–158. <https://doi.org/10.1016/j.jnoncrysol.2015.07.007>.
- (103) Saitoh, A.; Tricot, G.; Rajbhandari, P.; Anan, S.; Takebe, H. Effect of $\text{B}_2\text{O}_3/\text{P}_2\text{O}_5$ Substitution on the Properties and Structure of Tin Boro-Phosphate Glasses. *Mater. Chem. Phys.* **2015**, *149*, 648–656. <https://doi.org/10.1016/j.matchemphys.2014.11.021>.
- (104) Funke, L. M.; Eckert, H. Charge Compensation in Sodium Borophosphate Glasses Studied by ^{11}B $\{^{23}\text{Na}\}$ and ^{31}P $\{^{23}\text{Na}\}$ Rotational Echo Double Resonance Spectroscopy. *J. Phys. Chem. C* **2016**, *120* (6), 3196–3205. <https://doi.org/10.1021/acs.jpcc.5b11608>.
- (105) MacDonald, K.; Hanson, M. A.; Boyd, D. Modulation of Strontium Release from a Tertiary Borate Glass through Substitution of Alkali for Alkali Earth Oxide. *J. Non-Cryst. Solids* **2016**, *443*, 184–191.
- (106) Masai, H.; Koreeda, A.; Fujii, Y.; Ohkubo, T.; Kohara, S. Photoluminescence of Sn^{2+} -Centre as Probe of Transient State of Supercooled Liquid. *Opt. Mater. Express* **2016**, *6* (6), 1827–1836. <https://doi.org/10.1364/OME.6.001827>.
- (107) Svenson, M. N.; Youngman, R. E.; Yue, Y.; Rzoska, S. J.; Bockowski, M.; Jensen, L. R.; Smedskjaer, M. M. Volume and Structural Relaxation in Compressed Sodium Borate Glass. *Phys. Chem. Chem. Phys.* **2016**, *18* (43), 29879–29891. <https://doi.org/10.1039/C6CP06341A>.
- (108) Funke, L. M.; Bradtmüller, H.; Eckert, H. Recoupling Dipolar Interactions with Multiple $I=1$ Quadrupolar Nuclei: A ^{11}B $\{^6\text{Li}\}$ and ^{31}P $\{^6\text{Li}\}$ Rotational Echo Double Resonance Study of Lithium Borophosphate Glasses. *Solid State Nucl. Magn. Reson.* **2017**, *84*, 143–150.

- 1
2
3
4
5
6
7
8
9
10
11
12
13
14
15
16
17
18
19
20
21
22
23
24
25
26
27
28
29
30
31
32
33
34
35
36
37
38
39
40
41
42
43
44
45
46
47
48
49
50
51
52
53
54
55
56
57
58
59
60
- (109) Kim, Y.; Morita, K. Temperature Dependence and Cation Effects in the Thermal Conductivity of Glassy and Molten Alkali Borates. *J. Non-Cryst. Solids* **2017**, *471*, 187–194. <https://doi.org/10.1016/j.jnoncrysol.2017.05.034>.
- (110) Masai, H.; Okumura, S.; Ohkubo, T.; Yanagida, T. Luminescence of Sn²⁺ Center in Oxide Glass with a Tendency toward Phase Separation. *Opt. Mater. Express* **2017**, *7* (8), 2993–3002. <https://doi.org/10.1364/OME.7.002993>.
- (111) Torimoto, A.; Masai, H.; Okada, G.; Noriaki Kawaguchi; Yanagida, T.; Ohkubo, T. Emission Properties of Ce³⁺ Centers in Barium Borate Glasses Prepared from Different Precursor Materials. *Opt. Mater.* **2017**, *72*, 52–57. <https://doi.org/10.1016/j.optmat.2017.03.062>.
- (112) Storek, M.; Adjei-Acheamfour, M.; Christensen, R.; Martin, S. W.; Böhmer, R. Positive and Negative Mixed Glass Former Effects in Sodium Borosilicate and Borophosphate Glasses Studied by ²³Na NMR. *J. Phys. Chem. B* **2016**, *120* (19), 4482–4495. <https://doi.org/10.1021/acs.jpcc.6b00482>.
- (113) Zhang, R.; de Oliveira, M.; Wang, Z.; Fernandes, R. G.; de Camargo, A. S.; Ren, J.; Zhang, L.; Eckert, H. Structural Studies of Fluoroborate Laser Glasses by Solid State NMR and EPR Spectroscopies. *J. Phys. Chem. C* **2017**, *121* (1), 741–752. <https://doi.org/10.1021/acs.jpcc.6b11187>.
- (114) Curtis, B.; Hynek, D.; Kaizer, S.; Feller, S.; Martin, S. W. Composition Dependence of the Short Range Order Structures in 0.2Na₂O+0.8[xB₂O₃+ (1-x) GeO₂] Mixed Glass Formers. *J. Non-Cryst. Solids* **2018**, *500*, 61–69. <https://doi.org/10.1016/j.jnoncrysol.2018.05.035>.
- (115) de Oliveira Jr, M.; Oliveira, J. S.; Kundu, S.; Machado, N. M. P.; Rodrigues, A. C. M.; Eckert, H. Network Former Mixing Effects in Ion-Conducting Lithium Borotellurite Glasses: Structure/Property Correlations in the System (Li₂O)_y[2(TeO₂)_x(B₂O₃)_{1-x}]_{1-y}. *J. Non-Cryst. Solids* **2018**, *482*, 14–22. <https://doi.org/10.1016/j.jnoncrysol.2017.11.052>.
- (116) Fernandes, H. R.; Kapoor, S.; Patel, Y.; Ngai, K.; Levin, K.; Germanov, Y.; Krishtopa, L.; Kroeker, S.; Goel, A. Composition-Structure-Property Relationships in Li₂O–Al₂O₃–B₂O₃ Glasses. *J. Non-Cryst. Solids* **2018**, *502*, 142–151. <https://doi.org/10.1016/j.jnoncrysol.2018.08.005>.
- (117) Jin, T.; Bernard, G. M.; Miskolzie, M.; Terskikh, V. V.; Michaelis, V. K. A ¹¹B and ³¹P MAS NMR Study of the Impact of Ca²⁺ and Sr²⁺ Network Modifying Cations on the Structure of Borate and Borophosphate Glasses. *Phys. Chem. Glasses-Eur. J. Glass Sci. Technol. Part B* **2018**, *59* (4), 174–180. <https://doi.org/10.13036/17533562.59.4.048>.
- (118) Kapoor, S.; Youngman, R. E.; Zakharchuk, K.; Yaremchenko, A.; Smith, N. J.; Goel, A. Structural and Chemical Approach toward Understanding the Aqueous Corrosion of Sodium Aluminoborate Glasses. *J. Phys. Chem. B* **2018**, *122* (48), 10913–10927. <https://doi.org/10.1021/acs.jpcc.8b06155>.
- (119) Paterson, A. L.; Hannon, A. C.; Werner-Zwanziger, U.; Zwanziger, J. W. Structural Differences between the Glass and Crystal Forms of the Transparent Ferroelectric Nanocomposite, LaBGeO₅, from Neutron Diffraction and NMR Spectroscopy. *J. Phys. Chem. C* **2018**, *122* (36), 20963–20980. <https://doi.org/10.1021/acs.jpcc.8b05747>.
- (120) Torimoto, A.; Masai, H.; Okada, G.; Kawaguchi, N.; Yanagida, T.; Ohkubo, T. Correlation between Emission Properties, Valence States of Ce and Chemical Compositions of Alkaline Earth Borate Glasses. *J. Lumin.* **2018**, *197*, 98–103. <https://doi.org/10.1016/j.jlumin.2017.12.068>.
- (121) Tsuruyu, K.; Ohkubo, T.; Kakihara, T.; Iwadate, Y. Structural Roles of V and Mo in Borate

- and Silicate Glasses by Solid State NMR and Raman Spectroscopies. *Phys. Chem. Glasses-Eur. J. Glass Sci. Technol. Part B* **2018**, *59* (5), 234–240. <https://doi.org/10.13036/17533562.59.5.028>.
- (122) Doucet, J.; Tonkopi, E.; Nuschke, A.; Tremblay, M.; Brewer, K.; Beyea, S.; Filiaggi, M.; Abraham, R.; Werner-Zwanziger, U.; Boyd, D. Multi-Modal Imageability and Degradation Characteristics of High-Borate Glass Systems for Transient Embolization. *J. Non-Cryst. Solids* **2019**, *510*, 26–35. <https://doi.org/10.1016/j.jnoncrysol.2019.01.014>.
- (123) Januchta, K.; Youngman, R. E.; Jensen, L. R.; Smedskjaer, M. M. Mechanical Property Optimization of a Zinc Borate Glass by Lanthanum Doping. *J. Non-Cryst. Solids* **2019**, *520*, 119461. <https://doi.org/10.1016/j.jnoncrysol.2019.119461>.
- (124) Masuno, A.; Iwata, T.; Yanaba, Y.; Sasaki, S.; Inoue, H.; Watanabe, Y. High Refractive Index La-Rich Lanthanum Borate Glasses Composed of Isolated BO_3 Units. *Dalton Trans.* **2019**, *48* (29), 10804–10811. <https://doi.org/10.1039/C9DT01715A>.
- (125) Lepry, W. C.; Nazhat, S. N. The Anomaly in Bioactive Sol–Gel Borate Glasses. *Mater. Adv.* **2020**, *1* (5), 1371–1381. <https://doi.org/10.1039/D0MA00360C>.
- (126) Lee, A. C.; Lee, S. K. Effect of Composition on Structural Evolution and NMR Parameters of Quadrupolar Nuclides in Sodium Borate and Aluminoborosilicate Glasses: A View from High-Resolution ^{11}B , ^{27}Al , and ^{17}O Solid-State NMR. *J. Non-Cryst. Solids* **2021**, *555*, 120271. <https://doi.org/10.1016/j.jnoncrysol.2020.120271>.
- (127) Lee, S. K.; Lee, A. C.; Kweon, J. J. Probing Medium-Range Order in Oxide Glasses at High Pressure. *J. Phys. Chem. Lett.* **2021**, *12* (4), 1330–1338. <https://doi.org/10.1021/acs.jpcclett.1c00055>.
- (128) Ruckman, A.; Beckler, G.; Guthrie, W.; Jesuit, M.; Boyd, M.; Slagle, I.; Wilson, R.; Barrow, N.; Tagiara, N. S.; Kamitsos, E. I. Lithium Ion Sites and Their Contribution to the Ionic Conductivity of $\text{RLi}_2\text{O-B}_2\text{O}_3$ Glasses with $R \leq 1.85$. *Solid State Ion.* **2021**, *359*, 115530. <https://doi.org/10.1016/j.ssi.2020.115530>.
- (129) Chatzipanagis, K. I.; Tagiara, N. S.; Kamitsos, E. I.; Barrow, N.; Slagle, I.; Wilson, R.; Greiner, T.; Jesuit, M.; Leonard, N.; Phillips, A. Structure of Lead Borate Glasses by Raman, ^{11}B MAS, and ^{207}Pb NMR Spectroscopies. *J. Non-Cryst. Solids* **2022**, *589*, 121660. <https://doi.org/10.1016/j.jnoncrysol.2022.121660>.
- (130) Saini, R.; Kapoor, S.; Neuville, D. R.; Youngman, R. E.; Cerrutti, B. M.; McCloy, J. S.; Eckert, H.; Goel, A. Correlating Sulfur Solubility with Short-to-Intermediate Range Ordering in the Structure of Borosilicate Glasses. *J. Phys. Chem. C* **2022**, *126* (1), 655–674. <https://doi.org/10.1021/acs.jpcc.1c08654>.
- (131) Topper, B.; Tsekrekas, E. M.; Greiner, L.; Youngman, R. E.; Kamitsos, E. I.; Möncke, D. The Dual Role of Bismuth in $\text{Li}_2\text{O-Bi}_2\text{O}_3\text{-B}_2\text{O}_3$ Glasses along the Orthoborate Join. *J. Am. Ceram. Soc.* **2022**, *105* (12), 7302–7320. <https://doi.org/10.1111/jace.18699>.
- (132) Yang, J.; Sohn, I. Compositional Dependence of Thermophysical Properties in Binary Alkaline Earth Borate Melts: Insights from Structure in Short-Range and Intermediate-Range Order. *J. Mater. Sci. Technol.* **2022**, *131*, 195–203. <https://doi.org/10.1016/j.jmst.2022.05.037>.
- (133) Sukenaga, S.; Unozawa, H.; Chiba, Y.; Tashiro, M.; Kawanishi, S.; Shibata, H. Incorporation Limit of MoO_3 in Sodium Borosilicate Glasses. *J. Am. Ceram. Soc.* **2023**, *106* (1), 293–305. <https://doi.org/10.1111/jace.18760>.
- (134) Swanson, R.; Stebbins, J.; Yeo, T.; Xu, Y.; Hung, I.; Gan, Z.; McCormack, S.; Sen, S. Structure and Fragility of Normal and Invert Lanthanum Borate Glasses: Results from ^{11}B

- and ^{17}O NMR Spectroscopy and Calorimetry. *J. Non-Cryst. Solids* **2023**, *603*, 122119. <https://doi.org/10.1016/j.jnoncrysol.2022.122119>.
- (135) Topper, B.; Möncke, D.; Youngman, R. E.; Valvi, C.; Kamitsos, E. I.; Varsamis, C. P. Zinc Borate Glasses: Properties, Structure and Modelling of the Composition-Dependence of Borate Speciation. *Phys. Chem. Chem. Phys.* **2023**, *25* (8), 5967–5988. <https://doi.org/10.1039/D2CP05517A>.
- (136) Sharma, S.; Middha, S.; Khanna, A.; Chen, B.; Chen, B. Comparative Study of Eu^{3+} Doped Calcium Borate Glasses and Crystalline Calcium Hexaborate Phosphors. *J. Mater. Sci. Mater. Electron.* **2024**, *35* (2), 152. <https://doi.org/10.1007/s10854-023-11754-3>.
- (137) Song, L.; Feller, S.; Hawbaker, H.; Yin, W.; Li, W.; Hannon, A. C.; Zhou, Y.; Xu, J.; Zhu, F. Unveiling the Structure of Calcium Borate Glass by Neutron Diffraction, MAS-NMR, Raman and First-Principles Calculations. *Ceram. Int.* **2024**, *50* (4), 6634–6647. <https://doi.org/10.1016/j.ceramint.2023.11.412>.
- (138) Silver, A. H. *Nuclear Quadrupole Effects in Boron Compounds*; Rensselaer Polytechnic Institute, 1958.
- (139) Greenblatt, S.; Bray, P. A Discussion of Fraction of 4-Co-Ordinated Boron Atoms Present in Borate Glasses. *Phys. Chem. Glasses* **1967**, *8* (6), 213.
- (140) Taylor, P.; Friebele, E. On the Nature of Unique Boron Sites in Borate Glasses. *J. Non-Cryst. Solids* **1974**, *16* (3), 375–386. [https://doi.org/10.1016/0022-3093\(74\)90082-9](https://doi.org/10.1016/0022-3093(74)90082-9).
- (141) Dell, W.; Bray, P. The Determination of Phase Relations in the System $\text{MgO-B}_2\text{O}_3$ at the Metaborate Composition Using B^{11} NMR. *Phys. Chem. Glasses* **1982**, *23* (4), 126–128.
- (142) Bray, P. J.; Lui, M. L.; Hintenlang, D. E. NMR Studies of Structure and Ion Motion in Glasses. *Wiss. Z.* **1982**, *32*, 409–426.
- (143) Ratai, E.-M.; Janssen, M.; Epping, J.; Chan, J.; Eckert, H. Local and Medium Range Order in Alkali Borate Glasses: An Overview of Recent Solid State NMR Results. *Phys. Chem. Glasses* **2003**, *44* (2), 45–53.
- (144) Imre, A. W.; Voss, S.; Mehrer, H. Ionic Conduction, Diffusion and Glass Transition in $0.2[\text{XNa}_2\text{O} \cdot (1-\text{X})\text{Rb}_2\text{O}] \cdot 0.8\text{B}_2\text{O}_3$. *J. Non-Cryst. Solids* **2004**, *333* (3), 231–239. <https://doi.org/10.1016/j.jnoncrysol.2003.12.050>.
- (145) Nijhawan, S. Glass Transition Temperature of the Sodium Borosilicate System and An Analysis of the Structure of Rubidium Borate Glasses Using NMR Spectroscopy and Transition Temperatures. Honors Thesis, Coe College, Physics Department, 2003.
- (146) Moeller, A.; Olesiak, M.; Gao, J.; Giri, S.; Affatigato, M.; Feller, S.; Kodama, M. A Solution Approach to High Potassium Content Borate Glasses. *Phys. Chem. Glasses* **2003**, *44* (3), 237–240.
- (147) Michaelis, V. K. *Nuclear Magnetic Resonance Studies of Disorder and Local Structure in Borate and Germanate Materials*; University of Manitoba (Canada), 2011.
- (148) Ragueneau, B.; Tricot, G.; Silly, G.; Ribes, M.; Pradel, A. The Mixed Glass Former Effect in Twin-Roller Quenched Lithium Borophosphate Glasses. *Solid State Ion.* **2012**, *208*, 25–30. <https://doi.org/10.1016/j.ssi.2011.11.034>.
- (149) Christensen, R. The Mixed Glass Former Effect in $0.35 \text{Na}_2\text{O} + 0.65[\text{x}\text{B}_2\text{O}_3 + (1-\text{x}) \text{P}_2\text{O}_5]$ Glasses. **2012**. <https://doi.org/10.31274/etd-180810-2218>.
- (150) Pytalev, D.; Caurant, D.; Majérus, O.; Trégouët, H.; Charpentier, T.; Mavrin, B. Structure and Crystallization Behavior of $\text{La}_2\text{O}_3 \cdot 3\text{B}_2\text{O}_3$ Metaborate Glasses Doped with Nd^{3+} or Eu^{3+} Ions. *J. Alloys Compd.* **2015**, *641*, 43–55. <https://doi.org/10.1016/j.jallcom.2015.03.244>.
- (151) Tricot, G.; Saitoh, A.; Takebe, H. Intermediate Length Scale Organisation in Tin

- Borophosphate Glasses: New Insights from High Field Correlation NMR. *Phys. Chem. Chem. Phys.* **2015**, *17* (44), 29531–29540. <https://doi.org/10.1039/c5cp02095f>.
- (152) Wang, W.; Christensen, R.; Curtis, B.; Hynek, D.; Keizer, S.; Wang, J.; Feller, S.; Martin, S. W.; Kieffer, J. Elastic Properties and Short-Range Structural Order in Mixed Network Former Glasses. *Phys. Chem. Chem. Phys.* **2017**, *19* (24), 15942–15952. <https://doi.org/10.1039/C6CP08939A>.
- (153) Zielniok, D.; Cramer, C.; Eckert, H. Structure/Property Correlations in Ion-Conducting Mixed-Network Former Glasses: Solid-State NMR Studies of the System Na₂O–B₂O₃–P₂O₅. *Chemistry of materials* **2007**, *19* (13), 3162–3170.
- (154) Takaishi, T.; Jin, J.; Uchino, T.; Yoko, T. Structural Study of PbO–B₂O₃ Glasses by X-ray Diffraction and ¹¹B MAS NMR Techniques. *J. Am. Ceram. Soc.* **2000**, *83* (10), 2543–2548. <https://doi.org/10.1111/j.1151-2916.2000.tb01588.x>.
- (155) Krishnamurthy, A.; Wren, J. E.; Michaelis, V. K.; Kroeker, S. Composition-dependent Structural Role of Lead in Aluminoborate and Galloborate Glasses: A Solid-state NMR Study. *J. Am. Ceram. Soc.* **2024**, *107* (7), 4522–4535. <https://doi.org/10.1111/jace.19694>.
- (156) Aguiar, P. M. *Multinuclear Magnetic Resonance Investigations of Structure and Order in Borates and Metal Cyanides*; University of Manitoba, **2007**.
- (157) Nanba, T.; Nishimura, M.; Miura, Y. A theoretical interpretation of the chemical shift of ²⁹Si NMR peaks in alkali borosilicate glasses. *Geochim. Cosmochim. Acta* **2004**, *68* (24), 5103–5111. <https://doi.org/10.1016/j.gca.2004.05.042>
- (158) Sasaki, S.; Masuno, A.; Yanaba, Y.; Inoue, H.; Ohkubo, T. Survival of Fragmented BO₄ Units in Highly Modified Rare-Earth-Rich Borate Glasses. *Inorg. Chem.* **2024**, *63* (49), 23131–23140. <https://doi.org/10.1021/acs.inorgchem.4c03264>
- (159) Youngman, R. E.; Zwanziger, J. W. On the formation of tetracoordinate boron in rubidium borate glasses. *J. Am. Chem. Soc.* **1995**, *117* (4), 1397–1402. <https://doi.org/10.1021/ja00109a026>
- (160) Brow, R. K.; Tallant, D. R.; Turner, G. L. Polyhedral arrangements in lanthanum aluminoborate glasses. *J. Am. Chem. Soc.* **1997**, *80* (5), 1239–1244.
- (161) Youngman, R. E.; Zwanziger, J. W. Network modification in potassium borate glasses: structural studies with NMR and Raman spectroscopies. *J. Phys. Chem.* **1996**, *100* (41), 16720–16728.
- (162) Mustarelli, P.; Quartarone, E.; Benevelli, F. A ¹¹B and ⁷Li MAS-NMR study of sol-gel lithium triborate glass subjected to thermal densification. *Mater. Res. Bull.* **1997**, *32* (6), 679–687. [https://doi.org/10.1016/S0025-5408\(97\)00038-X](https://doi.org/10.1016/S0025-5408(97)00038-X)
- (163) Terashima, K.; Shimoto, T. H.; Yoko, T. Structure and nonlinear optical properties of PbO–Bi₂O₃–B₂O₃ glasses. *Phys. Chem. Glasses* **1997**, *38* (4), 211–217.
- (164) Terashima, K.; Uchino, T.; Hashimoto, T.; Yoko, T. Structure and nonlinear optical properties of BaO–TiO₂–B₂O₃ glasses. *J. Ceram. Soc. Jpn.* **1997**, *105* (1220), 288–293. <https://doi.org/10.2109/jcersj.105.288>
- (165) Grishchuk, E. V.; Efrushina, N. P.; Dotsenko, V. P.; Gubanova, E. R.; Structural study of fluoroborate glasses by NMR and IR-spectroscopy. *Neorg. Mater.* **1998**, *34* (5), 520–522.
- (166) Wang, S.; Stebbins, J. F. On the structure of borosilicate glasses: a triple-quantum magic-angle spinning ¹⁷O nuclear magnetic resonance study. *J. Non-Cryst. Solids* **1998**, *321* (3), 286–290. [https://doi.org/10.1016/S0022-3093\(98\)00703-0](https://doi.org/10.1016/S0022-3093(98)00703-0)
- (167) Jung, J. K.; Song, S. K.; Noh, T. H.; Han, O. H. ¹¹B NMR investigations in xV₂O₅–B₂O₃ and xV₂O₅–B₂O₃–PbO glasses. *J. Non-Cryst. Solids* **2000**, *270* (1–3), 97–102.

- [https://doi.org/10.1016/S0022-3093\(00\)00054-5](https://doi.org/10.1016/S0022-3093(00)00054-5)
- (168) Wang, D.; Zhang, J.; Zhang, D.; Wan, S.; Zhang, Q.; Sun, D.; Yin, S. Structural investigation of $\text{Li}_2\text{O}-\text{B}_2\text{O}_3-\text{MoO}_3$ glasses and high-temperature solutions: toward understanding the mechanism of flux-induced growth of lithium triborate crystal. *CrystEngComm* **2013**, *15* (2), 356-364. <https://doi.org/10.1039/C2CE26231B>
- (169) Chialanza, M. R.; Keuchkerian, R.; Cárdenas, A.; Olivera, A.; Vazquez, S.; Faccio, R.; Castiglioni, J.; Schneider, J. F.; Fornaro, L. Correlation between structure, crystallization and thermally stimulated luminescence response of some borate glass and glass-ceramics. *J. Non-Cryst. Solids* **2015**, *427*, 191-198. <https://doi.org/10.1016/j.jnoncrysol.2015.07.045>
- (170) Tokuda, Y.; Takahashi, Y.; Masai, H.; Kaneko, S.; Ueda, Y.; Fujimura, S.; Yoko, T. Local structure of alkalis in mixed-alkali borate glass to elucidate the origin of mixed-alkali effect. *J. Asian Ceram. Soc.* **2015**, *3* (4), 412-416. <https://doi.org/10.1016/j.jascer.2015.09.002>
- (171) Osipov, A. A.; Eremyashev, V. E.; Mazur, A. S.; Tolstoi, P. M.; Osipova, L. M. Coordination state of aluminum and boron in barium aluminoborate glass. *Glass Phys. Chem.* **2016**, *42* (3), 230-237. <https://doi.org/10.1134/S1087659616030111>
- (172) Song, L.; Wang, Y.; Zhai, T.; Sun, B.; Du, Y.; Feller, S.; Yin, W.; Xu, J.; Hannon, A. C.; Zhu, F. Revealing the microstructure and structural origin of glass-forming range of magnesium borate glass. *Ceram. Int.* **2025 (In Press)**, <https://doi.org/10.1016/j.ceramint.2025.02.075>
- (173) Jellison Jr, G.; Bray, P. A Structural Interpretation of B^{10} and B^{11} NMR Spectra in Sodium Borate Glasses. *J. Non-Cryst. Solids* **1978**, *29* (2), 187-206. [https://doi.org/10.1016/0022-3093\(78\)90113-8](https://doi.org/10.1016/0022-3093(78)90113-8).
- (174) Yun, Y.; Bray, P. J. B^{11} Nuclear Magnetic Resonance Studies of $\text{Li}_2\text{O}-\text{B}_2\text{O}_3$ Glasses of High Li_2O Content. *J. Non-Cryst. Solids* **1981**, *44* (2-3), 227-237. [https://doi.org/10.1016/0022-3093\(81\)90025-9](https://doi.org/10.1016/0022-3093(81)90025-9).
- (175) Terashima, K.; Hashimoto, T.; Uchino, T.; Kim, S.-H.; Yoko, T. Structure and Nonlinear Optical Properties of $\text{Sb}_2\text{O}_3-\text{B}_2\text{O}_3$ Binary Glasses. *J. Ceram. Soc. Jpn.* **1996**, *104* (1215), 1008-1014.
- (176) Button, D. P.; Tandon, R.; King, C.; Veléz, M. H.; Tuller, H. L.; Uhlmann, D. R. Insights into the structure of alkali borate glasses. *J. Non-Cryst. Solids* **1982**, *49* (1-3), 129-142. [https://doi.org/10.1016/0022-3093\(82\)90112-0](https://doi.org/10.1016/0022-3093(82)90112-0)
- (177) Button, D. P.; Tandon, R. P.; Tuller, H. L.; Uhlmann, D. R. Fast Li^+ ion conduction in chloroborate glasses. *J. Non-Cryst. Solids* **1980**, *42* (1-3), 297-302. [https://doi.org/10.1016/0022-3093\(80\)90031-9](https://doi.org/10.1016/0022-3093(80)90031-9)
- (178) Zhong, J. *Structural aspects of several oxide glasses as elucidated by multinuclear NMR*; Brown University, **1988**.
- (179) Voss, S.; Berkemeier, F.; Imre, A. W.; Mehrer, H. Mixed-alkali effect of tracer diffusion and ionic conduction in Na-Rb borate glasses as a function of total alkali content. *Z. Phys. Chem.* **2004**, *218* (12), 1353-1374. <https://doi.org/10.1524/zpch.218.12.1353.53833>
- (180) Christensen, R.; Byer, J.; Olson, G.; Martin, S. W. The glass transition temperature of mixed glass former $0.35\text{Na}_2\text{O} + 0.65[\text{x}\text{B}_2\text{O}_3 + (1 - \text{x})\text{P}_2\text{O}_5]$ glasses. *J. Non-Cryst. Solids* **2012**, *358* (4), 826-831. <https://doi.org/10.1016/j.jnoncrysol.2011.12.068>
- (181) Trégouët, H.; Caurant, D.; Majérus, O.; Charpentier, T.; Lerouge, T.; Cormier, L. Exploration of glass domain in the $\text{SiO}_2-\text{B}_2\text{O}_3-\text{La}_2\text{O}_3$ system. *J. Non-Cryst. Solids* **2017**, *476*, 158-172. <https://doi.org/10.1016/j.jnoncrysol.2017.09.048>
- (182) Jellison, Jr., G. E. Structural Determinations of Boron Oxide and Sodium Borate Glasses;

- Brown University, **1977**.
- (183) Zhong, J.; Wu, X.; Liu, M. L.; Bray, P. J. Structural modeling of lithium borosilicate glasses via NMR studies. *J. Non-Cryst. Solids* **1988**, 107 (1), 81-87. [https://doi.org/10.1016/0022-3093\(88\)90096-8](https://doi.org/10.1016/0022-3093(88)90096-8)
- (184) Reser, M. K. (ed.). *Phase Diagrams for Ceramists*. The American Ceramic Society **1964**.
- (185) Reser, M. K. (ed.). *Phase Diagrams for Ceramists (1975 Supplement)*. The American Ceramic Society **1975**.
- (186) Sastry, B. S. R., Hummel, F. A. Studies in lithium oxide systems: V, $\text{Li}_2\text{O-Li}_2\text{O-B}_2\text{O}_3$. *J. Am. Ceram. Soc.* **1959**, 42 (5), 216-218. <https://doi.org/10.1111/j.1151-2916.1959.tb15456.x>
- (187) Yu, H.; Jin, Z.; Chen, Q.; Hillert, M.; Thermodynamic assessment of the lithium-borate system. *J. Am. Ceram. Soc.* **2000**, 83 (12), 3082-3088. <https://doi.org/10.1111/j.1151-2916.2000.tb01686.x>
- (188) Morey, G. W.; Merwin, H. E.; Phase equilibrium relationships in the binary system, sodium oxide-boric oxide, with some measurements of the optical properties of the glasses. *J. Am. Ceram. Soc.* **1936**, 58 (11), 2248-2254. <https://doi.org/10.1021/ja01302a048>
- (189) Milman, T.; Bouaziz, R.; Contribution à l'étude des borates de sodium. *Ann. Chim.* **1968**, 3 (4), 311-312, as cited in Reser, M. K. (ed.). *Phase Diagrams for Ceramists (1975 Supplement)*. The American Ceramic Society **1975**.
- (190) Utlak, S. A.; Besmann, T. M. Thermodynamic assessment of the $\text{Na}_2\text{O-Al}_2\text{O}_3\text{-SiO}_2\text{-B}_2\text{O}_3$ pseudo-binary and -ternary systems. *J. Chem. Thermodyn.* **2019**, 130, 251-268. <https://doi.org/10.1016/j.jct.2018.09.001>
- (191) Rollet, A. P. Sur les borates de potassium: Étude du système $\text{K}_2\text{O-B}_2\text{O}_3$. *C. R. Hebd. Seances Acad. Sci.* **1935**, 200 (21), 1763-1765.
- (192) Rollet, A. P. Sur le polymorphisme du pentaborate de potassium $5\text{B}_2\text{O}_3\cdot\text{K}_2\text{O}$. *C. R. Hebd. Seances Acad. Sci.* **1936**, 202 (22), 1863-1866.
- (193) Toledano, P. Borates of Potassium and Rubidium. *Rev. Chim. Miner.* **1964**, 1 (3), 353-413, as cited in Shaw, R. R.; Uhlmann, D. R. Subliquidus immiscibility in binary alkali borates. *J. Am. Ceram. Soc.* **1968**, 51 (7), 377-382. <https://doi.org/10.1111/j.1151-2916.1968.tb11897.x>
- (194) Kocher, J. Study of rubidium and cesium borates. *Rev. Chim. Miner.* **1966**, 3 (2), 209, as cited in Reser, M. K. (ed.). *Phase Diagrams for Ceramists (1975 Supplement)*. The American Ceramic Society **1975**.
- (195) Bubnova, R. S.; Polyakova, I. G.; Filatov, S. K.; Krzhizhanovskaya, M. G. Crystal Structure and Thermal Behavior of Rubidium Borates in *Proceedings of II International Conference on Borate Glasses, Crystals, and Melts*, Sheffield: The Society of Glass Technology, **1997**, 120-127.
- (196) Krogh-Moe, J. Some new compounds in the system cesium oxide-boron oxide. *Arkiv for Kemi* **1958**, 12 (26), 247-249.
- (197) Rockett, T. J.; Foster, W. R. Phase relations in the system boron oxide-silica. *J. Am. Ceram. Soc.* **1965**, 48 (2), 75-80. <https://doi.org/10.1111/j.1151-2916.1965.tb11803.x>
- (198) Chen, H. M.; Chen, J. M.; Wang, S.; Li, W. T.; Meng, F. G.; Chen, W. J.; Li, L.; Yao, S. J. Thermodynamic Assessment of $\text{B}_2\text{O}_3\text{-SiO}_2$ Binary System. *Applied Mechanics and Materials* **2014**, 628, 68-72. <https://doi.org/10.4028/www.scientific.net/AMM.628.68>
- (199) Baret, G. R.; Madar, R.; Bernard, C. Silica-Based Oxide Systems: I. Experimental and Calculated Phase Equilibria in Silicon, Boron, Phosphorus, Germanium, and Arsenic Oxide

- Mixtures. *J. Electrochem. Soc.* **1991**, 138 (9), 2830-2835. <https://doi.org/10.1149/1.2086066>
- (200) Kocher, J.; Sadeghi, N. Sur les borates anhydres d'argent. *C. R. Acad. Sc. Paris, C* **1967**, 17, 1481-1484.
- (201) Geller, R. F.; Bunting, E. N. The system PbO-B₂O₃. *J. Res. Natl. Bur. Stand.* **1937**, 18 (5), 585-593. <https://doi.org/10.6028/jres.018.035>
- (202) Levin, E. M.; McDaniel, C. L. The System Bi₂O₃-B₂O₃. *J. Am. Ceram. Soc.* **1962**, 45 (8), 355-360. <https://doi.org/10.1111/j.1151-2916.1962.tb11168.x>
- (203) Levin, E. M. Liquid Immiscibility in Oxide Systems, In Alper, A. M. (ed.) *Phase Diagrams: Materials Science and Technology, Volume III* **1970**, 143-270.
- (204) Davis, H. M.; Knight, M. A. The System Magnesium Oxide-Boric Oxide. *J. Am. Ceram. Soc.* **1945**, 28 (4), 97-102. <https://doi.org/10.1111/j.1151-2916.1945.tb14519.x>
- (205) Carlson, E. T. The System CaO-B₂O₃. *J. Res. Natl. Bur. Stand.* **1932**, 9, 825-832. <https://doi.org/10.6028/jres.009.060>
- (206) Polyakova, I. G.; Litovchik, E. O. Crystallization of glasses in the SrO-B₂O₃ system. *Glass Phys. Chem* **2008**, 34 (4), 369-380. <https://doi.org/10.1134/S1087659608040056>
- (207) Witzmann, H.; Beulich, W. Zur Bildung wasserfreier Strontiumborate. Ein Beitrag zum Zustandsdiagramm des Systems SrO-B₂O₃. *Z. Phys. Chem.* **1963**, 225 (5-6), 336-341, as cited in Polyakova, I. G.; Litovchik, E. O. Crystallization of glasses in the SrO-B₂O₃ system. *Glass Phys. Chem* **2008**, 34 (4), 369-380. <https://doi.org/10.1134/S1087659608040056>
- (208) Pam, X. M.; Wang, C.; Jin, Z. P. Assessment of the thermodynamics and phase diagram of the SrO-B₂O₃ system. *Int. J. Mater. Res.* **2004**, 95 (1), 40-44. <https://doi.org/10.3139/ijmr-2004-0008>
- (209) Harrison, D. E.; Hummel, F. A. Phase Equilibria and Fluorescence in the System Zinc Oxide-Boric Oxide. *J. Electrochem. Soc.* **1956**, 103 (9), 491-498. <https://doi.org/10.1149/1.2430391>
- (210) Dimitriev, Y.; Kashchieva, E. Immiscibility in the TeO₂-B₂O₃ system. *J. Mater. Sci.* **1975**, 10, 1419-1424. <https://doi.org/10.1007/BF00540832>
- (211) Levin, E. M.; Robbins, C. R.; Waring, J. L. Immiscibility and the system lanthanum oxide-boric oxide. *J. Am. Ceram. Soc.* **1961**, 44 (2), 87-91. <https://doi.org/10.1111/j.1151-2916.1961.tb15356.x>
- (212) Subbarao, E. C.; Hummel, F. A. The System Cadmium Oxide-Boric Oxide: I. Phase Equilibria. *J. Electrochem. Soc.* **1956**, 103 (1), 29-33. <https://doi.org/10.1149/1.2430229>
- (213) Kim, Y.; Jung, I. Thermodynamic Evaluation and Optimization of the MnO-B₂O₃ and MnO-B₂O₃-SiO₂ Systems and Its Application to Oxidation of High-Strength Steels Containing Boron. *Metall. Mater. Trans. A* **2015**, 46A, 2736-2747. <https://doi.org/10.1007/s11661-015-2841-4>
- (214) Penin, N.; Seguin, L.; Gérard, B.; Touboul, M.; Nowogrocki, G. β-Tl₂B₄O₇: Compound containing a new three-dimensional borate anion. *J. Solid State Chem.* **2001**, 160 (1), 139-146. <https://doi.org/10.1006/jssc.2001.9207>
- (215) Wong, J.; Angell, C. A. *Glass: Structure by Spectroscopy*; Marcel Dekker Inc.: New York, 1976.
- (216) Kamitsos, E. Infrared Spectroscopy of Glasses. In *Modern glass characterization*; Affatigato, M., Ed.; The American Ceramic Society and John Wiley & Sons, Inc.: Hoboken, New Jersey, 2015; pp 32-73.
- (217) Almeida, R. M.; Santos, L. F. Raman Spectroscopy of Glasses. In *Modern glass*

- 1
2
3
4
5
6
7
8
9
10
11
12
13
14
15
16
17
18
19
20
21
22
23
24
25
26
27
28
29
30
31
32
33
34
35
36
37
38
39
40
41
42
43
44
45
46
47
48
49
50
51
52
53
54
55
56
57
58
59
60
- characterization; Affatigato, M., Ed.; The American Ceramic Society and John Wiley & Sons, Inc: Hoboken, New Jersey, 2015; pp 74–106.
- (218) Weir, C.; Lippincott, E. R. Infrared Studies of Aragonite, Calcite, and Vaterite Type Structures in the Borates, Carbonates, and Nitrates. *J. Res. Natl. Bur. Stand. Sect. Phys. Chem.* **1961**, *65* (3), 173–183. <https://doi.org/10.6028/jres.065A.021>.
- (219) Hart, P.; Smallwood, S. An Examination of the Infra-Red Spectra of Borate Anions. *J. Inorg. Nucl. Chem.* **1962**, *24* (9), 1047–1056. [https://doi.org/10.1016/0022-1902\(62\)80248-6](https://doi.org/10.1016/0022-1902(62)80248-6).
- (220) Weir, C.; Schroeder, R. Infrared Spectra of the Crystalline Inorganic Borates. *J. Res. Natl. Bur. Stand. Sect. Phys. Chem.* **1964**, *68* (5), 465–487. <https://doi.org/10.6028/jres.068A.045>.
- (221) Rulmont, A.; Almou, M. Vibrational Spectra of Metaborates with Infinite Chain Structure: LiBO_2 , CaB_2O_4 , SrB_2O_4 . *Spectrochim. Acta Part Mol. Spectrosc.* **1989**, *45* (5), 603–610. [https://doi.org/10.1016/0584-8539\(89\)80013-3](https://doi.org/10.1016/0584-8539(89)80013-3).
- (222) Chryssikos, G. D.; Kapoutsis, J.; Patsis, A.; Kamitsos, E. A Classification of Metaborate Crystals Based on Raman Spectroscopy. *Spectrochim. Acta Part Mol. Spectrosc.* **1991**, *47* (8), 1117–1126.
- (223) Anderson, S.; Bohon, R. L.; Kimpton, D. D. Infrared Spectra and Atomic Arrangement in Fused Boron Oxide and Soda Borate Glasses. *J. Am. Ceram. Soc.* **1955**, *38* (10), 370–377. <https://doi.org/10.1111/j.1151-2916.1955.tb14558.x>.
- (224) Jellyman, P.; Procter, J. Infrared Reflection Spectra of Glasses. *J. Soc. Glass Technol.* **1955**, *39*, 173–92T.
- (225) Moore, H. A Study of Glasses Consisting of the Oxides of Elements of Low Atomic Weight. Part II. The Absorption Characteristics of Certain of the Experimental Glasses. *J. Soc. Glass Technol.* **1956**, *40*, 97T–138T.
- (226) Parsons, J.; Milberg, M. Vibrational Spectra of Vitreous $\text{B}_2\text{O}_3 \cdot x\text{H}_2\text{O}$. *J. Am. Ceram. Soc.* **1960**, *43* (6), 326–330. <https://doi.org/10.1111/j.1151-2916.1960.tb13661.x>.
- (227) Krogh-Moe, J. Interpretation of Infrared Spectra of Boron Oxide and Alkali Borate Glasses. *Phys. Chem. Glasses* **1965**, *2*, 46–54.
- (228) Krogh-Moe, J. The Structure of Vitreous and Liquid Boron Oxide. *J. Non-Cryst. Solids* **1969**, *1* (4), 269–284. [https://doi.org/10.1016/0022-3093\(69\)90025-8](https://doi.org/10.1016/0022-3093(69)90025-8).
- (229) Goubeau, J.; Keller, H. Raman-Spektren Und Struktur von Boroxol-Verbindungen. *Z. Für Anorg. Allg. Chem.* **1953**, *272* (5-6), 303–312. <https://doi.org/10.1002/zaac.19532720510>.
- (230) Brill, T. Raman Spectroscopy of Crystalline and Glassy Borates. *Philips Res. Rep. Suppl.* **1976**, *2*, 1–114.
- (231) Galeener, F. L.; Lucovsky, G.; Mikkelsen Jr, J. Vibrational Spectra and the Structure of Pure Vitreous B_2O_3 . *Phys. Rev. B* **1980**, *22* (8), 3983–3990. <https://doi.org/10.1103/PhysRevB.22.3983>.
- (232) Windisch Jr, C. F.; Risen Jr, W. M. Vibrational Spectra of Oxygen-and Boron-Isotopically Substituted B_2O_3 Glasses. *J. Non-Cryst. Solids* **1982**, *48* (2–3), 307–323. [https://doi.org/10.1016/0022-3093\(82\)90168-5](https://doi.org/10.1016/0022-3093(82)90168-5).
- (233) Konijnendijk, W. L.; Stevels, J. The Structure of Borate Glasses Studied by Raman Scattering. *J. Non-Cryst. Solids* **1975**, *18* (3), 307–331. [https://doi.org/10.1016/0022-3093\(75\)90137-4](https://doi.org/10.1016/0022-3093(75)90137-4).
- (234) Tatsumisago, M.; Takahashi, M.; Minami, T.; Tanaka, M.; Umesaki, N.; Iwamoto, N. Structural Investigation of Rapidly Quenched $\text{Li}_2\text{O-B}_2\text{O}_3$ Glasses by Raman Spectroscopy. *Yogyo Kyokaiishi* **1986**, *94* (5), 464–469.

- 1
2
3
4
5
6
7
8
9
10
11
12
13
14
15
16
17
18
19
20
21
22
23
24
25
26
27
28
29
30
31
32
33
34
35
36
37
38
39
40
41
42
43
44
45
46
47
48
49
50
51
52
53
54
55
56
57
58
59
60
- (235) Kamitsos, E.; Karakassides, M.; Chryssikos, G. D. Vibrational Spectra of Magnesium-Sodium-Borate Glasses. 2. Raman and Mid-Infrared Investigation of the Network Structure. *J. Phys. Chem.* **1987**, *91* (5), 1073–1079. <https://doi.org/10.1021/j100289a014>.
- (236) Kamitsos, E. I.; Patsis, A.; Karakassides, M.; Chryssikos, G. D. Infrared Reflectance Spectra of Lithium Borate Glasses. *J. Non-Cryst. Solids* **1990**, *126* (1–2), 52–67. [https://doi.org/10.1016/0022-3093\(90\)91023-K](https://doi.org/10.1016/0022-3093(90)91023-K).
- (237) Kamitsos, E. I.; Chryssikos, G. D. Borate Glass Structure by Raman and Infrared Spectroscopies. *J. Mol. Struct.* **1991**, *247*, 1–16. [https://doi.org/10.1016/0022-2860\(91\)87058-P](https://doi.org/10.1016/0022-2860(91)87058-P).
- (238) Möncke, D.; Tricot, G.; Winterstein-Beckmann, A.; Wondraczek, L.; Kamitsos, E. I. On the Connectivity of Borate Tetrahedra in Borate and Borosilicate Glasses. *Phys. Chem. Glasses-Eur. J. Glass Sci. Technol. Part B* **2015**, *56* (5), 203–211. <https://doi.org/10.13036/17533562.56.5.203>.
- (239) Griscom, D. L. Borate Glass Structure. In *Borate glasses: Structure, properties, applications*; Plenum, L. D. P., Frechette, V. D., Kreidl, N. J., Eds.; Springer, 1978; pp 11–149.
- (240) Minami, T.; Tanaka, M. Structure and Ionic Transport of Superionic Conducting Glasses in the System AgI-Ag₂O-MoO₃. *J. Non-Cryst. Solids* **1980**, *38*, 289–294. [https://doi.org/10.1016/0022-3093\(80\)90433-0](https://doi.org/10.1016/0022-3093(80)90433-0).
- (241) Merzbacher, C. I.; White, W. B. Structure of Na in Aluminosilicate Glasses; a Far-Infrared Reflectance Spectroscopic Study. *Am. Mineral.* **1988**, *73* (9–10), 1089–1094.
- (242) Merzbacher, C. I.; White, W. B. The Structure of Alkaline Earth Aluminosilicate Glasses as Determined by Vibrational Spectroscopy. *J. Non-Cryst. Solids* **1991**, *130* (1), 18–34. [https://doi.org/10.1016/0022-3093\(91\)90152-V](https://doi.org/10.1016/0022-3093(91)90152-V).
- (243) Liu, C.; Angell, C. Mid-and Far-infrared Absorption of Alkali Borate Glasses and the Limit of Superionic Conductivity. *J. Chem. Phys.* **1990**, *93* (10), 7378–7386. <https://doi.org/10.1063/1.459413>.
- (244) Berreman, D. Infrared Absorption at Longitudinal Optic Frequency in Cubic Crystal Films. *Phys. Rev.* **1963**, *130* (6), 2193–2198. <https://doi.org/10.1103/PhysRev.130.2193>.
- (245) (a) Varsamis, C.; Kamitsos, E. I.; Chryssikos, G. D. Structure of Fast-Ion-Conducting AgI-Doped Borate Glasses in Bulk and Thin Film Forms. *Phys. Rev. B* **1999**, *60* (6), 3885–3898. <https://doi.org/10.1103/PhysRevB.60.3885>.
(b) Kamitsos, E. I.; Dussauze, M.; Varsamis, C.-P. E.; Vinatier, P.; Hamon, Y. Thin Film Amorphous Electrolytes: Structure and Composition by Experimental and Simulated Infrared Spectra. *J. Phys. Chem. C* **2007**, *111* (22), 8111–8119. <https://doi.org/10.1021/jp068617b>.
- (246) Amma S.; Luo J.; Pantano C. G.; Kim S. H. Specular reflectance (SR) and attenuated total reflectance (ATR) infrared (IR) spectroscopy of transparent flat glass surfaces: A case study for soda lime float glass. *J. Non-Cryst. Solids*, **2015**, *428* (15) 189-196. <http://dx.doi.org/10.1016/j.jnoncrysol.2015.08.015>
- (247) Kamitsos, E. I.; Patsis, A.; Chryssikos, G. D. Infrared Reflectance Investigation of Alkali Diborate Glasses. *J. Non-Cryst. Solids* **1993**, *152* (2–3), 246–257. [https://doi.org/10.1016/0022-3093\(93\)90258-Y](https://doi.org/10.1016/0022-3093(93)90258-Y).
- (248) Chryssikos, G. D.; Kapoutsis, J.; Kamitsos, E.; Patsis, A.; Pappin, A. Lithium-Sodium Metaborate Glasses: Structural Aspects and Vitrification Chemistry. *J. Non-Cryst. Solids* **1994**, *167* (1–2), 92–105. [https://doi.org/10.1016/0022-3093\(94\)90372-7](https://doi.org/10.1016/0022-3093(94)90372-7).

- 1
2
3 (249) Chatzipanagis, K.; Tagiara, N.; Möncke, D.; Kundu, S.; Rodrigues, A.; Kamitsos, E. I. Vibrational Study of Lithium Borotellurite Glasses. *J. Non-Cryst. Solids* **2020**, *540*, 120011. <https://doi.org/10.1016/j.jnoncrysol.2020.120011>.
- 4
5
6 (250) Feller, S. A. *Lithium-7, Boron-10, Boron-11, and Oxygen-17 Nuclear Magnetic Resonance Studies of Lithium Borate Glasses and Related Compounds*; Brown University, 1980.
- 7
8 (251) Feller, S. A.; Dell, W. J.; Bray, P. J. ^{10}B NMR Studies of Lithium Borate Glasses. *J. Non-Cryst. Solids* **1982**, *51* (1), 21–30. [https://doi.org/10.1016/0022-3093\(82\)90186-7](https://doi.org/10.1016/0022-3093(82)90186-7).
- 9
10 (252) Tatsumisago, M.; Shinkuma, Y.; Saito, T.; Minami, T. Formation of Frozen α -AgI in Superionic Glass Matrices at Ambient Temperature by Rapid Quenching. *Solid State Ion.* **1992**, *50* (3–4), 273–279. [https://doi.org/10.1016/0167-2738\(92\)90229-I](https://doi.org/10.1016/0167-2738(92)90229-I).
- 11
12 (253) Kowada, Y.; Adachi, H.; Tatsumisago, M.; Minami, T. Electronic States of Ag Ions in AgI-Based Superionic Conducting Glasses. *J. Non-Cryst. Solids* **1998**, *232–234*, 497–501. [https://doi.org/10.1016/S0022-3093\(98\)00478-5](https://doi.org/10.1016/S0022-3093(98)00478-5).
- 13
14 (254) Kapoutsis, J. A. A Structural Study of Silver Borate Glasses by Infrared Reflectance and Raman Spectroscopies. In *Proceedings of the Second International Conference on Borate Glasses, Crystals and Melts*; Wright, A. C., Feller, S. A., Hannon, A. C., Eds.; Sheffield, UK, **1997**; pp 303–312.
- 15
16 (255) Wright, A. C.; Sinclair, R. N.; Stone, C. E.; Shaw, J. L.; Feller, S. A.; Kiczanski, T.; Williams, R. B.; Berger, H. A.; Fischer, H. E.; Vedishcheva, N. M. A Neutron Diffraction Study of $2\text{M}_2\text{O}\cdot 5\text{B}_2\text{O}_3$ (M= Li, Na, K, Rb, Cs & Ag) and $2\text{MO}\cdot 5\text{B}_2\text{O}_3$ (M= Ca & Ba) Glasses. *Phys. Chem. Glasses-Eur. J. Glass Sci. Technol. Part B* **2012**, *53* (5), 191–204.
- 17
18 (256) Yiannopoulos, Y. D.; Kamitsos, E. I.; Chryssikos, G. D.; Kapoutsis, J. A. A Vibrational Spectroscopic Study of Alkaline Earth Borate Glasses. In *Proceedings of the Second International Conference on Borate Glasses, Crystals and Melts*; Wright, A. C., Feller, S. A., Hannon, A. C., Eds.; Sheffield, UK, **1997**; pp 514–521.
- 19
20 (257) Yiannopoulos, Y.; Chryssikos, G. D.; Kamitsos, E. Structure and Properties of Alkaline Earth Borate Glasses. *Phys. Chem. Glasses* **2001**, *42* (3), 164–172.
- 21
22 (258) Ohtori, N.; Takase, K.; Akiyama, I.; Suzuki, Y.; Handa, K.; Sakai, I.; Iwadate, Y.; Fukunaga, T.; Umesaki, N. Short-Range Structure of Alkaline-Earth Borate Glasses by Pulsed Neutron Diffraction and Molecular Dynamics Simulation. *J. Non-Cryst. Solids* **2001**, *293*, 136–145. [https://doi.org/10.1016/S0022-3093\(01\)00662-7](https://doi.org/10.1016/S0022-3093(01)00662-7).
- 23
24 (259) Alderman, O.; Benmore, C.; Holland, D.; Weber, J. Boron Coordination Change in Barium Borate Melts and Glasses and Its Contribution to Configurational Heat Capacity, Entropy, and Fragility. *J. Chem. Phys.* **2023**, *158* (22). <https://doi.org/10.1063/5.0153282>.
- 25
26 (260) (a) Dietzel, A. Die Kationenfeldstärken Und Ihre Beziehungen Zu Entglasungsvorgängen, Zur Verbindungsbildung Und Zu Den Schmelzpunkten von Silicaten. *Z. Für Elektrochem. Angew. Phys. Chem.* **1942**, *48* (1), 9–23.
- 27
28 (b) Dietzel, A. H. On the So-Called Mixed Alkali Effect. *Phys. Chem. Glasses* **1983**, *24* (6), 172–180.
- 29
30 (261) Shannon, R. D. Revised Effective Ionic Radii and Systematic Studies of Interatomic Distances in Halides and Chalcogenides. *Acta Crystallogr. Sect. A: Found. Crystallogr.* **1976**, *32* (5), 751–767. <https://doi.org/10.1107/S0567739476001551>.
- 31
32 (262) Lv P.; Wang C.; Stevansson B.; Yu Y.; Wang T.; Eden M. Impact of the cation field strength on physical properties and structures of alkali and alkaline-earth borosilicate glasses. *Ceram. Int.*, **2022**, *48*, 18094–18107. <https://doi.org/10.1016/j.ceramint.2022.03.022>
- 33
34 (263) Makris, N.; Varsamis, C.; Kamitsos, E. Structural Investigation of Lead Borate Glasses by
- 35
36
37
38
39
40
41
42
43
44
45
46
47
48
49
50
51
52
53
54
55
56
57
58
59
60

- Infrared Reflectance Spectroscopy. In *Proceedings of XXIV Panhellenic Conference in Solid State Physics*; 2008; pp 44–45.
- (264) Vedishcheva, N.; Shakhmatkin, B.; Wright, A.; Sinclair, R.; Grimley, D. A Combined Thermodynamic and Neutron Scattering Investigation of Glasses in the System PbO–B₂O₃; 1992; pp 41–46.
- (265) Ushida, H.; Iwadate, Y.; Hattori, T.; Nishiyama, S.; Fukushima, K.; Ikeda, Y.; Yamaguchi, M.; Misawa, M.; Fukunaga, T.; Nakazawa, T. Network Structure of B₂O₃–PbO and B₂O₃–PbO–PbBr₂ Glasses Analyzed by Pulsed Neutron Diffraction and Raman Spectroscopy. *J. Alloys Compd.* **2004**, *377* (1–2), 167–173. <https://doi.org/10.1016/j.jallcom.2003.12.038>.
- (266) Möncke, D.; Kamitsos, E. I.; Palles, D.; Limbach, R.; Winterstein-Beckmann, A.; Honma, T.; Yao, Z.; Rouxel, T.; Wondraczek, L. Transition and Post-Transition Metal Ions in Borate Glasses: Borate Ligand Speciation, Cluster Formation, and Their Effect on Glass Transition and Mechanical Properties. *J. Chem. Phys.* **2016**, *145* (12), 124501. <https://doi.org/10.1063/1.4962323>.
- (267) Ganguli, M.; Rao, K. Studies on the Effect of Li₂SO₄ on the Structure of Lithium Borate Glasses. *J. Chem. Phys.* **1999**, *103* (6), 920–930. <https://doi.org/10.1021/jp982930z>.
- (268) Liu, H.; Shen, G.; Wang, X.; Wei, J.; Shen, D. Viscosity and IR Investigations in the Li₂O–B₂O₃ System. *Prog. Cryst. Growth Charact. Mater.* **2000**, *40* (1–4), 235–241. [https://doi.org/10.1016/S0960-8974\(00\)00013-9](https://doi.org/10.1016/S0960-8974(00)00013-9).
- (269) Kashif, I.; Salem, S.; Soliman, A.; Farouk, H.; Mostafa, A.; Salah, S.; Sanad, A. Mossbauer, Infrared and Magnetic Susceptibility Studies of Iron Sodium Borate Glasses Doped by Sulphur. *J. Phys. Chem. Solids* **2006**, *67* (11), 2370–2375. <https://doi.org/10.1016/j.jpcs.2006.06.011>.
- (270) Doweidar, H.; Saddeek, Y. B. FTIR and Ultrasonic Investigations on Modified Bismuth Borate Glasses. *J. Non-Cryst. Solids* **2009**, *355* (6), 348–354. <https://doi.org/10.1016/j.jnoncrysol.2008.12.008>.
- (271) Gaafar, M.; Abd El-Aal, N.; Gerges, O.; El-Amir, G. Elastic Properties and Structural Studies on Some Zinc-Borate Glasses Derived from Ultrasonic, FT-IR and X-Ray Techniques. *J. Alloys Compd.* **2009**, *475* (1–2), 535–542. <https://doi.org/10.1016/j.jallcom.2008.07.114>.
- (272) Pascuta, P. Structural Investigations of Some Bismuth–Borate–Vanadate Glasses Doped with Gadolinium Ions. *J. Mater. Sci. Mater. Electron.* **2010**, *21*, 338–342. <https://doi.org/10.1007/s10854-009-9917-0>.
- (273) Kaur, A.; Khanna, A.; Bhatt, H.; González-Barriuso, M.; González, F.; Chen, B.; Deo, M. BO and TeO Speciation in Bismuth Tellurite and Bismuth Borotellurite Glasses by FTIR, ¹¹B MAS-NMR and Raman Spectroscopy. *J. Non-Cryst. Solids* **2017**, *470*, 19–26. <https://doi.org/10.1016/j.jnoncrysol.2017.04.028>.
- (274) Kaur, R.; Khanna, A.; González-Barriuso, M.; González, F.; Chen, B. Structural, Optical and Thermal Properties of Glass and Anti-Glass Phases in Strontium Tellurite and Borotellurite Systems Doped with Europium. *Mater. Res. Bull.* **2018**, *106*, 288–295. <https://doi.org/10.1016/j.materresbull.2018.06.020>.
- (275) Osipova, L.; Osipov, A.; Osipov, A. The Structure of Binary and Iron-Containing ZnO–B₂O₃ Glass by IR, Raman, and Mössbauer Spectroscopy. *Glass Phys. Chem.* **2019**, *45*, 182–190. <https://doi.org/10.1134/S1087659619030076>.
- (276) (a) Stehle, C.; Vira, C.; Hogan, D.; Feller, S.; Affatigato, M. Optical and Physical Properties of Bismuth Borate Glasses Related to Structure. *Phys. Chem. Glasses* **1998**, *39* (2), 83–86.

- (b) George, H.; Vira, C.; Stehle, C.; Meyer, J.; Evers, S.; Hogan, D.; Feller, S.; Affatigato, M. A Structural Analysis of the Physical Properties of Bismuth and Lead Based Glasses. *Phys. Chem. Glasses* **1999**, *40* (6), 326–332.
- (277) Ihara, R.; Honma, T.; Benino, Y.; Fujiwara, T.; Komatsu, T. Second-Order Optical Nonlinearities of Metastable BiBO₃ Phases in Crystallized Glasses. *Opt. Mater.* **2004**, *27* (3), 403–408. <https://doi.org/10.1016/j.optmat.2004.07.002>.
- (278) Dong, M.; Sayyed, M.; Lakshminarayana, G.; Ersundu, M. Ç.; Ersundu, A.; Nayar, P.; Mahdi, M. Investigation of Gamma Radiation Shielding Properties of Lithium Zinc Bismuth Borate Glasses Using XCOM Program and MCNP5 Code. *J. Non-Cryst. Solids* **2017**, *468*, 12–16. <https://doi.org/10.1016/j.jnoncrysol.2017.04.018>.
- (279) Varsamis, C.-P. E.; Makris, N.; Valvi, C.; Kamitsos, E. I. Short-Range Structure, the Role of Bismuth and Property–Structure Correlations in Bismuth Borate Glasses. *Phys. Chem. Chem. Phys.* **2021**, *23* (16), 10006–10020. <https://doi.org/10.1039/D1CP00301A>.
- (280) Topper, B.; Tagiara, N. S.; Herrmann, A.; Kamitsos, E. I.; Möncke, D. Yttrium and Rare-Earth Modified Lithium Orthoborates: Glass Formation and Vibrational Activity. *J. Non-Cryst. Solids* **2022**, *575*, 121152. <https://doi.org/10.1016/j.jnoncrysol.2021.121152>.
- (281) Lower, N.P.; Mcrae, J.L.; Feller, H.A.; Betzen, A.R.; Kapoor, S., Affatigato, M.; Feller, S.A. Physical properties and alkaline-earth and alkali borate glasses prepared over an extended range of composition. *J. Non-Cryst. Solids*, **2001**, 293-295, 669-675.
- (282) Kamitsos, E.; Karakassides, M. Structural Studies of Binary and Pseudo Binary Sodium Borate Glasses of High Sodium Content. *Phys. Chem. Glasses* **1989**, *30* (1), 19–26.
- (283) Zhong, J.; Bray, P. J. NMR Study of Structure of Sodium Boroaluminate Glass at High Sodium Content. *J. Non-Cryst. Solids* **1986**, *84* (1–3), 17–25. [https://doi.org/10.1016/0022-3093\(86\)90758-1](https://doi.org/10.1016/0022-3093(86)90758-1).
- (284) Chryssikos, G.D.; Kamitsos, E.I.; Karakassides, M.A. Structure of borate glasses. Part 2: The alkali-induced network modification schemes in terms of structure and properties. *Phys. Chem. Glasses*, **1990**, *31*, 109-116.
- (285) (a) Yano, T.; Kunimine, N.; Shibata, S.; Yamane, M. Structural Investigation of Sodium Borate Glasses and Melts by Raman Spectroscopy.: I. Quantitative Evaluation of Structural Units. *J. Non-Cryst. Solids* **2003**, *321* (3), 137–146. [https://doi.org/10.1016/S0022-3093\(03\)00158-3](https://doi.org/10.1016/S0022-3093(03)00158-3).
- (b) Yano, T.; Kunimine, N.; Shibata, S.; Yamane, M. Structural Investigation of Sodium Borate Glasses and Melts by Raman Spectroscopy. II. Conversion between BO₄ and BO₂O– Units at High Temperature. *J. Non-Cryst. Solids* **2003**, *321* (3), 147–156. [https://doi.org/10.1016/S0022-3093\(03\)00159-5](https://doi.org/10.1016/S0022-3093(03)00159-5).
- (286) Araujo, R. Statistical Mechanics of Chemical Disorder: Application to Alkali Borate Glasses. *J. Non-Cryst. Solids* **1983**, *58* (2–3), 201–208. [https://doi.org/10.1016/0022-3093\(83\)90024-8](https://doi.org/10.1016/0022-3093(83)90024-8).
- (287) Stebbins, J. F.; Ellsworth, S. E. Temperature Effects on Structure and Dynamics in Borate and Borosilicate Liquids: High-resolution and High-temperature NMR Results. *J. Am. Ceram. Soc.* **1996**, *79* (9), 2247–2256. <https://doi.org/10.1111/j.1151-2916.1996.tb08969.x>.
- (288) Akagi, R.; Ohtori, N.; Umesaki, N. Raman Spectra of K₂O–B₂O₃ Glasses and Melts. *J. Non-Cryst. Solids* **2001**, *293*, 471–476. [https://doi.org/10.1016/S0022-3093\(01\)00752-9](https://doi.org/10.1016/S0022-3093(01)00752-9).
- (289) Osipova, L.; Osipov, A.; Bykov, V. Structure of High-Alkali Melts in the Lithium Borate System from Vibrational Spectroscopic Data. *Glass Phys. Chem.* **2007**, *33*, 486–491.
- (290) Cormack, A.; Park, B. Molecular Dynamics Simulations of Borate Glasses. *Phys. Chem.*

- Glasses* **2000**, *41* (5), 272–277.
- (291) Varsamis, C.-P. E.; Vegiri, A.; Kamitsos, E. I. Molecular Dynamics Investigation of Lithium Borate Glasses: Local Structure and Ion Dynamics. *Phys. Rev. B* **2002**, *65* (10), 104203. <https://doi.org/10.1103/PhysRevB.65.104203>.
- (292) Majérus, O.; Cormier, L.; Calas, G.; Beuneu, B. Temperature-Induced Boron Coordination Change in Alkali Borate Glasses and Melts. *Physical Review B* **2003**, *67* (2), 024210.
- (293) Cormier, L.; Majérus, O.; Neuville, Dr.; Calas, G. Temperature-Induced Structural Modifications Between Alkali Borate Glasses and Melts. *J. Am. Ceram. Soc.* **2006**, *89* (1), 13–19. <https://doi.org/10.1111/j.1551-2916.2005.00657.x>.
- (294) Alderman, O. L.; Benmore, C. J.; Lin, A.; Tamalonis, A.; Weber, J. R. Borate Melt Structure: Temperature-dependent B–O Bond Lengths and Coordination Numbers from High-energy X-ray Diffraction. *J. Am. Ceram. Soc.* **2018**, *101* (8), 3357–3371. <https://doi.org/10.1111/jace.15529>.
- (295) Alderman, O.; Benmore, C.; Weber, J. Consequences of Sp^2 – Sp^3 Boron Isomerization in Supercooled Liquid Borates. *Appl. Phys. Lett.* **2020**, *117* (13), 131901. <https://doi.org/10.1063/5.0024457>.
- (296) Warren, B. The Diffraction of X-Rays in Glass. *Phys. Rev.* **1934**, *45* (10), 657. <https://doi.org/10.1103/PhysRev.45.657>.
- (297) Warren, B. X-Ray Diffraction Study of the Structure of Glass. *Chem. Rev.* **1940**, *26* (2), 237–255. <https://doi.org/10.1021/cr60084a007>.
- (298) Biscoe, J.; Pincus, A.; Smith Jr, C.; Warren, B. X-Ray Study of Lime-Phosphate and Lime-Borate Glass. *J. Am. Ceram. Soc.* **1941**, *24* (4), 116–119. <https://doi.org/10.1111/j.1151-2916.1941.tb14833.x>.
- (299) Green, R. L. X-Ray Diffraction and Physical Properties of Potassium Borate Glasses. *J. Am. Ceram. Soc.* **1942**, *25* (3), 83–89. <https://doi.org/10.1111/j.1151-2916.1942.tb14356.x>.
- (300) Mozzi, R.; Warren, B. The Structure of Vitreous Silica. *J. Appl. Crystallogr.* **1969**, *2* (4), 164–172. <https://doi.org/10.1107/S0021889869006868>.
- (301) Mozzi, R. L.; Warren, B. The Structure of Vitreous Boron Oxide. *J. Appl. Crystallogr.* **1970**, *3* (4), 251–257. <https://doi.org/10.1107/S0021889870006143>.
- (302) Neufeind, J.; Poulsen, H. Diffraction on Disordered Materials Using “Neutron-like” Photons. *Phys. Scr.* **1995**, *1995* (T57), 112. <https://doi.org/10.1088/0031-8949/1995/T57/019>.
- (303) Poulsen, H.; Neufeind, J.; Neumann, H.-B.; Schneider, J.; Zeidler, M. Amorphous Silica Studied by High Energy X-Ray Diffraction. *J. Non-Cryst. Solids* **1995**, *188* (1–2), 63–74. [https://doi.org/10.1016/0022-3093\(95\)00095-X](https://doi.org/10.1016/0022-3093(95)00095-X).
- (304) Yasui, I.; Hasegawa, H.; Saito, Y. Structure of Borate Glasses Containing Tl and Ba Oxide. *J. Non-Cryst. Solids* **1988**, *106* (1–3), 30–33. [https://doi.org/10.1016/0022-3093\(88\)90221-9](https://doi.org/10.1016/0022-3093(88)90221-9).
- (305) Yasui, I.; Hasegawa, H.; Saito, Y.; Akasaka, Y. Structure of Borate Glasses Containing Heavy Metal Ions. *J. Non-Cryst. Solids* **1990**, *123* (1–3), 71–74. [https://doi.org/10.1016/0022-3093\(90\)90774-G](https://doi.org/10.1016/0022-3093(90)90774-G).
- (306) Vedishcheva, N. M.; Shakhmatkin, B. A.; Wright, A. C.; Grimley, D. I.; Etherington, G.; Sinclair, R. N. Structural Order in Lead Borate Glasses: A Test of Recent Thermodynamic Predictions. *Fundam. Glass Sci. Technol.* **1993**, 459–462.
- (307) Wright, A.; Sinclair, R.; Crimley, D.; Hulme, R.; Vedishcheva, N.; Shakhmatkin, B.; Hannon, A.; Feller, S.; Meyer, B.; Royle, M. Borate Glasses, Superstructural Units and the

- 1
2
3 Random Network Theory 1. *Glass Phys. Chem.* **1996**, 22 (4), 268–278.
- 4 (308) Kita, Y.; Misawa, M.; Umesaki, N.; Kirihara, T.; Fukunaga, T.; Iida, T. Structural Analysis
5 of Na₂O-B₂O₃ Melts by Pulsed Neutron Total Scattering Method and Molecular Dynamics
6 Simulation. *ISIJ Int.* **1993**, 33 (1), 188–194. <https://doi.org/10.2355/isijinternational.33.188>.
- 7 (309) Herms, G.; Sakowski, J.; Gerike, W.; Stachel, D. Structural Changes in Two Different Types
8 of Oxide Glass Melts: Borates and Metaphosphates. *Z. Für Naturforschung A* **1998**, 53 (10–
9 11), 874–882. <https://doi.org/10.1515/zna-1998-10-1111>.
- 10 (310) Herms, G.; Sakowski, J. X-ray Diffraction Studies of Structural Changes in Molten Borate
11 Glasses. *Phys. Chem. Glasses* **2000**, 41 (5), 309–312.
- 12 (311) Alderman, O.; Liska, M.; Machacek, J.; Benmore, C.; Lin, A.; Tamalonis, A.; Weber, J.
13 Temperature-Driven Structural Transitions in Molten Sodium Borates Na₂O–B₂O₃: X-Ray
14 Diffraction, Thermodynamic Modeling, and Implications for Topological Constraint
15 Theory. *J. Phys. Chem. C* **2016**, 120 (1), 553–560.
16 <https://doi.org/10.1021/acs.jpcc.5b10277>.
- 17 (312) Alderman, O. L.; Benmore, C. J.; Reynolds, B.; Royle, B.; Feller, S.; Weber, R. J. Liquid
18 Fragility Maximum in Lithium Borate Glass-forming Melts Related to the Local Structure.
19 *Int. J. Appl. Glass Sci.* **2023**, 14 (1), 52–68. <https://doi.org/10.1111/ijag.16611>.
- 20 (313) Hoppe, U.; Walter, G.; Barz, A.; Stachel, D.; Hamon, A. The PO Bond Lengths in Vitreous
21 P₂O₅ Probed by Neutron Diffraction with High Real-Space Resolution. *J. Phys. Condens.*
22 *Matter* **1998**, 10 (2), 261. <https://doi.org/10.1088/0953-8984/10/2/004>.
- 23 (314) Brown, I. D.; Altermatt, D. Bond-Valence Parameters Obtained from a Systematic Analysis
24 of the Inorganic Crystal Structure Database. *Acta Crystallogr. B* **1985**, 41 (4), 244–247.
25 <https://doi.org/10.1107/S0108768185002063>.
- 26 (315) Alderman, O. L.; Ferlat, G.; Baroni, A.; Salanne, M.; Micoulaut, M.; Benmore, C.; Lin, A.;
27 Tamalonis, A.; Weber, J. Liquid B₂O₃ up to 1700 K: X-Ray Diffraction and Boroxol Ring
28 Dissolution. *J. Phys. Condens. Matter* **2015**, 27 (45), 455104. <https://doi.org/10.1088/0953-8984/27/45/455104>.
- 29 (316) Suzuya, K.; Yoneda, Y.; Kohara, S.; Umesaki, N. High Energy X-ray Study of the Structure
30 of Vitreous B₂O₃. *Physics and chemistry of glasses* **2000**, 41 (5), 282–285.
- 31 (317) Gurr, G.; Montgomery, P.; Knutson, C.; Gorres, B. The Crystal Structure of Trigonal
32 Diboron Trioxide. *Acta Crystallogr. B* **1970**, 26 (7), 906–915.
33 <https://doi.org/10.1107/S0567740870003369>.
- 34 (318) Warren, B.; Krutter, H.; Morningstar, O. Fourier Analysis of X-ray Patterns of Vitreous
35 SiO₂ and B₂O₂. *J. Am. Ceram. Soc.* **1936**, 19 (1-12), 202–206.
36 <https://doi.org/10.1111/j.1151-2916.1936.tb19822.x>.
- 37 (319) Sugiyama, K.; Nomura, K.; Kimura, S. X-Ray Diffraction Study on the Structure of Liquid
38 Li₂O-B₂O₃. *High Temp. Mater. Process.* **1995**, 14 (2), 131–136.
39 <https://doi.org/10.1515/HTMP.1995.14.2.131>.
- 40 (320) Kajinami, A.; Kotake, T.; Deki, S.; Kohara, S. The Structural Analysis of Manganese Borate
41 Glass by High-Energy X-Ray Diffraction Measurement. *Nucl. Instrum. Methods Phys. Res.*
42 *Sect. B Beam Interact. Mater. At* **2003**, 199, 34–37.
- 43 (321) Brazhkin, V.; Katayama, Y.; Trachenko, K.; Tsiok, O.; Lyapin, A.; Artacho, E.; Dove, M.;
44 Ferlat, G.; Inamura, Y.; Saitoh, H. Nature of the Structural Transformations in B₂O₃ Glass
45 under High Pressure. *Phys. Rev. Lett.* **2008**, 101 (3), 035702.
46 <https://doi.org/10.1103/PhysRevLett.101.035702>.
- 47 (322) Johnson, P. A.; Wright, A. C.; Sinclair, R. N. A Neutron Diffraction Investigation of the
48
49
50
51
52
53
54
55
56
57
58
59
60

- Structure of Vitreous Boron Trioxide. *J. Non-Cryst. Solids* **1982**, *50* (3), 281–311. [https://doi.org/10.1016/0022-3093\(82\)90092-8](https://doi.org/10.1016/0022-3093(82)90092-8).
- (323) Misawa, M. Structure of Vitreous and Molten B_2O_3 Measured by Pulsed Neutron Total Scattering. *J. Non-Cryst. Solids* **1990**, *122* (1), 33–40. [https://doi.org/10.1016/0022-3093\(90\)90221-7](https://doi.org/10.1016/0022-3093(90)90221-7).
- (324) Hannon, A. C.; Barney, E. R.; Holland, D. The Structure of Tin Borate Based Glasses. *Phys. Chem. Glasses-Eur. J. Glass Sci. Technol. Part B* **2009**, *50* (5), 271–283. [https://doi.org/10.1016/Phys. Chem. Glasses-Eur. J. Glass Sci. Technol. Part B](https://doi.org/10.1016/j.jnoncrystol.2007.02.045).
- (325) Zeidler, A.; Wezka, K.; Whittaker, D. A.; Salmon, P. S.; Baroni, A.; Klotz, S.; Fischer, H. E.; Wilding, M. C.; Bull, C. L.; Tucker, M. G. Density-Driven Structural Transformations in B_2O_3 Glass. *Phys. Rev. B* **2014**, *90* (2), 024206. <https://doi.org/10.1103/PhysRevB.90.024206>.
- (326) Alderman, O. L. G. Boroxol ring dissolution in molten and glassy B_2O_3 by neutron and x-ray diffraction difference methods. *J. Chem. Phys* **2025**, *162* (5), 054502.
- (327) Lelong, G.; Cormier, L.; Hennet, L.; Michel, F.; Rueff, J.-P.; Ablett, J. M.; Monaco, G. Lithium Borates from the Glass to the Melt: A Temperature-Induced Structural Transformation Viewed from the Boron and Oxygen Atoms. *Inorg. Chem.* **2021**, *60* (2), 798–806. <https://doi.org/10.1021/acs.inorgchem.0c02844>.
- (328) Wright, A. C.; Sinclair, R. N.; Stone, C. E.; Shaw, J. L.; Feller, S. A.; Williams, R. B.; Fischer, H. E.; Vedishcheva, N. M. A Neutron Diffraction Study of Sodium, Rubidium and Cæsium Borate Glasses. *Phys. Chem. Glasses-Eur. J. Glass Sci. Technol. Part B* **2014**, *55* (2), 74–84.
- (329) Swenson, J.; Börjesson, L.; Howells, W. Structure of Borate Glasses from Neutron-Diffraction Experiments. *Phys. Rev. B* **1995**, *52* (13), 9310. <https://doi.org/10.1103/PhysRevB.52.9310>.
- (330) Cormier, L.; Calas, G.; Beuneu, B. Quantification of Boron Coordination Changes between Lithium Borate Glasses and Melts by Neutron Diffraction. *Phys. Chem. Glasses-Eur. J. Glass Sci. Technol. Part B* **2009**, *50* (3), 195–200.
- (331) Suzuki, Y.; Ohtori, N.; Takase, K.; Handa, K.; Itoh, K.; Fukunaga, T.; Umesaki, N. Pulsed Neutron Diffraction Studies of $RO \cdot xB_2O_3$ Glasses: R=Ca, Sr and Ba; X=2, 3 and 4. *Phys. Chem. Glasses* **2003**, *44* (2), 150–154.
- (332) Handa, K.; Kita, Y.; Kohara, S.; Suzuya, K.; Fukunaga, T.; Misawa, M.; Iida, T.; Iwasaki, H.; Umesaki, N. Structure of $M_2O-B_2O_3$ (M: Na and K) Glasses and Melts by Neutron Diffraction. *J. Phys. Chem. Solids* **1999**, *60* (8–9), 1465–1471. [https://doi.org/10.1016/S0022-3697\(99\)00143-2](https://doi.org/10.1016/S0022-3697(99)00143-2).
- (333) Cormier, L.; Calas, G.; Beuneu, B. Structure of Single and Mixed Alkali Li–Rb Borate Glasses by Neutron Diffraction. *J. Non-Cryst. Solids* **2007**, *353* (18–21), 1779–1784. <https://doi.org/10.1016/j.jnoncrystol.2007.02.045>.
- (334) Shaw, J.; Wright, A.; Sinclair, R.; Frueh, J.; Williams, R.; Nelson, N.; Affatigato, M.; Feller, S.; Scales, C. A Neutron Diffraction Investigation of the Structure of Caesium Borate Glasses. *Phys. Chem. Glasses* **2003**, *44*, 256–259.
- (335) Kajinami, A.; Harada, Y.; Inoue, S.; Deki, S.; Umesaki, N. The Structural Analysis of Zinc Borate Glass by Laboratory EXAFS and X-Ray Diffraction Measurements. *Jpn. J. Appl. Phys.* **1999**, *38* (S1), 132.
- (336) Youngman, R. E.; Cornelius, L. K.; Koval, S. E.; Hogue, C. L.; Ellison, A. J. Structure–Property Studies of $SrBr_2-SrO-B_2O_3$ Glasses. *Phys. Chem. Glasses-Eur. J. Glass Sci.*

- Technol. Part B* **2009**, *50* (3), 175–182.
- (337) Matsumura, S.; Watanabe, M.; Mizuno, A.; Kohara, S. Supercooled Barium Boric Oxide Melts: X-ray Diffraction Measurements and Glass Formation. *J. Am. Ceram. Soc.* **2007**, *90* (3), 742–745. <https://doi.org/10.1111/j.1551-2916.2006.01475.x>.
- (338) Gejke, C.; Swenson, J.; Delaplané, R.; Börjesson, L. Neutron Diffraction Study of Microscopic Structure of SnB₂O₄ Glass. *Phys. Rev. B* **2002**, *65* (21), 212201. <https://doi.org/10.1103/PhysRevB.65.212201>.
- (339) Holland, D.; Smith, M.; Howes, A.; Davies, T.; Barrett, L. Influence of the Borate Anomaly on the Sn (II) Environment in Tin Borate Glasses. *Phys. Chem. Glasses* **2003**, *44* (2), 59–63.
- (340) Hayashi, A.; Nakai, M.; Tatsumisago, M.; Minami, T. Structure and Properties of Glasses in the System Li₂O–SnO–B₂O₃. *Comptes Rendus Chim.* **2002**, *5* (11), 751–757.
- (341) Wright, A. C.; Etherington, G.; Feller, S. A.; Gnappi, G.; Grimley, D.; Montenero, A.; Sinclair, R. N.; Stone, C. Neutron Diffraction Studies of Binary Network Glasses Containing PbO and Bi₂O₃. *Glass Sci. Technol.* **2002**, *75* (C2), 139–144.
- (342) Orman, R. G. Characterisation of Novel Antimony (III) Oxide-Containing Glasses, University of Warwick, 2010. <https://pugwash.lib.warwick.ac.uk/record=b2334501~S15>.
- (343) Stone, C.; Wright, A.; Sinclair, R.; Feller, S.; Affatigato, M.; Hogan, D.; Nelson, N.; Vira, C.; Dimitriev, Y.; Gattef, E. Structure of Bismuth Borate Glasses. *Phys. Chem. Glasses* **2000**, *41* (6), 409–412.
- (344) (a) Tagiara, N. S.; Palles, D.; Simandiras, E. D.; Psycharis, V.; Kyritsis, A.; Kamitsos, E.I., Synthesis, thermal and structural properties of pure TeO₂ glass and zinc-tellurite glasses. *J. Non-Cryst. Solids* **2017**, *457*, 116–125. <https://doi.org/10.1016/j.jnoncrsol.2016.11.033>.
(b) Tagiara, N. S.; Moayedi, E.; Kyritsis, A.; Wondraczek, L.; Kamitsos, E.I., Short-Range Structure, Thermal and Elastic Properties of Binary and Ternary Tellurite Glasses. *J. Phys. Chem. B* **2019**, *123*, 7905–7918. <https://dx.doi.org/10.1021/acs.jpcc.9b04617>.
(c) Papadopoulos, A.G.; Tagiara, N. S.; Simandiras, E. D.; Kamitsos, E.I., On the Absence of Doubly Bonded Te=O Groups in TeO₂ Glass. *J. Phys. Chem. B* **2020**, *124*, 5746–5753. <https://dx.doi.org/10.1021/acs.jpcc.0c02499>.
- (345) Milberg, M.; Meller, F. Structure of Vitreous B₂O₃·½H₂O. *J. Chem. Phys.* **1959**, *31* (1), 126–129. <https://doi.org/10.1063/1.1730278>.
- (346) Meller, F.; Milberg, M. The Structure of Some B₂O₃-H₂O Glasses. *J. Am. Ceram. Soc.* **1960**, *43* (7), 353–356. <https://doi.org/10.1111/j.1151-2916.1960.tb13670.x>.
- (347) Brüning, R.; Patterson, S. Thermal and Structural Properties of B₂O₃-H₂O Glasses. *J. Mater. Res.* **2003**, *18* (10), 2494–2500. <https://doi.org/10.1557/JMR.2003.0347>.
- (348) Brüning, R.; Galbraith, J. B.; Braedley, K. E.; Johnstone, J.; Robichaud, J.; Balaji, S.; Djaoued, Y. X-Ray Diffraction and Micro-Raman Study of Structural Transformations in (B₂O₃)_{1-x}(H₂O)_x Glasses and Liquids. *J. Am. Ceram. Soc.* **2010**, *93* (11), 3745–3751. <https://doi.org/10.1111/j.1551-2916.2010.03921.x>.
- (349) Wright, A. C. The Structural Chemistry of B₂O₃. *Phys. Chem. Glasses-Eur. J. Glass Sci. Technol. Part B* **2018**, *59* (2), 65–87. <https://doi.org/10.13036/17533562.59.2.034>.
- (350) Sen, S. Temperature Induced Structural Changes and Transport Mechanisms in Borate, Borosilicate and Boroaluminates Liquids: High-Resolution and High-Temperature NMR Results. *J. Non-Cryst. Solids* **1999**, *253* (1–3), 84–94. [https://doi.org/10.1016/S0022-3093\(99\)00346-4](https://doi.org/10.1016/S0022-3093(99)00346-4).
- (351) Alderman, O. Borate Melt Structure: A Short Review. *Phys. Chem. Glasses-Eur. J. Glass*

- Sci. Technol. Part B* **2018**, 59 (1), 1–10. <https://doi.org/10.13036/17533562.59.1.016>.
- (352) Li, D.; Bancroft, G.; Fleet, M.; Hess, P.; Yin, Z. Coordination of B in K₂O-SiO₂-B₂O₃-P₂O₅ Glasses Using BK-Edge XANES. *Am. Mineral.* **1995**, 80 (9–10), 873–877. <https://doi.org/10.2138/am-1995-9-1001>.
- (353) Fleet, M.; Muthupari, S. Coordination of Boron in Alkali Borosilicate Glasses Using XANES. *J. Non-Cryst. Solids* **1999**, 255 (2–3), 233–241. [https://doi.org/10.1016/S0022-3093\(99\)00386-5](https://doi.org/10.1016/S0022-3093(99)00386-5).
- (354) Yamamoto, K.; Fujita, M.; Tsuji, J.; Kojima, K.; Wada, N.; Taniguchi, K.; Ikeda, S.; Perera, R. Boron K-Edge X-Ray Absorption and Emission Spectroscopic Studies in Sodium Borate Glasses. *Mem. SR Cent. Ritsumeikan Univ.* **2001**, 3, 15–20.
- (355) Lee, S. K.; Eng, P. J.; Mao, H.; Shu, J. Probing and Modeling of Pressure-Induced Coordination Transformation in Borate Glasses: Inelastic x-Ray Scattering Study at High Pressure. *Phys. Rev. B—Condensed Matter Mater. Phys.* **2008**, 78 (21), 214203. <https://doi.org/10.1103/PhysRevB.78.214203>.
- (356) Lee, S. K.; Eng, P. J.; Mao, H.; Meng, Y.; Shu, J. Structure of Alkali Borate Glasses at High Pressure: B and Li K-Edge Inelastic X-Ray Scattering Study. *Phys. Rev. Lett.* **2007**, 98 (10), 105502. <https://doi.org/10.1103/PhysRevLett.98.105502>.
- (357) Brazhkin, V.; Farnan, I.; Funakoshi, K.; Kanzaki, M.; Katayama, Y.; Lyapin, A.; Saitoh, H. Structural Transformations and Anomalous Viscosity in the B₂O₃ Melt under High Pressure. *Phys. Rev. Lett.* **2010**, 105 (11), 115701.
- (358) Buscemi, M. Investigation of Boro-Germanate and Germanium Disulfide Glasses: Relation between Structure and Properties, University of Bath, 2019.
- (359) Sasaki, S.; Masuno, A.; Ohara, K.; Yanaba, Y.; Inoue, H.; Watanabe, Y.; Kohara, S. Structural Origin of Additional Infrared Transparency and Enhanced Glass-Forming Ability in Rare-Earth-Rich Borate Glasses without B–O Networks. *Inorg. Chem.* **2020**, 59 (19), 13942–13951. <https://doi.org/10.1021/acs.inorgchem.0c01567>.
- (360) Shannon, R. t; Prewitt, C. Revised Values of Effective Ionic Radii. *Acta Crystallogr. B* **1970**, 26 (7), 1046–1048. <https://doi.org/10.1107/S0567740870003576>.
- (361) Shannon, R. T.; Prewitt, C. T. Effective Ionic Radii in Oxides and Fluorides. *Acta Crystallogr. B* **1969**, 25 (5), 925–946. <https://doi.org/10.1107/S0567740869003220>.
- (362) Dronskowski, R. Computational Chemistry of Solid State Materials. *Materials Today* **2006**, 9 (3), 53. [https://doi.org/10.1016/S1369-7021\(06\)71391-8](https://doi.org/10.1016/S1369-7021(06)71391-8).
- (363) Barney, E. R.; Hannon, A. C.; Laorodphan, N.; Holland, D. Influence of Lone-Pair Cations on the Germanate Anomaly in Glass. *J. Phys. Chem. C* **2011**, 115 (30), 14997–15007. <https://doi.org/10.1021/jp202279b>.
- (364) Hannon, A. C.; Vaishnav, S.; Alderman, O. L.; Bingham, P. A. The Structure of Sodium Silicate Glass from Neutron Diffraction and Modeling of Oxygen-oxygen Correlations. *J. Am. Ceram. Soc.* **2021**, 104 (12), 6155–6171. <https://doi.org/10.1111/jace.17993>.
- (365) Hoppe, U.; Walter, G.; Kranold, R.; Stachel, D. Structural Specifics of Phosphate Glasses Probed by Diffraction Methods: A Review. *J. Non-Cryst. Solids* **2000**, 263, 29–47. [https://doi.org/10.1016/S0022-3093\(99\)00621-3](https://doi.org/10.1016/S0022-3093(99)00621-3).
- (366) Baugher, J.; Bray, P. B¹¹ NMR in Germanium Borate Glasses. *Phys. Chem. Glasses* **1972**, 13 (2), 63.
- (367) Lower, N. P.; McRae, J. L.; Feller, H. A.; Betzen, A. R.; Kapoor, S.; Affatigato, M.; Feller, S. A. Physical Properties of Alkaline-Earth and Alkali Borate Glasses Prepared over an Extended Range of Compositions. *J. Non-Cryst. Solids* **2001**, 293, 669–675.

- 1
2
3 [https://doi.org/10.1016/S0022-3093\(01\)00768-2](https://doi.org/10.1016/S0022-3093(01)00768-2).
- 4 (368) Schurko, R. W. Ultra-Wideline Solid-State NMR Spectroscopy. *Acc. Chem. Res.* **2013**, *46*
5 (9), 1985–1995. <https://doi.org/10.1021/ar400045t>.
- 6 (369) Pell, A. J.; Pintacuda, G.; Grey, C. P. Paramagnetic NMR in Solution and the Solid State.
7 *Prog. Nucl. Magn. Reson. Spectrosc.* **2019**, *111*, 1–271.
8 <https://doi.org/10.1016/j.pnmrs.2018.05.001>.
- 9 (370) Pell, A. J.; Pintacuda, G. Broadband Solid-State MAS NMR of Paramagnetic Systems.
10 *Prog. Nucl. Magn. Reson. Spectrosc.* **2015**, *84*, 33–72.
11 <https://doi.org/10.1016/j.pnmrs.2014.12.002>.
- 12 (371) Stebbins, J. F.; McCarty, R. J.; Palke, A. C. Toward the Wider Application of ²⁹Si NMR
13 Spectroscopy to Paramagnetic Transition Metal Silicate Minerals and Glasses: Fe (II), Co
14 (II), and Ni (II) Silicates. *Am. Mineral.* **2018**, *103* (5), 776–791. [https://doi.org/10.2138/am-](https://doi.org/10.2138/am-2017-6176)
15 [2017-6176](https://doi.org/10.2138/am-2017-6176).
- 16 (372) Zhu, F.; Bowron, D. T.; Gärtner, S.; Fang, C.; Zhou, Y.; Liu, H.; Hannon, A. C. Structural
17 Analysis of Potassium Borate Solutions. *Phys. Chem. Chem. Phys.* **2023**, *25* (17), 12207–
18 12219. <https://doi.org/10.1039/D2CP05331D>.
- 19 (373) Laorodphan, N.; Pooddee, P.; Kidkhunthod, P.; Kunthadee, P.; Tapala, W.; Puntharod, R.
20 Boron and Pentavalent Vanadium Local Environments in Binary Vanadium Borate Glasses.
21 *J. Non-Cryst. Solids* **2016**, *453*, 118–124. <https://doi.org/10.1016/j.jnoncrysol.2016.10.005>.
- 22 (374) Vedishcheva, N. M. and Wright, A. C. in *Glass: Selected properties and crystallization*,
23 edited by J. W. P. Schmelzer (de Gruyter, Berlin, 2014), pp. 269-299.
24
25
26
27
28
29
30
31
32
33
34
35
36
37
38
39
40
41
42
43
44
45
46
47
48
49
50
51
52
53
54
55
56
57
58
59
60